

1985

The preparation and characterization of chalcogenide derivatives of hemerythrin

Gudrun Susanne Lukat
Iowa State University

Follow this and additional works at: <https://lib.dr.iastate.edu/rtd>

 Part of the [Inorganic Chemistry Commons](#)

Recommended Citation

Lukat, Gudrun Susanne, "The preparation and characterization of chalcogenide derivatives of hemerythrin " (1985). *Retrospective Theses and Dissertations*. 7868.
<https://lib.dr.iastate.edu/rtd/7868>

This Dissertation is brought to you for free and open access by the Iowa State University Capstones, Theses and Dissertations at Iowa State University Digital Repository. It has been accepted for inclusion in Retrospective Theses and Dissertations by an authorized administrator of Iowa State University Digital Repository. For more information, please contact digirep@iastate.edu.

INFORMATION TO USERS

This reproduction was made from a copy of a document sent to us for microfilming. While the most advanced technology has been used to photograph and reproduce this document, the quality of the reproduction is heavily dependent upon the quality of the material submitted.

The following explanation of techniques is provided to help clarify markings or notations which may appear on this reproduction.

1. The sign or "target" for pages apparently lacking from the document photographed is "Missing Page(s)". If it was possible to obtain the missing page(s) or section, they are spliced into the film along with adjacent pages. This may have necessitated cutting through an image and duplicating adjacent pages to assure complete continuity.
2. When an image on the film is obliterated with a round black mark, it is an indication of either blurred copy because of movement during exposure, duplicate copy, or copyrighted materials that should not have been filmed. For blurred pages, a good image of the page can be found in the adjacent frame. If copyrighted materials were deleted, a target note will appear listing the pages in the adjacent frame.
3. When a map, drawing or chart, etc., is part of the material being photographed, a definite method of "sectioning" the material has been followed. It is customary to begin filming at the upper left hand corner of a large sheet and to continue from left to right in equal sections with small overlaps. If necessary, sectioning is continued again—beginning below the first row and continuing on until complete.
4. For illustrations that cannot be satisfactorily reproduced by xerographic means, photographic prints can be purchased at additional cost and inserted into your xerographic copy. These prints are available upon request from the Dissertations Customer Services Department.
5. Some pages in any document may have indistinct print. In all cases the best available copy has been filmed.

**University
Microfilms
International**

300 N. Zeeb Road
Ann Arbor, MI 48106

8514420

Lukat, Gudrun Susanne

THE PREPARATION AND CHARACTERIZATION OF CHALCOGENIDE
DERIVATIVES OF HEMERYTHRIN

Iowa State University

PH.D. 1985

University
Microfilms
International 300 N. Zeeb Road, Ann Arbor, MI 48106

PLEASE NOTE:

In all cases this material has been filmed in the best possible way from the available copy. Problems encountered with this document have been identified here with a check mark .

1. Glossy photographs or pages _____
2. Colored illustrations, paper or print _____
3. Photographs with dark background _____
4. Illustrations are poor copy _____
5. Pages with black marks, not original copy _____
6. Print shows through as there is text on both sides of page _____
7. Indistinct, broken or small print on several pages
8. Print exceeds margin requirements _____

9. Tightly bound copy with print lost in spine _____
10. Computer printout pages with indistinct print _____
11. Page(s) _____ lacking when material received, and not available from school or author.
12. Page(s) _____ seem to be missing in numbering only as text follows.
13. Two pages numbered _____. Text follows.
14. Curling and wrinkled pages _____
15. Dissertation contains pages with print at a slant, filmed as received _____
16. Other _____

University
Microfilms
International

The preparation and characterization of
chalcogenide derivatives of hemerythrin

by

Gudrun Susanne Lukat

A Dissertation Submitted to the
Graduate Faculty in Partial Fulfillment of the
Requirements for the Degree of
DOCTOR OF PHILOSOPHY

Department: Chemistry
Major: Inorganic Chemistry

Approved:

Signature was redacted for privacy.

In Charge of Major Work

Signature was redacted for privacy.

~~For the Major Department~~

Signature was redacted for privacy.

For the Graduate College

Iowa State University
Ames, Iowa

1985

TABLE OF CONTENTS

	Page
ABBREVIATIONS	xiv
I. INTRODUCTION	1
A. Molecular Properties of Hemerythrin	2
B. Structure and Properties of the Iron Site	8
C. Previous Work on Sulfide Derivatives of Hemerythrin	25
D. Statement of the Problem	31
E. Spectroscopic Techniques	35
II. EXPERIMENTAL PROCEDURES	50
A. Isolation of OxyHr	50
B. Preparation of MetHr and DeoxyHr	51
C. Instrumentation	53
D. Preparation and Characterization of μ -Sulfidosemi-metHr	56
E. Preparation and Characterization of μ -Selenidosemi-metHr	62
F. Preparation and Characterization of μ -SulfidometHr	63
G. Attempts at Preparation of μ -SelenidometHr	70
H. Preparation and Detection of a Sulfide Complex of DeoxyHr (deoxys ²⁻)	71
I. Reactivity of the SulfideHrs	75
III. RESULTS AND DISCUSSION	86
A. Preparation and Characterization of μ -Sulfidosemi-metHr	86
B. Preparation and Characterization of μ -Selenidosemi-metHr	116

C.	Preparation and Characterization of μ -SulfidometHr	120
D.	Attempts at Preparation of μ -SelenidometHr	133
E.	Preparation and Detection of a Sulfide Complex of DeoxyHr	135
F.	Reactivity of the SulfidehHrs	136
IV.	CONCLUSIONS	187
A.	Formation and Structure of the Chalcogenide Derivatives of Hemerythrin	187
B.	Comparison of Reactivity of the μ -Sulfide-hemerythrins and μ -oxo Containing Hemerythrins	190
C.	Comparisons of the Iron Site in the μ -S ²⁻ hemerythrins with Those of Other Fe-S Centers	191
D.	Comparison of the Reactivity of the μ -S ²⁻ hemerythrins with Sulfide Metabolism	195
V.	LITERATURE CITED	199
VI.	ACKNOWLEDGEMENTS	208
VII.	APPENDIX A: EPR MICROWAVE POWER SATURATION CURVES FOR HEMERYTHRIN DERIVATIVES AND THREE COPPER STANDARDS	209
VIII.	APPENDIX B: IODOMETRIC TITRATION FOR THE DETERMINATION OF SULFIDE CONCENTRATIONS	217
IX.	APPENDIX C: CALCULATION OF Fe-S-Fe BRIDGING ANGLE IN μ -SULFIDOMETHEMERYTHRIN FROM VIBRATIONAL FREQUENCIES	220
A.	Calculation of Fe-S-Fe Angle from Resonance Raman Data	220
B.	Fe-S-Fe Angle Calculations Based on Retention of Fe-Fe Distance upon Replacement of S for O	222

LIST OF FIGURES

		Page
Figure I-1.	Primary structure of hemerythrin from erythrocytes of <u>Phascolopsis gouldii</u>	4
Figure I-2.	Tertiary structure of myohemerythrin	5
Figure I-3.	Quaternary structure of hemerythrin from <u>Phascolopsis gouldii</u>	7
Figure I-4.	Summary of oxidation states available to the binuclear iron site in hemerythrin	9
Figure I-5.	Active site structures of hemerythrin at 2.0 Å resolution	11
Figure I-6.	UV-visible absorption spectra for derivatives of hemerythrin	14
Figure I-7.	UV-visible spectrum of 3.5×10^{-4} M semi-metN ₃ ⁻ in 50 mM Tris/acetate pH 8.0	24
Figure I-8.	The removal of the degeneracy of the electron spin states for a spin 1/2 system by an applied magnetic field H	36
Figure I-9.	Zero-field and magnetic field splitting for high spin Fe(III) and Fe(II) ions	38

Figure I-10.	Ladder of magnetic states produced as a result of antiferromagnetic coupling of two high-spin ferric ions (A) and one high-spin ferric ion with a high-spin ferrous ion (B)	40
Figure I-11.	Isomer shift and quadrupole splitting of ^{57}Fe in a non-cubic electronic environment	44
Figure I-12.	Magnetic and quadrupole splitting in a ferromagnetic ^{57}Fe compound	45
Figure I-13.	Differences between non-resonance and resonance Raman effects	48
Figure II-1.	A standard working curve for sulfide determination based on the formation of methylene blue	68
Figure II-2.	Absorption spectra observed during the anaerobic incubation of 0.12 mM oxyHr with 1.23 mM sulfide in 50 mM Tris/acetate pH 8.0 at room temperature	73
Figure III-1.	Resonance Raman spectrum of 2 mM $\mu\text{-S}^{2-}$ semi-metHr in 50 mM Tris/perchlorate pH 8.0	87
Figure III-2.	Mössbauer spectra of crystalline $\mu\text{-S}^{2-}$ semi-metHr	89
Figure III-3.	Derivative EPR spectrum of $\mu\text{-S}^{2-}$ semi-metHr	93

Figure III-4.	Absorbance at 530 nm versus the ratio of total stoichiometric sulfide concentration, $[(\text{H}_2\text{S}) + (\text{HS}^-) + (\text{S}^{2-})]$, to Hr concentration	95
Figure III-5.	UV-visible spectra for titration of metHr with sulfide	96
Figure III-6.	Plot of percent Hr in the $\mu\text{-S}^{2-}$ -semi-metHr form versus reaction time of metHr plus sulfide	99
Figure III-7.	EPR spectra of (semi-met) _R titrated with sulfide	105
Figure III-8.	UV-visible titration of (semi-met) _R with sulfide	106
Figure III-9.	Titration of (semi-met) _O with sulfide as monitored by EPR spectroscopy	107
Figure III-10.	EPR spectra of the reaction of metHr with sulfide liberated from MoS_4^{2-} during its aquation	112
Figure III-11.	EPR spectra of metHr reacted with polysulfide	114
Figure III-12.	Derivative EPR spectra resulting from the addition of Na_2Se to 1.48 mM metHr in 50 mM Bis/tris/sulfate, pH 6.1	118
Figure III-13.	Absorption spectrum of μ -selenidosemi-metHr	119

Figure III-14.	Absorption spectra of μ -S ²⁻ -metHr and μ -S ²⁻ -semi-metHr in anaerobic 50 mM Tris/acetate pH 8.0	124
Figure III-15.	Mössbauer spectrum of a frozen solution of 6.25 mM μ -S ²⁻ -metHr on 50 mM Tris/perchlorate pH 8.0. The spectrum was taken in a 1.7 kG perpendicular applied field at 100 K	126
Figure III-16.	Resonance Raman spectrum of 2 mM μ -S ²⁻ -metHr in 50 mM Tris/perchlorate pH 8.0	130
Figure III-17.	EPR spectra observed for the titration of deoxyN ₃ ⁻ by sulfide	137
Figure III-18.	Plots of E_{soln} versus $\log \frac{[\mu\text{-S}^{2-}\text{-metHr}]}{[\mu\text{-S}^{2-}\text{-semi-metHr}]}$	140
Figure III-19.	EPR simulations of various ratios of (semi-met) _O and (semi-met) _R	147
Figure III-20.	UV-visible and EPR spectra for μ -S ²⁻ -metHr equilibration with Fe ²⁺ cyt c at room temperature for 50 minutes in 50 mM Tris/perchlorate pH 8.0	150
Figure III-21.	EPR spectra following the extended anaerobic dialysis of μ -S ²⁻ -semi-metHr: 2.1 mM protein in 50 mM Tris/acetate pH 8.0 at 4 °C	153

- Figure III-22. Absorption spectra obtained during aerobic incubation of 0.16 mM μ -S²⁻semi-metHr in 50 mM Tris/acetate pH 8.0 at room temperature 157
- Figure III-23. EPR spectra observed during incubation of 1.94 mM μ -S²⁻semi-met in 50 mM Tris/acetate pH 8.0 at room temperature 158
- Figure III-24. EPR spectra observed during aerobic incubation of 1.94 mM μ -S²⁻semi-met in 50 mM Tris/perchlorate pH 8.0 at room temperature 159
- Figure III-25. EPR spectra obtained during anaerobic incubation of (semi-met)_O for the indicated times in 50 mM Tris/acetate pH 8.0 161
- Figure III-26. Conversion of (semi-met)_O towards (semi-met)_R in 50 mM Tris/perchlorate pH 8.0 at room temperature as monitored by EPR 162
- Figure III-27. Absorption spectra obtained during aerobic incubation of 0.125 mM μ -S²⁻semi-metHr in 50 mM Tris/acetate pH 8.0 at room temperature in the presence of 6.5 mM NaN₃ 166
- Figure III-28. Aerobic reaction of μ -S²⁻semi-metHr with excess azide in 50 mM Tris/perchlorate at room temperature 167

- Figure III-29. EPR spectra observed at the indicated 173
times during anaerobic incubation at room
temperature of 1.78 mM μ -S²⁻-metHr in
50 mM Tris/perchlorate pH 8.0
- Figure III-30. EPR spectra observed during anaerobic 175
incubation at room temperature of 1.48 mM
 μ -S²⁻-metHr in 50 M Tris/acetate pH 8.0
in the presence of 0.84 M NaN₃
- Figure III-31. Absorption spectra observed during aerobic 180
incubation of 53.9 μ M μ -S²⁻-metHr in 50 mM
Tris/perchlorate pH 8.0 at room temperature
- Figure III-32. EPR spectra observed during aerobic 183
incubation at room temperature of 1.41 mM
 μ -S²⁻-metHr in 50 mM Tris/acetate pH 8.0
in the presence of 0.76 M NaN₃
- Figure III-33. Absorption spectra observed during aerobic 184
incubation at room temperature of 0.35 mM
 μ -S²⁻-metHr in 50 mM Tris/perchlorate pH 8.0
containing 0.16 M NaN₃
- Figure IV-1. Iron site of the μ -S²⁻-Hrs 188
- Figure A-1. Plot of $\log [S/\sqrt{P_0}]$ versus $\log P_0$ for 210
1.50 mM μ -S²⁻-semi-metHr in 50 mM Tris/
acetate pH 8.0
- Figure A-2. Plot of $\log [S/\sqrt{P_0}]$ versus $\log P_0$ for 211
0.8 mM (semi-met)_R in 50 mM Tris/acetate
pH 8.0

- Figure A-3. Plot of $[S/\sqrt{P_0}]$ versus $\log P_0$ for 1.45 mM (semi-met) $_0$ in 50 mM Tris/acetate pH 8.0 212
- Figure A-4. Plot of $\log [S/\sqrt{P_0}]$ versus $\log P_0$ for 3.4 mM semi-met N_3^- in 50 mM Bis/tris/sulfate pH 6.0 213
- Figure A-5. Plot of $[S/\sqrt{P_0}]$ versus $\log P_0$ for 1.02 mM deoxy N_3^- in 50 mM Tris/acetate pH 8.0 214
- Figure A-6. Plots of $[S/\sqrt{P_0}]$ versus $\log P_0$ for 0.8 mM CuEDTA (A), 0.52 mM $CuCl_2 \cdot 6H_2O$ (B) and 1.00 mM $CuSO_4 \cdot 5H_2O$ (C) 215
- Figure A-7. Plot of $[S/\sqrt{P_0}]$ versus $\log P_0$ for $g = 2.02$ signal observed for the reaction of $\mu\text{-S}^{2-}$ -semi-metHr with O_2 in 50 mM Tris/acetate pH 8.0 216

LIST OF TABLES

		Page
Table I-1.	Structural Properties of the Active Site of Four Forms of Hemerythrin	10
Table I-2A.	Absorption Spectra of Hemerythrin Complexes	15
Table I-2B.	Absorption Spectra of Model Complexes	16
Table I-3.	Mössbauer and Magnetic Data for Hemerythrin and Model Complexes	17
Table I-4A.	Vibrational Spectral Data for μ -oxo Bridges in Hemerythrin Derivatives	19
Table I-4B.	Vibrational Spectral Data for μ -oxo Bridges in Model Complexes	20
Table I-5.	g-Values for Various Semi-methemerythrin Derivatives	22
Table I-6.	Reduction Potentials of Hemerythrin Derivatives at 25 °C, $I=0.15$ M and pH 8.2 versus NHE	26
Table I-7A.	Fundamental Fe-S Stretching Modes of Some Iron-sulfur Proteins	28
Table I-7B.	Observed Fe-S (and Fe-Cl) and S-S Frequencies	29

LIST OF TABLES

		Page
Table I-1.	Structural Properties of the Active Site of Four Forms of Hemerythrin	10
Table I-2A.	Absorption Spectra of Hemerythrin Complexes	15
Table I-2B.	Absorption Spectra of Model Complexes	16
Table I-3.	Mössbauer and Magnetic Data for Hemerythrin and Model Complexes	17
Table I-4A.	Vibrational Spectral Data for μ -oxo Bridges in Hemerythrin Derivatives	19
Table I-4B.	Vibrational Spectral Data for μ -oxo Bridges in Model Complexes	20
Table I-5.	g-Values for Various Semi-methemerythrin Derivatives	22
Table I-6.	Reduction Potentials of Hemerythrin Derivatives at 25 °C, I=0.15 <u>M</u> and pH 8.2 versus NHE	26
Table I-7A.	Fundamental Fe-S Stretching Modes of Some Iron-sulfur Proteins	28
Table I-7B.	Observed Fe-S (and Fe-Cl) and S-S Frequencies	29

Table I-8.	Reduction Potentials of Various Half-reactions	33
Table III-1.	Mössbauer parameters for crystalline $\mu\text{-S}^{2-}$ semi-metHr. Quadrupole splittings, ΔE_{q} , and isomer shifts, δ_{Fe} , of the three components A, B and D at 60 K, 100 K and 200 K	90
Table III-2.	$(\text{Semi-met})_{\text{R}}$ reaction with sulfide	103
Table III-3.	Titration of $(\text{semi-met})_{\text{O}}$ with sulfide	108
Table III-4.	Data for reaction of metHr with sulfide liberated by thiomolybdate hydrolysis	111
Table III-5.	Data for parallel sulfide and iron analyses of $\mu\text{-S}^{2-}$ -metHr	122
Table III-6.	Data for parallel sulfide plus sulfane and iron analysis of $\mu\text{-S}^{2-}$ -metHr. Determination of the $(\text{S}^{2-} + \text{S}^0)/2\text{Fe}$ ratio	123
Table III-7.	Resonance Raman vibrational frequencies and assignments for $\mu\text{-S}^{2-}$ -metHr and $\mu\text{-S}^{2-}$ -semi-metHr	128
Table III-8.	Midpoint reduction potentials (E_{m}) for the $\mu\text{-S}^{2-}$ -metHr/ $\mu\text{-S}^{2-}$ -semi-metHr couple at 25 °C, $I = 0.15 \text{ mM}$ and pH 8.0	141

Table III-9. Concentrations of μ -S²⁻semi-metHr present 178
in reaction mixtures of μ -S²⁻metHr plus one
equivalent of dithionite. Reactions carried
out at 25 °C in 50 mM Tris/acetate pH 8.0

ABBREVIATIONS

Hr	hemerythrin
metN ₃ ⁻	metazidohemerythrin
(semi-met) _O , (SM) _O	semi-methemerythrin in the O conformation
(semi-met) _R , (SM) _R	semi-methemerythrin in the R conformation
μ-S ²⁻ semi-metHr	μ-sulfidosemi-methemerythrin
μ-S ²⁻ metHr	μ-sulfidomethemerythrin

Tris	Tris(hydroxymethyl)aminomethane
Bis/tris	Bis(2-hydroxyethyl)imino-tris(hydroxymethyl)methane

Cys	cysteine	His	histidine
Asp	aspartic acid	Glu	glutamic acid

EPR	electron paramagnetic resonance
EXAFS	extended X-ray absorption fine structure
LMCT	ligand to metal charge transfer
NHE	normal hydrogen electrode

cyt c	cytochrome c
DCIP	2,6-dichlorophenolindophenol
DMPD	N,N-dimethyl-p-phenylenediamine
DPPH	diphenylpicrylhydrazide
DSS	2,2-dimethyl-2-silapentane-5-sulfonate
DTT	dithiothreitol
EDTA	ethylenediamine tetraacetate

HBpz ₃	tri-l-pyrazolyborate
phen	o-phenanthroline
S ₂ -o-xyl	o-xyl-α,α'-dithiolate

I. INTRODUCTION

Hemerythrin (Hr) is a non-heme iron respiratory protein found in several phyla of marine invertebrates. It exists in all sipunculids examined to date, two brachiopods, two priapulids and one annelid. Sipunculids are marine worms 3 to 15 centimeters in length. Most of their estimated life span of 25 years is spent burrowed in the substratum. They are distributed widely throughout the oceans of the world, being found from the tropics to the poles, in intertidal shores and in depths of up to 7000 meters. There are several species found off of the east and west coasts of the United States (1).

All the work reported here deals with the North American Atlantic coast sipunculid Phascolopsis (syn. Golfingia) gouldii. Hemerythrin occurs in the erythrocytes of the coelomic cavity of these animals. Oxygen is absorbed through the body wall into the coelomic cavity where the physiologically significant reaction of hemerythrin, reversible combination with molecular oxygen, takes place. The function of coelomic hemerythrin is predominantly one of oxygen storage (2). This function is revealed by several physiological properties of hemerythrin that differ significantly from the properties of its mammalian counterpart hemoglobin, whose primary function is oxygen transport.

Hemerythrin has a much stronger affinity for oxygen (oxygen pressure at half-saturation, $P_{50} \sim 3-5$ mm) (3,4) than hemoglobin ($P_{50} \sim 20-40$ mm) (5). Unlike the oxygen binding curve for hemoglobin, the plot of O_2 partial pressure versus the fractional saturation for P. gouldii hemerythrin shows no sigmoidal character indicating no cooperativity in oxygen binding (6). This hemerythrin also lacks a Bohr effect, i.e., oxygenation is independent of pH (7). These characteristics of hemerythrin are consistent with its function as an oxygen storage protein. In this case, it is not necessary for the protein to respond to small differences in oxygen tension as it would if it were part of a vascular network for oxygen transport, like hemoglobin. It is in oxygen transport that the sigmoidal shape and pH dependence of oxygen equilibrium curves are functionally important characteristics (8).

A. Molecular Properties of Hemerythrin

Coelomic hemerythrin from P. gouldii occurs as an octamer of $M_r = 108,000$ and consists of identical subunits (9, 10). Minor genetic variants are present but seem to have little or no effect on the chemical and physical properties of the octameric protein (11). Although the octameric form of the protein is the most commonly encountered quaternary structure, there are species in which hemerythrin exists as a dimer,

trimer, tetramer or monomer (1). Myohemerythrin (myo = monomer) was first reported by Manwell, who detected its presence in the retractor muscle of Themiste zostericola (12). Myohemerythrin has a molecular weight of 13,900 which corresponds closely to the molecular weight of a subunit of the octameric protein (13,500) (10).

The complete amino acid sequence for the P. gouldii hemerythrin subunit has been established and is illustrated in Figure I-1 (13, 14, 15). It is noteworthy that of 113 amino acid residues, there is only a single cysteine (position 50). Extensive chemical modification studies of P. gouldii hemerythrin show that the reaction of Cys-50 with sulfhydryl reagents such as p-hydroxymercuribenzoate, N-ethylmaleimide or silylorganic acid results in dissociation of the octamer into monomers (16). Dissociation can also be caused by dilution of the octameric protein. When dilution is performed below pH 7.5, no intermediates (dimers, trimers, etc.) are formed; only octamers and monomers are present (17, 18). At pHs above 7.5, several intermediates are detected (19, 20). Interestingly, monomeric hemerythrins do not have an SH group at residue 50 (21, 22).

Crystallographic work supports the evidence from circular dichroism (9, 23) showing that helices comprise 70 to 75 percent of the secondary structure. Helices are incorporated into the tertiary structure of the protein as illustrated in

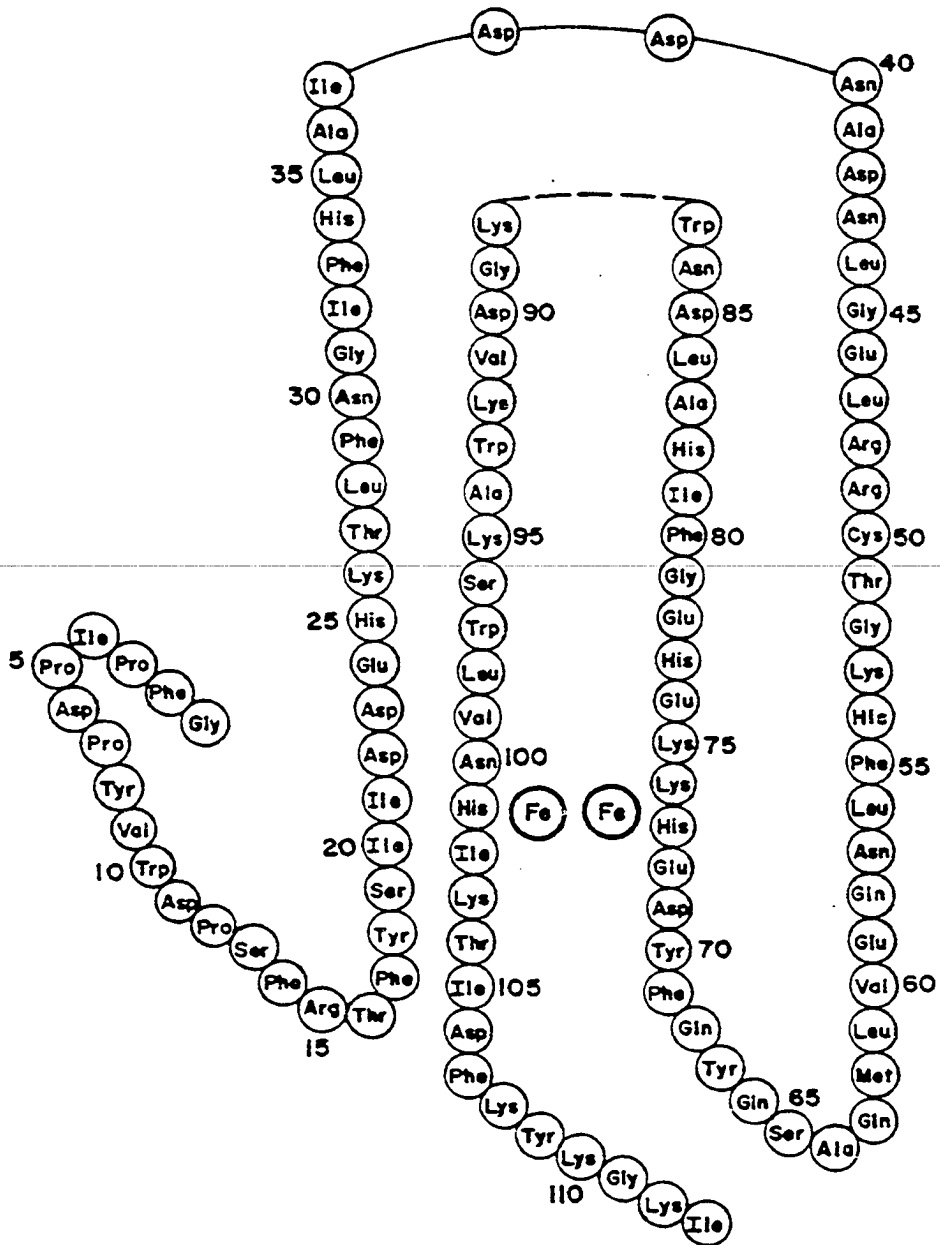


Figure I-1. Primary structure of hemerythrin from erythrocytes of *Phascolopsis gouldii*

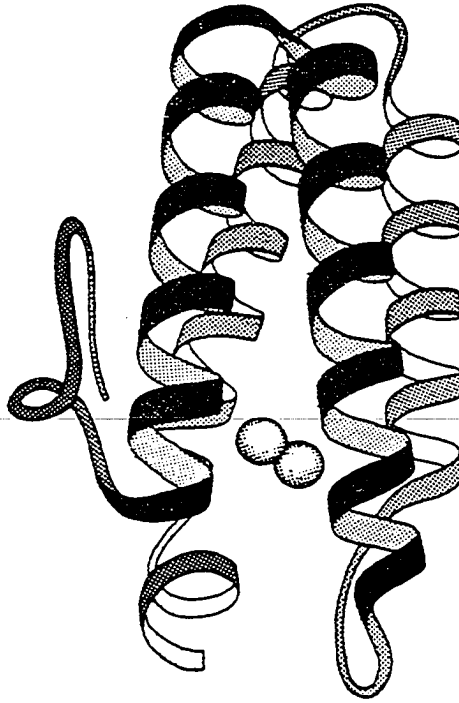


Figure I-2. Tertiary structure of myohemerythrin

Figure I-2 (24). Independent crystallographic examinations of the tertiary structure of P. gouldii and Themiste dyscritum octameric hemerythrins reveal that they have essentially identical structures. These low resolution X-ray diffraction studies indicate that the monomer is folded into four quasi-parallel helices, 30 to 40 Å in length (25, 26). This four parallel helical structure motif is also found in cytochrome b_{562} , cytochrome c', ferritin subunits and tobacco mosaic virus subunits (27). In hemerythrin, the helices are connected by short non-helical turns and by amino acid ligation to the two irons in the active site. N-terminal residues make up a non-helical section which runs forth and back along one side of the molecule. In contrast, the carboxyl terminal end is a short helical stub (25).

The quaternary structure of hemerythrin is depicted in Figure I-3. The subunit arrangement in P. gouldii results in the molecules resembling square donuts having approximate external dimensions of 75 x 75 x 50 Å. The donut has D_4 symmetry and is composed of two layers, each a square of subunits related by the four fold axis (R) in an end-side arrangement. The four fold axis passes through the center of a square channel having sides 20 Å long. This channel widens to a chamber 30 Å in diameter and 15 Å high in the center of the molecule (28).

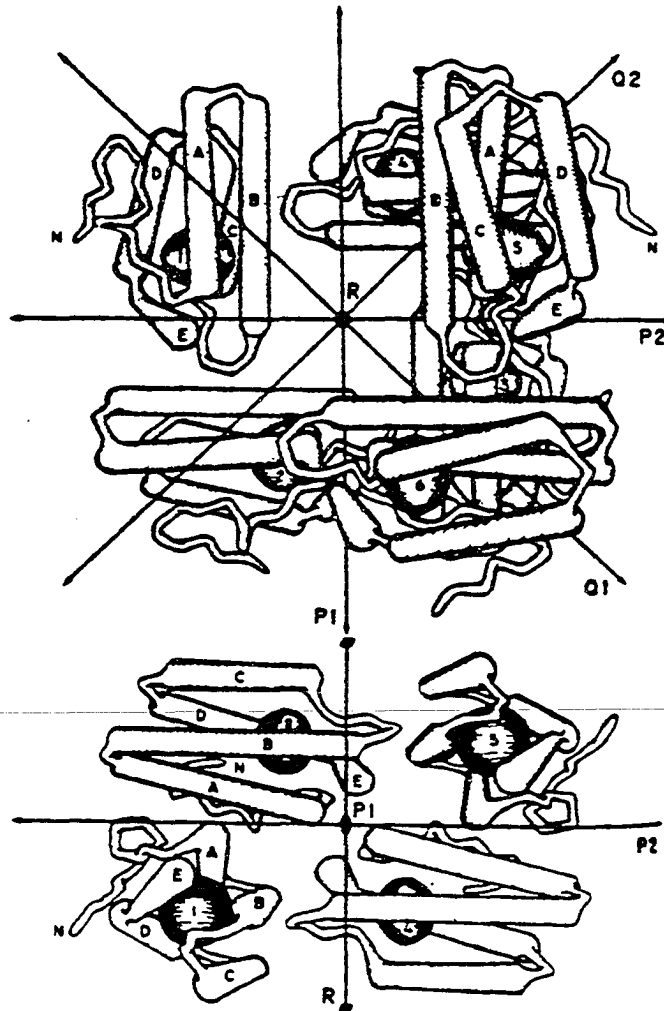


Figure I-3. Quaternary structure of hemerythrin from Phascolopsis gouldii

Subunits are drawn as schematic representations of the polypeptide chain. The helical segments are labelled A through E in accordance with the notation for myohemerythrin from Themiste dyscritum, and the amino-terminal arm is designated by N. The oblate spheroids represent the iron centers and are marked with subunit numbers

B. Structure and Properties of the Iron Site

Each of the subunits of octameric hemerythrin contains a binuclear iron site which reversibly binds one molecule of oxygen. Transformations between various oxidation levels of the iron site are diagrammed in Figure I-4. Extensive chemical and spectroscopic investigations have established that upon oxygenation the two high spin Fe(II) ions in deoxyHr are oxidized to high spin Fe(III) in oxyHr, and the bound dioxygen is reduced to the peroxide oxidation state (1, 29, 30). Addition of two or more oxidizing equivalents to either deoxyHr or oxyHr results in a form of the protein known as metHr. Autooxidation of oxyHr to metHr occurs over a period of several days and may occur by loss of peroxide (31). MetHr contains two high spin Fe(III) ions and forms complexes with a number of small anions such as N_3^- , SCN^- , CN^- , and Cl^- . MetHr does not bind oxygen. However, it can be converted back to the oxygen binding form with reducing agents (32).

Important structural features of the iron site as deduced from X-ray crystallography and EXAFS studies are summarized in Table I-1 (33, 34, 35, 36). Figure I-5A illustrates the structure of the binuclear center of metaquoHr at 2.0 Å resolution. The two iron atoms, separated by approximately 3.27 Å, are bridged by the spectroscopically predicted oxo ion and the carboxylate side chains of Glu-58 and Asp-106. One

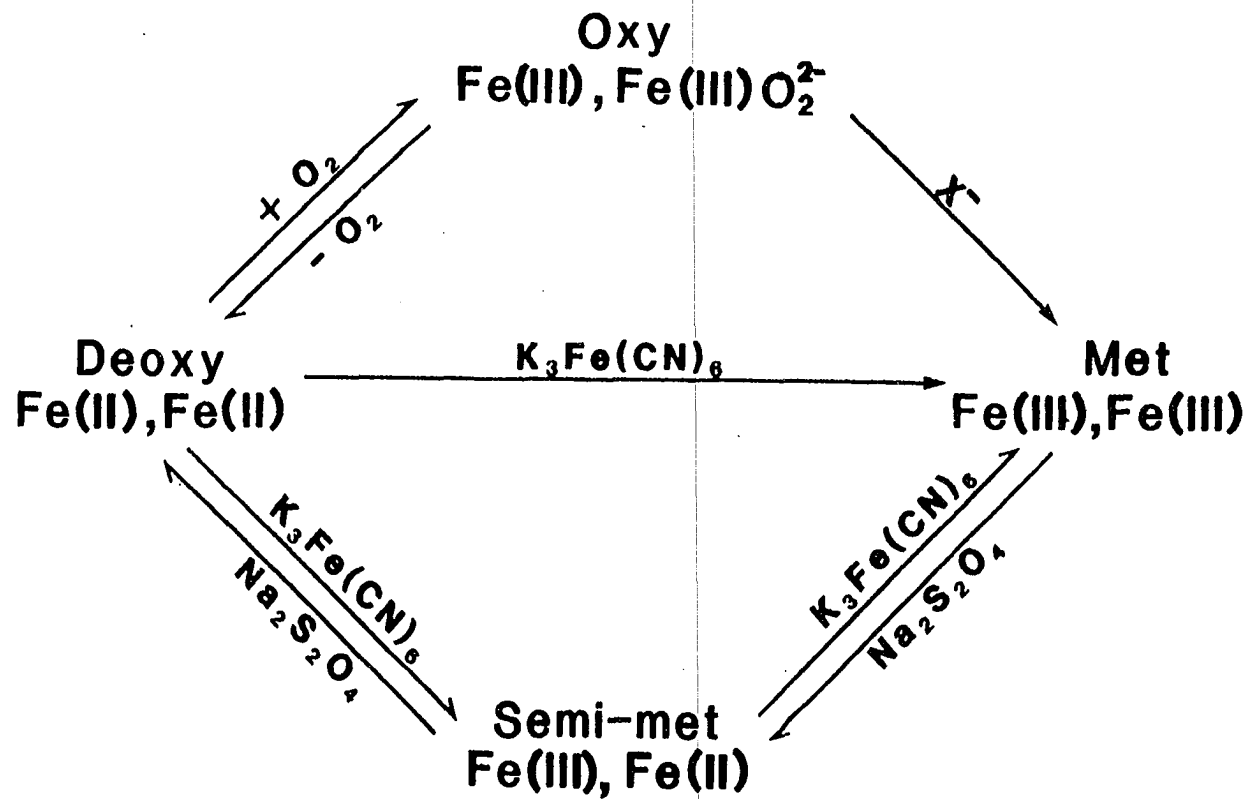


Figure I-4. Summary of oxidation states available to the binuclear iron site in hemerythrin

Table I-1. Structural Properties of the Active Site of Four Forms of Hemerythrin^a

Hemerythrin Derivative	OxyHr	Methr (high pH)	MetN ₃ ⁻	DeoxyHr
Fe···Fe dist., Å				
EXAFS ^b	3.57	3.54	3.38 ^c , 3.49	3.13 ^d
X-RAY ^e	n.d.	3.20	3.27	n.d.
Fe-O-Fe angle, deg.				
EXAFS ^b	155(+25/-13)	153(+27/-13)	152(+28/-13)	n.d.
X-RAY ^e	n.d.	127	135	n.d.
Fe-O μ-oxo dist., Å				
EXAFS ^b	1.83	1.82	1.80	n.d.
X-RAY ^e	n.d.	1.68, 1.92	1.64, 1.89	n.d.
Fe-L dist., Å				
Average of (O, N)				
EXAFS ^b	2.16	2.15	2.15	2.14 ^d
X-RAY ^e				
Fe-O _{carboxy}	n.d.	mean 2.11 (2.03-2.28)	mean 2.23 (2.16-2.33)	n.d.
Fe-N	n.d.	mean 2.21 (2.15-2.31)	mean 2.23 (2.13-2.29)	n.d.

^aValues not determined are designated n.d.

^bReference 33.

^cReference 34.

^dReference 35.

^eReference 36.

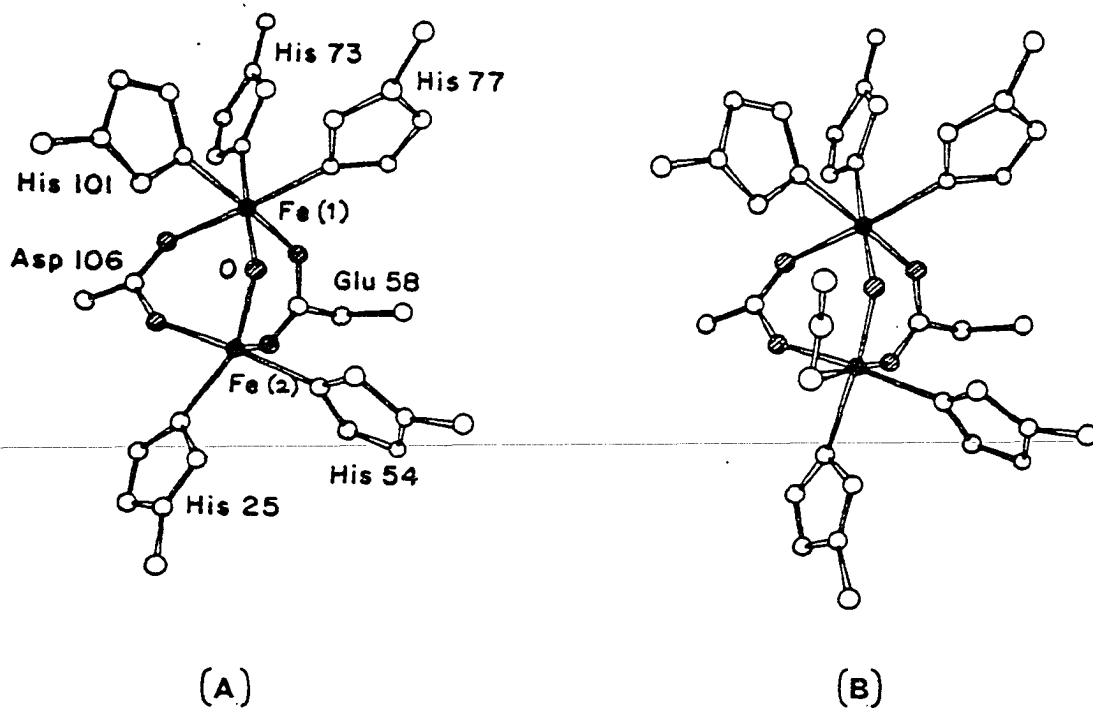


Figure I-5. Active site structures of hemerythrin at 2.0 Å resolution

- A) Metaquoemerythrin
- B) Metazidoemerythrin

iron atom is hexacoordinate with the side chains of His-73, His-77 and His-101 completing its coordination sphere. Side chains of His-25 and His-54 are coordinated to the second iron. Since no exogenous ligand is bound to the pentacoordinate iron, its coordination polyhedron is best described as trigonal bipyramidal (37).

Addition of azide converts aquometHr to metazidoHr in which both iron atoms are octahedrally coordinated. The structure of metazidoHr at 2.0 Å resolution is depicted in Figure I-5B (36). In addition to X-ray crystallography, resonance Raman spectroscopy (38, 39) and EXAFS (33, 34) have been used to investigate the mode of azide binding which was found to be end-on rather than bridging. Spectroscopic data indicate that dioxygen binding in oxyHr is analogous to azide binding in metazidoHr (33, 39). A 2.2 Å resolution crystallographic study of oxyHr is consistent with this mode of binding. The dioxygen binds to the iron that is pentacoordinate in metaquoHr, the same binding site found for azide in the metazidoHr form (40). Presently the structure of deoxyHr is not as well defined; it is not clear from X-ray crystallographic and EXAFS studies whether the μ -oxo bridge is retained in deoxyHr (35).

There are several anions such as ClO_4^- and NO_3^- which bind to hemerythrin, but not directly at the iron site. If the crystallographic data for T. dyscritum are applicable to P.

gouldii, then the perchlorate binding site is in the inner cavity of the octamer near Cys-50. Perchlorate binding causes structural changes in regions near the active site which affect the stability and reactivity of metHr coordination complexes (41).

The UV-visible absorption spectra of oxyHr, deoxyHr, metHr and metazidoHr are shown in Figure I-6. Table I-2 lists the characteristics of the absorption spectra of a number of hemerythrin derivatives and model compounds (32, 42). The electronic spectra of the met anion complexes are pH independent (32). A pH dependence is observed for the spectrum of metHr; its acid-base transformation has a pK_a of 7.8. Perchlorate binding raises the pK_a to 8.7 (43). Originally the low and high-pH forms of metHr were designated "metaquo" and "methydroxo" hemerythrin, respectively (32). However, the crystal structure of "metaquo" Hr shows no water molecule coordinated to the iron (37) suggesting that the nature of the acid-base change is simply binding of hydroxide to the originally five coordinate iron at high pH.

The first suggestion of the presence of a μ -oxo bridge between the irons in metHr and oxyHr came from the correlation of absorption spectra with Mössbauer and magnetic data (23). Mössbauer (42, 44, 45) and magnetic data (46, 47) are summarized in Table I-3. Magnetic susceptibility measurements on the oxy and met forms indicate strong antiferromagnetic

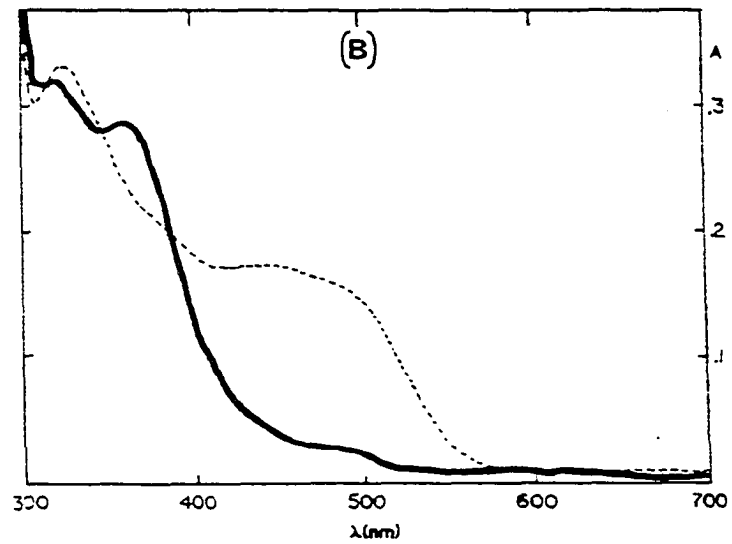
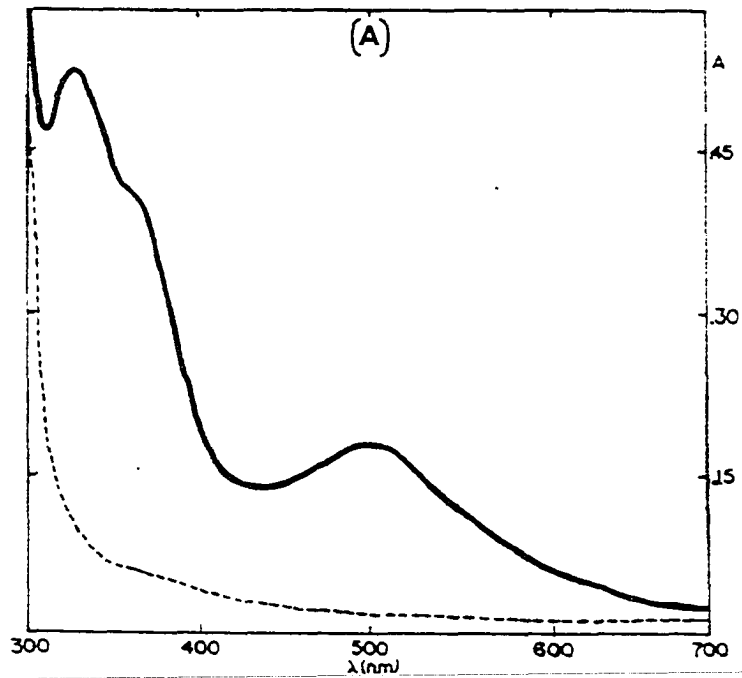


Figure I-6. UV-visible absorption spectra for derivatives of hemerythrin

A) OxyHr and DeoxyHr ($7.7 \times 10^{-5} \text{ M}$). B) MetHr and MetN₃⁻ ($4.9 \times 10^{-5} \text{ M}$)

Table I-2A. Absorption Spectra of Hemerythrin Complexes^a

Hemerythrin Derivatives	LMCT ^b (O ²⁻ →Fe)		Exogeneous		LMCT ^b		⁶ A ₁ → ⁴ T ₂ (⁴ G)		⁶ A ₁ → ⁴ T ₁ ^c	
	λ(nm)	ε _M	λ(nm)	ε _M	λ(nm)	ε _M	λ(nm)	ε _M	λ(nm)	ε _M
OxyHr	330 360	6800 5450	500	2200	750	200	990	10		
MetHr "hydroxy" high pH form	320 362	6800 5900	480sh	550	597	200	990	8		
MetHr "aquo" low pH form	355	6400	480sh	600	580sh	200	n.d.			
MetN ₃ ⁻	326 380	6750 4300	446	3700	680	190	1010	10.2		15
MetSCN ⁻	327	7200	452	5100	674	200	n.d.			
MetCN ⁻	330	6400	493	770	695	140	n.d.			
MetCl ⁻	329 380	6600 6000	490sh	750	656	180	n.d.			

^aReference 32.

^bLMCT, ligand to metal charge transfer transition.

^cTransitions not determined are designated n.d.

Table I-2B. Absorption Spectra of Model Complexes^a

Model Complexes	LMCT ^b (O ²⁻ →Fe)		Unassigned		⁶ A ₁ → ⁴ T ₂ (⁴ G)		⁶ A ₁ → ⁴ T ₁ ^c	
	λ(nm)	ε _M	λ(nm)	ε _M	λ(nm)	ε _M	λ(nm)	ε _M
[Fe ₂ O(O ₂ CCH ₃) ₂] ²⁻ (HBpz ₃) ₂ ^b	262	6750	457 ^d	1010	695	140	995	7
	339	9270	492 ^d	920				
	358 ^{sh}							
[Fe ₂ O(O ₂ CH) ₂] ²⁻ (HBpz ₃) ₂ ^b	342 ^d	10200	460 ^d	1080	692	140	n.o.	
	489 ^d	980						
[Fe ₂ O(O ₂ CPh) ₂] ²⁻ (HBpz ₃) ₂ ^b	336 ^d	9000	455 ^d	960	691	130	n.o.	
	490 ^d	860						

^aReference 42.^bHBpz₃, tri-l-pyrazolylborate.^cTransitions not observed are designated n.o.^dUnassigned transitions.

Table I-3. Mössbauer and Magnetic Data for Hemerythrin and Model Complexes

Hemerythrin ^a Derivatives	δ (mm/s) ^b	ΔE_q (mm/s) ^c	Temp. (K)	J (cm ⁻¹) ^d
OxyHr ^c	0.52	1.92	77	-77
	0.48	1.00	77	
	0.54	1.92	4.2	
	0.51	1.09	4.2	
MetHr pH 7.0	0.46	1.57	77	-134
MetN ₃ ⁻	0.50	1.91	77	
MetSCN ⁻	0.55	1.92	77	
MetCl ⁻	0.50	2.04	77	
DeoxyHr	1.15	2.86	77	small
	1.17	2.89	4.2	

Model ^{e,f} Complexes				

[Fe ₂ O(O ₂ CCH ₃) ₂] ⁻ (HBpz ₃) ₂] ^g	0.52	1.60	4.2	-121
[Fe ₂ (OH)(O ₂ CCH ₃) ₂] ⁻ (HBpz ₃) ₂] ^{+h}	n.d.	n.d.	----	-17

^a Reference 44 and 45.

^b δ , isomer shift.

^c ΔE_q , quadrupole splitting.

^d Reference 46.

^e HBpz₃, tri-l-pyrazolylborate.

^f Mössbauer parameters not determined are designated by n.d.

^g Reference 42.

^h Reference 47.

coupling between the irons ($J \sim -100 \text{ cm}^{-1}$) leading to a diamagnetic ground state (46). At an iron-iron distance in the range of 3.2-3.6 Å for oxy- and metHrs (Table I-1) (33, 34, 36), the antiferromagnetic coupling must occur predominantly through the bridging ligands. Comparison to synthetic molecules indicates that the strength of the coupling can be entirely accounted for by the presence of the μ -oxo bridge (42, 48). The presence of the μ -oxo bridge in oxy and metHrs has also been independently verified by resonance Raman studies of oxygen isotope exchange (49, 50, 51). The vibrational frequencies for the stretching and deformation modes of the Fe-O-Fe cluster in various hemerythrin derivatives and model compounds are presented in Table I-4.

In the analyses of the kinetics of reduction of metHr to deoxyHr by dithionite, Harrington, de Waal and Wilkins suggested that this reduction passes through a previously unknown oxidation level containing an Fe(II)Fe(III) pair at each iron site (52). The existence of this so-called semi-met oxidation level has been confirmed by EPR spectroscopy (53, 54). The importance of this observation is that an intermediate with this oxidation level could lie on the pathway for reversible oxygenation. Semi-metHr can be prepared either by one-electron reduction of metHr to give (semi-met)_R or by one electron oxidation of deoxyHr to give

Table I-4A. Vibrational Spectral Data for μ -oxo Bridges
in Hemerythrin Derivatives^{a,b}

Hemerythrin Derivative	ν_s Fe-O-Fe symmetric stretch, cm^{-1}	ν_{as} Fe-O-Fe asymmetric stretch, cm^{-1}	δ Fe-O-Fe deformation, cm^{-1}	Reference
OxyHr	486(475)	~753(720)	n.o.	49
MetHr (low pH form)	510(496)	~750(720)	n.o.	49
MetHr (high pH form)	508(n.d.)	780(~750)	n.o.	49
MetN ₃ ⁻	507(493)	768(733)	292(286)	49
MetSCN ⁻	514(498)	780(742)	~290(~285)	49
MetCN ⁻	512(499)	780(n.d.)	n.o.	49,50
MetCl ⁻	509(n.d.)	n.d.(n.d.)	n.d.(n.d.)	46

^aNumber in parentheses is the ¹⁸O shifted value.

^bVibrations not observed are designated n.o.; vibrations not determined are designated n.d.

Table I-4B. Vibrational Spectral Data for μ -oxo Bridges
in Model Complexes^{a,b}

Model Complexes	ν_s Fe-O-Fe symmetric stretch, cm^{-1}	ν_{as} Fe-O-Fe asymmetric stretch, cm^{-1}	δ Fe-O-Fe deformation, cm^{-1}	Reference
$[\text{Fe}_2\text{O}(\text{O}_2\text{CCH}_3)_2]^{2-}$ $(\text{HBpz}_3)_2^c$	528(511)	751(721)	283(269)	42
$[\text{Fe}_2\text{OCl}_6]^{2-}$	458(440)	870(826)	203(198)	51

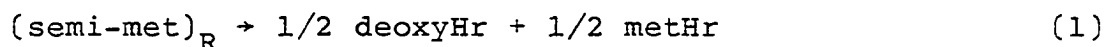
^aNumber in parentheses is the ¹⁸O shifted value.

^bVibrations not observed are designated n.o.; vibrations not determined are designated n.d.

^cHBpz₃, tri-l-pyrazolylborate.

(semi-met)_O (53). These two forms can be distinguished on the basis of their distinctive optical and EPR spectra (52). Semi-met anion complexes can be made by addition of anions like N₃⁻, SCN⁻, CN⁻ and Cl⁻ to either (semi-met)_R or (semi-met)_O. Spectrally the semi-met anion complexes formed from (semi-met)_R and (semi-met)_O appear identical (55). EPR spectra of the semi-metHrs are consistent with an S=1/2 ground state indicating retention of antiferromagnetic coupling (54, 56). Some characteristic g values for semi-metHrs are listed in Table I-5.

The amplitude of the (semi-met)_R spectrum decreases with time when the sample is incubated at room temperature because of the disproportionation reaction given in reaction 1. The extent of this disproportionation varies from



species to species; for P. gouldii Harrington and Wilkins report that ~ 20 percent of the protein disproportionates (55). This disproportionation is significantly depressed by addition of those anions which form complexes with semi-metHr (ligand anions) (54, 55). P. gouldii (semi-met)_O does not disproportionate directly; it first isomerizes to (semi-met)_R, which then disproportionates. When followed by EPR spectroscopy (1), the O → R conversion is complete in

Table I-5. g-Values for Various Semi-methemerythrin Derivatives

Species	Derivatives	g-Values	Reference
octameric <u>P. gouldii</u>	(semi-met) _O , pH 8.2	1.94, 1.71	1
octameric <u>P. gouldii</u>	(semi-met) _R , pH 8.2	1.95, 1.87, 1.65	1
		1.93, 1.86, 1.68	53
octameric <u>P. gouldii</u>	(semi-met) _R , pH 6.5	1.96, 1.86, 1.66	56
octameric <u>T. zostericola</u>	(semi-met) _O , pH 8.2	1.95, 1.72	54
octameric <u>T. zostericola</u>	(semi-met) _R , pH 8.2	1.96, 1.88, 1.66	54
octameric <u>T. zostericola</u>	semi-metN ₃ ⁻ , pH 8.2	1.94, 1.85, 1.57	54
octameric <u>T. zostericola</u>	semi-metN ₃ ⁻ , pH 8.2	1.90, 1.81, 1.49	54
octameric <u>P. gouldii</u>	semi-metN ₃ ⁻ , pH 8.2	1.90, 1.81, 1.49	54
octameric <u>P. gouldii</u>	semi-metNO ₂ ⁻ , pH 6.5	1.93, 1.87, 1.66	56

~ 26 minutes ($k = 1.30 \times 10^{-3} \text{ sec}^{-1}$, 25 °C, pH 8.0) for P. gouldii (57) and in ~ 7 minutes for myoHr from T. zostericola (58).

Presently the semi-metN₃⁻ complex is the most thoroughly studied semi-met derivative. Its UV-visible spectrum, shown in Figure I-7, has a maximum at 470 nm ($\epsilon = 2400 \text{ M}^{-1} \text{ cm}^{-1}$) and a shoulder at 315 nm (55). Integration of EPR spectra shows that there are 1.0 ± 0.1 spins per Fe₂ pair (59) consistent with the original assignment of the mixed valence oxidation state, Fe(II)Fe(III), to each monomer (53). In keeping with this formulation, the reduction of metHr to semi-metHr requires one equivalent of dithionite. UV-visible titrations indicate that azide combines with the semi-metHr thus formed in a ratio of ~ 1:1 (60).

Comparison of the resonance Raman data for the semi-metN₃⁻ derivative with that of the corresponding metN₃⁻ form shows that, although the internal azide stretch occurs at the same frequency, the position of the Fe-N stretching frequency shifts from 374 cm^{-1} to 357 cm^{-1} and the symmetric Fe-O-Fe stretch assigned to the μ -oxo bridge is absent. Since it is difficult to predict the degree of resonance enhancement that should be observed, the absence of a Fe-O-Fe stretch cannot rule out the presence of an oxo bridge in the semi-met form of the protein. Use of ¹⁵N¹⁴N₂⁻ in preparing semi-metN₃⁻ results in a splitting of the Fe-N band; this result is

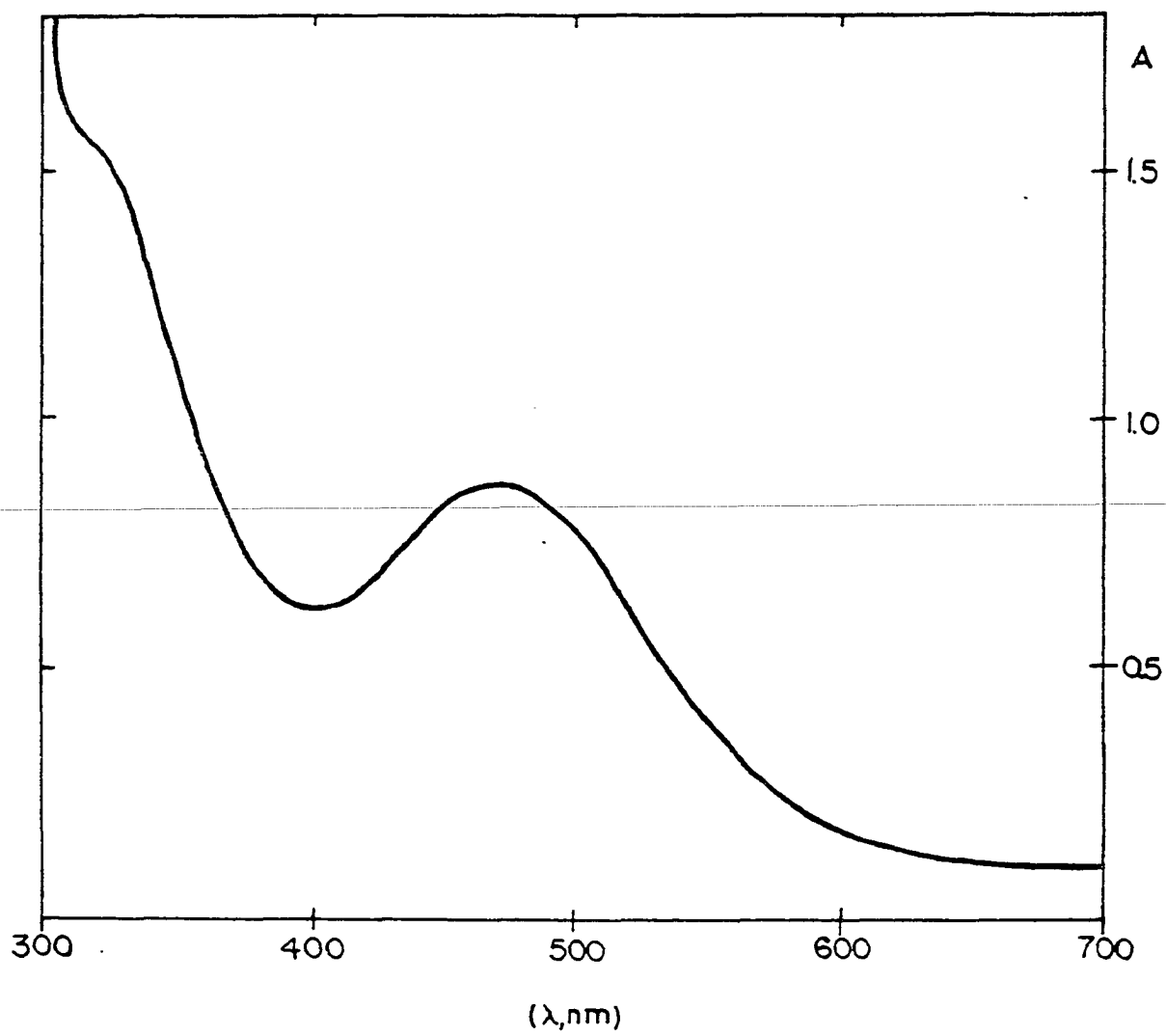


Figure I-7. UV-visible spectrum of 3.5×10^{-4} M semi-metN₃⁻ in 50 mM Tris/acetate, pH 8.0

consistent with end-on binding of the azide to one iron atom and a structure analogous to that of metazidoHr (60).

The ^1H NMR spectrum of semi-metN $_3^-$ contains resonances at 73 and 54 ppm downfield of DSS which are assigned to the exchangeable protons of the histidines coordinated to the ferric and ferrous ions, respectively. Integration of the peaks shows that the ratio of the areas is 2:3 illustrating that the iron bound to two histidines is the Fe(III) in semi-metN $_3^-$. Study of the temperature dependence of the semi-metN $_3^-$ NMR spectrum allows estimation of a value for the antiferromagnetic coupling constant J of $-10 \pm 3 \text{ cm}^{-1}$ (61). ~~This value is an order of magnitude less than that of oxyHr or metHr (Table I-3).~~

The reduction potentials of the met/(semi-met) $_R$ and (semi-met) $_O$ /deoxy couples are given in Table I-6 (57, 62). In those cases where reduction potentials have been determined for the same redox couples in hemerythrins from different species, only small differences in the measured reduction potentials are observed (57).

C. Previous Work on Sulfide Derivatives of Hemerythrin

When H_2S or Na_2S is added to an oxygen-free solution of metHr at pH 8.0, a purple complex is formed. First reported by Keresztes-Nagy and Klotz in 1965, this complex has an

Table I-6. Reduction Potentials of Hemerythrin Derivatives at 25 °C, I=0.15 M and pH 8.2 versus NHE^a

Couple	Species	Reduction Potential(V)	Redox Partner
(Semi-met) _O /deoxyHr	<u>T. zostericola</u>	0.30	Fe(CN) ₆ ³⁻ /excess Fe(CN) ₆ ⁴⁻
	<u>P. gouldii</u> ^b	0.30	Fe(CN) ₆ ³⁻ /excess Fe(CN) ₆ ⁴⁻
(Semi-met) _O /oxyHr	<u>T. zostericola</u>	0.40	Fe(CN) ₆ ³⁻
MetHr/deoxyHr	<u>T. zostericola</u>	0.23	Cytochrome c(II)/(III)
MetHr/(semi-met) _R	<u>T. zostericola</u>	0.11	DCIP _{red} /DCIP _{ox} ^c
	<u>P. gouldii</u>	0.11	DCIP _{red} /DCIP _{ox}
Metmyo/(semi-metmyo) _R	<u>T. zostericola</u>	0.07	DCIP _{red} /DCIP _{ox}

^aReference 57.

^bReference 62.

^cDCIP, 2,6,-dichlorophenolindophenol.

absorption maximum at 510 nm and a shoulder at 340 nm (63). Anaerobic dialysis of this derivative against 25:75 (v/v) ethanol:water produces crystals of the hemerythrin complex. Based on the study of these crystals, Bayer et al. proposed that the sulfur was bound to metHr as S_2^{2-} analogous to the binding of O_2^{2-} in oxyHr. This suggestion stemmed from three experimental features: the similarity of the UV-visible absorption spectrum of (metHr + S^{2-}) to that of oxyHr, indirect chemical evidence that the sulfur was not in the reduced S^{2-} state and elemental analysis of washed (metHr + S^{2-}) crystals showing two sulfurs per two irons (64).

~~According to Freier et al. the purple complex formed upon addition of sulfide to metHr contains two iron (III) ions and one sulfide at the active site (65). Their stoichiometry of sulfide binding is determined by a spectrophotometric titration of metHr with solutions of H_2S . They could not generate this sulfide complex upon addition of H_2S to deoxyHr or upon addition of Na_2S_2 to either deoxyHr or metHr.~~

The resonance Raman spectrum of this hemerythrin derivative contains only one peak at 444 cm^{-1} . Vibrational information for several pertinent Fe-S containing proteins and synthetic systems is cited in Table I-7 (65, 66). Comparison of the 444 cm^{-1} vibration of the sulfideHr with those observed for iron-sulfur compounds of known structure does not allow unambiguous assignment of this frequency.

Table I-7A. Fundamental Fe-S Stretching Modes of Some Iron-sulfur Proteins

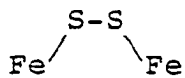
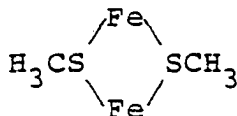
Molecule	ν (cm ⁻¹)	Assignment ^a
Oxidized Rubredoxin ^b (<i>C. pasteurianum</i>)	365	ν_3 of Fe-S ₄ tetrahedron
$\begin{array}{c} \text{CysS} \backslash \quad / \text{SCys} \\ \quad \quad \quad \text{Fe} \\ \text{CysS} / \quad \backslash \text{SCys} \end{array}$	311	ν_1 of Fe-S ₄ tetrahedron
Oxidized Adrenodoxin ^c	418	Fe-S _b
$\begin{array}{c} \text{CysS} \backslash \quad \text{S} \quad / \text{SCys} \\ \quad \quad \quad \text{Fe} \quad \quad \text{Fe} \\ \text{CysS} / \quad \text{S} \quad \backslash \text{SCys} \end{array}$	392	Fe-S _b
	347	Fe-S _t
	328	Fe-S _t
	290	Fe-S _b
Oxidized Spinach Ferrodoxin ^c	425	Fe-S _b
$\begin{array}{c} \text{CysS} \backslash \quad \text{S} \quad / \text{SCys} \\ \quad \quad \quad \text{Fe} \quad \quad \text{Fe} \\ \text{CysS} / \quad \text{S} \quad \backslash \text{SCys} \end{array}$	395	Fe-S _b
	336	Fe-S _t
	328	Fe-S _t
	284	Fe-S _b

^aSubscript b indicates primarily Fe-bridging S stretching. Subscript t indicates primarily Fe-terminal S stretching.

^bReference 65.

^cReference 66.

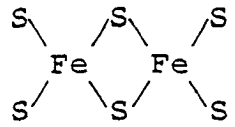
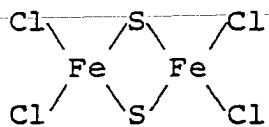
Table I-7B. Observed Fe-S (and Fe-Cl) and S-S Frequencies

Molecule	$\nu(\text{cm}^{-1})$	Assignment ^a
$\text{S}_2\text{Fe}_2(\text{CO})_6^{\text{b}}$	554	S-S
	329	Fe-S
$(\text{SCH}_3)_2\text{Fe}(\text{CO})_6^{\text{b}}$	350	Fe-S
		
$\text{Na}_2\text{S}_2^{\text{b}}$	451	S-S
$\text{H}_2\text{S}_2^{\text{b}}$	509	S-S

^aSubscript b indicates primarily Fe-bridging S stretching. Subscript t indicates primarily Fe-terminal S stretching.

^bReference 65.

Table I-7B. (Continued)

Molecule	ν (cm ⁻¹)	Assignment ^a
$\text{Fe}_2\text{S}_2(\text{S}_2\text{-o-xyl})_2^{2-}$ ^b	417	Fe-S _b
	392	Fe-S _b
	347	Fe-S _t
	338	Fe-S _t
	326	Fe-S _t
	324	Fe-S _t
	279	Fe-S _b
$\text{Fe}_2\text{S}_2\text{Cl}_4^{2-}$ ^c	415	Fe-S _b
	401	Fe-S _b
	345	Fe-Cl
	334	Fe-Cl
	331	Fe-Cl
	318	Fe-S _b
	287	Fe-S _b

^cReference 66.

Isotopic replacement with ^{34}S results in a frequency shift which is more consistent with assigning the 444 cm^{-1} band to an Fe-S stretching vibration than an S-S vibration. No shift is observed when D_2S is added to a solution of metHr in D_2O suggesting that S^{2-} rather than $-\text{SH}^-$ is the ligand involved. Since terminal $\text{Fe}^{3+}-\text{S}^{2-}$ coordination is unlikely, the 444 cm^{-1} band is assigned to the symmetric stretch of an Fe-S-Fe unit (65).

Once sulfide has been incorporated into the active site, Freier et al. found that exposure of the protein to dioxygen and laser excitation of 514.5 nm result in the production of oxyHr. On the basis of resonance Raman studies simultaneous binding of azide and sulfide to metHr is not possible. Sulfide does not seem to affect the active-site structure of metazidoHr, and likewise no perturbations of the sulfide derivative's active-site structure are observed in the presence of azide (65).

D. Statement of the Problem

Conflicting reports on the nature of the sulfide containing ligand (64, 65) leave some question as to whether a sulfide or a persulfide is bound to the active site of the purple sulfide derivatives of hemerythrin. Furthermore, all previous reports have assumed that this sulfide derivative is

at the met oxidation level. The possibility of sulfide acting as a reducing agent has not been considered even though a comparison of E° ' for S°/H_2S given in Table I-8 (67, 68, 69) with those of hemerythrin (Table I-6) indicate that a redox reaction is feasible.

Our preliminary characterization of this purple sulfide derivative determined that it is in fact at the semi-met oxidation level. This new information has made a detailed study of the redox chemistry of this derivative possible. The study of the redox chemistry has resulted in the discovery of a sulfide derivative at the met oxidation level. The physical and chemical characterization of this latter derivative has led to the conclusion that a single sulfide bridges the two irons in the sulfideHrs.

Introduction of a sulfide into the active site of hemerythrin confers new structural and electronic properties and reactivity patterns on the binuclear iron center which can be usefully compared to the physiologically relevant μ -oxo bridge containing forms of the protein. In addition, the properties of this "semi-synthetic" iron-sulfur center can be compared to those of $[2Fe-2S]$ centers in iron-sulfur proteins. In particular, Rieske-type iron-sulfur centers (70, 71) exhibit some physical and chemical properties which are quite similar to those of the sulfideHrs. Those similarities in turn suggest some structural similarities in the two types of

Table I-8. Reduction Potentials of Various Half-reactions^a

Half-reaction	E° (V vs NHE) ^b	E°' (V vs NHE) ^c
$S_2O_8^{2-} + 2e^- = 2SO_4^{2-}$	2.01	
$H_2O_2 + 2e^- = 2H_2O$	1.776	
$O_2(g) + 4H^+ + 4e^- = 2H_2O(l)$	1.229	0.815
$SeO_4^{2-} + 4H^+ + 2e^- = H_2SeO_3 + H_2O$	1.150	
$S_2O_4 + 2H^+ + 4e^- = S_2O_3^{2-} + H_2O$	1.03	0.484
$Fe^{3+} + e^- = Fe^{2+}$	0.771	0.771
$H_2SeO_3(aq) + 4H^+ + 4e^- =$ $Se(gray) + 3H_2O$	0.740	
$O_2(g) + 2H^+ + 2e^- = H_2O_2$	0.682	0.295
$S_2O_6^{2-} + 4H^+ + 2e^- = 2H_2SO_3$	0.570	
$4H_2SO_3 + 4H^+ + 6e^- = S_4O_6^{2-} + 6H_2O$	0.510	
$S_2O_3^{2-} + 4e^- = 2S + 3H_2O$	0.500	
$H_2SO_3 + 4H^+ + 4e^- = S + 3H_2O$	0.450	
$2H_2SO_3 + 2H^+ + 4e^- = S_2O_3^{2-} + 3H_2O$	0.400	
$Fe(CN)_6^{3-} + e^- = Fe(CN)_6^{4-}$	0.36	(0.43) ^d

^aReference 67.

^bE° refers to a standard state in which the hydrogen ion activity = 1. Temperature is 25 °C.

^cE°' refers to a standard state of pH 7, 25 °C.

^dReference 68. E° value at pH = 8.

Table I-8. (Continued)

Half-reaction	E° (V vs NHE) ^b	E° ^c (V vs NHE) ^c
$\text{Co(phen)}_3^{3+} + e^- = \text{Co(phen)}_3^{2+}$		0.37
cytochrome c(Fe^{3+}) + $e^- =$ cytochrome c(Fe^{2+})		0.26 ^{d,e}
$\text{DCIP}_{\text{ox}} + e^- = \text{DCIP}_{\text{red}}^{\text{f}}$		0.217(0.14) ^g
$\text{SO}_4^{2-} + 4\text{H}^+ + 2e^- = \text{H}_2\text{SO}_3 + \text{H}_2\text{O}$	0.172	
$\text{S(rhombic)} + 2\text{H}^+ + 2e^- = \text{H}_2\text{S}_{(\text{aq})}$	0.142	-0.243
$\text{S}_4\text{O}_6^{2-} + 2e^- = 2\text{S}_2\text{O}_3^{2-}$	0.080	
$\text{SeO}_4^{2-} + \text{H}_2\text{O} + 2e^- = \text{SeO}_3^{2-} + 2\text{OH}^-$	0.050	
$2\text{H}_2\text{SO}_3 + \text{H}^+ + 2e^- = \text{HS}_2\text{O}_4^- + 2\text{H}_2\text{O}$	-0.082	
$2\text{SO}_4^{2-} + 4\text{H}^+ + 2e^- = \text{S}_2\text{O}_6^{2-} + 2\text{H}_2\text{O}$	-0.220	
$\text{SeO}_3^{2-} + 3\text{H}_2\text{O} + 4e^- = \text{Se} + 6\text{OH}^-$	-0.366	
$\text{Se} + 2\text{H}^+ + 2e^- = \text{H}_2\text{Se}_{(\text{aq})}$	-0.399	
$2\text{SO}_3^{2-} + 2\text{H}_2\text{O} + 2e^- = \text{S}_2\text{O}_4^{2-} + 4\text{OH}^-$	-0.500	
$\text{Se} + 2e^- = \text{Se}^{2-}$	-0.920	
$\text{SO}_4^{2-} + 2\text{H}^+ + 2e^- = \text{SO}_3^{2-} + \text{H}_2\text{O}$	-0.93	-0.454

^eReference 69.

^fDCIP, 2,6-dichlorophenolindolphenol.

^g E° at pH 8. Reference 57.

centers. For these reasons, this thesis consists of a detailed description and discussion of the preparation and properties of the sulfideHrs.

E. Spectroscopic Techniques

1. Electron paramagnetic resonance

Electron paramagnetic resonance (EPR) has contributed significantly to the characterization of the structure and function of paramagnetic centers found in proteins. With this technique, it is possible to study species possessing electrons with unpaired spins; such species are often not readily observed by other methods. These statements apply particularly to proteins containing transition metal ions. In this section, a brief summary of EPR spectroscopy is given with particular reference to binuclear iron centers in proteins.

Interaction of unpaired electron spin moment with an applied magnetic field results in removal of the degeneracy of electron spin states. For a system with $S=1/2$, there are two spin populations, one aligned with the field and the other antiparallel to the field. The difference in energy between these two populations, $g\beta H$, can be determined from the electronic Zeeman Hamiltonian given in equation (1).

$$\mathcal{H} = -g\beta S \cdot H = -g\beta S_z H_z \quad (1)$$

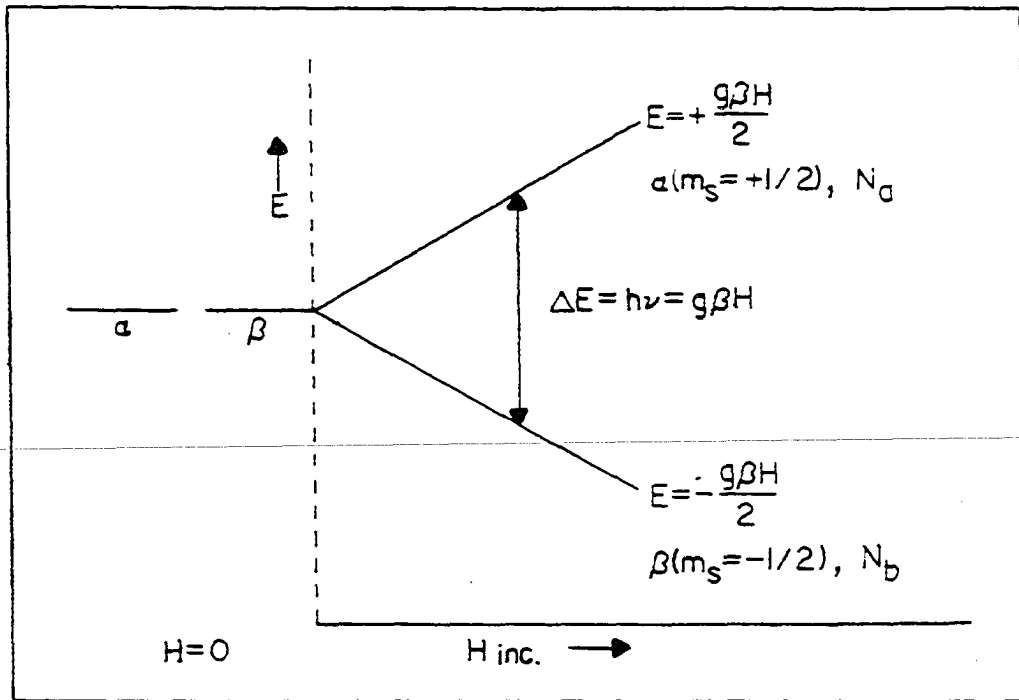


Figure I-8. The removal of the degeneracy of the electron spin states for a spin-1/2 system by an applied magnetic field H

S_z is the component of the electronic spin (along the z direction); H_z is the strength of the applied field; β is the electron Bohr magneton having a value of $9.274096 \pm (0.000050) \times 10^{-21}$ erg/gauss; and g for a free electron equals 2.0023193. Figure I-8 illustrates the splitting of spin states in a magnetic field. The energy of the transition is reflected in the g value. In a typical EPR experiment, the frequency is fixed, and the magnetic field is swept. The spectra are plotted as the first derivative of the absorption curve versus the strength of the magnetic field (72).

The spin populations are controlled by a Boltzmann distribution, $N_a/N_b = \exp(-g\beta H/kT)$, where N_a and N_b represent the populations of the upper and lower energy levels, respectively, and T is the absolute temperature. Transitions induced by the applied microwave field are dependent on a difference in those populations. Spin-lattice relaxation tends to preserve the Boltzmann distribution while the microwave field has a tendency to equalize the populations. Saturation occurs when the microwave power is so intense that the rate at which the upper state is populated is fast enough to equalize the spin populations. The result is a decrease in the intensity of the observed signal. When the relaxation process is dominant, a decrease in temperature will cause the ratio N_a/N_b to decrease. The net absorption then increases, which is particularly useful for biological macromolecules (73).

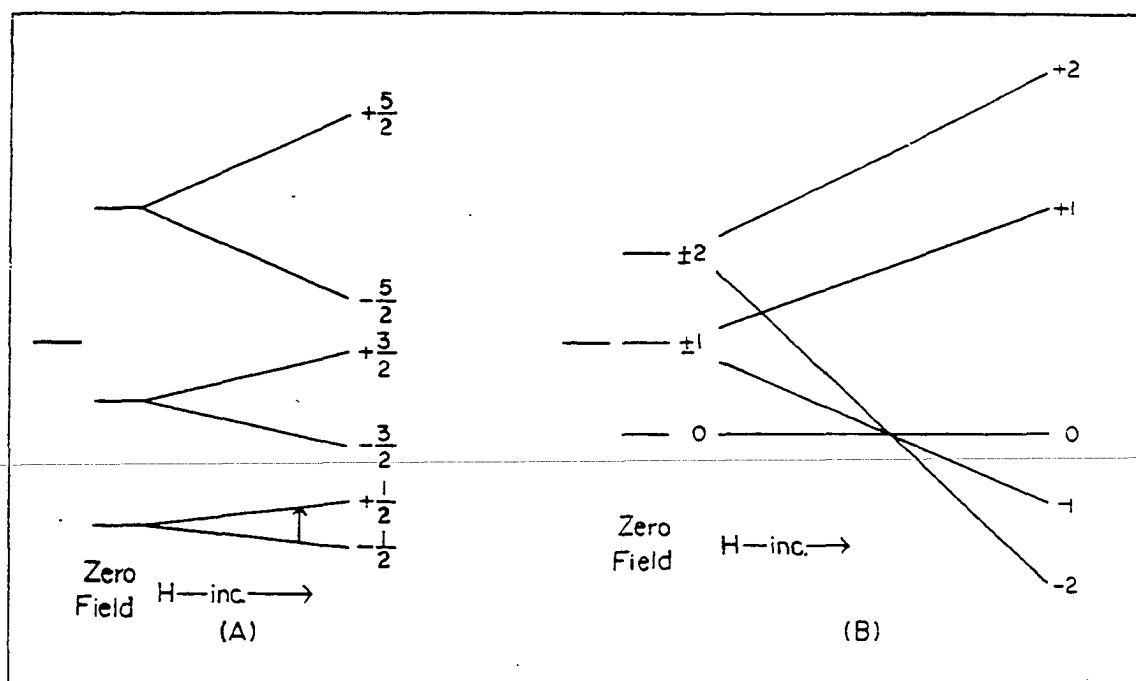


Figure I-9. Zero-field and magnetic field splitting for high-spin Fe(III) and Fe(II) ions.

A) Zero-field and magnetic field splitting for a d^5 ion in a strong tetragonal field B) Zero-field and magnetic field splitting for a d^6 ion

In a number of proteins, the presence of iron results in paramagnetism. High spin Fe(III) generally has long electron spin lifetimes making it easily observed at room temperature in all symmetry crystal fields. Kramers' degeneracy is present even with large zero field splitting. Figure I-9A shows the energy levels expected for a high spin Fe(III) in a strong tetragonal field. In the case of high spin Fe(II), EPR spectra are usually not obtainable because of rapid relaxation and the lack of a ground state Kramers' doublet (72). The zero-field and magnetic field splitting for a high spin d^6 are illustrated in Figure I-9B.

In multinuclear iron sites, it is not uncommon for the spins to be antiferromagnetically coupled through polarization of bonding electrons on intervening ligands. For example, [2Fe-2S] ferredoxins contain two high spin Fe(III)($S=5/2$) ions in their oxidized form; the ground state of this form is diamagnetic at low temperatures, i.e., it has a net $S=0$. Addition of one electron to the cluster results in a coupled mixed valence dimer having a net spin $S=1/2(5/2-4/2)$ and an observable EPR spectrum. In ferredoxins, the antiferromagnetic exchange interaction between the spins occurs predominantly through the bridging sulfides and in the reduced form gives an EPR spectrum similar to those of semi-metHrs (74, 75).

The energy of the coupled state depends on the relative orientations of the two spins and is given by $-2J\mathbf{S}_A \cdot \mathbf{S}_B$. These

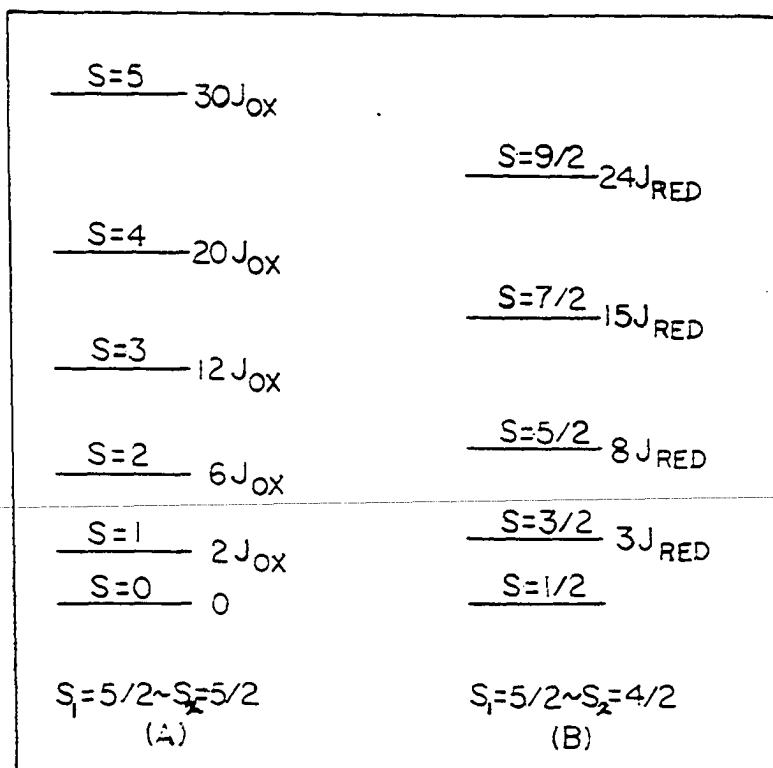


Figure I-10. Ladder of magnetic states produced as a result of antiferromagnetic coupling of two high-spin ferric ions (A) and one high-spin ferric ion with a high-spin ferrous ion(B)

Each state is associated with a resultant spin(S). The energy of each of the spin states relative to the lowest is given by $-J[S(S + 1)]$

states are populated according to a Boltzmann population given by $N_a/N_b = \exp(-2JS_A \cdot S_B/kT)$. The degree of spin pairing is dependent on temperature in such a way that all the molecules will be in the state of lowest S (0 and 1/2, respectively, for examples in Figure I-10) when $T \ll J$. At temperatures much larger than J , the electron spins are maximally unpaired (73). Figure I-10 depicts the ladder of magnetic states available to coupled systems having ground states of $S=0$ ($S_A=5/2$, $S_B=5/2$) and $S=1/2$ ($S_A=5/2$, $S_B=2$).

The absolute number of unpaired spins in a sample can be ascertained by determining the area under the EPR signal by double integration. The area of the unknown is compared to the area of a standard of known spin concentration. Typical standards are DPPH, $\text{CuSO}_4 \cdot 5\text{H}_2\text{O}$, $\text{CuCl}_2 \cdot 2\text{H}_2\text{O}$ and CuEDTA (76).

2. Mössbauer spectroscopy

Mössbauer spectroscopy is a powerful tool used in studying the chemical state and environment of iron atoms. This technique observes nuclear transitions (a change in the nuclear spin quantum number, I) which result from the absorption of gamma-rays by the sample. The Mössbauer effect involves transitions between the nuclear excited and ground states with the selection rules $\Delta m_I = 0, \pm 1$ and $\Delta m_S = 0$ (77).

A distinctive feature of this technique is that the source of the radiation must be a radioactive nucleus of the

same isotope in which the absorption occurs. In ^{57}Fe Mössbauer spectroscopy a source of radioactive ^{57}Co prepared by diffusing a radioactive cobalt salt into a metal foil matrix is generally used. The ^{57}Co decays to ^{57}Fe in an excited state via electron capture. The excited ^{57}Fe then decays to the stable ^{57}Fe ground state by emission of gamma radiation. Having an excited Fe isotope as the source insures that the absorption lines can only be attributed to iron. The radiation from the source is scanned by moving the source back and forth with respect to the sample. Due to the electromagnetic Doppler effect, movement of the source results in a shift of the energy of the gamma radiation to higher or lower values as the source is moved towards and away from the sample. Absorption energy is measured in velocity (mm/s) of the source (78).

The three main parameters obtained from a Mössbauer spectrum are the isomer shift, the quadrupole splitting and the magnetic hyperfine splitting. The isomer shift, the energy of the center of the absorption spectrum with respect to a standard, is a measure of the electromagnetic interaction of the charge distribution in the nucleus with the s-electron density at the nucleus. The s-electrons can be shielded from the nucleus by interactions with the d-electrons. Since the amount of shielding is dependent on the number of d-electrons, the isomer shift can be used to measure the valence of the

iron being examined. The isomer shift, however, does not always allow unambiguous assignment of oxidation state because the s-electron density can be altered by covalent interactions with neighboring ligands. The quadrupole splitting results from the symmetry and local structure of the iron atoms. Any symmetry less than cubic in the arrangement of valence electrons or neighboring ligands causes an electric field gradient at the iron nucleus. Since the $I = 3/2$ excited state of ^{57}Fe has a quadrupole moment, this asymmetry removes the degeneracy of the excited state energy levels (77, 79). This effect is diagrammed in Figure I-11.

Magnetic hyperfine interactions can cause further splitting of these energy levels as shown in Figure I-12. Since both the excited and ground nuclear states of ^{57}Fe have magnetic moments in addition to quadrupole moments, then a more complex spectrum will result in the presence of a magnetic field. The applied field will split the levels seen in the zero field spectrum. The effective magnetic field may be a result of nuclear interactions with unpaired electrons or may originate from an external source. Biological systems are generally magnetically dilute so the major mechanism for electron spin relaxation is via the temperature-dependent spin-lattice rather than spin-spin interaction. Lowering the temperature sometimes increases the spin-lattice relaxation time enough that the time average of electronic spin

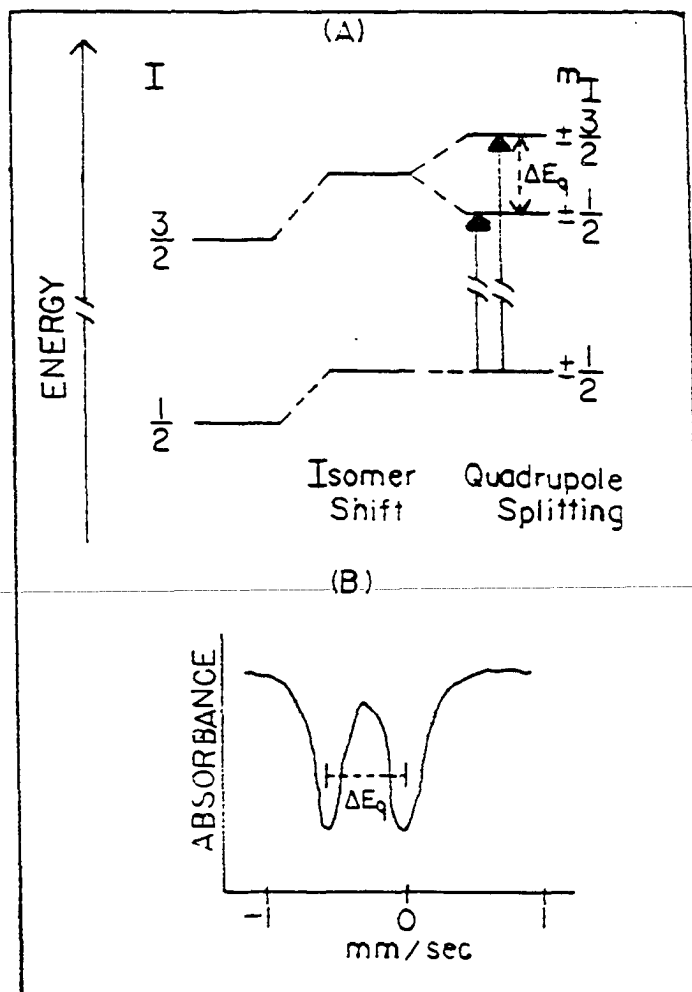


Figure I-11. Isomer shift and quadrupole splitting of ^{57}Fe in a non-cubic electronic environment

A) Nuclear energy levels B) The corresponding Mössbauer spectrum

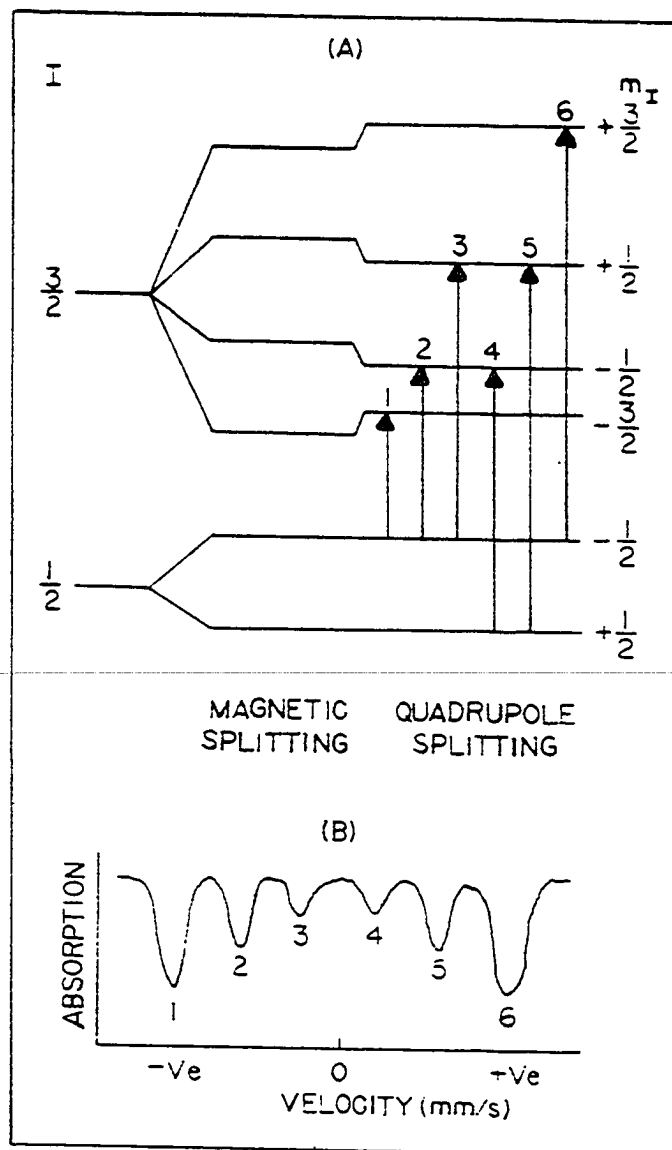


Figure I-12. Magnetic and quadrupole splitting in a ferromagnetic ^{57}Fe compound

- A) Superimposition of the magnetic and quadrupole hyperfine interactions for iron
- B) Expected Mössbauer spectrum

interaction with the nuclear spin is nonzero over the time of the nuclear spin precession. This nonzero interaction is manifested by splitting of the lines in the Mössbauer spectrum. In the ideal case of one iron environment in a single crystal with only one orientation in the magnetic field, a six line spectrum like the one illustrated in Figure I-12 is obtained. In a powder or frozen solution, there are usually many different orientations of the magnetic moment for each orientation of the electric field gradient. The magnitude of the magnetic splitting is slightly different for each orientation and the resulting spectrum is usually a broad absorption spread over several mm/s (77, 79).

Since ^{57}Fe is only 2 % naturally abundant, most biological Mössbauer samples are enriched with ^{57}Fe . Enrichment is accomplished either by growing the organism from which the protein is isolated on separated isotope ^{57}Fe or by introducing the ^{57}Fe by chemical exchange (77).

3. Resonance Raman spectroscopy

Vibrational spectroscopy yields electronic and structural information not easily obtained by other spectroscopic methods. Raman spectroscopy is a technique that provides vibrational data by monitoring the inelastic scattering of the incident light on a molecule. The incident photon has a different energy than the scattered photon; this energy

difference is caused by the electromagnetic radiation changing a molecular vibrational mode and the polarizability of the electron cloud of the molecule. Since a nonlinear molecule with N atoms has $3N-6$ normal modes of vibration, the Raman spectrum of a protein generally contains a large number of low intensity peaks making it impossible to examine vibrational characteristics of a specific site. Thus, normal Raman spectroscopy is not very useful for studying specific identifiable sites in macromolecules (80).

The method of choice for obtaining vibrational information for a metal site in a biological macromolecule is resonance Raman spectroscopy. The resonance Raman scattering effect is the increase in intensity of some Raman spectral lines when a compound is excited with incident laser light of a frequency within an electronic absorption band of the scattering molecule. This enhancement results from a coupling of vibrational and electronic transitions. Since the enhanced lines are due to vibrational modes of the chromophore or adjacent groups of atoms, selective information about the chromophore can be obtained, usually without interference from non-resonanced enhanced lines. The difference between non-resonance and resonance Raman effects is diagrammed in Figure I-13 (81).~

Excitation profiles, measuring the relative intensity of a given vibrational peak using various excitation frequencies,

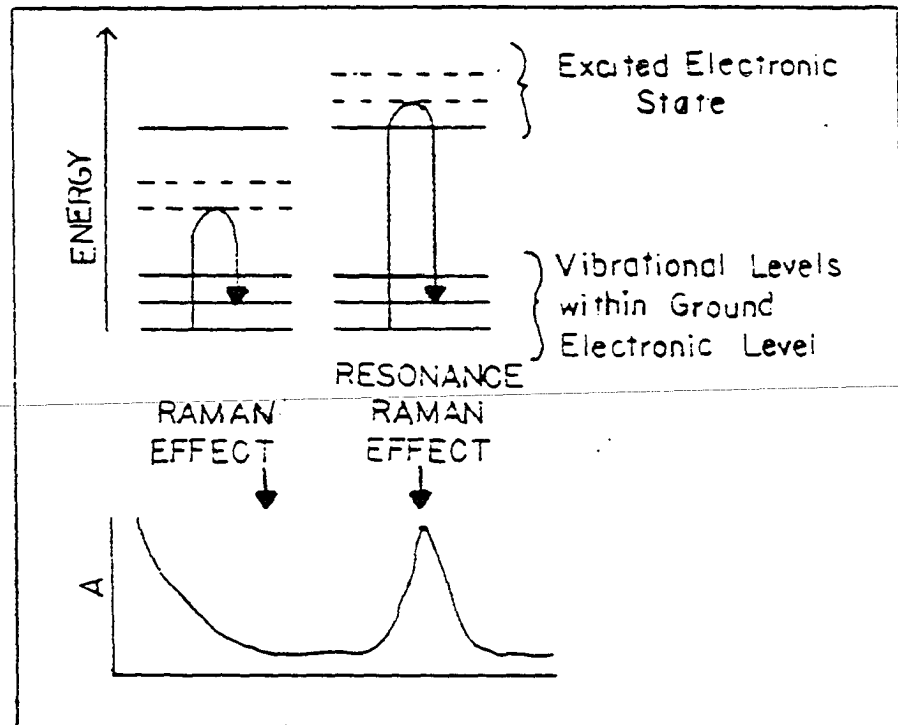


Figure I-13. Differences between non-resonance and resonance Raman effects

Non-resonance Raman photons occupy a virtual state during the scattering process. Resonance Raman photons occupy a level within an excited electronic state

are used to determine whether a vibrational peak is coupled to a specific electronic transition. The electronic transitions giving rise to resonance enhancement are usually charge transfer transitions and assignment of vibrational frequencies often provides information about which atoms are involved in the charge transfer (81).

Vibrational information can be employed in the characterization of bridged systems such as occurs in hemerythrin (Table I-4). In the case of mono and dioxobridged systems, a major consideration is the extreme sensitivity of the observed vibrational frequencies to the M-O-M bond angle. A monooxo-bridged metal dimer system can be treated as a three body system bent at an angle θ and having two bridging vibrations. When the vibrational frequencies and the corresponding force constants are available, the secular equations of Wing and Callahan can be used to estimate the M-X-M bridging angle (82). Calculations of this type have been used to rationalize the values of the symmetric and asymmetric Fe-O-Fe stretching modes in oxy and metHrs (49).

II. EXPERIMENTAL PROCEDURES

A. Isolation of OxyHr

Using a standard procedure (83) for the isolation of hemerythrin from Phascolopsis gouldii, 300 worms purchased from the Marine Biological Laboratory, Woods Hole, Massachusetts, normally yielded 5 to 8 grams of crystalline oxyHr. The entire operation was carried out at 4 °C. The worms were slit lengthwise and bled into a large porcelain evaporating dish. The coelomic fluid was allowed to settle overnight. Cells and debris were then filtered through several layers of cheese cloth. Removal of the fatty layer was accomplished next in a series of steps that consisted of spinning down the cells in a clinical centrifuge, removing the fatty layer with a Pasteur pipette and resuspending the cells in sea water. This sequence was repeated (usually 2 to 3 times) until the sediment was virtually free of any fatty layer. The cells were transferred to an Erlenmeyer flask containing 2.5 times their volume of 0.4 % by weight NaCl solution. This mixture was stirred overnight to ensure that all the cells were lysed. The cell debris was then removed by a low speed centrifugation in the clinical centrifuge followed by 2 one hour high speed centrifugations (15,000 rpm) in a Sorvall centrifuge. The reddish-purple solution was dialyzed

against a large volume of a 0.4 % NaCl in a 20:80 (v/v) ethanol:water solution. In later preparations of the protein, the NaCl was omitted from the solution used for crystallization because of difficulties encountered due to Cl^- binding to hemerythrin. The oxyHr crystals thus obtained were stored in glass containers at 4 °C until used. Kept in this fashion, the protein was usable for 4 to 5 months; slow autooxidation to metHr took place during this period.

B. Preparation of MetHr and DeoxyHr

For most experiments, either metHr or deoxyHr was the starting material. MetHr was prepared from crystals of oxyHr dissolved in the appropriate buffer (usually 50 mM Tris/acetate pH 8.0) and treated with a small excess of potassium ferricyanide. The reaction was incubated at room temperature until completion, usually several hours. The excess ferricyanide and ferrocyanide formed were removed by dialysis against several changes of buffer at 4 °C. When prepared in this fashion at pH 8.0 and stored at 4 °C, metHr was sufficiently stable to be used over a period of several weeks.

Concentrations of metHr were determined by formation of metazidoHr. At least a ten-fold molar excess of sodium azide was added to a sample of metHr. The extinction coefficients at 447 nm and 326 nm were used (see Table I-2A). All the Hr

concentrations in this thesis are expressed in terms of Hr monomer (i.e., binuclear iron site).

DeoxyHr was prepared from either metHr or oxyHr. The protein was dialyzed at 4 °C overnight against a solution of 2-3 mM dithionite, which had been prepared by addition of solid sodium dithionite to a thoroughly degassed liter of buffer. Removal of excess dithionite was achieved by further dialysis against anaerobic buffer. The deoxyHr was used as quickly as possible after removal of excess dithionite. Removal of the deoxyHr from dialysis bags required anaerobic conditions to prevent reoxygenation. This was accomplished by placing a vial inside a 24/40 Schlenck-type flask which was stoppered with a rubber septum and attached to the vacuum line. The vial and flask were degassed; the septum was removed with a strong flow of argon over the top of the flask. The dialysis bags containing the deoxyHr were cut open in the flask just above the vial and under the flow of argon. Once the deoxyHr was in the vial, the system was immediately evacuated. Then the deoxyHr was kept under positive argon pressure until use which was usually within two hours. Protein concentrations were determined by reoxygenation to oxyHr. Extinction coefficients for 500 nm, 360 nm and 330 nm were utilized (see Table I-2A), and an average hemerythrin concentration was calculated.

C. Instrumentation

UV-visible absorption spectra were obtained on a Perkin-Elmer Model 554 spectrophotometer. A double septum sealed quartz cuvette (84) with high vacuum teflon stopcocks was used when anaerobic conditions were required.

EPR spectra were generally obtained on 0.1-0.2 mL samples of protein ranging in concentration from 0.4-3.0 mM. Solutions of various hemerythrin derivatives were injected, anaerobically when necessary, into 4 mm O.D. quartz tubes and frozen in liquid nitrogen. The tubes were then evacuated, flame sealed and stored in liquid nitrogen until the spectrometer was available for use. X-band spectra were obtained on a Bruker Model ER220D spectrometer equipped with an Oxford ESR-10 helium flow system. Samples were examined routinely at temperatures ranging from 4.0-5.0 K.

In order to quantitate the semi-methHr EPR signals, double integrations of the spectra were obtained. $\text{CuSO}_4 \cdot 5\text{H}_2\text{O}$, $\text{CuCl}_2 \cdot 6\text{H}_2\text{O}$ or CuEDTA were used as concentration standards (76). Values for the double integrations were generated by an integration program available with the spectrometer. These values were inserted into equation (1).

$$[X] = \frac{GN_s MA_s (P_s)^{1/2} (\text{scan}_x)^2 g_{ps} R_x \text{Int2}_x y_x [\text{STD}]}{GN_x MA_x (P_x)^{1/2} (\text{scan}_s)^2 g_{px} R_s \text{Int2}_s y_s} \quad (1)$$

The subscripts s and x denote the values for the standard and the unknown respectively. The parameters are abbreviated as follows: GN, receiver gain; MA, modulation amplitude; P, power in watts; scan, scan width in gauss; Int2, value of the double integral generated by computer; y, height of the integral; [X] and [STD], concentrations of unknown and standard, respectively. The term R takes into account the degeneracy of any of the lines in the spectrum. $R = (\sum_j D_j) / D_r$ where D_r is the degeneracy of the most intense line and D_j is the sum of the degeneracies of the most intense lines in the spectrum (85). Since the g-value is proportional to the integrated intensity of the field-swept EPR spectra, the average intensity factor g_p was incorporated into the equation. According to Aasa and Vanngard, $g_p = 2/3((g_x^2 + g_y^2 + g_z^2)/3)^{1/2} + 1/3(g_x + g_y + g_z)/3$ (86). For the most consistent integrated concentration values, instrumental parameters for the unknown and standard were kept as similar as possible.

To insure that the area was a true reflection of the amount of paramagnetic material present, all spectra were run under non-saturating conditions. Power saturation curves for the

copper standards and of the paramagnetic hemerythrin derivatives were determined. These curves and an explanation of their usage are given in Appendix A.

Resonance Raman spectra were collected at the Oregon Graduate Center on a computer-interfaced Jarrell-Ash spectrophotometer equipped with Spectra Physics 164-05 (Ar) and 164-01 (Kr) ion lasers, an RCA C31034 photomultiplier tube and an ORTEC Model 9302 amplifier/discriminator. Spectra of anaerobic solutions of hemerythrin approximately 2 mM in monomer were obtained at 77 K. Samples were transferred via gas-tight syringe to capillary tubes which were sealed with putty at both ends. Temperature was controlled by placing the capillary in the cold-finger of a liquid N₂ Dewar or by placing the capillary in a flow of cold N₂ gas which was obtained by regulating the rate of boiloff from a Dewar of liquid N₂ (87). Thawed solutions of μ -sulfidometHr tended to bleach in the laser beam whereas no bleaching was detected in samples run at 77 K. In all cases, 180° backscattering geometry was used, and multiple scans were collected and averaged to enhance the signal-to-noise ratio. Laser power at the sample ranged from 30-130 mW for visible excitation and 12-15 mW for UV excitation. Slit widths of 3-10 cm⁻¹ were used. Estimates of peak intensity at various excitation wavelengths were made relative to that of ν_1 of perchlorate at 935 cm⁻¹.

Mössbauer spectra were collected at the University of Illinois on a constant acceleration spectrometer equipped with a variable temperature cryostat. All velocities were determined relative to metallic iron at 300 K. Crystalline samples were centrifuged into half-inch diameter cylindrical nylon cups and solution samples were transferred via syringe into the Mössbauer cups which were placed at the bottom of disposable syringes in order to facilitate transferring the protein into the cup under anaerobic conditions. Both types of samples were frozen and then stored in liquid N₂. The samples ranged from 6-16 mM in Hr monomer; these high concentrations were required because of the low natural abundance of ⁵⁷Fe coupled with the fact that no method has yet been discovered for enrichment of hemerythrin in ⁵⁷Fe. Removal of the irons usually results in protein denaturation and/or precipitation (63, 88, 89).

D. Preparation and Characterization of μ -Sulfidosemi-metHr

1. Preparation of μ -sulfidosemi-metHr

For routine use, μ -sulfidosemi-metHr (μ -S²⁻semi-metHr) was prepared by anaerobic dialysis of metHr against 3-5 mM sulfide. The sulfide dialyzate was made by dissolving appropriate amounts of either reagent grade Na₂S·9H₂O or NaSH in 1 liter volumes of nitrogen-saturated 50 mM Tris/acetate or

50 mM Tris/perchlorate at pH 8.0. NaSH was prepared from H₂S gas as described in the literature (90). At 4 °C formation of the μ -S²⁻-semi-metHr was complete after dialysis for 10 to 24 hours depending on the concentration of Hr and the excess of sulfide present. When required, excess sulfide was removed by anaerobic dialysis of μ -S²⁻-semi-metHr against two changes of nitrogen-saturated buffer or by passage of the protein over a Sephadex G-25 column.

Samples of μ -S²⁻-semi-metHr for Mössbauer and EPR studies were prepared as described in Section II-C. When crystals were used, the protein derivative was crystallized by an additional step, namely, dialysis against a solution with 20:80 (v/v) ratio of ethanol to water (64). Samples of μ -S²⁻-semi-metHr for resonance Raman studies were prepared in the crystalline form as described above and also in solution by direct addition of Na₂S·9H₂O to metHr in a molar ratio of 4:1.

2. Stoichiometry of the sulfide reaction with metHr

For titrations of metHr with sulfide, the anaerobic stock solutions of Hr were typically 2.0-2.6 mM in monomer. The titrations were conducted at pH 6.2 in 50 mM Bis/tris/acetate or at pH 8.0 in 50 mM Tris/acetate. For each point on the titration curve, 300 μ L of the stock protein solution was transferred to a degassed vial via gas-tight syringe. After addition of the desired amount of sulfide, the reaction

mixtures were diluted to the same total volume, usually around 350 μL . For EPR titrations, the samples were used without further dilution. Samples were frozen at various intervals to determine the time required to obtain the maximum EPR signal. The corresponding UV-visible spectra were obtained from dilutions of the reaction mixtures equilibrated for either 30-60 minutes or 100-150 minutes; the samples for UV-visible spectra were generally 0.3-0.5 mM in monomer.

Stock sulfide solutions were made by dissolving either $\text{Na}_2\text{S}\cdot 9\text{H}_2\text{O}$ or NaSH in the appropriate degassed 0.5 M buffer. The concentrations of these sulfide solutions were determined by a standard iodometric method which is described in Appendix B.

3. Alternate methods of $\mu\text{-S}^{2-}$ semi-metHr preparation

Several other possible methods for preparing $\mu\text{-S}^{2-}$ semi-metHr were also examined. Unless noted otherwise, all of these reactions were carried out in argon-saturated or nitrogen-saturated buffer. The methods examined were:

- (semi-met)_R plus sulfide,
- (semi-met)_O plus sulfide,
- metHr plus thiomolybdate,
- metHr plus polysulfide (S_4^{2-}),
- metHr plus gaseous hydrogen sulfide, and
- metHr plus sulfide and excess azide.

a) (Semi-metHr)_R + NaSH (Semi-met)_R was generated by reduction of metHr with 16 equivalents of dithionite.

Concentrations of stock solutions of $\text{Na}_2\text{S}_2\text{O}_4$ were determined by titration with $\text{K}_3\text{Fe}(\text{CN})_6$ solutions whose concentrations were determined using $\epsilon_{420}=1030 \text{ M}^{-1}\text{cm}^{-1}$ (91). Production of $(\text{semi-met})_{\text{R}}$ was verified by EPR. A 12-fold molar excess of sulfide was added immediately after addition of dithionite. EPR again provided a measure of the reaction that had taken place. The concentration of the stock NaSH solution was determined iodometrically before and after use as described in Appendix B.

A second set of experiments was conducted using one equivalent of dithionite to reduce metHr followed by addition of varying amounts of sulfide. This titration was followed by both UV-visible and EPR spectroscopies.

b) $(\text{Semi-met})_{\text{O}} + \text{NaSH}$ $(\text{Semi-met})_{\text{O}}$ was generated by addition of one equivalent of $\text{Fe}(\text{CN})_6^{3-}$ to deoxyHr, which was then titrated with sulfide. EPR samples were frozen immediately after addition of sulfide. The concentrations of stock solutions were determined in the manner described for the reactions of $(\text{semi-met})_{\text{R}}$ with sulfide in the preceding two paragraphs.

c) $\text{MetHr} + \text{MoS}_4^{2-}$ The stock solutions of metHr and $(\text{NH}_4)_2\text{MoS}_4$ (prepared by Robert Anglin as described in the literature (92)) were prepared in 50 mM Tris/acetate pH 8.0 at concentrations of 1.15 mM and 0.0328 M respectively. Under anaerobic conditions the metHr and MoS_4^{2-} were combined in a

mole ratio of 1.00:1.76. At room temperature, this reaction was monitored by EPR for 15 hours. The initial thiomolybdate concentration was determined by use of the published extinction coefficient, $11,850 \text{ M}^{-1}\text{cm}^{-1}$ at 467 nm (93). The intense absorbance of the thiomolybdate made it impossible to monitor reaction of the protein directly via its UV-visible spectrum. Attempts to follow the rate of MoS_4^{2-} hydrolysis via the UV-visible spectrum by monitoring a blank which contained only buffer and the same concentration of thiomolybdate present in the protein reaction mixture were unsuccessful. When no protein was present, very little change was observed in the thiomolybdate UV-visible spectrum during the time period which $[\text{metHr} + \text{MoS}_4^{2-}]$ reaction was monitored. However, the change in the absorbance at 467 nm due to reaction of the thiomolybdate in the presence of metHr gave an indication of the degree to which the thiomolybdate had hydrolyzed.

d) MetHr + S_4^{2-} The reaction was carried out under two sets of conditions. In one case the reaction mixture contained metHr and S_4^{2-} in a 1:1 molar ratio, and in the second case the molar ratio was 1:0.25 (or 1:0.92 metHr to sulfur atoms). The stock polysulfide solutions were prepared by weighing sodium tetrasulfide (Na_2S_4 , purchased from Alfa Products) under argon and dissolving it in argon-saturated 50 mM Tris/acetate pH 8.0. These solutions were used

immediately (while they were still a clear golden color) because a yellow precipitate appeared within five minutes. Both reactions were monitored by EPR and UV-visible spectroscopies.

e) MetHr + hydrogen sulfide MetHr was prepared in 0.5 mM Tris/acetate pH 8.0. Samples 1.22 mM in protein and 0.6 mL in volume were degassed in three septum-stoppered vials. One of the samples was placed under an atmosphere of hydrogen sulfide gas. For the other two samples, hydrogen sulfide was slowly bubbled through metHr in 1:1 and 2:1 molar ratios via syringe. The volumes of H₂S gas used were calculated from the ideal gas law. The experimental conditions were 27.5 °C, 736 mm Hg and 7.32×10^{-7} moles of gas required for one equivalent. EPR samples were frozen at various times for all three reaction mixtures. UV-visible spectra were taken as soon as possible after the introduction of hydrogen sulfide to the system.

f) MetHr + NaSH + NaN₃ Sodium sulfide and sodium azide were added simultaneously to metHr such that the resulting reaction mixture contained the molar ratio of 1 sulfide:36 azide:1 Hr. The attempt at preparation of $\mu\text{-S}^{2-}$ semi-metHr under these less than ideal conditions was monitored by UV-visible and EPR spectroscopies.

E. Preparation and Characterization of
 μ -Selenidosemi-metHr

Anaerobic solutions of metHr in 50 mM Bis/tris/sulfate, pH 6.1, were prepared in septum-capped vials. The stock solutions of selenide were prepared by weighing Na_2Se (purchased from Alfa Products, 95 % pure) under argon and dissolving it in 0.5 M Bis/tris/sulfate, pH 6.1. The selenide solutions were used immediately after preparation. Three reaction mixtures with different iron to selenide ratios were examined. A typical titration of metHr with selenide involved the addition of aliquots of a 0.074 M Na_2Se solution via gas-tight syringe to one mL volumes of 1.48 mM metHr. Reaction progress was followed by both EPR and UV-visible spectroscopies. The analogous experiment was performed at pH 8.0 in 50 mM Tris/sulfate. Dialysis of metHr against an Na_2Se solution was also tried as a method of preparation of μ -selenidosemi-metHr ($\mu\text{-Se}^{2-}$ -semi-metHr).

Attempts to crystallize $\mu\text{-Se}^{2-}$ -semi-metHr consisted of dialysis of the selenide derivative prepared by direct addition of Se^{-2} to metHr against anaerobic 80:20 (v/v) 5 mM Tris/sulfate pH 8.0:ethanol solutions at 4 °C.

Two Mössbauer samples of $\mu\text{-Se}^{2-}$ -semi-metHr using Se^{2-} :monomer ratios of ~ 2:1 and ~ 4:1 were frozen. The samples were 2.00 mM and 1.89 mM in hemerythrin monomer,

respectively, and were prepared at pH 8.0 by direct addition of a Na_2Se solution to metHr. Attempts to make the Mössbauer samples more concentrated were unsuccessful due to protein precipitation upon addition of selenide to concentrated stock solutions of metHr. Concentration of the Se^{-2} derivative after formation was not feasible because the selenide and protein product are very air-sensitive.

F. Preparation and Characterization of μ -SulfidometHr

1. Preparation of μ -sulfidometHr

All solutions and dialysis buffers were degassed before use and all operations were carried out at 4 °C under Ar or N_2 unless noted otherwise. Two to five mL of 1-2 mM metHr in 50 mM Tris/acetate or Tris/perchlorate pH 8.0 were dialyzed against 1 L of buffer containing 2-3 mM sulfide added as either $\text{Na}_2\text{S}\cdot 9\text{H}_2\text{O}$ or NaSH (63). After 6-10 hours, the dialysis sack containing purple colored $\mu\text{-S}^{2-}$ -semi-metHr was transferred to 1 L of buffer 2 mM in $\text{K}_3\text{Fe}(\text{CN})_6$. Following approximately 8 hours of dialysis, the excess ferricyanide and ferrocyanide were removed by aerobic passage through a small column of Sephadex G-25 or by anaerobic dialysis for a total of 8 hours against two changes of 1 L of buffer. Alternatively, stock solutions of sulfide ($\text{Na}_2\text{S}\cdot 9\text{H}_2\text{O}$ or NaSH) and $\text{K}_3\text{Fe}(\text{CN})_6$ were prepared. Reagents were transferred via gas-tight syringes.

A four-fold molar excess of sulfide was added to a sample of metHr. After one hour incubation at room temperature, four equivalents of $K_3Fe(CN)_6$ were added. Within two minutes the protein solution had turned from purple to deep red. Although the dialysis procedure was more lengthy, it gave more reproducible and reliable results. Attempts at oxidizing $\mu-S^{2-}$ -semi-metHr to $\mu-S^{2-}$ -metHr with $Co(phen)_3^{3+}$ were performed using a procedure analogous to that described for the ferricyanide dialysis method. $[Co(phen)_3]Cl_3 \cdot 9H_2O$ was prepared as described in the literature (94).

2. Characterization of μ -sulfidometHr

EPR samples of μ -sulfidometHr ($\mu-S^{2-}$ -metHr) were prepared using both methods described above and were frozen in liquid N_2 . Samples for resonance Raman and Mössbauer spectroscopies were prepared from the same batch of $\mu-S^{2-}$ -metHr, which had been prepared by the dialysis method in 50 mM Tris/perchlorate pH 8.0. Excess reagents were removed by dialysis against two changes of anaerobic buffer. At this point, the solution was divided in half. The first half, approximately 2 mM in $\mu-S^{2-}$ -metHr, was frozen for resonance Raman experiments. The second half, 2.5 mL, was concentrated using a PM30 Amicon membrane to approximately 800 μ L. Five hundred microliters of $\mu-S^{2-}$ -metHr (6.25 mM) were frozen in a Mössbauer cup under argon.

The possibility of a pH dependence of the UV-visible spectrum of $\mu\text{-S}^{2-}\text{metHr}$ was examined by equilibrating $\mu\text{-S}^{2-}\text{metHr}$ anaerobically for an hour in buffers having a pH ranging from 6.0 to 9.7. Above pH 10.5, the spectrum of $\mu\text{-S}^{2-}\text{metHr}$ is completely bleached and cannot be regenerated by lowering the pH.

3. Determination of extinction coefficients for $\mu\text{-S}^{2-}\text{metHr}$

Extinction coefficients for $\mu\text{-S}^{2-}\text{metHr}$ were determined using the same wet chemical method of analysis for iron (95) which was used previously for Hr. The reagents required for the iron analysis were 0.06 M H_2SO_4 ; 0.8 M $\text{NH}_2\text{OH}\cdot\text{HCl}$; 0.254 mg o-phenanthroline/mL 5×10^{-3} M H_2SO_4 . After measuring the absorbance of the protein in Tris/acetate at 464 nm, 500 nm, 544 nm and 680 nm, 2 to 3 mL of a solution of Hr, 2×10^{-5} to 4×10^{-5} M in iron, were denatured by addition of 1 mL of 0.06 M H_2SO_4 . One-tenth milliliter of 0.08 M $\text{NH}_2\text{OH}\cdot\text{HCl}$ was then added to reduce the iron. Five milliliters of the o-phenanthroline solution were added to the Fe(II) containing mixture. The mixture was then heated to 40 °C for 15 to 30 minutes. After cooling to room temperature, the mixture was centrifuged to remove precipitated protein. The iron content of the supernatant was then determined by measuring the absorbance of the Fe(II)-phenanthroline complex at 570 nm ($\epsilon_{570} = 1.096 \times 10^4 \text{ M}^{-1}\text{cm}^{-1}$).

4. Analysis of labile sulfide and of sulfide plus sulfane sulfur in μ -S²⁻-metHr

In conjunction with iron analyses of μ -S²⁻-metHr, a standard wet chemical method for analysis of sulfide and sulfide plus sulfane sulfur (96, 97, 98) was used with a few modifications. For the sulfide analyses, the required reagents were 1 % zinc acetate [$\text{Zn}(\text{C}_2\text{H}_3\text{O}_2)_2 \cdot 2\text{H}_2\text{O}$]; 12 % aqueous NaOH; 0.1 % N,N-dimethyl-p-phenylenediamine (DMPD) monohydrochloride in 5 N HCl; 23 mM FeCl₃ in 1.2 N HCl; Na₂S·9H₂O in 0.1 N NaOH. Using the following procedure, five different protein samples were assayed concurrently. A small magnetic stir bar was placed at the bottom of a 15 mL polypropylene conical centrifuge tube. Four milliliters of protein ($\sim 2 \times 10^{-4}$ M in Fe) were transferred to the centrifuge tube. Two milliliters of the 1 % zinc acetate solution were added to the protein followed immediately by addition of 0.1 mL 12 % NaOH. Then the mixture was gently stirred until the schlieren of the NaOH had disappeared. Next the mixture was allowed to sit at room temperature for 15 to 20 minutes. One milliliter of the 0.1 % DMPD solution was slowly added underneath the mixture already present in the centrifuge tube. It was then gently stirred so that only a top 2 mm layer of zinc hydroxide remained undissolved. The layer of zinc hydroxide and addition of reagents to the mixture underneath the surface were used to prevent loss of

sulfide to the atmosphere. A 0.2 mL aliquot of 23 mM FeCl_3 was injected under the surface, and the motion of the stir bar was immediately accelerated in order to quickly homogenize the solution. The mixture then sat at 25 °C for one hour after which time a low speed centrifugation was used to spin down the precipitated protein. The absorbance of the final product, methylene blue, was monitored at 670 nm ($\epsilon_{670}=3.45 \times 10^4 \text{ M}^{-1}\text{cm}^{-1}$). In general only the absorbance at 670 nm was measured; however, the appropriate ratios between the maxima at 670 nm and 750 nm and the minimum at 710 nm were assurances that the absorbance at 670 nm was due essentially only to methylene blue. Although the ratios were not entirely constant, for routine use a sufficient approximation was $A_{670}:A_{750}:A_{710}=3:2:1$.

A standard working curve shown in Figure II-1 was generated using a $\text{Na}_2\text{S}\cdot 9\text{H}_2\text{O}$ solution in place of the protein in the previously described procedure. A stock $\text{Na}_2\text{S}\cdot 9\text{H}_2\text{O}$ solution was independently standardized iodometrically (Appendix B) and diluted with buffer to the desired sulfide concentration.

For determinations of sulfide plus sulfane sulfur in $\mu\text{-S}^2\text{-metHr}$, the following reagents were used in addition to those used for the previously described sulfide analysis: guanidine hydrochloride, saturated solution at room temperature in water; 100 mM dithiothreitol (DTT) (for

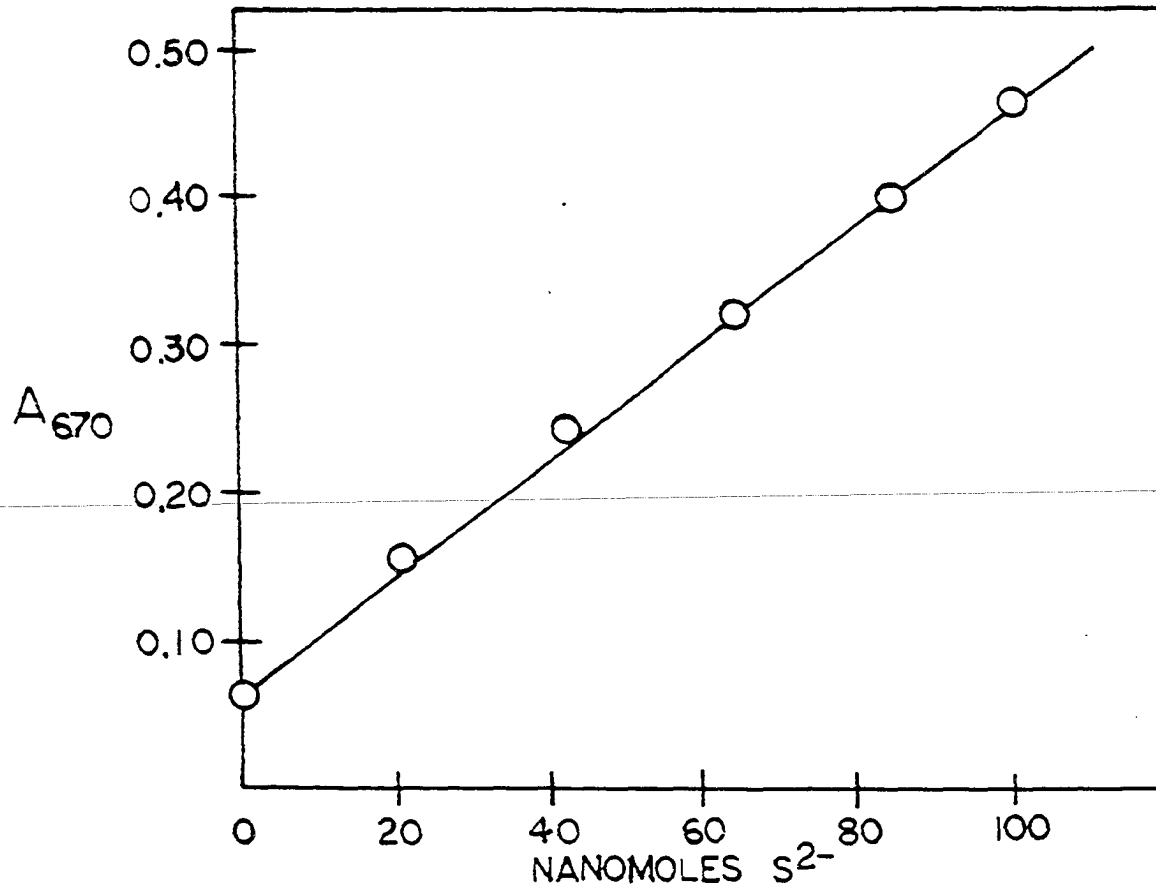


Figure II-1. A standard working curve for sulfide determination based on the formation of methylene blue

reduction of S^0) in 20 mM EDTA ($Na_2C_{10}H_{14}O_8N_2 \cdot 2H_2O$); CsCl, saturated solution at room temperature in water; 50 mM $FeCl_3$ in 1.2 N HCl. Several determinations were carried out simultaneously. Various volumes of a stock $\mu-S^{2-}$ -metHr solution were diluted with 50 mM Tris/acetate pH 8.0 to a final volume of 560 μ L. A 220 μ L volume of saturated CsCl was added to each of these protein solutions. In conical centrifuge tubes containing small magnetic stir bars, 2 mL water (pH 11.0) were mixed with 14 μ L of the DTT/EDTA solution. Next a guanidine·HCl/DTT/EDTA solution consisting of 25 mL saturated guanidine·HCl and 1.25 mL DTT/EDTA solutions was prepared. Each sample was subjected to the following steps. A pipet was used to underlay the water in the centrifuge tube with 270 μ L of the guanidine·HCl/DTT/EDTA mixture. The 780 μ L Hr/CsCl mixture was placed on the very bottom of the tube and then underlaid by 270 μ L of the guanidine·HCl/DTT/EDTA solution. This resulted in the protein solution being dispersed between the two guanidine·HCl layers. The guanidine·HCl was used to unfold the protein so that any sulfide buried in the protein structure protected from the DMPD would be exposed. A 2.87 mL volume of water (pH ~ 11.0) was carefully layered on the top of the liquid column, so that the layers remained undisturbed. The tube was stoppered and allowed to sit at room temperature. After two hours, the tube was opened, and 1 mL 0.1 % DMPD solution was added at the

bottom of the centrifuge tube. Stirring was initiated followed by injection of 200 μ L 50 mM FeCl_3 under the surface. The mixture was incubated at 25 °C for 30 minutes to an hour to ensure complete methylene blue formation. Centrifugation was usually not required because no protein precipitated. The absorbance at 670 nm was then used to determine sulfide plus sulfane sulfur concentration.

G. Attempts at Preparation of μ -SelenidometHr

μ -Se²⁻-semi-metHr was prepared by direct addition of a 4 to 8-fold molar excess of Na_2Se to anaerobic solutions of metHr as described in section II-E. One experiment was conducted in 50 mM Bis/tris/acetate at pH 6.3, and a second was performed at pH 8.0 in 50 mM Tris/perchlorate. In both cases, formation of μ -Se²⁻-semi-metHr was verified by EPR. The μ -Se²⁻-semi-metHr prepared at pH 6.3 was dialyzed against a nitrogen-saturated 2.34 mM $\text{K}_3\text{Fe}(\text{CN})_6$ solution at 4 °C for 12 hours. The protein was then transferred to a nitrogen-saturated liter of 50 mM Bis/tris/acetate pH 6.3 and allowed to dialyze for 6 hours anaerobically at 4 °C to remove excess ferricyanide. Four equivalents of a stock $\text{K}_3\text{Fe}(\text{CN})_6$ solution were added directly to the pH 8.0 protein via gas-tight syringe. After 20 minutes reaction time, the protein mixture was dialyzed anaerobically against a liter of the appropriate

buffer for removal of excess ferricyanide. The reaction progress was monitored by UV-visible spectroscopy.

H. Preparation and Detection of a Sulfide Complex of DeoxyHr (deoxyS²⁻)

Three approaches were utilized to examine interactions of sulfide with deoxyHr. The first of these methods was based on monitoring the formation of μ -S²⁻-metHr upon oxidation of deoxyHr equilibrated with sulfide. The second procedure involved examination of the EPR spectrum of a Hr adduct formed by addition of excess azide to deoxyHr (deoxyN₃⁻) in the presence of excess sulfide. Finally, attempts were made to reduce μ -S²⁻-semi-metHr to the deoxy oxidation level with dithionite. All procedures were carried out anaerobically. All of the dialysis reactions were performed at 4 °C in nitrogen-saturated buffer in flasks which were sealed off from air under an atmosphere of nitrogen.

1. Method one: Oxidation of deoxyHr plus sulfide

DeoxyHr was prepared in 50 mM Tris/acetate at pH 8.0 as described in Section II-B. The 1.37 mM deoxyHr was transferred to a liter of buffer which contained 4.6 mM Na₂S·9H₂O. After forty hours equilibration time at 4 °C, the

protein solution still appeared to be colorless. A second liter of nitrogen-saturated buffer was used to prepare a 2.58 mM $K_3Fe(CN)_6$ solution. The dialysis bag containing the deoxyHr/sulfide equilibration was placed in this ferricyanide solution and allowed to dialyze overnight. For removal of the excess ferricyanide, the dialysis sack was then transferred to a final liter of anaerobic buffer for overnight dialysis. Some precipitate was visible in the final reaction mixture. A UV-visible spectrum was taken to determine the product(s) and the protein concentration.

Since the reaction of the oxyHr with sulfide results in the bleaching of the characteristic oxyHr UV-visible spectrum, i.e., the formation of deoxyHr (see Figure II-2), it was used as a means of equilibrating deoxyHr with excess sulfide. An oxyHr sample 1.4 mM in protein was placed in a dialysis bag and dialyzed against a liter of buffer containing 3.5 mM $Na_2S \cdot 9H_2O$. After 20 hours reaction time, the colorless protein was placed in an anaerobic buffer solution of 2.1 mM ferricyanide. After 13 hours of dialysis, the sack was transferred to a liter of buffer and dialyzed to remove the excess reagents. UV-visible spectroscopy was used to monitor the reaction product(s).

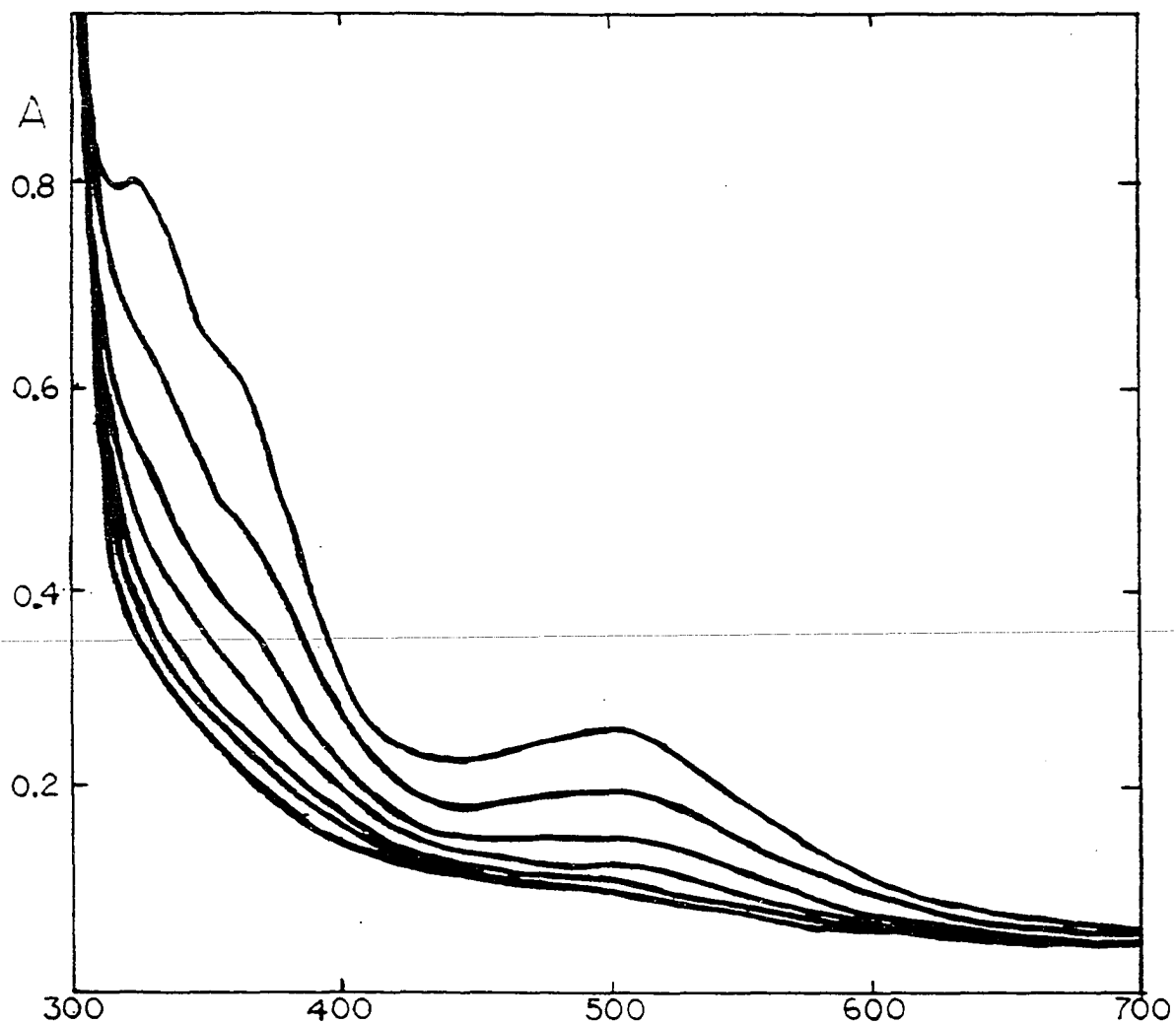


Figure II-2. Absorption spectra observed during the anaerobic incubation of 0.12 mM oxyHr with 1.23 mM sulfide in 50 mM Tris/acetate pH 8.0 at room temperature

Cell pathlength = 1 cm. Spectra were taken at 20 minute intervals

2. Method two: EPR titration of deoxyN₃⁻ with sulfide

Four separate sets of EPR experiments were conducted in which various mixtures of deoxyHr, sulfide and/or azide were used. 1) DeoxyN₃⁻ EPR samples were made up as standards using N₃⁻ to deoxyHr molar ratios of 36:1 and 110:1. EPR samples containing reaction mixtures of sulfide and deoxyHr in molar ratios of 39:1 and 112:1 were frozen. 2) 7.42×10^{-4} M deoxyHr was equilibrated with a 36-fold molar excess of NaSH (0.0265 M sulfide). At various times during the equilibration, 0, 25, and 55 minutes, a 37-fold molar excess of NaN₃ was added. EPR samples were frozen immediately after introduction of azide into the system. 3) A 36-fold molar excess of NaN₃ (0.0273 M) was added to 7.42×10^{-4} M deoxyHr sample. Addition of azide was followed by immediate addition of a 37-fold molar excess of NaSH and freezing of an EPR sample. 4) Nine hundred microliters of 1.29 mM deoxyHr were mixed with 80 μ L 48.9 mM NaN₃. The reaction mixture was divided into five samples which were placed in degassed EPR tubes that contained various amounts of a stock sulfide solution; each sample had a final volume of 180 μ L. Molar ratios of deoxyHr:azide:sulfide were as follows: 1:38:0. 1:38:57, 1:38:96, 1:38:153 and 1:38:196.

3. Method three: Reduction of $\mu\text{-S}^{2-}$ -semi-metHr

$\mu\text{-S}^{2-}$ -semi-metHr prepared by the dialysis method was transferred into dialyzate buffer containing 2 mM $\text{Na}_2\text{S}_2\text{O}_4$. During anaerobic dialysis at 4 °C over a period of four days, the reaction was monitored by UV-visible and EPR spectroscopies.

I. Reactivity of the SulfideHrs

1. Reduction potentials

The midpoint reduction potential of the $\mu\text{-S}^{2-}$ -metHr/ $\mu\text{-S}^{2-}$ -semi-metHr couple was determined using $\text{Fe}(\text{CN})_6^{3-}/\text{Fe}(\text{CN})_6^{4-}$ and cytochrome c (Fe^{3+})/cytochrome c (Fe^{2+}) couples as redox partners. Stock solutions of $\mu\text{-S}^{2-}$ -metHr were prepared by the dialysis method described in Section II-F. $\mu\text{-S}^{2-}$ -semi-metHr stock solutions were made by direct addition of one equivalent of dithionite to $\mu\text{-S}^{2-}$ -metHr in 50 mM Tris/perchlorate pH 8.0 or by dialysis of metHr against sulfide in an anaerobic Tris/acetate pH 8.0 solution. Concentrations of the stock protein solutions were between 1 and 3 mM with the excess reagents being removed by quick passage over several columns of Sephadex G-25 equilibrated in the appropriate buffer. All measurements were made anaerobically in 50 mM buffer containing 50 mM Na_2SO_4 at pH 8.0 and 25 °C.

Keeping the total concentration of $\text{Fe}(\text{CN})_6^{3-}$ plus

$\text{Fe}(\text{CN})_6^{4-}$ constant at either 40 or 80 mM, anaerobic solutions containing various ratios of $\text{K}_3\text{Fe}(\text{CN})_6$ to $\text{K}_4\text{Fe}(\text{CN})_6$ were prepared in either Tris/acetate or Tris/perchlorate pH 8.0. A value of $E_{\text{pH } 8.0} = 430$ mV versus NHE was used for the $\text{Fe}(\text{CN})_6^{3-}/\text{Fe}(\text{CN})_6^{4-}$ couple (68). The absorbance of each $\text{Fe}(\text{CN})_6^{3-}/\text{Fe}(\text{CN})_6^{4-}$ solution was background corrected against an $\text{Fe}(\text{CN})_6^{4-}$ stock solution before addition of the protein. Aliquots of $\mu\text{-S}^{2-}\text{-metHr}$ or $\mu\text{-S}^{2-}\text{-semi-metHr}$ stock solutions were added to the ferri/ferrocyanide solutions such that the total protein concentrations fell into the range of 0.10-0.16 mM. Relative concentrations of $\mu\text{-S}^{2-}\text{-metHr}$ and $\mu\text{-S}^{2-}\text{-semi-metHr}$ at equilibrium were determined from absorbances at 500 and 544 nm. The molar extinction coefficients used for $\mu\text{-S}^{2-}\text{-metHr}$ were $\epsilon_{500} = 3920 \text{ M}^{-1}\text{cm}^{-1}$ and $\epsilon_{544} = 3300 \text{ M}^{-1}\text{cm}^{-1}$ (determined by iron analyses described in Section II-F); $\epsilon_{500} = 1100 \text{ M}^{-1}\text{cm}^{-1}$ and $\epsilon_{544} = 1000 \text{ M}^{-1}\text{cm}^{-1}$ (65) were the values for $\mu\text{-S}^{2-}\text{-semi-metHr}$. Equilibrium was attained in approximately 30 minutes in Tris/perchlorate and approximately 15 minutes in Tris/acetate. Least squares analyses of data points from 3-6 titrations were used to generate the lines from which the midpoint potentials were extracted.

For the equilibration of the two sulfide derivatives with cytochrome c, oxidized horse heart cytochrome c ($\text{Fe}^{3+}\text{cyt c}$) Type III was purchased from Sigma. Ferrocycytochrome c ($\text{Fe}^{2+}\text{cyt c}$) was obtained from $\text{Fe}^{3+}\text{cyt c}$ either by dialysis

against or direct addition of dithionite. Cytochrome c concentrations were determined by visible absorbances at 550 nm and 528 nm ($\epsilon_{550}=29,500 \text{ M}^{-1}\text{cm}^{-1}$ for Fe^{2+} cyt c, $\epsilon_{550}=9000 \text{ M}^{-1}\text{cm}^{-1}$ and $\epsilon_{528}=11,200 \text{ M}^{-1}\text{cm}^{-1}$ for Fe^{3+} cyt c) (99, 100). The reactions of $\mu\text{-S}^{2-}$ metHr with Fe^{2+} cyt c and of $\mu\text{-S}^{2-}$ semi-metHr with Fe^{3+} cyt c were monitored at 500 nm with the reaction mixtures being equimolar in cyt c and hemerythrin. All initial sulfideHr concentrations were 0.11 mM. Visible absorbances could not be used in determination of $\mu\text{-S}^{2-}$ metHr and $\mu\text{-S}^{2-}$ semi-metHr concentrations at equilibrium because of the intense absorbance due to cytochrome c. Therefore these concentrations were estimated by double integration of the $\mu\text{-S}^{2-}$ semi-metHr and Fe^{3+} cyt c EPR spectra. These two spectra do not overlap. An $E_{\text{pH } 8.0}$ of 0.26 V versus NHE was used for cytochrome c (69, 101); this is the same value used by Armstrong et al. in calculating reduction potentials of other derivatives of hemerythrin (see Table I-6) (57).

2. General reaction conditions

Generally all reactions described below were monitored by UV-visible and EPR spectroscopies. EPR samples were 6.0×10^{-4} to 2.0×10^{-3} M in protein. The UV-visible samples, which were dilutions of the EPR samples, were 1.0×10^{-4} to 2.0×10^{-4} M in protein. All reactions were conducted in 50 mM Tris/acetate pH 8.0 unless noted differently. Dialyzate

solutions typically were one liter volumes kept at 4 °C for the duration of the reaction. For reactions requiring direct addition of reagents, stock solutions were prepared by dissolving reagent grade commercial samples of the sodium salts of azide, chloride, thiocyanate, cyanide and fluoride in the appropriate buffer. Direct addition reactions were carried out at room temperature. In reactions of the $\mu\text{-S}^{2-}\text{Hrs}$ with O_2 , stirred solutions were left open to air at room temperature. No attempts were made to add known quantities of O_2 .

3. Stability of $\mu\text{-S}^{2-}$ semi-metHr

Four samples of $\mu\text{-S}^{2-}$ semi-metHr were prepared using the dialysis method. After formation of the desired protein product, three dialysis bags were transferred to anaerobic sulfide-free buffer for extended dialysis at 4 °C. An EPR sample was prepared from the fourth sample to be used as a reference. The remaining protein samples were transferred to fresh nitrogen-saturated buffer every 24 hours. EPR samples and UV-visible spectra were obtained for these samples after 3, 7 and 20 days of dialysis. Addition of excess azide to the UV-visible samples was helpful in characterizing the final product.

4. $\mu\text{-S}^{2-}$ semi-metHr + ligand anions

The reaction of $\mu\text{-S}^{2-}$ semi-metHr with azide was carried out by dialysis or by direct addition of azide to $\mu\text{-S}^{2-}$ semi-metHr via gas-tight syringe. Typically 2-3 mL of 1 mM $\mu\text{-S}^{2-}$ semi-metHr were dialyzed against nitrogen-saturated buffer containing 2.0-6.5 mM NaN_3 . Dialysis experiments were monitored for a maximum of 16 days. In the case of direct addition of azide, $\mu\text{-S}^{2-}$ semi-metHr concentrations ranged from 1.1×10^{-4} to 6.1×10^{-4} M and a 20 to 50-fold molar excess of azide was utilized. These reactions were carried out at room temperature and monitored for approximately 4 hours. Interaction of excess fluoride added directly to $\mu\text{-S}^{2-}$ semi-metHr was examined for a reaction time of 30 minutes at room temperature.

5. $\mu\text{-S}^{2-}$ semi-metHr + O_2

Excess sulfide was removed from $\mu\text{-S}^{2-}$ semi-metHr prepared via dialysis by passage over a Sephadex G-25 column. A disposable Pasteur pipet was used to bubble air through a 6.2×10^{-4} M $\mu\text{-S}^{2-}$ semi-metHr sample which was monitored by UV-visible spectroscopy for 11 hours. Reaction mixtures containing 1.0-1.8 mM $\mu\text{-S}^{2-}$ semi-metHr left stirring open to air were monitored by EPR for time periods ranging from 40 minutes to 9 hours. After being exposed to O_2 for 1 1/2 hours, one reaction sample was passed over a Sephadex G-25

column and a second sample was treated with excess azide before they were frozen for inspection by EPR. In a separate experiment, μ -S²⁻-semi-metHr was exposed to air for 40 minutes; after this time, the reaction mixture was divided into four samples. One sample was frozen as a reference. A 40-fold molar excess of dithiothreitol (DTT) was added to the second sample 4 minutes before it was frozen for EPR. The third sample was reacted with a 40-fold molar excess of ascorbate 5 minutes prior to freezing. The final sample was treated with a 40-fold molar excess azide also as a reference.

A stock solution of μ -S²⁻-semi-metHr was prepared in 50 mM Tris/perchlorate pH 8.0. The reaction of this stock solution with O₂ after removal of excess sulfide was monitored for ~ 6 hours. The EPR samples contained 1.94 mM protein. A power saturation study was performed on the final EPR sample. The temperature dependence of this final EPR sample's spectrum was done to ascertain any differences in the behavior of the g = 2.02 signal compared to the typical semi-metHr EPR signals. The UV-visible spectra were obtained from 0.18 mM samples which were obtained by dilution of the stock protein used for the EPR samples. Fresh UV-visible samples were prepared for each spectrum. Addition of a 50-fold molar excess of azide to these UV-visible samples were used to characterize the product.

The reaction mixture of 1.94 mM μ -S²⁻-semi-metHr prepared

in Tris/perchlorate pH 8.0 and azide in a molar ratio of 1:265 left open to air was monitored for ~ 6 hours by EPR. During this time period, UV-visible spectra were obtained from dilutions of the reaction mixture.

6. (Semi-met)_O → (semi-met)_R conversion

Because the μ -S²⁻semi-metHr plus O₂ reaction generated EPR spectra which resembled that of (semi-met)_O, the (semi-met)_O → (semi-met)_R conversion was monitored under comparable conditions. (Semi-met)_O was generated by addition of one equivalent of ferricyanide to deoxyHr and allowed to incubate at room temperature. Both UV-visible and EPR samples were taken periodically. The reaction performed with 0.55 mM protein in Tris/acetate pH 8.0 was monitored for 50 minutes. The same reaction conducted in Tris/perchlorate pH 8.0 utilized 0.80 mM protein and was followed for 350 minutes.

7. Stability of μ -S²⁻metHr

μ -S²⁻metHr samples 0.58 to 1.78 mM in Hr were prepared in 50 mM Tris/acetate pH 8.0 and in 50 mM Tris/perchlorate pH 8.0. One to two milliliter samples were placed in argon-filled septum-capped vials and incubated at room temperature under positive argon pressure. These anaerobic samples were monitored by EPR spectroscopy for periods of time ranging from 50 to 88 hours. The corresponding UV-visible samples were

8.0×10^{-5} to 2.2×10^{-4} M in monomer and were monitored in a double-septum quartz cell for times of 30 to 55 hours.

One preparation of $\mu\text{-S}^{2-}\text{metHr}$ in Tris/perchlorate was divided into two 800 μL samples. One sample was incubated anaerobically at room temperature as described in the previous paragraph. A 12.5 μL volume of 0.038 M $\text{K}_3\text{Fe}(\text{CN})_6$ solution was added via syringe to the second 0.58 mM $\mu\text{-S}^{2-}\text{metHr}$ sample. In the presence of one equivalent of ferricyanide, the second sample was incubated under the same conditions as the first sample. Both samples were monitored for 88 hours by EPR spectroscopy.

8. $\mu\text{-S}^{2-}\text{metHr}$ + ligand anions

The anaerobic reactions of $\mu\text{-S}^{2-}\text{metHr}$ with azide, chloride and cyanide were performed by direct addition of stock solutions of the desired reagent. The reaction of $\mu\text{-S}^{2-}\text{metHr}$ with azide was carried out using $\text{N}_3^-/\mu\text{-S}^{2-}\text{metHr}$ molar ratios (concentration of Hr) of 36(0.66 mM), 180(0.35 mM) and 570(1.48 mM). The reaction mixtures, 0.66 mM and 1.48 mM in Hr, were monitored by EPR spectroscopy for 24 hours. All three reaction mixtures were followed by UV-visible spectroscopy for 10-24 hours. The reactions of 0.15 mM $\mu\text{-S}^{2-}\text{metHr}$ with a 685-fold molar excess of chloride and a 100-fold molar excess of cyanide were monitored for 9 hours by UV-visible spectroscopy. After 9 hours, excess azide was

added to both reaction mixtures in an effort to identify the products.

Five aerobic 1.05 mL samples 9.5×10^{-5} M in μ -S²⁻metHr were prepared in Tris/perchlorate pH 8.0 for UV-visible spectroscopy. Ten microliters of a stock ligand anion solution were added to each UV-visible sample. The resulting ligand anion/ μ -S²⁻metHr molar ratios were: 99 N₃⁻, 248 N₃⁻, 129 CN⁻, 162 SCN⁻ and 110 Cl⁻. The reactions were monitored for 5 to 30 minutes after which time they were stored at 4 °C for 3 days. After three days, the UV-visible spectra were examined. A similar experiment was performed in Tris/acetate pH 8.0.

A reaction mixture of μ -S²⁻metHr in Tris/perchlorate with a 200-fold molar excess of azide was exposed to the light of a projector bulb for 55 minutes. Changes in the UV-visible spectrum were followed during this same time period. A similar experiment was attempted using a 200-fold molar excess of SCN⁻. However, in this case, the protein was considerably less stable upon irradiation making the reaction difficult to monitor.

9. μ -S²⁻met-Hr + sulfide

The reaction of μ -S²⁻metHr with sulfide was carried out using several different sources of sulfide. Stock sulfide solutions were made up from either sodium sulfide or sodium

hydrogen sulfide; the sulfide concentration was determined by iodometric titration of the stock solution (see Appendix B). Two-tenths to four molar equivalents of sulfide were added to anaerobic solutions of $\mu\text{-S}^{2-}\text{metHr}$. The volume of $\text{H}_2\text{S}_{(g)}$ required for addition of four equivalents of sulfide to stock $\mu\text{-S}^{2-}\text{metHr}$ was calculated using the ideal gas law. All three reactions were monitored with time by UV-visible and EPR spectroscopies for up to 4 hours.

10. $\mu\text{-S}^{2-}\text{metHr}$ + reducing agents

Addition of one reducing equivalent of dithionite to $\mu\text{-S}^{2-}\text{metHr}$ yielded $\mu\text{-S}^{2-}\text{semi-metHr}$. The dithionite concentration was determined by a ferricyanide titration similar to the one described earlier in this section. The reaction product was characterized by use of EPR and UV-visible spectroscopies. Reduction was also attempted with excesses of ferrocyanide, thiosulfate and sulfite added from stock solutions of the sodium salts.

11. $\mu\text{-S}^{2-}\text{metHr}$ + O_2

The reaction of $\mu\text{-S}^{2-}\text{metHr}$ with O_2 was examined in both Tris/acetate and Tris/perchlorate by EPR and UV-visible spectroscopies. The reaction was followed for ~ 6 hours in Tris/acetate and ~ 12 hours in Tris/perchlorate. Excess azide was added to the final product in all cases.

The aerobic reaction of $\mu\text{-S}^{2-}\text{metHr}$ with azide was also examined in Tris/acetate and Tris/perchlorate. The azide concentrations ranged from a 35-fold to a 550-fold molar excess of Hr. The azide was added to the solutions of $\mu\text{-S}^{2-}\text{metHr}$ immediately after the protein was opened to air.

12. $\mu\text{-S}^{2-}\text{metHr}$ + other oxidizing agents

Two potential oxidizing agents other than molecular oxygen were added to solutions of $\mu\text{-S}^{2-}\text{metHr}$ under anaerobic conditions. Hydrogen peroxide was added to the protein in molar ratios $\text{H}_2\text{O}_2:\mu\text{-S}^{2-}\text{metHr}$ of 1:1 and 16:1. The second oxidizing agent ferricyanide was added in a 32-fold molar excess over Hr. Both reactions were followed for 7-12 hours by UV-visible spectroscopy.

III. RESULTS AND DISCUSSION

A. Preparation and Characterization of μ -Sulfidosemi-metHr

The absorption spectrum of the purple sulfide derivative of Hr prepared by reaction of metHr with sulfide contains a prominent shoulder at 340 nm and a broad maximum near 500 nm (see Figure III-5D). The resonance Raman spectrum of this derivative obtained with 368.8 nm excitation is shown in Figure III-1. The spectral features are the same as those obtained previously by Freier and co-workers using 514.5 nm excitation (65). As mentioned in Section I-C, the peak at 444 cm^{-1} is assigned to the symmetric vibration of an Fe-S-Fe moiety. This 444 cm^{-1} is approximately five-fold more intense with 363.8 nm excitation than with 514.5 nm excitation, indicating that the absorption band at 340 nm has considerable $S^{2-} \rightarrow Fe$ charge transfer character.

^{57}Fe Mössbauer spectra of crystals of this purple derivative are given in Figure III-2. The spectra recorded at $T > 60\text{ K}$ can be resolved into four Lorentzians of roughly equal areas and a minor doublet accounting for $11 \pm 2\%$ of the total area, as illustrated for the 200 K spectrum in Figure III-2a. The four major components can be assigned to two quadrupole doublets, A and B, on the basis of the temperature dependence of their energies (see Table III-1). A crystalline

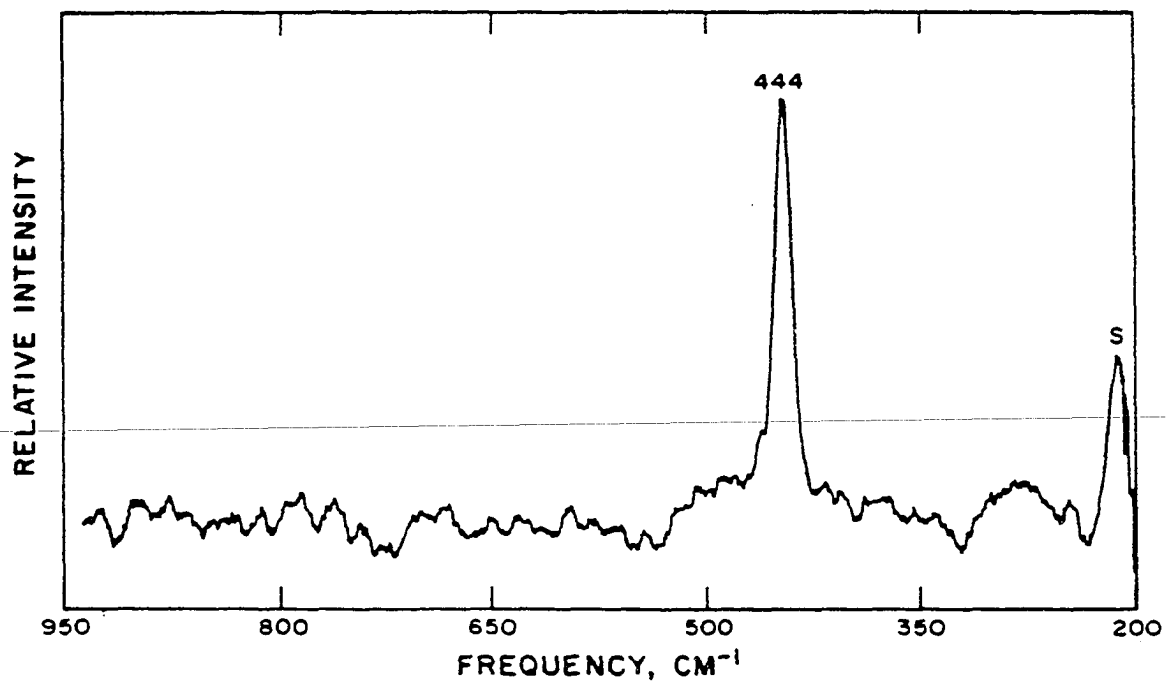


Figure III-1. Resonance Raman spectrum of 2 mM μ -S²-semi-met. Hr in 50 mM Tris/perchlorate pH 8.0

Condition: temperature, 243 K; excitation, 363.8 nm, 12 mW; scan rate, 1 cm⁻¹/s; slit width, 8 cm⁻¹; 11 scans averaged

Figure III-2. Mössbauer spectra of crystalline $\mu\text{-S}^{2-}$ -semimetal

Spectra were taken in zero field at 200 K(a) and 4.2 K(b). The solid line in (a) which traces the observed spectrum is a simulation assuming one minor and two major doublets D, A and B accounting for 12.5, 45 and 42 percent of the total area, respectively. The solid line in (a) above the observed-spectrum depicts the minor doublet, D. The much larger splitting in spectrum (b) is evidence for magnetic hyperfine interactions at both major iron sites. A sharp quadrupole doublet at 0.49 and 1.55 mm/s, due to a minor diamagnetic species, D accounting for 12 percent of the total area, has been subtracted from (b)

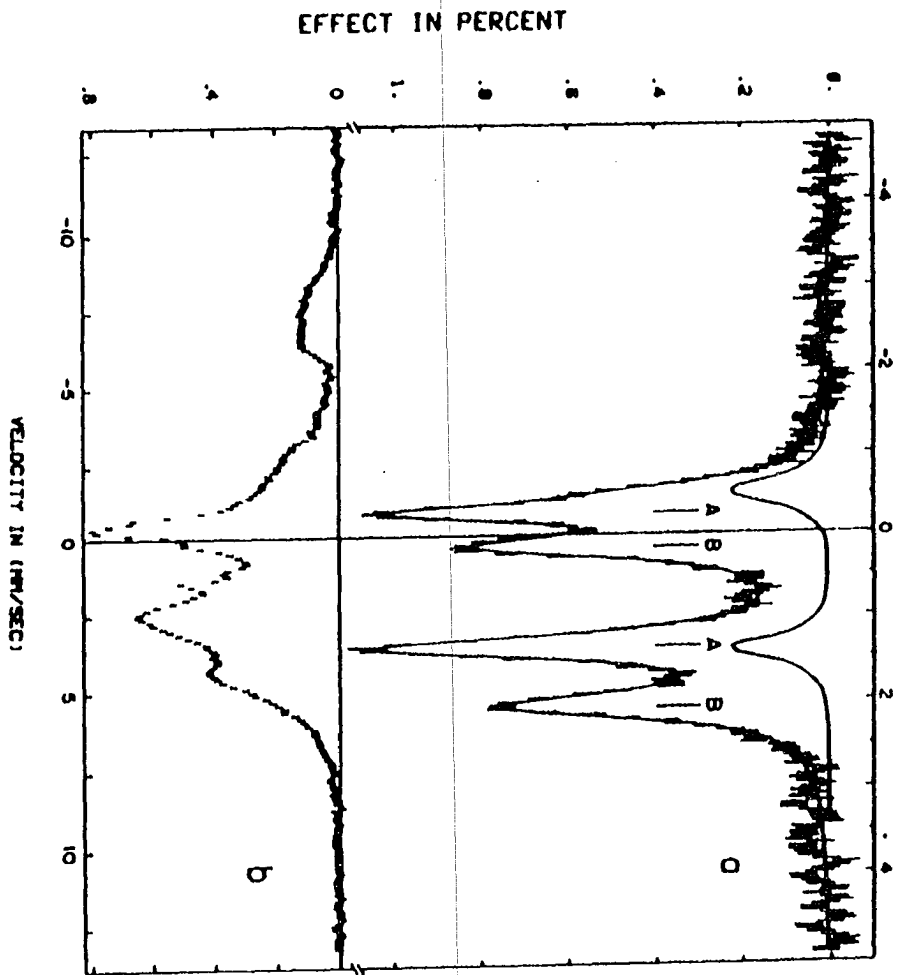


Table III-1. Mössbauer parameters for crystalline $\mu\text{-S}^{2-}$ semi-methr. Quadrupole splittings, ΔE_q , and isomer shifts, δ_{Fe} , of the three components A, B and D at 60 K, 100 K and 200 K

T	60	100	200	K
ΔE_q (A)	1.57	1.58	$1.63 \pm .02$	mm/s
δ_{Fe} (A)	0.57	0.58	0.53	mm/s

ΔE_q (B)	2.59	2.43	1.88	mm/s
δ_{Fe} (B)	1.16	1.14	1.10	mm/s

ΔE_q (D)	2.04	2.05	$1.92 \pm .05$	mm/s
δ_{Fe} (D)	0.53	0.53	0.43	mm/s

sample of aquometHr (high spin ferric) gave the quadrupole splittings, ΔE_q (isomer shift, δ_{Fe}) in mm/s of 1.61(0.48) at 4.2 K, 1.62(0.47) at 100 K, and 1.62(0.43) at 200 K. Published values for deoxyHr (high spin ferrous) are 2.89(1.17) at 4.2 K, 2.86(1.15) at 77 K and 2.75(1.11) at 195 K (see Table I-3) (44, 45). By comparison with these data, the two doublets, A and B in Figure III-2a can be assigned to an Fe(III), $S_A=5/2$, and Fe(II), $S_B=2$, respectively. A solution obtained by addition of 0.1 M Na_2S to crystalline aquometHr yields a Mössbauer spectrum at 200 K very similar to the one in Figure III-2a, including the contribution of the minor doublet. Resolution of two quadrupole doublets, one for Fe(II) and another for Fe(III), indicates that electron exchange within the [Fe(II), Fe(III)] pair must be slow relative to the Mössbauer time scale (10^{-7} s).

In contrast to all previously published Mössbauer spectra of hemerythrin derivatives (44, 45, 102, 103), those of this purple sulfide derivative recorded at 4.2 K show resolved magnetic hyperfine splittings. MetHr and oxyHr each contain a pair of high-spin ferric ions which are antiferromagnetically coupled to give a diamagnetic ground state (see Figure I-10). Thus, in contrast to that in Figure III-2b, magnetic splitting of their Mössbauer spectra is not observed in zero applied field. The minor component D of Figure III-2a must be similar

in nature to iron sites in oxyHr and metHr because it remains a sharp quadrupole doublet in all magnetically split spectra. However, $\Delta E_q(D)$ and $\delta_{Fe}(D)$ are different from those of metHr and oxyHr (see Table I-3), and the D component remains unidentified. Mössbauer spectra of the purple sulfide derivative measured in weak applied fields (~350 G) at 4.2 K show overall splittings of ~7.5 mm/s and vary substantially with the direction of the field; such field dependence is a strong indication of an EPR active center.

Examination of crystalline and solution samples of the purple sulfide derivative by EPR spectroscopy reveals an EPR active center at temperatures below 30 K. The EPR spectrum is shown in Figure III-3 and has g-values of 1.883 ± 0.004 , 1.709 ± 0.007 and 1.400 ± 0.006 . These values are close to those of semi-metN₃⁻ (see Table I-5) although the spectrum of μ -S²⁻-semi-metHr is significantly broader. The combined Mössbauer and EPR data can be explained by the standard spin-coupling model based on strong isotropic exchange (74), using a Hamiltonian $\mathcal{H} = JS_A \cdot S_B$ with $J < 0$. According to this model, the ground state has a net spin $S = 1/2$ and g-tensor $g = 7/3g_A - 4/3g_B$, where g_A and g_B are the intrinsic g-tensors of the high spin ferric, $S_A = 5/2$, and ferrous, $S_B = 2$, ions, respectively. This coupling leads to the same ladder of spin states described in Section I-E for the reduced [2Fe-2S] ferredoxins (74, 75). Double integration of the EPR signal

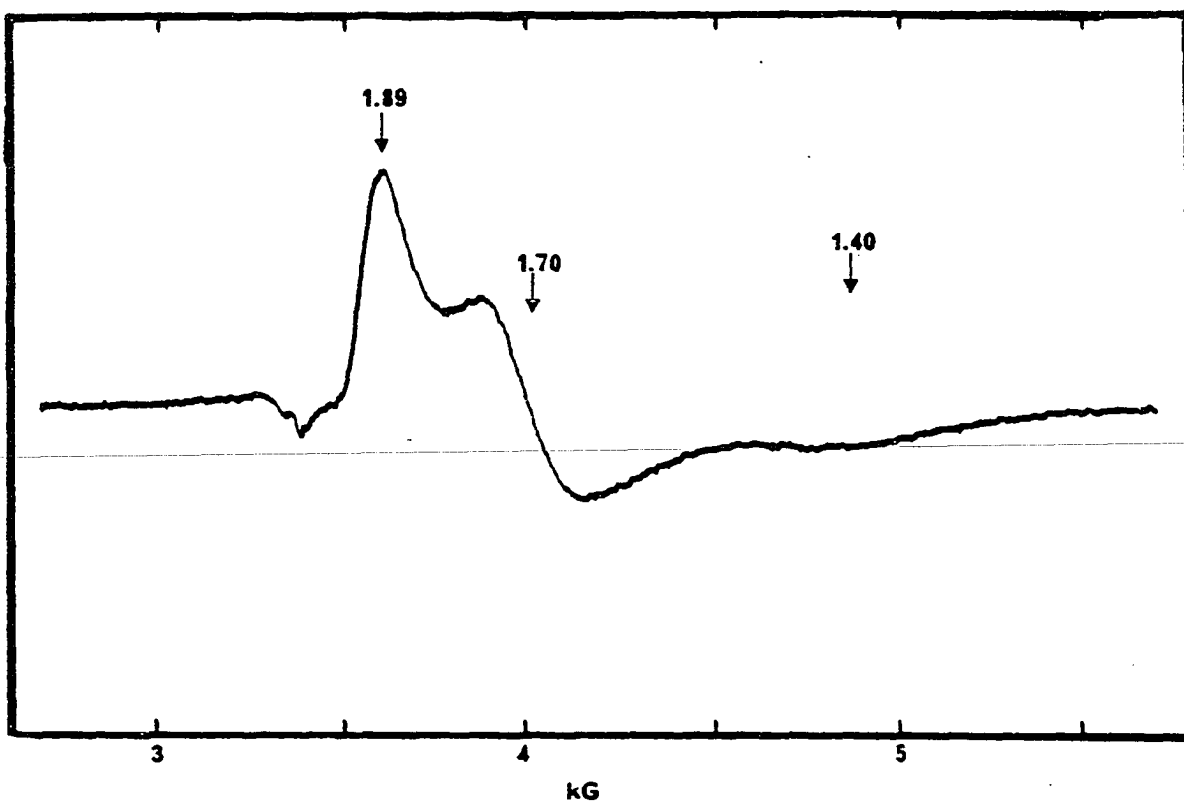


Figure III-3. Derivative EPR spectrum of $\mu\text{-S}^{2-}$ -semi-metHr

$\mu\text{-S}^{2-}$ -semi-metHr was prepared by dialysis of metHr against $\text{Na}_2\text{S}\cdot 9\text{H}_2\text{O}$ in 50 mM Tris/acetate pH 8.0. Instrument parameters: temperature, 4.1 K; frequency, 9.658; power, 100 μW ; modulation amplitude, 16 G at 100 kHz; time constant, 0.2 s; receiver gain, 2.0×10^4

confirms that there is one spin per binuclear iron site. If one substitutes the spin only value $g_A=2$ for the high spin ferric g -tensor, the model predicts g_B values of 2.10, 2.22 and 2.45 for the ferrous site, which indicate unexpectedly large contributions to the magnetic moment from spin-orbit interaction among the t_{2g} orbitals. Relatively low-lying orbital states of the ferrous ion can be inferred also from the strong temperature dependence of the quadrupole splitting $\Delta E_q(B)$ (see Table III-1).

The combination of Mössbauer and EPR data establishes the charge and spin states of the individual iron atoms in the purple sulfide derivative as Fe(III), $S_A=5/2$, and Fe(II), $S_B=2$ and the existence of an antiferromagnetic exchange interaction that couples the two spins to a resultant spin of $S=1/2$. Thus, the purple sulfide derivative of Hr will henceforth be referred to as μ -sulfidosemi-metHr.

1. Stoichiometry of the sulfide reaction with metHr

Having established that sulfide reduces metHr to the semi-met oxidation level, titrations of metHr with sulfide were undertaken in an attempt to determine the stoichiometry of the metHr/sulfide reaction and the nature of the sulfide containing ligand. A titration curve obtained by monitoring the absorbance change at 530 nm of metHr reacted with sulfide at various molar ratios is shown in Figure III-4. The

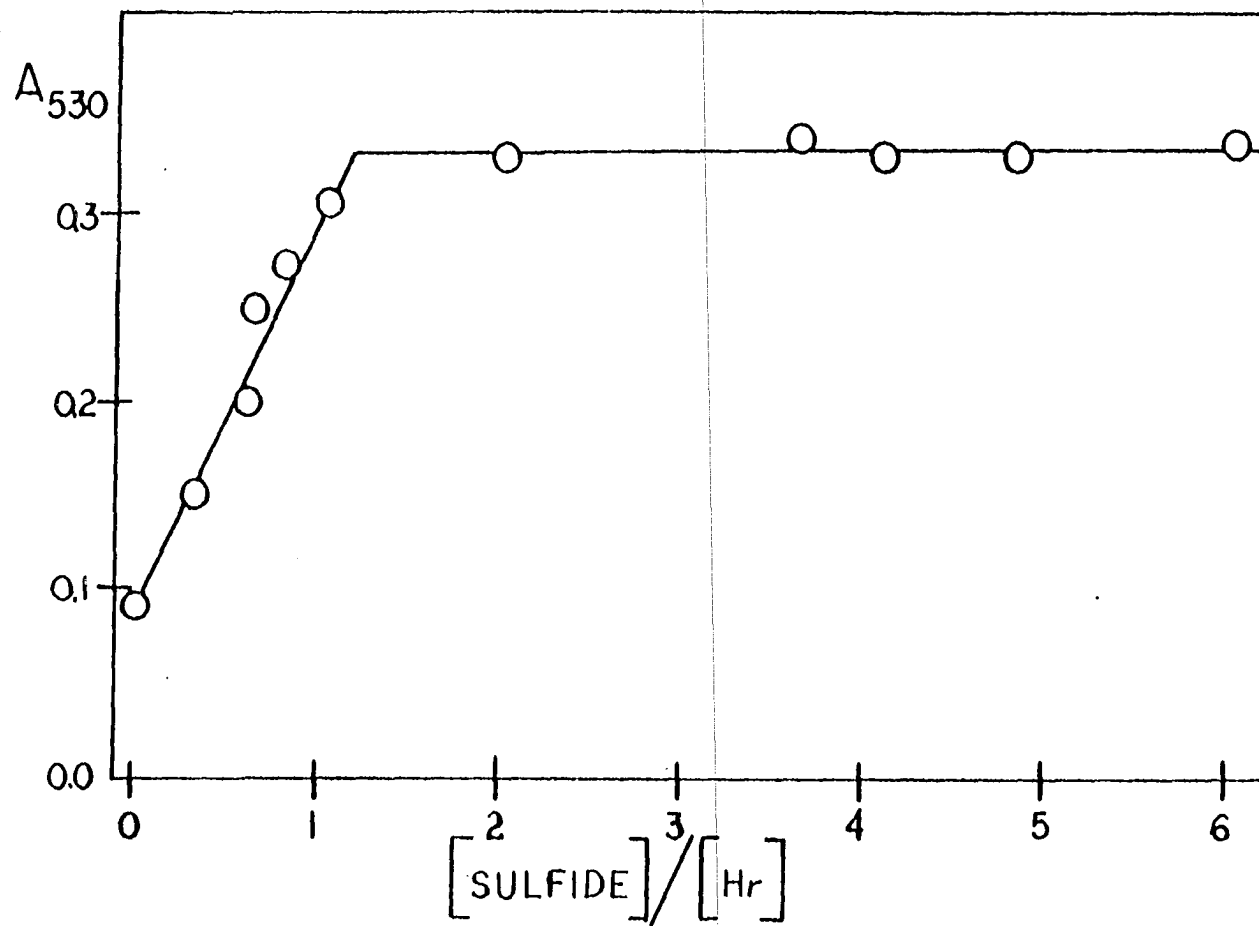


Figure III-4. Absorbance at 530 nm versus the ratio of total stoichiometric sulfide concentration, $[(H_2S) + (HS^-) + (S^{2-})]$, to hemerythrin concentration. (All samples contained 0.30 mM hemerythrin in 50 mM Tris/acetate pH 8.0, 25 °C)

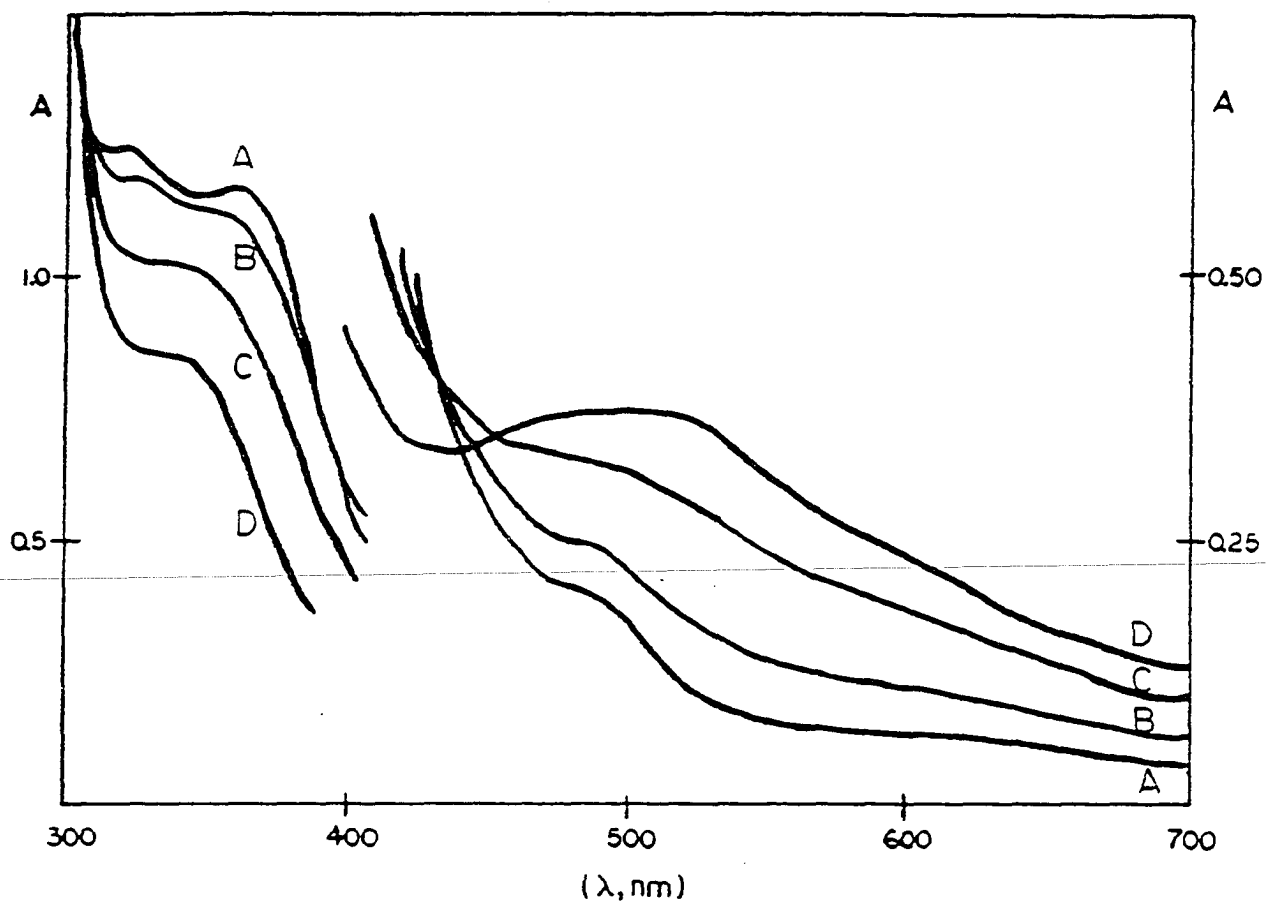
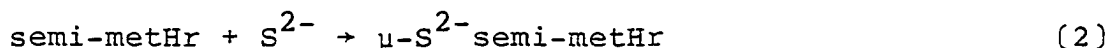
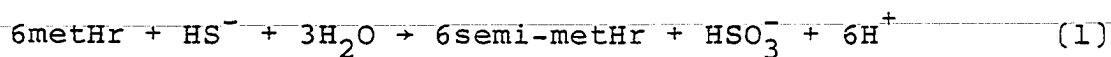


Figure III-5. UV-visible spectra for titration of metHr with sulfide

All samples contained 0.30 mM hemerythrin in 50 mM Tris/acetate pH 8.0, 25 °C. [sulfide]: [Hr], 0, A; 0.36, B; 0.85, C; 1.21, D

UV-visible spectra for some of the points are shown in Figure III-5. Similar curves are obtained at pH 8.0 and pH 6.0. Using least squares analyses to draw the best lines, the endpoints of these titrations are found to be 1.23 ± 0.09 mol sulfide/mol Hr at pH 8.0 and 1.22 ± 0.04 mol sulfide/mol Hr at pH 6.0. The reported values are based on three independent titrations at pH 8.0 and two titrations at pH 6.0. These titrations indicate that 1.2 mol sulfide/mol Hr are required for complete formation of $\mu\text{-S}^{2-}$ -semi-metHr. Theoretically, the consecutive reactions 1 and 2 would require 1.17 mol



sulfide/mol Hr. The reduction potentials of -120 mV (pH 7.0) for the $\text{SO}_3^{2-}/\text{H}_2\text{S}$ half-reaction (104) and 110 mV (pH 8.2) for the metHr/semi-metHr couple (57) indicate that the six electron redox reaction 1 is thermodynamically feasible. Freier and co-workers report a titration curve for metHr with sulfide giving an endpoint of 1.0 mol sulfide/mol Hr (65); it should be noted that an endpoint of 1.2 mol sulfide/mol Hr is within the uncertainty of their data. A sulfide/Hr mol ratio of 1.0 can explain the binding of one sulfide per binuclear iron site, but it cannot account for the fact that the protein

product is at the semi-met oxidation level. A sulfide/Hr mol ratio of 1.2 can explain both reduction of the protein and the incorporation of one sulfide.

When the time course of the reaction of metHr with sulfide is examined by EPR spectroscopy, mixtures of semi-metHr and $\mu\text{-S}^{2-}$ -semi-metHr are seen at reaction times of less than five minutes. Only $\mu\text{-S}^{2-}$ -semi-metHr is observed in the EPR spectra of samples frozen at longer reaction times. Figure III-6 illustrates the EPR time course of the reaction of metHr with various quantities of sulfide using $\text{Na}_2\text{S}\cdot 9\text{H}_2\text{O}$ as the sulfide source. The maximum percentage of Hr in the $\mu\text{-S}^{2-}$ -semi-met form ascertained from EPR integrations is obtained within a range of 5 to 50 minutes. Using NaSH as the sulfide source results in a slightly slower build-up of EPR intensity with the maximum amount of $\mu\text{-S}^{2-}$ -semi-met being present after 60 minutes reaction time. When a molar ratio of 1.0 sulfide/Hr is used (regardless of the sulfide source employed) the EPR intensity decreases after reaching a maximum. Thus, in order to obtain accurate titrations, reaction times of less than one hour must be used. As an illustration two titration curves were obtained for samples which had been allowed to react for 100 to 180 minutes rather than ~ 45 minutes as in the previously described titrations. The longer reaction times gave endpoints of ~ 1.4 mol sulfide/mol Hr.

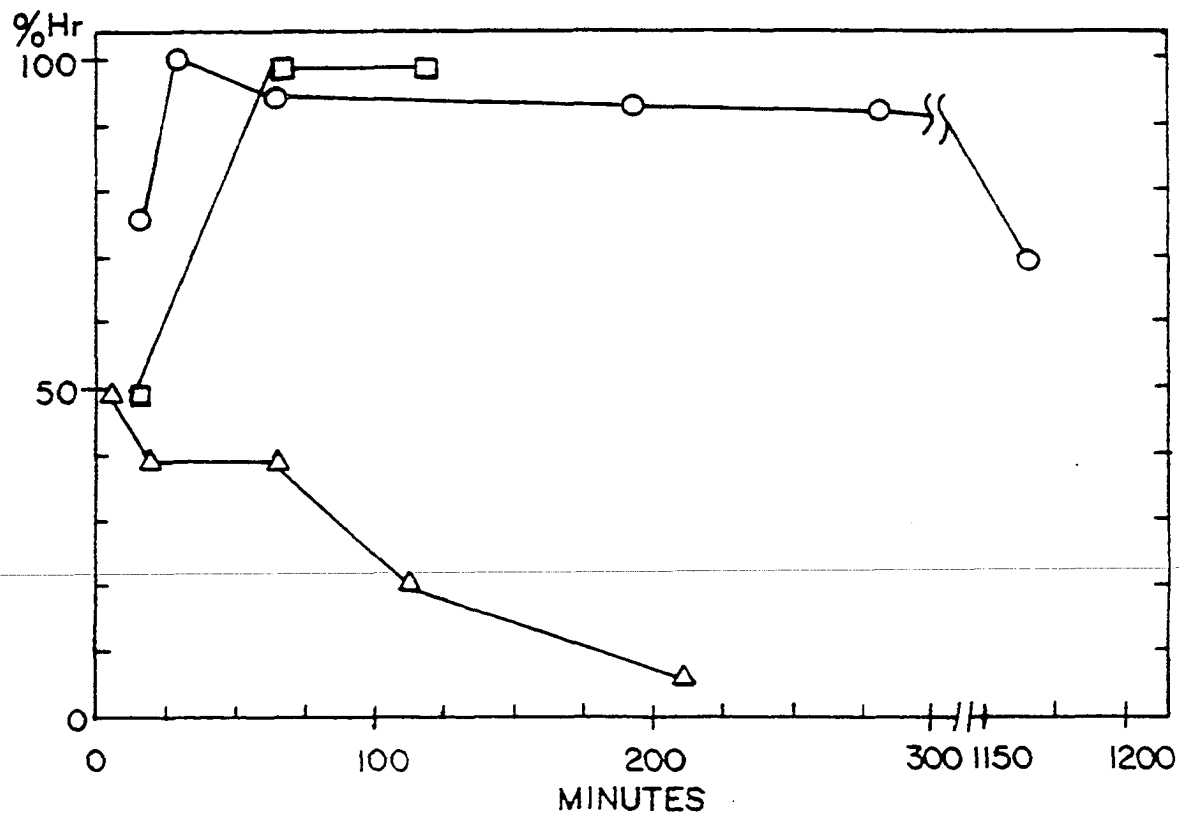
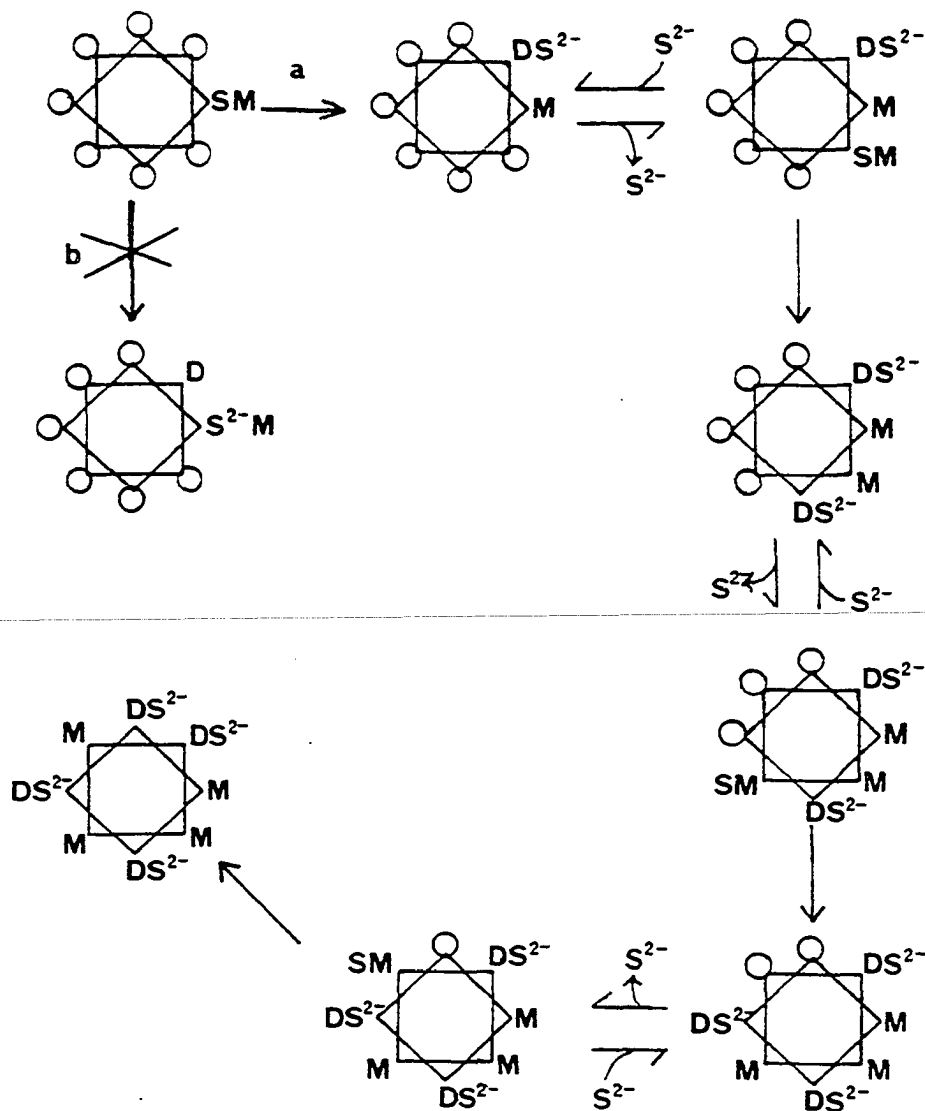


Figure III-6. Plot of percent Hr in the $\mu\text{-S}^{2-}$ -semi-metHr form (as determined by EPR integration) versus reaction time of metHr plus sulfide

The protein was in 50 mM Tris/acetate pH 8.0, 25 °C, $\text{Na}_2\text{S}\cdot 9\text{H}_2\text{O}$ sulfide source. Molar ratio [sulfide]/[Hr] ([Hr]): 1.0 (2.7 mM), Δ ; 2.0 (2.6 mM), \square ; 4.2 (2.5 mM), \circ

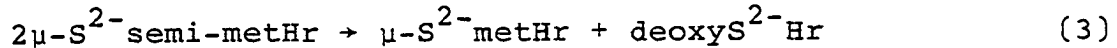
Observation of semi-metHr at early stages of the EPR time course suggests that reduction of metHr occurs initially followed by binding of sulfide. The time course experiments also indicate that binding of sulfide must be relatively strong since the ultimate reduced product is $\mu\text{-S}^{2-}$ -semi-metHr even when sulfide is not present in excess. The explanation for long term instability of the $\mu\text{-S}^{2-}$ -semi-metHr when all the Hr present is not converted to the sulfide derivative (i.e. at a molar ratio of < 1.2 sulfide/Hr) is not clear. One can postulate that decomposition is facilitated by one or more of the subunits of the octamer not binding sulfide thereby remaining in the semi-met form. As illustrated in pathway a of Scheme III-1, disproportionation of these subunits could destabilize the $\mu\text{-S}^{2-}$ -semi-metHr subunit in the octamer resulting in the release of bound sulfide and further disproportionation. UV-visible spectra of reaction solutions with a sulfide/Hr molar ratio of ~ 1 show increases in their absorbance between 300 and 400 nm at long reaction times, indicative of the formation of metHr. This observation supports the idea that the decomposition is due to the disproportionation of semi-metHr via pathway a of Scheme III-1 rather than the disproportionation of fully formed $\mu\text{-S}^{2-}$ -semi-metHr (reaction 3) or pathway b of Scheme III-1. Since the UV-visible spectra do not reflect the formation of $\mu\text{-S}^{2-}$ -metHr which has an intense absorbance at 464 nm

Scheme III-1



μ -S²⁻ semi-met subunits in the Hr octamer are represented by O. Subunits at the met and semi-met oxidation level are abbreviated M and SM, respectively. DS²⁻ and S²⁻M represent subunits at the deoxy and met oxidation levels with a sulfide at the iron site

(Section III-C), pathway b or the disproportionation reaction 3 must not occur to an appreciable extent.



2. Alternate methods of $\mu\text{-S}^{2-}$ semi-metHr preparation

The other methods for preparation of $\mu\text{-S}^{2-}$ semi-metHr, which are discussed below, yield further information about the chemical and physical nature of the adduct.

a) Semi-met_R + NaSH Addition of excess sulfide to (semi-met)_R, which was prepared by reduction of metHr with excess dithionite, results in the formation of $\mu\text{-S}^{2-}$ semi-metHr. Monitoring of the reaction by EPR shows that (semi-met)_R is quantitatively converted to $\mu\text{-S}^{2-}$ semi-metHr, i.e., double integrations of EPR spectra yield concentrations of $\mu\text{-S}^{2-}$ semi-metHr equal to the initial concentrations of (semi-met)_R (see Table III-2). In these experiments, 100 % of the protein is not always accounted for in a paramagnetic state. Reaction times of metHr with excess dithionite are kept short in order to minimize production of deoxyHr. Reaction times following the addition of sulfide to the metHr/dithionite reaction mixture are also kept short to ensure that the only reaction which occurs is ligation of sulfide to (semi-met)_R. With the excesses of sulfide that were employed, reduction of any unreacted metHr by sulfide (or

polysulfide) is a possible reaction. Since reaction 2, ligation of sulfide to $(\text{semi-met})_R$, appears to occur more quickly than reaction 1, reduction of metHr to $(\text{semi-met})_R$, use of short reaction times may prevent contributions of reaction 1 to the amount of Hr which ultimately is converted to $\mu\text{-S}^{2-}$ semi-metHr in these experiments.

Table III-2. $(\text{Semi-met})_R$ reaction with sulfide^a

$[(\text{semi-met})_R]$ (mM)	$[\mu\text{-S}^{2-}\text{semi-metHr}]^b$ (mM)	$\frac{[(\text{semi-met})_R]}{[\mu\text{-S}^{2-}\text{semi-metHr}]}$
1.86	2.18	0.85
1.50	1.57	0.96
1.29	1.34	0.96

^aSemi-met concentrations determined by double integration of EPR spectra.

^bConcentrations of Hr are corrected for dilution due to addition of sulfide to $(\text{semi-met})_R$ solutions so that the $(\text{semi-met})_R$ and $\mu\text{-S}^{2-}$ semi-metHr concentrations can be compared directly.

$(\text{Semi-met})_R$ is generated quantitatively within 15 minutes after addition of one equivalent of dithionite to metHr. When $(\text{semi-met})_R$ prepared in this fashion is titrated with sulfide, one observes the EPR spectra shown in Figure III-7. In this

case, one mole of sulfide/mole Hr results in quantitative formation of $\mu\text{-S}^{2-}$ -semi-metHr from $(\text{semi-met})_{\text{R}}$ when the EPR samples are frozen immediately after addition of sulfide. The corresponding UV-visible titration curve (Figure III-8, ~ 30 minutes reaction time) indicates that one sulfide is required per 2Fe to ensure the complete conversion of $(\text{semi-met})_{\text{R}}$ to $\mu\text{-S}^{2-}$ -semi-metHr. The fact that $\mu\text{-S}^{2-}$ -semi-metHr is the product of the reaction of $(\text{semi-met})_{\text{R}}$ and sulfide lends credence to the suggestion that reduction of metHr (reaction 1) is followed by ligation of sulfide (reaction 2).

b) $(\text{Semi-met})_{\text{O}} + \text{NaSH}$ The EPR spectra obtained for the titration of $(\text{semi-met})_{\text{O}}$ with sulfide are shown in Figure III-9. Table III-3 lists the molar ratios of sulfide to Hr and the percentage of the protein maintained in the semi-met form after the addition of sulfide. The integrated value of the $(\text{semi-met})_{\text{O}}$ concentration of samples containing molar ratios of sulfide/ $(\text{semi-met})_{\text{O}}$ greater than 0.67 is relatively uncertain because of the weak EPR signal and the presence of the background signal of the EPR cavity which is seen at the high gains required to detect the small amounts of semi-metHr. Formation of deoxyHr in this reaction is indicated by the UV-visible spectra for the samples containing ratios of sulfide/ $(\text{semi-met})_{\text{O}} \geq 0.67$. The typical UV-visible spectrum of $\mu\text{-S}^{2-}$ -semi-metHr is not observed; the featureless spectrum of deoxyHr is obtained. This featureless spectrum is

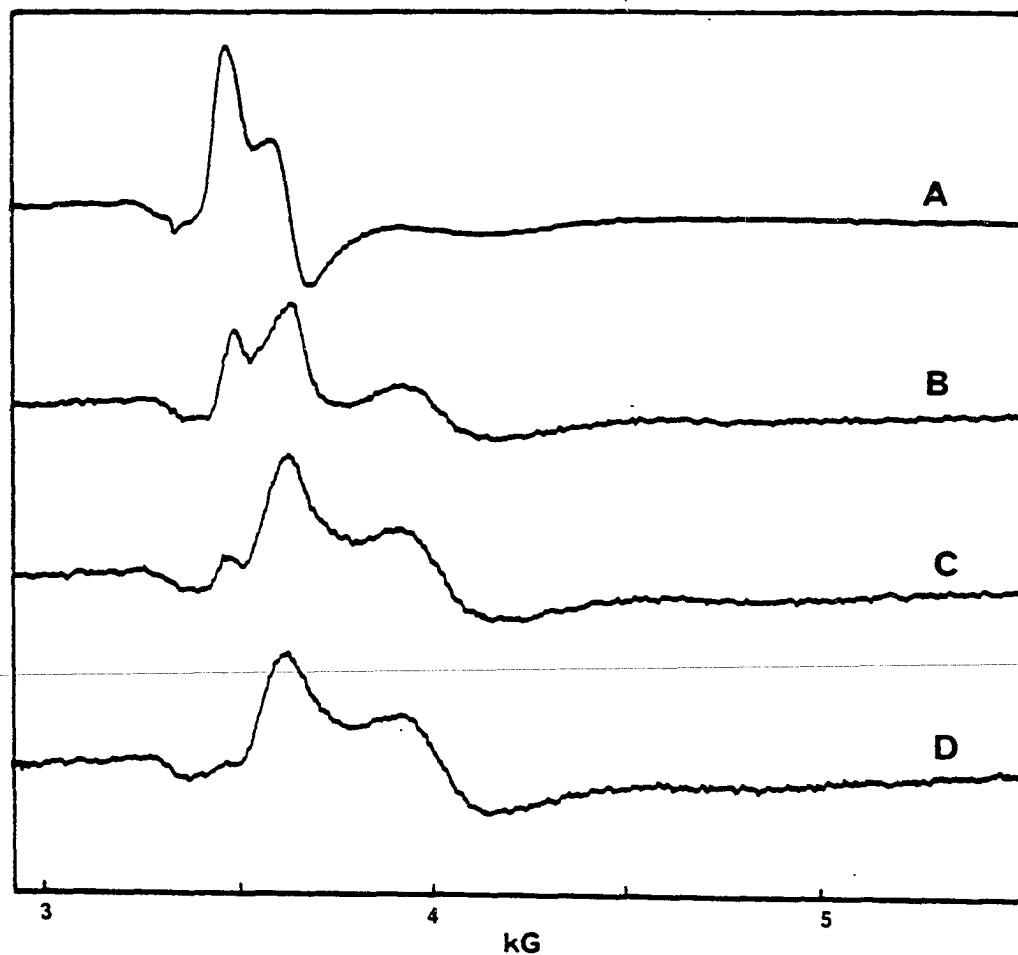


Figure III-7. EPR spectra of (semi-met)_R titrated with sulfide

0.25 mM Hr in 50 mM Tris/perchlorate pH 8.0, 25 °C. Sulfide/(semi-met)_R ratios: 0.0, A; 0.4 B; 0.8 C; 1.0, D. Instrument parameters: temperature, 4.2 K; frequency, 9.5730 GHz; power, 100 μW; modulation amplitude, 16 G at 100 kHz; time constant, 0.2 s; receiver gain, 1.25×10^5

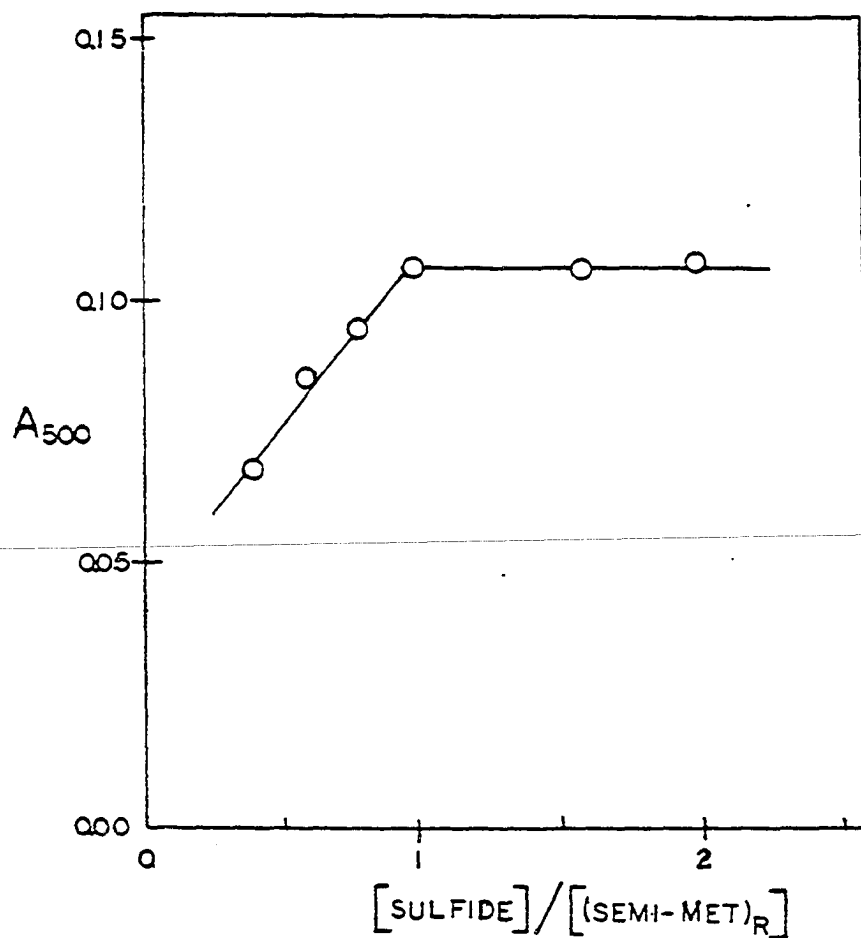


Figure III-8. UV-visible titration of (semi-met)_R with sulfide

All samples, 0.14 mM hemerythrin in 50 mM Tris/perchlorate pH 8.0, were equilibrated 30 minutes with various amounts of sulfide (from a stock Na₂S·9H₂O solution) at 25 °C

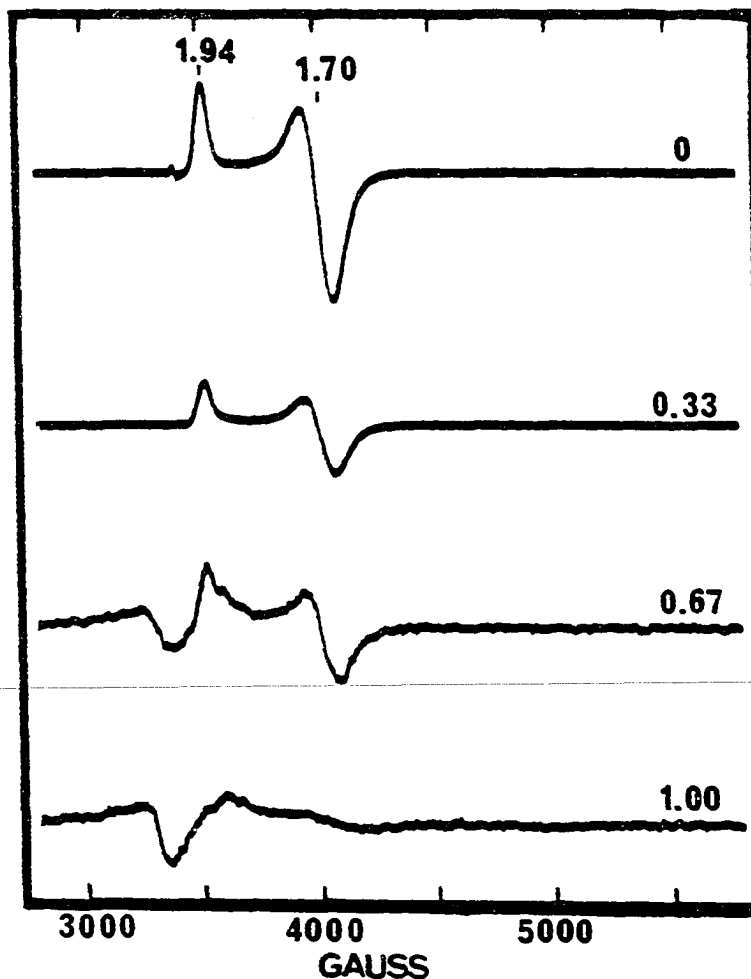


Figure III-9. Titration of $(\text{semi-met})_0$ with sulfide as monitored by EPR spectroscopy

1.45 mM hemerythrin in 50 mM Tris/acetate pH 8.0 was reacted anaerobically with sulfide from a stock NaSH solution. $[\text{sulfide}]/[\text{Hr}]$ ratios are listed next to each spectrum. Instrument parameters: temperature, 4.3 K; frequency, 9.569 GHz; power, 100 μW , modulation amplitude 16 G at 100 kHz; time constant, 0.2 s; receiver gain, 6.3×10^5 (0.67, 1.00)

converted to that of oxyHr when the sample is opened to air. These data indicate that sulfide does not bind to (semi-met)_O; instead it reduces the protein to deoxyHr.

Table III-3. Titration of (semi-met)_O with sulfide

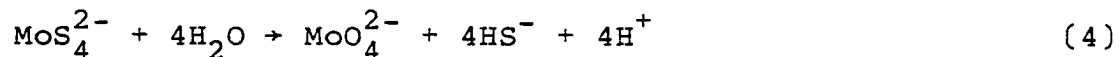
[sulfide]/[Hr] (<u>M</u> / <u>M</u>)	[(semi-met) _O] ^a (<u>mM</u>)	Percent of total [Hr] as (semi-met) _O
0.00	1.35	93%
0.33	0.48	33%
0.67	0.14	10%
1.00	0.05	3%
1.34	0.12	9%
1.67	0.09	7%

^a(Semi-met)_O concentrations determined by double integration of EPR spectra.

The difference in reactivity of (semi-met)_O and (semi-met)_R with sulfide can be explained in two ways. If the difference between (semi-met)_O and (semi-met)_R is reversal of the oxidation states of the irons in the dimer and if sulfide can reduce only the exposed five-coordinate iron, then sulfide reduction of (semi-met)_O is indicative of the five-coordinate iron being the Fe(III) in this form. The exposed iron would then have to be the Fe(II) in (semi-met)_R. An alternate explanation is that the O and R forms of (semi-met) are due to

conformational differences in the protein backbone. The O conformation, being, "deoxy-like" is more susceptible to reduction while the R conformer, being "met-like" binds the sulfide.

c) MetHr + MoS₄²⁻ The fact the EPR samples frozen very early on in the time course of the reaction of metHr with sulfide contain a mixture of (semi-met)_R and μ-S²⁻semi-metHr suggests that reduction occurs first, i.e., that reactions 1 and 2 occur sequentially. Supportive evidence for this order can also be obtained by using the aquation of MoS₄²⁻ (reaction 4) (105) as a source of sulfide.



The rate of thiomolybdate hydrolysis in the presence of metHr is greater than that of the hydrolysis in buffer alone. Harmer and Sykes report a half-life of 50 hours for reaction 5 and that subsequent stages of the aquation are at least an order of magnitude faster (105). This method of slowly adding sulfide to metHr allows separation of the reduction and ligation steps in the formation of μ-S²⁻semi-metHr. Table III-4 summarizes the results of the reaction of metHr with sulfide liberated via thiomolybdate hydrolysis. The

corresponding EPR spectra are illustrated in Figure III-10. These spectra show the build-up of (semi-met)_R, followed by a mixture of (semi-met)_R and $\mu\text{-S}_4^{2-}$ -semi-metHr, and then finally only $\mu\text{-S}_4^{2-}$ -semi-metHr is present. The maximum paramagnetic concentration is reached after 127 minutes. After this time, the amount of EPR active protein remains constant, and the only change observed is the incorporation of the sulfide. Unfortunately the EPR signal reflects only 4.7 % of the total protein concentration; some other process, most likely disproportionation, is apparently occurring more quickly than the release of sufficient sulfide from MoS_4^{2-} to reduce the protein quantitatively. The possibility exists that the rate and extent of disproportionation for P. gouldii increases when only some of the monomers with an octameric unit are reduced to the semi-met level. Disproportionation would result in formation of metHr and deoxyHr; reaction products (if any exist) of deoxyHr and sulfide are not detectable by UV-visible and EPR spectroscopies. The series of reactions postulated in pathway a of Scheme III-1 is also a possible explanation for the incomplete formation of $\mu\text{-S}_4^{2-}$ -semi-metHr in this reaction.

d) MetHr + S_4^{2-} The possibility of polysulfides being present in stock solutions of $\text{NaS}_2 \cdot 9\text{H}_2\text{O}$ or NaSH dictated the investigation of the reaction of metHr with S_4^{2-} . The UV-visible spectra of the reaction of metHr with S_4^{2-} in a ratio of ~ 1:0.25 (1:0.92 metHr to S atoms) do not have the

Table III-4. Data for reaction of metHr with sulfide liberated by thiomolybdate hydrolysis

Reaction time (minutes)	[MoS ₄ ²⁻] decrease due to hydrolysis ^a (mM)	Concentration of paramagnetic Hr species (mM) ^b	Percent total [Hr] ^c
17	0.15	0.01	0.93
50	0.18	0.03	2.8
127	0.40	0.05	4.5
181	0.57	0.05	4.5
236	0.62	0.05	4.5
350	0.75	0.05	4.5
930	0.84	0.04	3.7

^aOriginal MoS₄²⁻ concentration was 1.90 mM. Amount lost due to aquation determined by the difference of the initial MoS₄²⁻ concentration and the MoS₄²⁻ concentration at a given reaction time.

^bConcentration of paramagnetic species determined by double integration of EPR spectra.

^cTotal [Hr] was 1.08 mM.

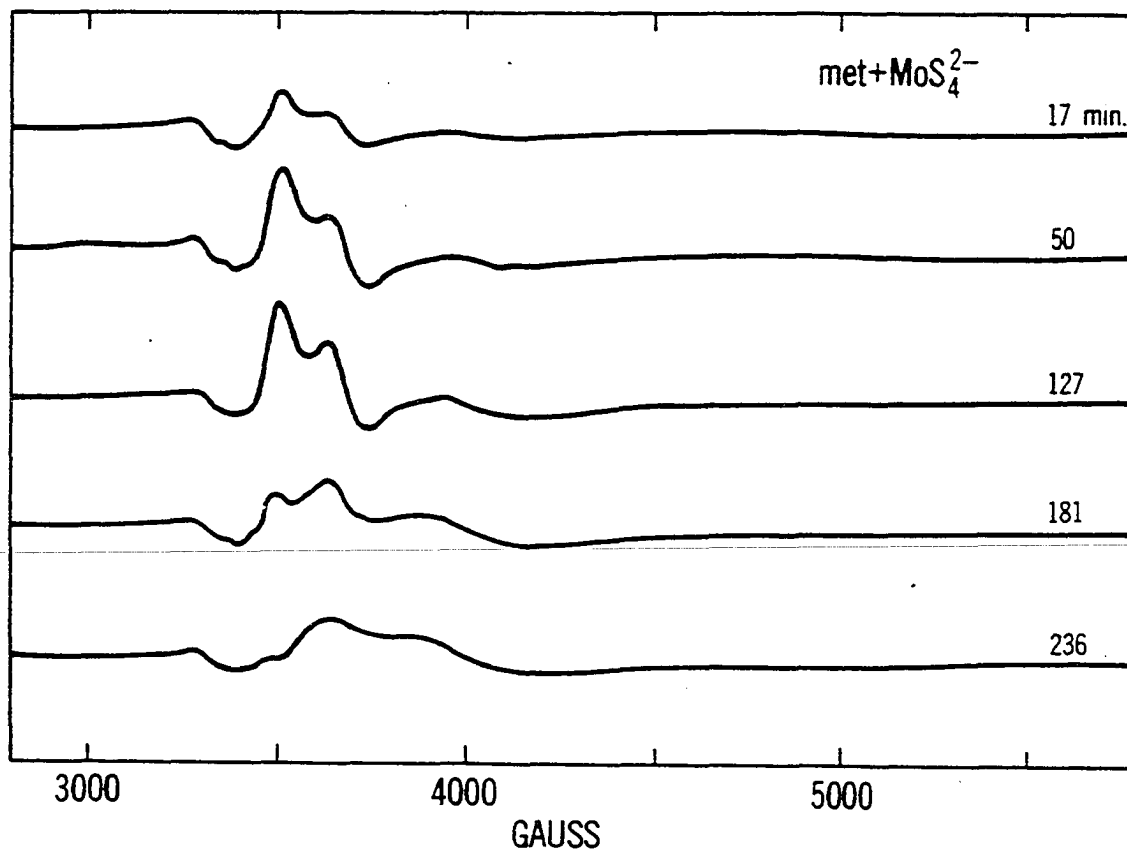


Figure III-10. EPR spectra of the reaction of the metHr with sulfide liberated from MoS_4^{2-} during its aquation

Hr: MoS_4^{2-} ratio was initially 1:1.8.
 Instrument parameters: temperature, 4.1 K;
 frequency, 9.5709 GHz; power, 100 μW ;
 modulation, 16 G at 100 kHz; time constant
 0.2 s; receiver gain, 8.0×10^4

broad peak at 500 nm expected for $\mu\text{-S}_4^{2-}$ -semi-metHr. An isosbestic point is observed at 500 nm indicating the presence of only two species. On the basis of the EPR spectra obtained for this reaction, the two species are metHr and (semi-met)_R. Double integrations of EPR spectra of all the samples (2, 15, 30 and 40 minutes reaction times) show (semi-met)_R as the major reaction product. Therefore, polysulfide S_4^{2-} is capable of reducing metHr to the semi-met oxidation level. The major reaction product of metHr and S_4^{2-} in ~ 1:1 molar ratio is $\mu\text{-S}_4^{2-}$ -semi-metHr. The EPR spectrum obtained for the 5 minute reaction time sample is shown in Figure III-11 and accounts for 66 % of the protein being present in the $\mu\text{-S}_4^{2-}$ -semi-metHr form. After 30 minutes reaction time, 100 % of the reaction mixture protein is observed as $\mu\text{-S}_4^{2-}$ -semi-metHr. Considering the higher concentration of tetrasulfide present in this second reaction mixture, formation of $\mu\text{-S}_4^{2-}$ -semi-metHr is not totally unexpected. It is known that for tetrasulfide the equilibrium properties of the aqueous solution may be ascribed to 64 % S_4^{2-} , 27 % S_5^{2-} and 9 % S_6^{2-} and that the equilibrium composition is rapidly established (10^{-2} s) (106).

The first experiment utilizing a molar ratio of ~ 1:0.25 of metHr to S_4^{2-} shows that it is possible to obtain the majority of the protein in the semi-met form under these conditions. The second experiment using a ~ 1:1 metHr to S_4^{2-} molar ratio illustrates that there is free sulfide in the

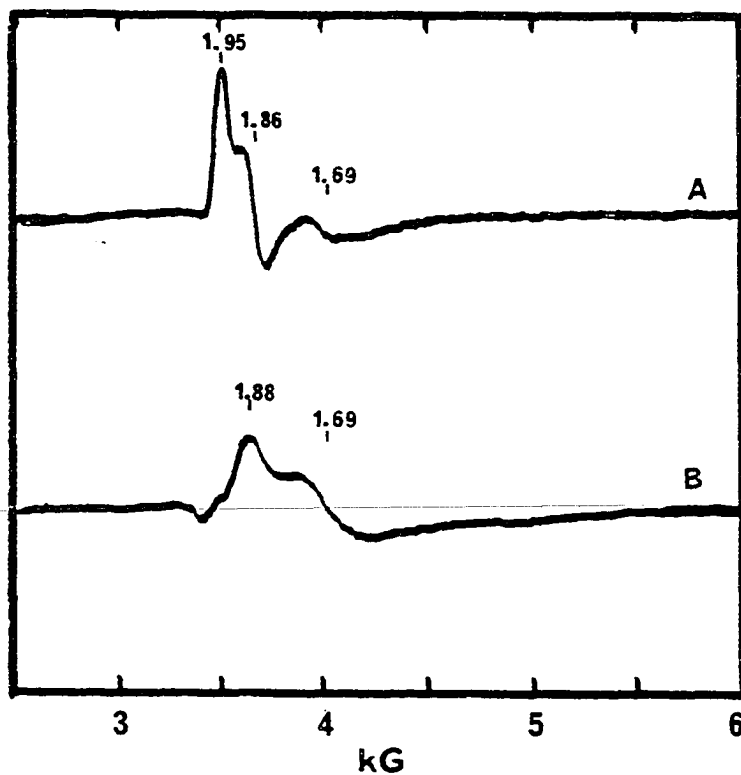


Figure III-11. EPR spectra of methHr reacted with polysulfide

A) 1 methHr:0.25 S_4^{2-} in 50 mM Tris/acetate pH 8.0 yields 1.60 mM (semi-met)_R in 40 minutes. B) 1 methHr:1 S_4^{2-} in 50 mM Tris/acetate pH 8.0 yields 1.64 mM μ - S_4^{2-} -semi-methHr in 30 minutes reaction time. Instrument parameters: temperature, 4.6 K; frequency, 9.5598 GHz; power, 100 μ W; modulation amplitude, 20 G at 100 kHz; time constant, 0.2 s; receiver gain, 8.0×10^4

aqueous solutions of tetrasulfide to ligate the semi-metHr which if formed. Experimental results discussed earlier in this section are in agreement with the binding of sulfide to (semi-met)_R. Using the percentages cited above for the polysulfide equilibria, the molar ratio of sulfide/metHr would be 0.09:1. In order to explain the formation of $\mu\text{-S}^{2-}$ semi-metHr, one must assume that the binding or oxidation of sulfide by the protein shifts the tetrasulfide equilibrium towards the production of sulfide. Both experiments with tetrasulfide indicate that if polysulfide is present in the stock solutions of $\text{Na}_2\text{S}\cdot 9\text{H}_2\text{O}$ or NaSH, it can reduce metHr and ultimately produce $\mu\text{-S}^{2-}$ semi-metHr. However, it should be noted that all of the sulfide titrations discussed above can be explained satisfactorily by invoking sulfide alone as the initial reactant.

e) MetHr + hydrogen sulfide The reaction of metHr with hydrogen sulfide gas yields the same protein product as that of the reaction using NaSH or $\text{Na}_2\text{S}\cdot 9\text{H}_2\text{O}$ as the sulfide source. The UV-visible spectrum obtained 45 minutes after addition of 2 molar equivalents of $\text{H}_2\text{S}_{(g)}$ to metHr is identical to the $\mu\text{-S}^{2-}$ semi-metHr prepared by other methods. EPR spectra were obtained for reaction mixtures containing molar ratios of $\text{H}_2\text{S}_{(g)}:\text{Hr}$ equal to one and two. With a molar ratio of one, 30 % of the protein can be accounted for in the semi-met state after 30 minutes reaction time. With a molar ratio of two,

100 % of the protein is in the $\mu\text{-S}^{2-}$ semi-metHr form within 45 minutes. The higher sulfide/Hr stoichiometry is most likely due to slow or incomplete dissolution of $\text{H}_2\text{S}_{(g)}$ when small volumes are injected into solutions of metHr. Since polysulfides are not as likely to be present in $\text{H}_2\text{S}_{(g)}$, this result suggests that one need not invoke polysulfides as the predominant reactants in the reactions conducted with stock sulfide solutions prepared from $\text{Na}_2\text{S}\cdot 9\text{H}_2\text{O}$ or NaSH.

f) MetHr + NaSH + NaN_3 Simultaneous anaerobic addition of sulfide and azide to metHr results in the production of metN_3^- ; azide binding (36-fold molar excess of N_3^- over Hr and sulfide) occurs quickly enough that the reduction of metHr by sulfide (reaction 1) cannot compete against it effectively.

On the basis of the Mössbauer and EPR data, the purple sulfide derivative of Hr contains a mixed valence $[\text{Fe}(\text{III}), \text{Fe}(\text{II})]$ dimer. Titrations of metHr with various sources of sulfide are consistent with the mixed valence dimer being due to reduction of metHr to semi-metHr and with subsequent incorporation of one sulfide ligand into the iron site.

B. Preparation and Characterization of μ -Selenidosemi-metHr

The selenide derivative ($\mu\text{-Se}^{2-}$ semi-metHr) analogous to $\mu\text{-S}^{2-}$ semi-metHr discussed in Section III-A is best generated by direct addition of stock solutions of Na_2Se to metHr.

Success at preparation of μ -Se²⁻-semi-metHr by dialysis of metHr against solutions of Na₂Se was quite limited. Attempts to crystallize μ -Se²⁻-semi-metHr by dialysis of the derivative against 80:20 (v/v) 5 mM Tris/sulfate pH 8.0:ethanol were unsuccessful.

The EPR spectra obtained for the titration of metHr in Bis/tris/sulfate pH 6.1 with selenide are shown in Figure III-12. Similar results are obtained at pH 8.0 in Tris/sulfate buffer. The three samples, frozen after 10 minutes reaction time, reveal that the reduction and ligation steps in this system are well separated in contrast to the case with sulfide. The EPR spectrum for the sample with a Se²⁻:Hr molar ratio of ~ 1:1 shows g values (1.94, 1.86 and 1.67) nearly identical to those reported for P. gouldii (semi-met)_R (see Table I-5) (56). Selenide to Hr molar ratios of ~ 2:1 and ~ 4:1 generate much broader EPR spectra having g values of 1.76 and 1.32. These EPR results are more supportive evidence that formation of μ -S²⁻-semi-metHr occurs via a similar two-step process of reduction to the semi-met oxidation level followed by ligation of a sulfide.

Comparison of Figures III-5 and III-13 shows that μ -Se²⁻-semi-metHr exhibits an optical spectrum very similar to that of μ -S²⁻-semi-metHr. This spectrum is observed for the Se²⁻:monomer ratio of ~ 2:1 and ~ 4:1 but not ~ 1:1. Since the selenide half-reaction can involve anywhere from 2 to 8

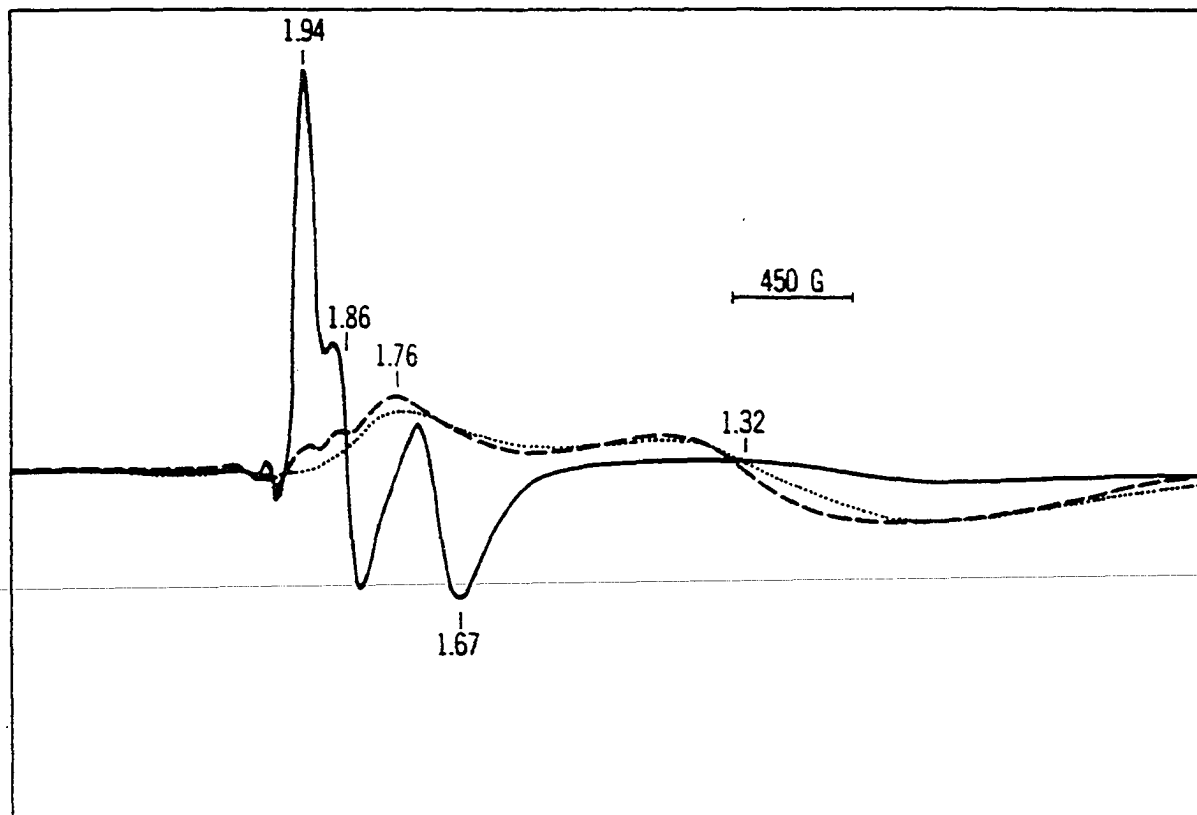


Figure III-12. Derivative EPR spectra resulting from the addition of Na_2Se to 1.48 mM methr in 50 mM Bis/tris/sulfate, pH 6.1

Instrument parameters: temperature, 4.2 K; frequency, 9.5730 GHz; power, 2 mW; time constant, 0.1 s. Spectra are shown for $\sim 1\text{Se}^{2-}:2\text{Fe}$, receiver gain, 2×10^4 (---); $\sim 2\text{Se}^{2-}:1\text{Fe}$, receiver gain, 3.2×10^4 (...)

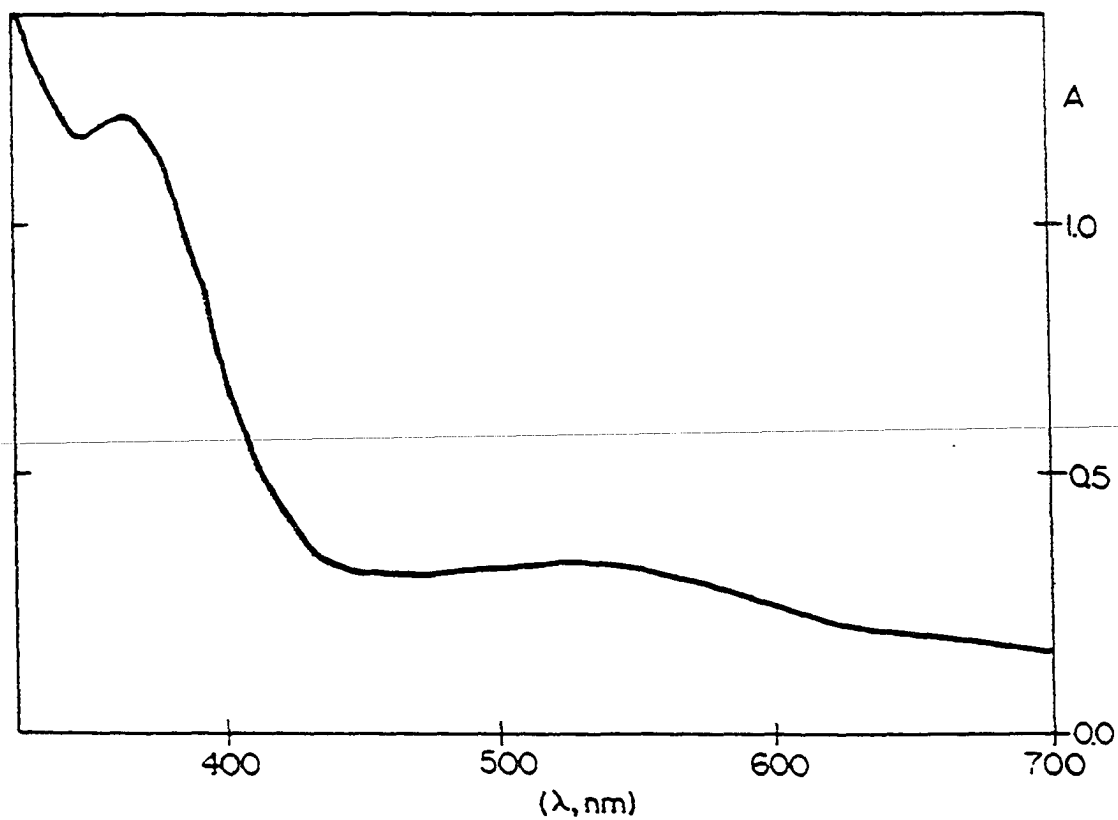


Figure III-13. Absorption spectrum of μ -selenidosemi-metHr

$2\text{Se}^{2-} : 1\text{Fe}$ reaction mixture after ten minutes.
 1.48×10^{-4} M in 50 mM Bis/tris/sulfate, pH 6.1

electrons (see Table I-8), it is difficult to determine at what $\text{Se}^{2-}:\text{Hr}$ molar ratio reduction should be complete. Assuming one selenide is required for ligation, the molar ratio of $\text{Se}^{2-}:\text{Hr}$ for complete formation of the $\mu\text{-Se}^{-2}\text{semi-metHr}$ must lie between the ratios 1.17:1 and 2:1. The instability of stock solutions of selenide makes a titration of the type shown in Figure III-4 impractical.

C. Preparation and Characterization of $\mu\text{-SulfidometHr}$

The discovery that the previously reported purple sulfide derivative of hemerythrin is at the semi-met oxidation level suggested the possibility of preparation of a sulfide derivative of Hr at the met oxidation level. Addition of one equivalent of $\text{Fe}(\text{CN})_6^{3-}$ to $\mu\text{-S}^{2-}\text{semi-metHr}$ accomplishes the oxidation handily as does anaerobic dialysis against $\text{Fe}(\text{CN})_6^{3-}$.

Since preparation of $\mu\text{-S}^{2-}\text{metHr}$ by dialysis ensures the absence of excess sulfide in protein solutions, this method of preparation yields $\mu\text{-S}^{2-}\text{metHr}$ sufficient for the determination of the bound sulfide to iron ratio. Sulfide and iron analyses carried out in parallel give a ratio of $0.89 \pm 0.11 \text{ S}^{2-}$ per 2Fe (average of nine determinations, Table III-5). Analyses for sulfide plus sulfane carried out in a similar manner yield a ratio of $0.97 \pm 0.08 (\text{S}^{-2} + \text{S}^0)$ per

2Fe (average of five determinations, Table III-6). These results indicate that $1S^{2-}/2Fe$ is the correct mole ratio in $\mu-S^{2-}$ -metHr and that no significant amounts of persulfide (S_2^{2-}) or sulfane sulfur are present.

Oxidation of $\mu-S^{2-}$ -semi-metHr to $\mu-S^{2-}$ -metHr results in increased absorbance throughout the visible and near UV region; the resulting UV-visible spectrum is shown in Figure III-14. The spectral parameters for $\mu-S^{2-}$ -metHr [λ , nm (ϵ , $M^{-1}cm^{-1}$)] are: 464(4500), 516sh, 544sh(3300), and 680sh(1200). The ~ 4 fold increase in absorbance of the main visible transition upon conversion of $\mu-S^{2-}$ -semi-metHr ($\epsilon_{500}=1100 M^{-1}cm^{-1}$) (65) to $\mu-S^{2-}$ -metHr is similar to that observed upon oxidation of the [2Fe-2S] protein adrenodoxin from the Fe(III)Fe(II) level to Fe(III)Fe(III) level (107) and contrasts with the ~ 1.5 fold increase in absorbance of the main visible transition upon conversion of semi-metN₃⁻ to metN₃⁻ (1, 32). However, the more significant differences between spectra of $\mu-S^{2-}$ -metHr and those of the oxo-bridged species appear in the near UV region. Spectra of oxyHr, metHr, all other anion adducts of metHr and a synthetic analogue of metHr contain two intense peaks ($\epsilon \sim 6,000-10,000 M^{-1}cm^{-1}$) at ~ 320 nm and ~ 360 nm one or both of which have been assigned to bridging $O^{2-} \rightarrow Fe$ charge transfer (see Table I-2) (32, 42, 49). The absence of well-resolved near UV bands from the spectrum of $\mu-S^{2-}$ -metHr is evidence against the

Table III-5. Data for parallel sulfide and iron analyses of $\mu\text{-S}^{2-}\text{-metHr}^a$

A_{670}	Nanomoles sulfide	Nanomoles Fe	Sulfide/2Fe mole ratio
0.141	18.0	41.4	0.87
0.172	26.1	62.0	0.84
0.225	40.2	80.4	0.78
0.230	41.4	82.8	1.00
0.250	46.5	102.4	0.91
0.272	52.3	113.8	0.92
0.276	53.4	125.3	0.85
0.298	59.5	124.0	0.96
0.322	65.3	145.0	0.90

Average 0.89 ± 0.11

^aAnalyses were carried out as described in Section II-F. Values for nanomoles of sulfide were determined using a least squares analysis of the working curve shown in Figure II-1.

Table III-6. Data for parallel sulfide plus sulfane and iron analysis of μ -S²⁻-metHr.^a Determination of the (S²⁻ + S⁰)/2Fe ratio

A ₆₇₀	Nanomoles (S ²⁻ + S ⁰)	Nanomoles Fe	(S ²⁻ + S ⁰)/2Fe mole ratio
0.154	21.5	41.2	1.04
0.195	32.2	61.4	1.05
0.227	40.6	81.8	0.99
0.242	44.4	101.8	0.87
0.282	54.9	121.8	<u>0.90</u>
Average			0.97 ± 0.08

^aAnalyses were carried out as described in Section II-F. Values for nanomoles of sulfide were determined using a least squares analysis of the working curve shown in Figure II-1.

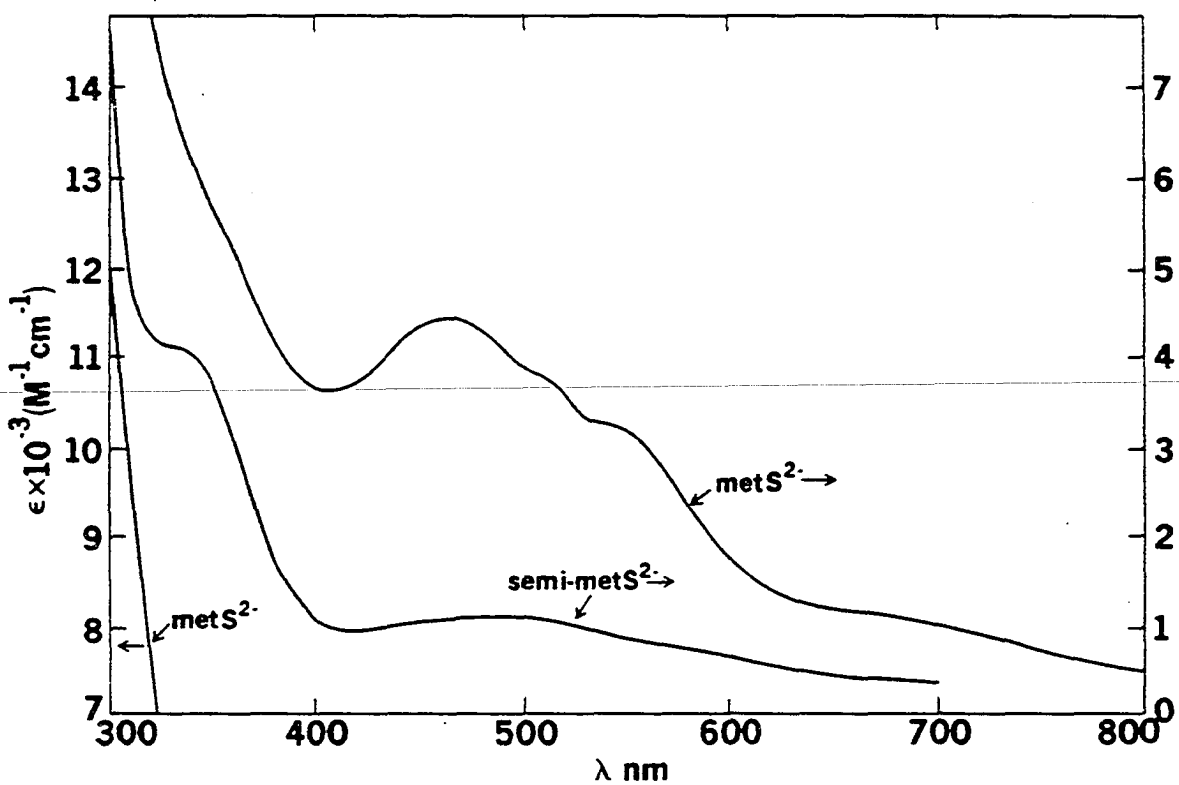


Figure III-14. Absorption spectra of $\mu\text{-S}^{2-}\text{metHr}$ and $\mu\text{-S}^{2-}\text{semi-metHr}$ in anaerobic 50 mM Tris/acetate pH 8.0

presence of a μ -oxo bridge at the iron site.

EPR and Mössbauer spectroscopies of this new derivative show that it is at the met oxidation level. μ -S²⁻-metHr gives no EPR signal at 4 K or 77 K. The Mössbauer spectrum at 100 K in an applied field of 1.7 kG, shown in Figure III-15, consists of a single doublet, each component being ~ 0.34 mm/s wide at half-height. The quadrupole splitting ΔE_q is 0.99 mm/s, and the isomer shift δ_{Fe} is 0.50 mm/s. This isomer shift is typical of metHr derivatives (see Table I-3) (44, 45). No significant differences are observed at 4.2 K. The lack of magnetic hyperfine interactions at low temperatures or in a weak applied field together with the lack of an EPR spectrum are typical of hemerythrin at the met oxidation level, i.e., of an antiferromagnetically coupled pair of high spin Fe(III) ions (23, 74, 75). The value of ΔE_q for μ -S²⁻-metHr is approximately 40 % smaller than that of metHr. A similar trend is observed in the Mössbauer spectra of $[Fe(salen)]_2X$ (X=O or S) where replacement of the μ -oxo bridge by a μ -sulfido bridge results in almost no change in the isomer shift, but a significant reduction in the quadrupole splitting (108). One would expect a terminal sulfide to result in two iron environments reflected in two quadrupole doublets in the Mössbauer spectrum like those observed for oxyHr (44, 45). From that point of view, a single doublet in the Mössbauer spectrum of S²⁻-metHr is evidence for a bridging

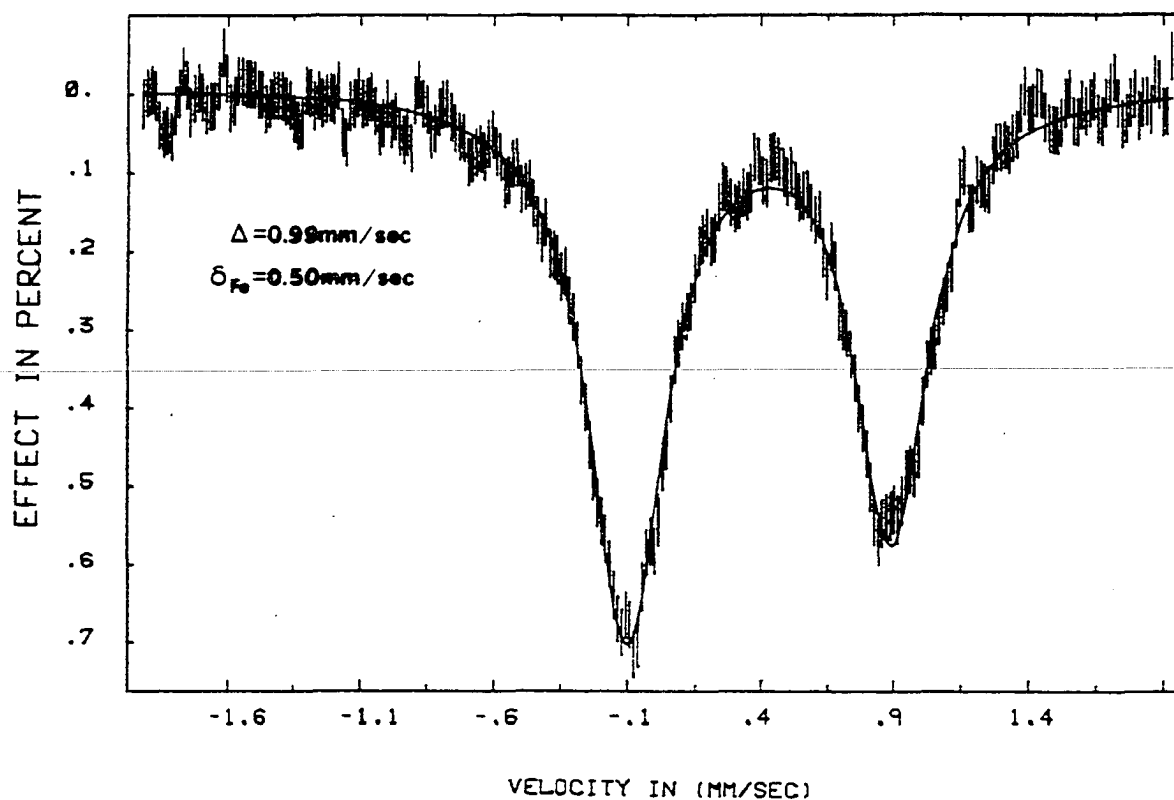


Figure III-15. Mössbauer spectrum of a frozen solution of 6.25 mM $\mu\text{-S}^{2-}$ -metHr in 50 mM Tris/perchlorate pH 8.0. The spectrum was taken in a 1.7 kG perpendicular applied field at 100 K

sulfide geometry. However, the Mössbauer spectra of a number of metHr anion complexes where the ligand is known to be terminally bound such as metN_3^- also contain only one quadrupole doublet. Thus, it is difficult to draw any conclusions about the ligand geometry based solely on the Mössbauer spectrum. However, it should be noted that metHr, which is known to contain one six-coordinate and one five-coordinate iron, also gives a single quadrupole doublet. Therefore, the Mössbauer spectrum of Figure III-15 is consistent with a bridging sulfide.

The resonance Raman spectrum of $\mu\text{-S}^{2-}\text{metHr}$ in Figure III-16 is strikingly different from that of $\mu\text{-S}^{2-}\text{semi-metHr}$ in that it contains at least 7 resonance-enhanced vibrational modes. Table III-7 summarizes the analysis of the frequencies indicating that the peaks at 653, 757, 858 and 1282 cm^{-1} are overtones and combinations of the fundamentals at 327 and 431 cm^{-1} . Similar frequency progressions are observed in the resonance Raman spectrum of oxidized $[\text{2Fe-2S}]$ iron-sulfur proteins. Overtones and combinations are not observed in resonance Raman spectra for the reduced $[\text{Fe(III),Fe(II)}]$ forms of $[\text{2Fe-2S}]$ iron-sulfur proteins (107); the same is true for $\mu\text{-S}^{2-}\text{semi-metHr}$ whose spectrum contains only a single band at 444 cm^{-1} (Figure III-1).

The resonance Raman spectra of all of the metHr anion complexes examined to date have the symmetric stretching

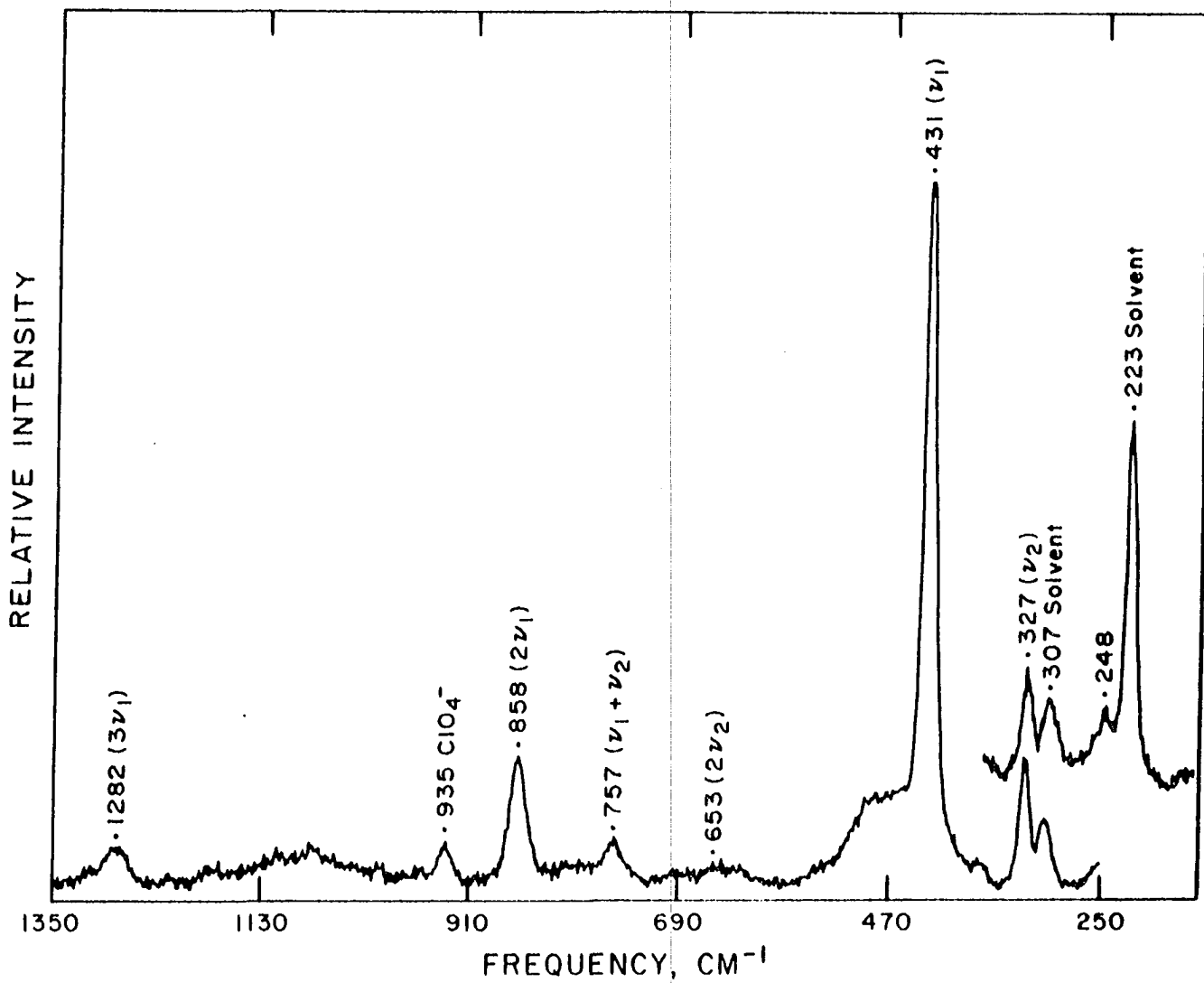
Table III-7. Resonance Raman vibrational frequencies and assignments for $\mu\text{-S}^{2-}\text{metHr}$ and $\mu\text{-S}^{2-}\text{semi-metHr}$

Frequency (cm^{-1})	Assignment
$\mu\text{-S}^{2-}\text{metHr}$	
327	$\nu_{\text{asym}}(\text{Fe-S-Fe})$
431	$\nu_{\text{sym}}(\text{Fe-S-Fe})$
653	$2\nu_{\text{asym}}$
757	$\nu_{\text{asym}} + \nu_{\text{sym}}$
858	$2\nu_{\text{sym}}$
1282	$3\nu_{\text{sym}}$
$\mu\text{-S}^{2-}\text{semi-metHr}$	
444	$\nu_{\text{sym}}(\text{Fe-S-Fe})^{\text{a}}$

^aReference 54.

Figure III-16. Resonance Raman spectrum of 2 mM μ -S²⁻metHr in 50 mM Tris/perchlorate pH 8.0

The solution contains ~ 0.4 M NaClO₄ as an internal standard. Instrument parameters: temperature, 77 K; excitation, 488.0 nm, 130 mW; scan rate, 1 cm⁻¹/s; slit width, 8 cm⁻¹; 34 scans averaged. Peaks at 223 and 307 cm⁻¹ in a 5:1 intensity ratio are characteristic of frozen solvent at 77 K. Broad feature between 450 and 500 cm⁻¹ is due to glass



vibration of the Fe-O-Fe unit appearing around 500 cm^{-1} (see Table I-4) (29, 49, 50). The absence of the 500 cm^{-1} band in the resonance Raman spectrum of $\mu\text{-S}^{2-}\text{metHr}$ is further evidence that the system does not contain a μ -oxo bridge between the two irons with sulfide being bound terminally to one of the irons.

The 431 cm^{-1} fundamental in the resonance Raman spectrum of $\mu\text{-S}^{2-}\text{metHr}$ is assigned to the symmetric Fe-S-Fe stretching vibration since totally symmetric modes generally show the greatest Raman intensities and resonance enhancements (109). The 327 cm^{-1} fundamental is assigned to the asymmetric Fe-S-Fe vibration by analogy to the vibrational modes in the Fe_2S_2 unit: ν_s at $\sim 400\text{ cm}^{-1}$; ν_{as} at $\sim 420(\text{w})$, $\sim 370(\text{w})$ and $\sim 290(\text{s})\text{ cm}^{-1}$ (107). The occurrence of an asymmetric mode at lower energy than the symmetric mode is indicative of a small Fe-S-Fe angle (82) as in the Fe_2S_2 clusters where the angle is 75° (110). Although the Fe-O-Fe angle is $\sim 127^\circ$ in metHr (36), substitution of S for O is expected to result in approximately a 0.35 \AA lengthening of each of the bridge bonds (38, 110). If the iron atoms in $\mu\text{-S}^{2-}\text{metHr}$ are constrained by the protein so that the geometric change associated with sulfur replacement of the oxo bridge occurs at the sulfur atom, the resulting Fe-S-Fe angle is calculated to be $\sim 98^\circ$. Using the secular equations of Wing and Callahan (82) for an Fe-S-Fe system, good agreement with the observed $\nu_s(\text{Fe-S-Fe})$ and

$\nu_{as}(\text{Fe-S-Fe})$ of $\mu\text{-S}^{2-}\text{metHr}$ can be achieved with values of 172 Nm^{-1} for the Fe-S stretching force constant, 27 Nm^{-1} for the bending force constant and 79.6° for the Fe-S-Fe bridge angle. These calculations are given in Appendix C. The value for the bending force constant is similar to that established for the Fe_2S_2 system; however, the stretching force constant is $\sim 30 \text{ Nm}^{-1}$ higher (107), which is reasonable for a single sulfur bridge.

The 13 cm^{-1} decrease in $\nu_s(\text{Fe-S-Fe})$ in $\mu\text{-S}^{2-}\text{metHr}$ relative to $\mu\text{-S}^{2-}\text{semi-metHr}$ is surprising. For example, in adrenodoxin the analogous one-electron oxidation results in $16\text{-}24 \text{ cm}^{-1}$ increases in bridge stretching vibrations (107) as expected for increased bond strengths at higher oxidation states. In $\mu\text{-S}^{2-}\text{metHr}$, structural or electronic changes accompanying oxidation must be compensating for the increase in net charge of the complex. A similar conclusion has been reached in the comparison of resonance Raman spectra of oxyHr and metHr where $\nu_s(\text{Fe-O-Fe})$ differs by $\sim 20 \text{ cm}^{-1}$ without any changes in the formal oxidation states of the iron atoms (49).

The Raman intensities of both the 431 cm^{-1} and 327 cm^{-1} bands relative to the perchlorate internal standard vary with excitation wavelength in the order $488.0 \text{ nm} > 530.9 \text{ nm} > 406.7 \text{ nm}$. Transitions at $\sim 450 \text{ nm}$ and $\sim 570 \text{ nm}$ in the absorption spectra of $[\text{2Fe-2S}]$ ferredoxins and in the synthetic analogues are assigned to bridging $\text{S}^{2-} \rightarrow \text{Fe}^{3+}$ charge

transfer based on Raman excitation profiles. The intensity variation in the resonance Raman spectra of $\mu\text{-S}^{2-}\text{metHr}$ is consistent with a similar assignment for its visible absorption spectrum, in particular, the maximally absorbing component at 464 nm (see Figure III-14).

In light of the discussion just presented, the physical data for the sulfideHr derivative at the met oxidation level suggest that the sulfide is bound to the iron dimer in a bridging position replacing the original $\mu\text{-oxo}$ bridge. This interpretation is consistent with the considerably larger number of bridging than terminal sulfide geometries for ~~Fe(III)-sulfide complexes (108, 110, 111)~~. Failure to discover $\mu\text{-S}^{2-}\text{metHr}$ by addition of sulfide to metHr indicates that the semi-met oxidation level is required to labilize the $\mu\text{-oxo}$ bridge and facilitate its replacement by sulfide. The spectroscopic and analytical data are consistent with a single sulfide replacing the $\mu\text{-oxo}$ bridge in the sulfideHrs, and the results of the reactivity studies, which are discussed in Section III-F, strengthen this interpretation.

D. Attempts at Preparation of $\mu\text{-SelenidometHr}$

Reaction of $\mu\text{-Se}^{2-}\text{semi-metHr}$ with ferricyanide performed by direct addition at pH 8.0 or dialysis at pH 6.3 does not yield $\mu\text{-selenidometHr}$. UV-visible spectra of the reaction

mixtures after removal of excess $\text{Fe}(\text{CN})_6^{3-}$ indicate that metHr is the predominant species present. The inability to form $\mu\text{-Se}^{2-}\text{metHr}$ can be rationalized in terms of the very negative reduction potential of Se/Se^{2-} couple, i.e., $\text{Fe}(\text{CN})_6^{3-}$ could oxidize the selenide as well as the iron in $\mu\text{-Se}^{2-}\text{semi-metHr}$. Comparison of the reduction potentials of $[\text{Fe}_2\text{X}_2(\text{SC}_6\text{H}_5)_4]^{2-/3-}$ where $\text{X} = \text{S}$ or Se reveals almost no change in the $[\text{Fe}(\text{III}), \text{Fe}(\text{II})]/[(\text{FeIII}), \text{Fe}(\text{II})]$ potential when S is replaced by Se (112). If one assumes that there is little or no change in the reduction potential of the irons in $\mu\text{-S}^{2-}\text{Hr}$ and $\mu\text{-Se}^{2-}\text{Hr}$ couples, the difference between the $\mu\text{-X}^{2-}\text{semi-metHr}$ ($\text{X} = \text{S}, \text{Se}$) is the ease with which the bridging ligand is oxidized. Since the reduction potential for the Se/Se^{2-} couple is considerably more negative than the S/S^{2-} , $\mu\text{-S}^{2-}\text{metHr}/\mu\text{-S}^{2-}\text{semi-metHr}$ and $\text{Fe}(\text{CN})_6^{3-/4-}$ potentials (see Table I-8), it is not unreasonable to propose that metHr is the product of the reaction of $\mu\text{-Se}^{2-}\text{semi-metHr}$ with ferricyanide because of oxidation of the bridging selenide to Se^0 followed by conversion of the remaining semi-metHr to metHr by reaction with excess ferricyanide. Other oxidants such as $\text{Co}(\text{phen})_3^{3+}$ and O_2 appear to react with the bridging sulfide in $\mu\text{-S}^{2-}\text{metHr}$. Thus even in the preparation of $\mu\text{-S}^{2-}\text{metHr}$, the choice of oxidant is crucial in obtaining $\mu\text{-S}^{2-}\text{metHr}$ as opposed to metHr.

E. Preparation and Detection of a Sulfide Complex of DeoxyHr

Attempts at reduction of $\mu\text{-S}^{2-}$ -semi-metHr by dialysis against excess dithionite (Method 3, Section II-H) do not yield the $[\text{Fe(II)},\text{Fe(II)}]\text{S}^{2-}\text{Hr}$. No reaction between dithionite and the protein is detected. If this lack of reaction is thermodynamically controlled, the $\mu\text{-S}^{2-}$ -semi-metHr \rightarrow " $\mu\text{-S}^{2-}$ -deoxyHr" reduction potential must be quite negative. The inability to reduce $\mu\text{-S}^{2-}$ -semi-metHr with retention of the sulfide is analogous to the lack of reduction by dithionite of $[2\text{Fe-2S}]$ centers in ferredoxins beyond the $\text{Fe(III)},\text{Fe(II)}$ level.

Interactions of sulfide with deoxyHr would be difficult to detect spectrophotometrically because of the lack of any intense bands in the visible, near UV or near IR spectrum of deoxyHr. However, recently Reem and Solomon (113) discovered an EPR signal at $g = 13$ due to deoxyN_3^- . They assigned this signal to a "forbidden" $M_s = \pm 2$ transition of an uncoupled high spin Fe(II) . Such an EPR signal is not observed for deoxyHr equilibrated with excess sulfide (Method 2, Section II-H). However, when excess azide is added to a sulfide/deoxyHr mixture, the deoxyN_3^- EPR signal is observed only after 55 minutes at room temperature. In the absence of sulfide, the EPR signal is generated immediately after addition of azide to deoxyHr. The slower binding of N_3^-

indicates that the sulfide is interacting with the deoxyHr in some fashion. If the order of sulfide and azide addition is reversed, the deoxyN₃⁻ EPR signal gradually disappears upon titration with excess sulfide. EPR spectra for such a titration are shown in Figure III-17. These EPR spectra suggest a weak association of sulfide with deoxyHr, since the formation constant for deoxyN₃⁻ is estimated to be 70 M⁻¹ (114). Disappearance of the g = 13 EPR signal is consistent with magnetic coupling of the unpaired spins on each Fe(II).

If sulfide is incorporated into a bridging position in deoxyHr, one should in principle be able to generate $\mu\text{-S}^{2-}\text{-metHr}$ or $\mu\text{-S}^{2-}\text{-semi-metHr}$ by oxidizing deoxyHr which has been equilibrated with excess sulfide (Method 1, Section II-H). However, regardless of the manner in which deoxyHr was equilibrated with sulfide, i.e., either dialysis of deoxyHr against excess sulfide or reaction of oxyHr with sulfide, the product of the equilibrated sulfide/deoxyHr mixture and ferricyanide is metHr. Thus, the nature of the product of the reaction of deoxyHr with sulfide remains unclear.

F. Reactivity of the SulfideHrs

1. Reduction potentials

Measurement of the reduction potential of the $\mu\text{-S}^{2-}\text{-metHr}/\mu\text{-S}^{2-}\text{-semi-metHr}$ couple makes use of the equilibrium given

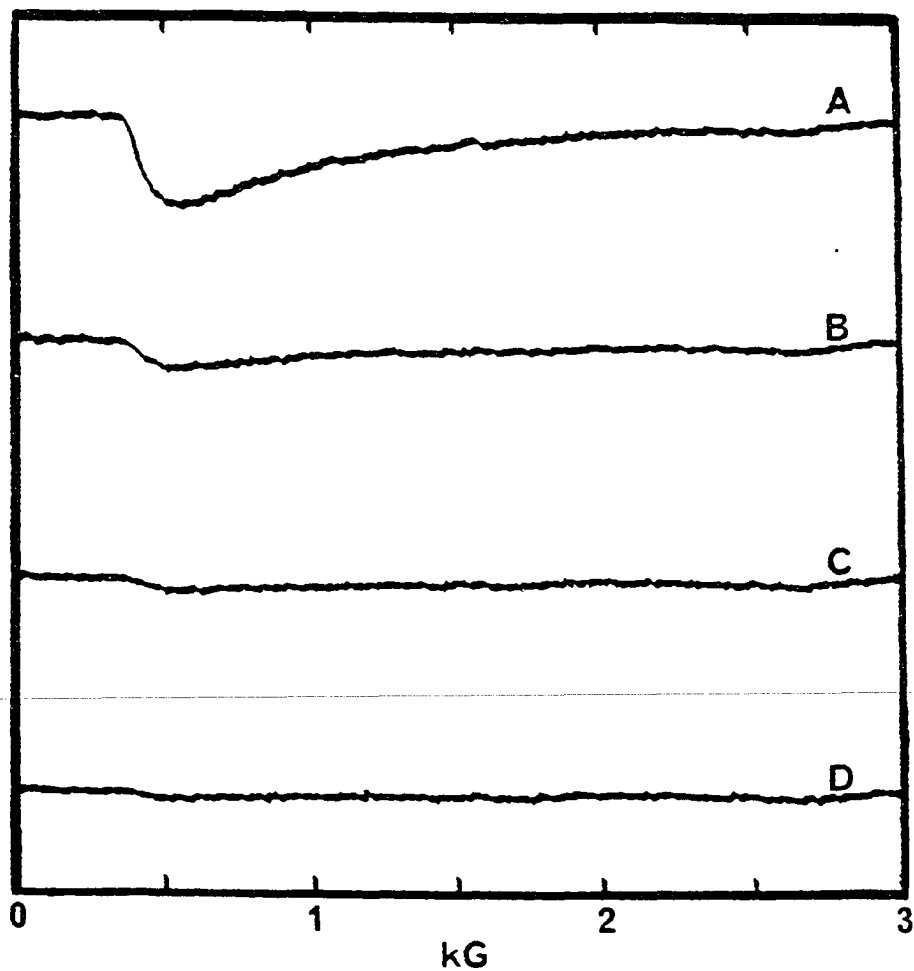
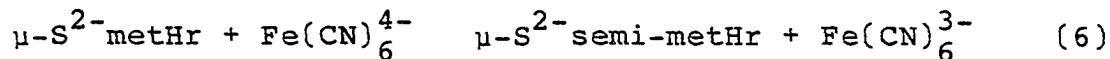


Figure III-17. EPR spectra observed for the titration of deoxyN₃⁻ by sulfide

Protein concentration is 0.72 mM. Azide concentration is 0.027 M. Sulfide concentration in A, 0; B, 0.041 M; C, 0.069 M and D, 0.109 M. Instrument parameters: temperature, 4 K; frequency, 9.5660 GHz; power, 32 μ W; modulation amplitude, 16 G at 100 kHz; time constant 0.2 s; receiver gain, 1×10^5

in reaction 6.



For this one electron redox process in the presence of a large excess of $\text{Fe}(\text{CN})_6^{3-/4-}$, the solution potential (E_{soln}) is determined by the $\text{Fe}(\text{CN})_6^{3-/4-}$ ratio. Under equilibrium conditions equation 1 holds.

$$\begin{aligned} E_{\text{soln}} &= E_{\text{pH } 8.0}^{\circ} \text{Fe}(\text{CN})_6^{3-/4-} + 0.0591 \log \frac{[\text{Fe}(\text{CN})_6^{3-}]}{[\text{Fe}(\text{CN})_6^{4-}]} \\ &= E_{\text{pH } 8.0}^{\circ} \mu\text{-S}^{2-}\text{metHr}/\mu\text{-S}^{2-}\text{semi-metHr} \quad (1) \\ &\quad + 0.0591 \log \frac{[\mu\text{-S}^{2-}\text{metHr}]}{[\mu\text{-S}^{2-}\text{semi-metHr}]} \end{aligned}$$

Plots of E_{soln} versus $\log [\mu\text{-S}^{2-}\text{metHr}]/[\mu\text{-S}^{2-}\text{semi-metHr}]$ should yield a straight line with a slope of 59 mV, and the point where $\log [\mu\text{-S}^{2-}\text{metHr}]/[\mu\text{-S}^{2-}\text{semi-metHr}] = 0$ gives the standard reduction potential under the conditions employed. Figure III-18 shows the plots for the redox titrations starting from either $\mu\text{-S}^{2-}\text{semi-metHr}$ or $\mu\text{-S}^{2-}\text{metHr}$ prepared in Tris/acetate by dialysis. The slopes in Figure III-18 are 59 ± 1 mV, confirming the one-electron nature of the process.

The midpoint potentials are listed in Table III-8. Stabilization of the reduced form of a redox couple leads to more positive measured $E_{\text{pH } 8.0}^{\circ}$'s while stabilization of the oxidized form is characterized by more negative $E_{\text{pH } 8.0}^{\circ}$ values. Therefore the 29 mV difference observed in the midpoint potentials determined when starting from either $\mu\text{-S}^{2-}\text{metHr}$ or $\mu\text{-S}^{2-}\text{semi-metHr}$ can be rationalized in terms of two conformers. When the met or semi-met sulfide derivatives are prepared via dialysis in Tris/acetate, the resulting conformation is that which stabilizes the met or semi-met oxidation level, respectively. These two conformers are designated *m* and *sm* in Scheme III-2. Relative to the time scale of the redox titrations, the vertical equilibria shown in Scheme III-2 must be slow in order for the conformational differences to be reflected in the measured midpoint potentials. Since $\mu\text{-S}^{2-}\text{semi-metHr}$ prepared by direct addition of one equivalent of dithionite to $\mu\text{-S}^{2-}\text{metHr}$ yields the same midpoint potential as the $\mu\text{-S}^{2-}\text{semi-metHr}$ made by dialysis, one must assume that dithionite but not ferrocyanide can induce the conformational change, *m* \rightarrow *sm*. The different results caused by these two reagents may be due to their mode of interaction with the protein. Dithionite, as $\text{SO}_2^{-\cdot}$, is capable of reacting directly at the iron site as an inner sphere reductant (52). Interaction at the iron site with small anions such as azide is known to result in

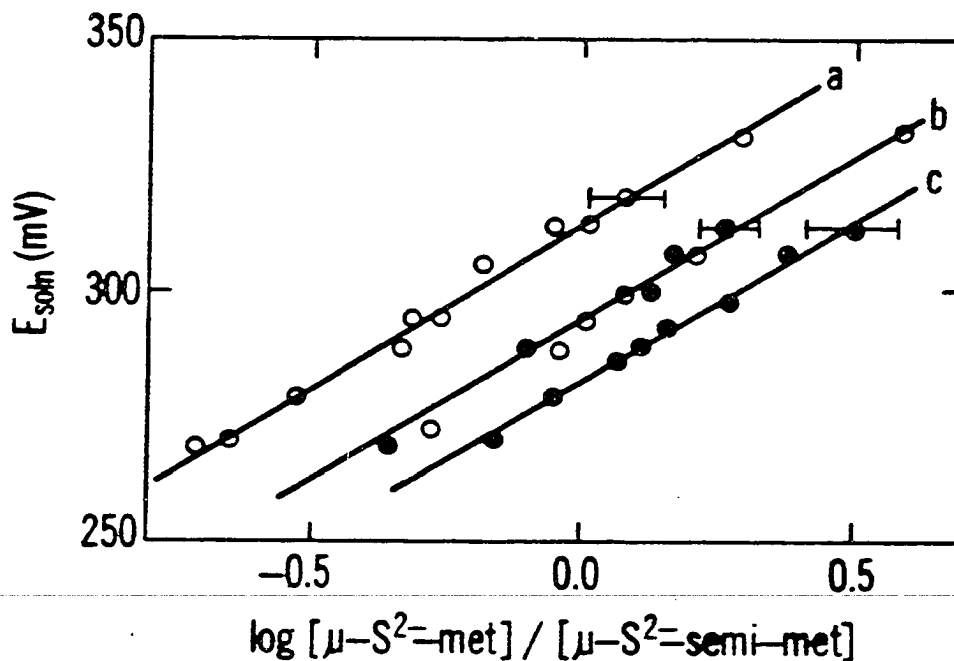


Figure III-18. Plots of E_{soln} versus $\log \frac{[\mu\text{-S}^{2-}\text{-metHr}]}{[\mu\text{-S}^{2-}\text{-semi-metHr}]}$

Data points are each the average of values obtained from three separate redox titrations using A_{544} to measure $[\mu\text{-S}^{2-}\text{-metHr}]$ and $[\mu\text{-S}^{2-}\text{-semi-metHr}]$. Conditions: 0.13-0.14 mM Hr; pH 8.0; $I = 0.15 \text{ M}$; 25 °C. Open circles represent titrations starting from $\mu\text{-S}^{2-}\text{-semi-metHr}$, filled circles represent titrations starting from $\mu\text{-S}^{2-}\text{-metHr}$. Data points for lines a and c were obtained in 50 mM Tris/acetate; data points for line b were obtained in 50 mM Tris/perchlorate

Table III-8. Midpoint reduction potentials (E_m) for the $\mu\text{-S}^{2-}\text{metHr}/\mu\text{-S}^{2-}\text{semi-metHr}$ couple at 25 °C, $I = 0.15 \text{ mM}$ and pH 8.0^a

Conditions	E_m (mV) vs NHE ^b	Redox Partner
M or SM ^c (ClO_4^-)	295 ± 5	$\text{Fe}(\text{CN})_6^{4-}/3-$
M (OAc^-)	283 ± 8	$\text{Fe}(\text{CN})_6^{4-}/3-$
SM (OAc^-)	312 ± 5	$\text{Fe}(\text{CN})_6^{4-}/3-$
M (ClO_4^-)	287 ± 25 ^d	$\text{Fe}^{2+}\text{cyt c}/\text{Fe}^{3+}\text{cyt c}$

^a50 mM Tris buffer with the counterion listed in parentheses at ~ 25 mM.

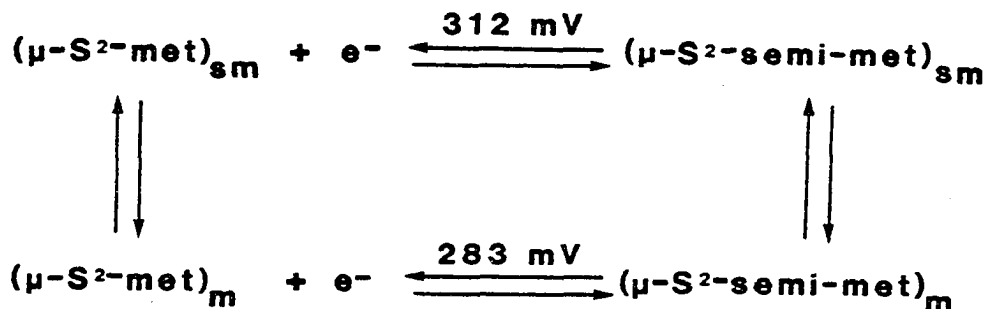
^bEach value represents the average from 3-6 separate redox titrations.

^cM and SM refer to titrations starting from $\mu\text{-S}^{2-}\text{metHr}$ (M) or $\mu\text{-S}^{2-}\text{semi-metHr}$ (SM).

^dAverage of six EPR plus UV-visible titrations.

conformational changes (63). Ferrocyanide, on the other hand, reacts in an outer sphere fashion and therefore, may not affect the conformation around the iron site.

Scheme III-2



One possible explanation for the lower potential of the m conformer is that it has a higher affinity for the negatively charged $\text{Fe}(\text{CN})_6^{3-/4-}$. In this case the midpoint potential should depend on the total concentration of $\text{Fe}(\text{CN})_6^{3-/4-}$ (115). However, the midpoint potential starting from $\mu\text{-S}^{2-}$ metHr in Tris/acetate is the same (within 8 mV) when measured using total $\text{Fe}(\text{CN})_6^{3-/4-}$ concentrations of either 40 or 80 mM.

When the reduction potential is measured for the $\mu\text{-S}^{2-}$ metHr/ $\mu\text{-S}^{2-}$ semi-metHr couple prepared in the presence of perchlorate, only one value is obtained regardless of which oxidation level is initially equilibrated with the $\text{Fe}(\text{CN})_6^{3-/4-}$ solutions. The plot of E_{soln} versus $\log [\mu\text{-S}^{2-}\text{metHr}]/[\mu\text{-S}^{2-}\text{semi-metHr}]$ for the protein prepared in

Tris/perchlorate is shown in Figure III-18b. One can offer several explanations for the observation of only one reduction potential for the $\mu\text{-S}^{2-}\text{Hr}$ couple in the presence of perchlorate. It is known that the perchlorate binding site in hemerythrin is 12-15 Å away from the iron site (38), that bound perchlorate slows the rate of ligand binding to metHr and that an iron site related pK_a is raised from 7.8 to 8.7 in the presence of perchlorate (39, 116, 117) (see Section I-B). Autoreduction of $\mu\text{-S}^{2-}\text{metHr}$ and the conversion of $(\text{semi-met})_O$ towards $(\text{semi-met})_R$ are also slowed down by the presence of perchlorate (see Section III-F). Assuming the existence of two conformers in the Tris/acetate experiment, the observation of only one reduction potential in Tris/perchlorate can be interpreted as being due to the stabilization of only one conformer by bound perchlorate. This one conformation could be dictated by the manner in which perchlorate binds rather than any conformational preference of $\mu\text{-S}^{2-}\text{metHr}$ or $\mu\text{-S}^{2-}\text{semi-metHr}$. Since the E_{pH}° 8.0 in the presence of perchlorate falls between the E_{pH}° 8.0 for the sm and m conformers in Tris/acetate, this perchlorate induced form can be viewed as an intermediate conformer, i.e., a conformation that is encountered during the interconversion of the sm and m conformers. Another possibility is that both sulfide derivatives in perchlorate are in the sm conformation because of the method of preparation used to generate the two

derivatives. Both $\mu\text{-S}^{2-}\text{-metHr}$ and $\mu\text{-S}^{2-}\text{-semi-metHr}$ are prepared by initial formation of $\mu\text{-S}^{2-}\text{-semi-metHr}$. Initial introduction of the sulfide into the iron site puts the protein in the sm conformation; once the sulfide is present the rigidity due to bound perchlorate decreases the likelihood of conversion to the m conformer. In this case, the effect of perchlorate can be rationalized as a stabilization of the sm conformer. The decrease from 312 to 295 mV would then be due predominantly to the electrostatic effect of the bound perchlorate (118). Yet another explanation is that ClO_4^- causes rapid equilibration of the m and sm conformers such that an average E° is obtained. However, the slower rates of various reactions of Hr in the presence of perchlorate mentioned above make this explanation less likely.

If the difference in the two conformations (m and sm) is at the iron site, differences might be expected in the EPR spectra. Assuming that the primary effect of bound perchlorate is electrostatic and that perchlorate stabilizes the sm conformer, one would expect differences in the EPR signal observed for $(\mu\text{-S}^{2-}\text{-semi-metHr})_m(\text{acetate})$ and $(\mu\text{-S}^{2-}\text{-semi-metHr})_{sm}(\text{acetate})$ or $(\mu\text{-S}^{2-}\text{-semi-metHr})_{sm}(\text{ClO}_4^-)$. EPR spectra of $\mu\text{-S}^{2-}\text{-semi-metHr}$ prepared three different ways in the presence of perchlorate at pH 8.0 as described in Section II-D (dialysis method and methods 1 and 5) show an identical signal ($g = 1.894, 1.707$ and 1.404) regardless of

the reaction time allowed. For $\mu\text{-S}^{2-}$ -semi-metHr prepared in Tris/acetate pH 8.0 by six different reactions (see Section II-D and II-I), the EPR signal ($g = 1.883, 1.709$ and 1.400) observed is practically identical to that observed for the derivative in perchlorate. The fact that the $\mu\text{-S}^{2-}$ -semi-metHr EPR signal is quite broad (~ 2000 G) may hinder detection of perturbations of the EPR signal, especially if the conformational changes are small or removed from the immediate environment of the iron site. Thus the m and sm conformations of $\mu\text{-S}^{2-}$ -semi-metHr cannot be readily distinguished by EPR spectroscopy.

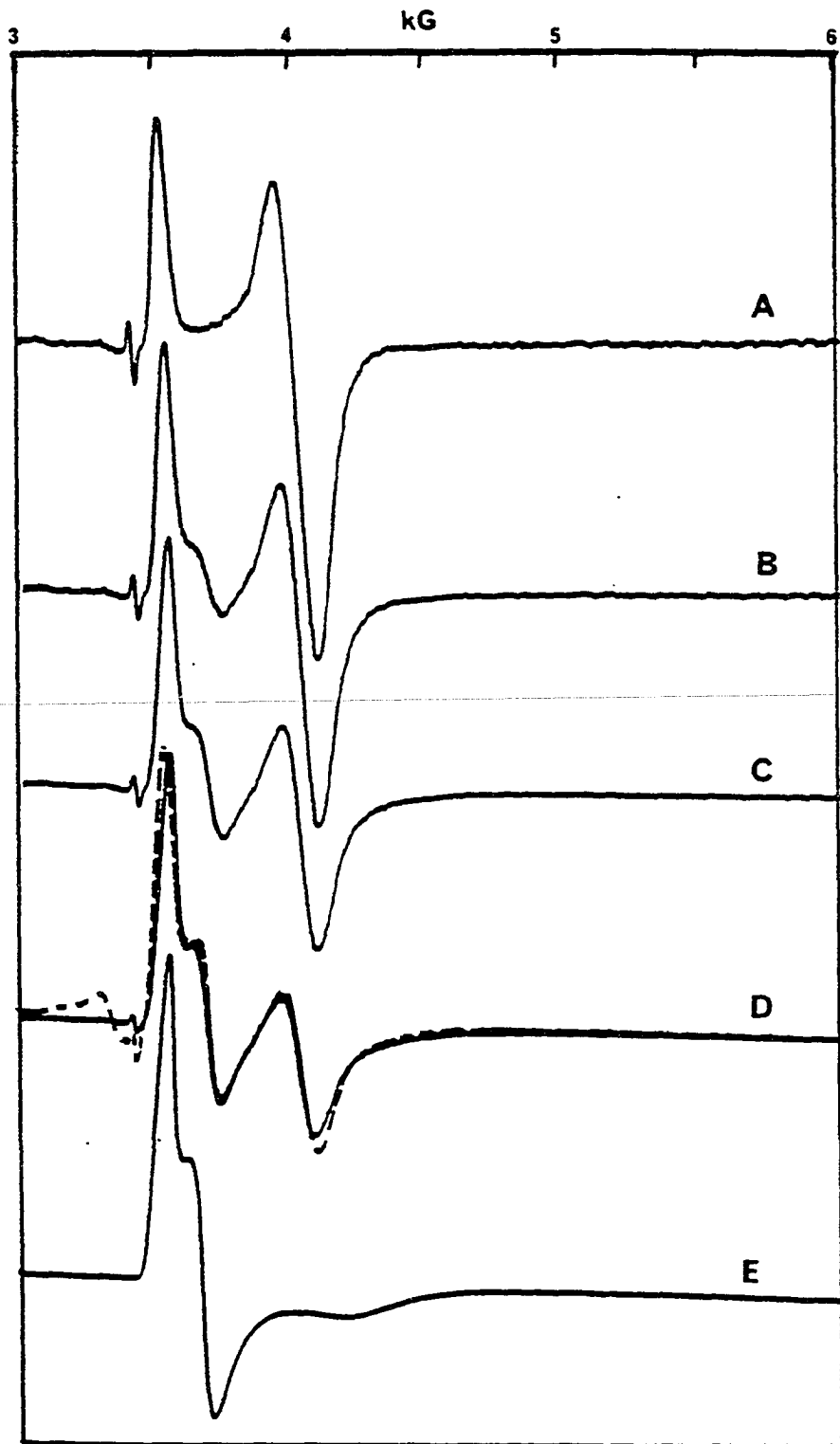
Although only slight differences are observed in the EPR spectra of $\mu\text{-S}^{2-}$ -semi-metHr prepared in Tris/perchlorate versus Tris/acetate, the EPR spectrum resulting from oxidative loss of sulfide from $\mu\text{-S}^{2-}$ -semi-metHr, discussed later in this section, resembles that of $(\text{semi-met})_O$. Hence, it is tempting to associate the sm conformer with $(\text{semi-met})_O$ and the m conformer with $(\text{semi-met})_R$. There is no evidence linking the two conformers of the $\mu\text{-S}^{2-}$ -Hrs with acidic and basic forms of the iron sites, such as occurs in metHr (1, 32). Both EPR and optical spectra of the $\mu\text{-S}^{2-}$ -Hrs remain essentially constant between pH 6.5 and 9.5.

Whatever the explanation for the range of values, the significant result is that replacement of the μ -oxo bridge by a μ -sulfido bridge in Hr results in an ~ 200 mV increase in

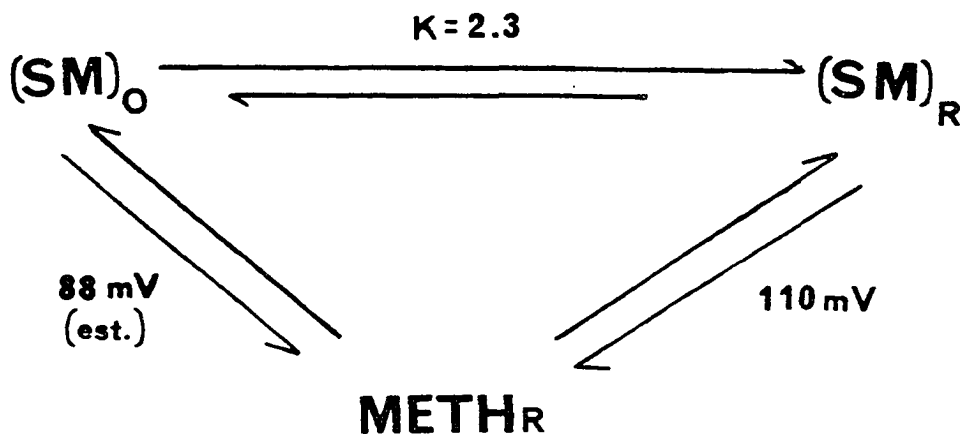
the met/semi-met reduction potential. This increase is most likely due predominantly to intrinsic differences in the potential of the iron sites rather than conformational differences between Hr and $\mu\text{-S}^{2-}\text{Hr}$. Comparing potentials of what appear to be similar conformers, i.e., those of $\text{metHr}/(\text{semi-met})_{\text{R}}$ and $(\mu\text{-S}^{2-}\text{metHr})_{\text{m}}/(\mu\text{-S}^{2-}\text{semi-metHr})_{\text{m}}$, gives an 173 mV increase in reduction potential upon incorporation of sulfide into the iron site. Since metHr is presumed to exist only in the R conformation (53), there is no value known for a " $(\text{metHr})_{\text{O}}/(\text{semi-met})_{\text{O}}$ " potential available for comparison with the $(\mu\text{-S}^{2-}\text{metHr})_{\text{sm}}/(\mu\text{-S}^{2-}\text{semi-metHr})_{\text{sm}}$ potential. As illustrated in Figures III-19, the $(\text{semi-met})_{\text{O}} = (\text{semi-met})_{\text{R}}$ equilibrium clearly lies towards $(\text{semi-met})_{\text{R}}$ for P. gouldii Hr. Thus, the reduction potential for $\text{metHr}/(\text{semi-met})_{\text{O}}$ must be less positive than the value for $\text{metHr}/(\text{semi-met})_{\text{R}}$ of + 110 mV. On the basis of the EPR spectral simulations shown in Figure III-19, one can estimate an equilibrium constant of 2.3 for $(\text{semi-met})_{\text{O}} \rightleftharpoons (\text{semi-met})_{\text{R}}$. The calculated value of the $\text{metHr}/(\text{semi-met})_{\text{O}}$ reduction potential is 22 mV less positive than the potential of the $\text{metHr}/(\text{semi-met})_{\text{R}}$ couple (see Scheme III-3). Thus using either reduction potential from Scheme III-3, an ~ 200 mV increase in the met/semi-met reduction potential occurs when the bridging oxide is replaced by a bridging sulfide.

Figure III-19. EPR simulations of various ratios of
(semi-met)_O and (semi-met)_R

Ratio of (semi-met)_O/(semi-met)_R: 100/0, A;
70/30, B; 50/50, C; 30/70, D; 0/100, E. The
dashed spectrum on D is the spectrum observed
after anaerobic incubation of (semi-met)_O for
49 minutes at room temperature in 50 mM
Tris/acetate pH 8.0. (Semi-met)_O/(semi-met)_R
ratio of 30:70 was used for equilibrium
constant calculation



Scheme III-3



Measurement of the $\mu\text{-S}^{2-}\text{Hr}$ reduction potential by a second independent method yields a value (Table III-8) in good agreement with the value obtained using $\text{Fe}(\text{CN})_6^{3-/4-}$ equilibration method. Visible absorption spectra of the reactions of equimolar concentrations of $\mu\text{-S}^{2-}\text{metHr}$ with $\text{Fe}^{2+}\text{cyt c}$ and of $\mu\text{-S}^{2-}\text{semi-metHr}$ with $\text{Fe}^{3+}\text{cyt c}$ are identical at equilibrium which is attained within 30 to 45 minutes reaction time; one such absorption spectrum is depicted in Figure III-20. Using concentrations of $\mu\text{-S}^{2-}\text{semi-metHr}$ and $\text{Fe}^{3+}\text{cyt c}$ determined by double integration of EPR spectra (see Figure III-20) and $E_{\text{pH } 8.0}^{\circ} = 260 \text{ mV}$ for the $\text{Fe}^{3+}/\text{Fe}^{2+}\text{cyt c}$ redox couple (68) in the Nernst equation, the $\mu\text{-S}^{2-}\text{metHr}/\mu\text{-S}^{2-}\text{semi-metHr}$ reduction potential can be calculated.

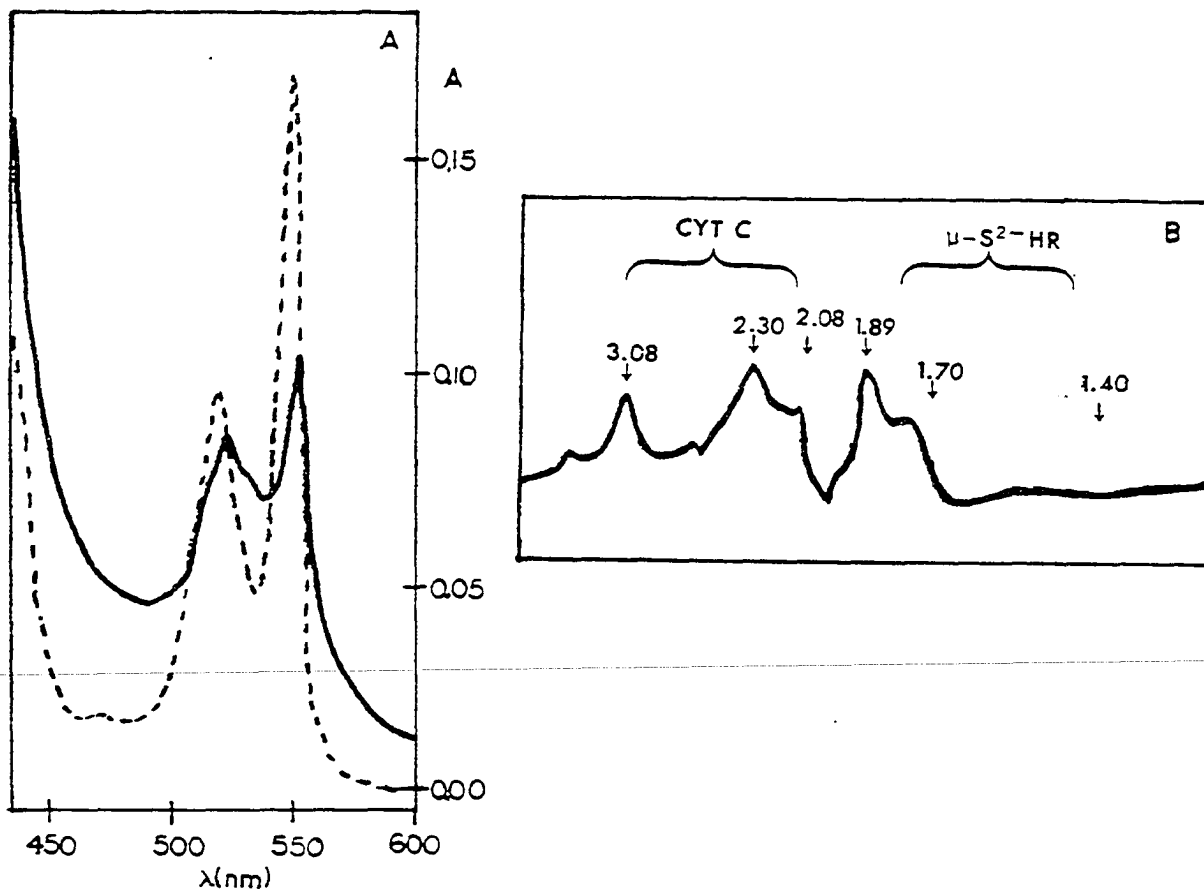


Figure III-20. UV-visible and EPR spectra for μ -S²⁻-metHr equilibration with Fe²⁺ cyt c at room temperature for 50 minutes in 50 mM Tris/perchlorate pH 8.0

A) UV-visible sample: 0.1.09 mM Hr, 0.111 mM cyt c. Dotted spectrum is that of Fe²⁺ cyt c before addition of Hr. B) EPR sample: 0.77 mM Hr, 0.76 mM cyt c. Instrument parameters: temperature, 4.2 K; frequency, 9.5689 GHz; power, 100 μ W; modulation amplitude, 16 G at 100 kHz; time constant, 0.2 s; receiver gain, 5.0×10^4

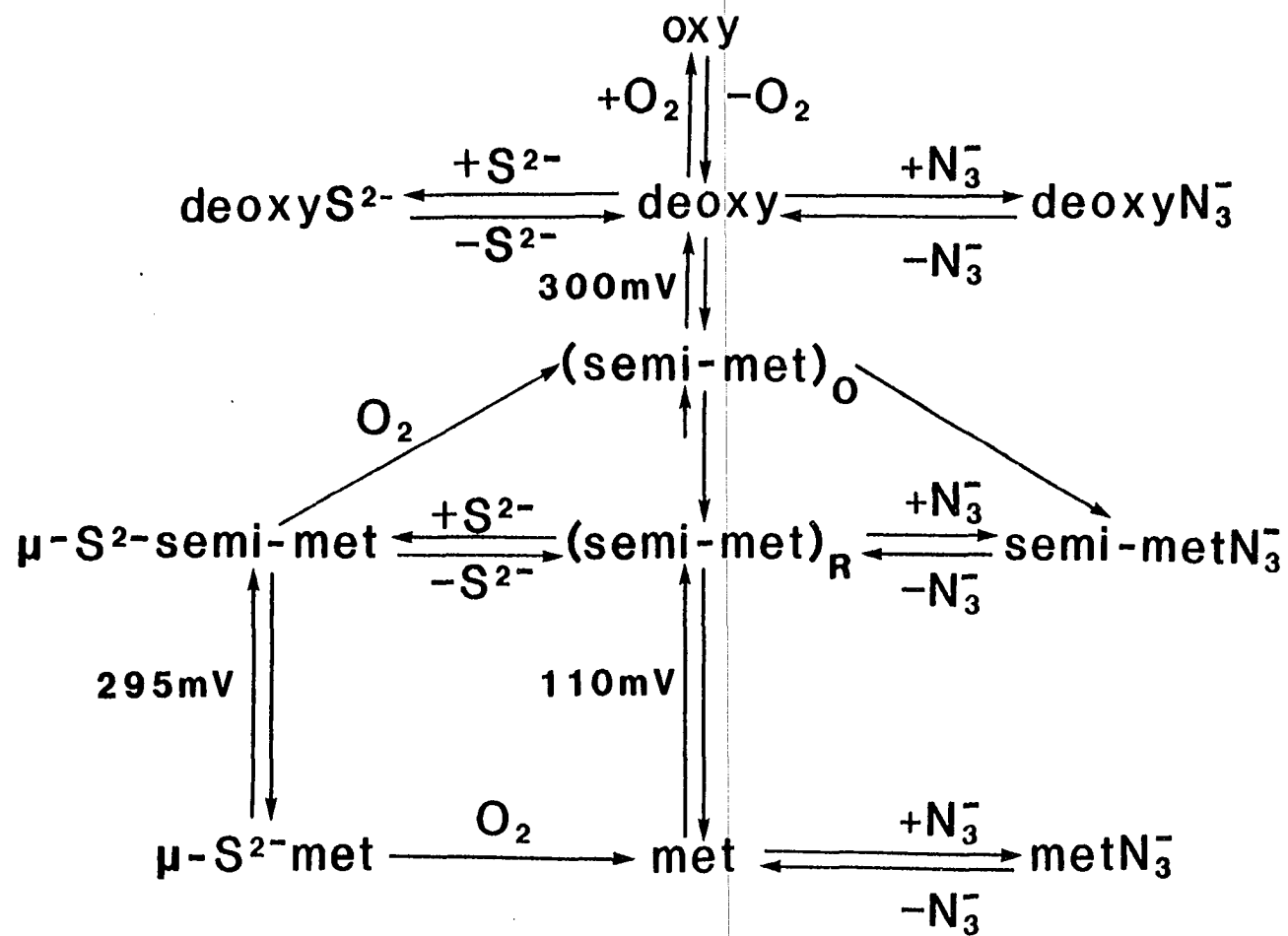
calculated. The best results are obtained by monitoring the development of EPR signals during equilibrations of $\mu\text{-S}^{2-}\text{-metHr}$ with $\text{Fe}^{2+}\text{cyt c}$ (both initial forms are EPR silent). The changes in the EPR intensities are difficult to measure when the alternative equilibrations of $\mu\text{-S}^{2-}\text{-semi-metHr}$ with $\text{Fe}^{3+}\text{cyt c}$ are monitored. The lower precision is due to the larger uncertainty in the concentrations obtained using integrations of EPR spectra in comparison to concentrations obtained from optical spectra. The value reported is the average of six independent equilibration experiments.

The reactivity of $\mu\text{-S}^{2-}\text{-semi-metHr}$ and $\mu\text{-S}^{2-}\text{-metHr}$ can be summarized in terms of Scheme III-4. The following discussion considers the stability and reactivity of the $\mu\text{-S}^{2-}\text{-Hrs}$ in order to explain and justify Scheme III-4.

2. Anaerobic stability of $\mu\text{-S}^{2-}\text{-semi-metHr}$

$\mu\text{-S}^{2-}\text{-semi-metHr}$ can be maintained over a period of several weeks if kept under anaerobic conditions in the presence of excess sulfide at 4 °C. Extended anaerobic dialysis of $\mu\text{-S}^{2-}\text{-semi-metHr}$ against Tris/acetate results in dissociation of the bound sulfide. As illustrated by the EPR spectra in Figure III-21, the removal of sulfide in such a manner results in solutions giving a mixture of semi-metHr and $\mu\text{-S}^{2-}\text{-semi-metHr}$ EPR signals. Comparisons of simulated EPR spectra for various ratios of $\mu\text{-S}^{2-}\text{-semi-metHr}$ to $(\text{semi-met})_0$

Scheme III-4



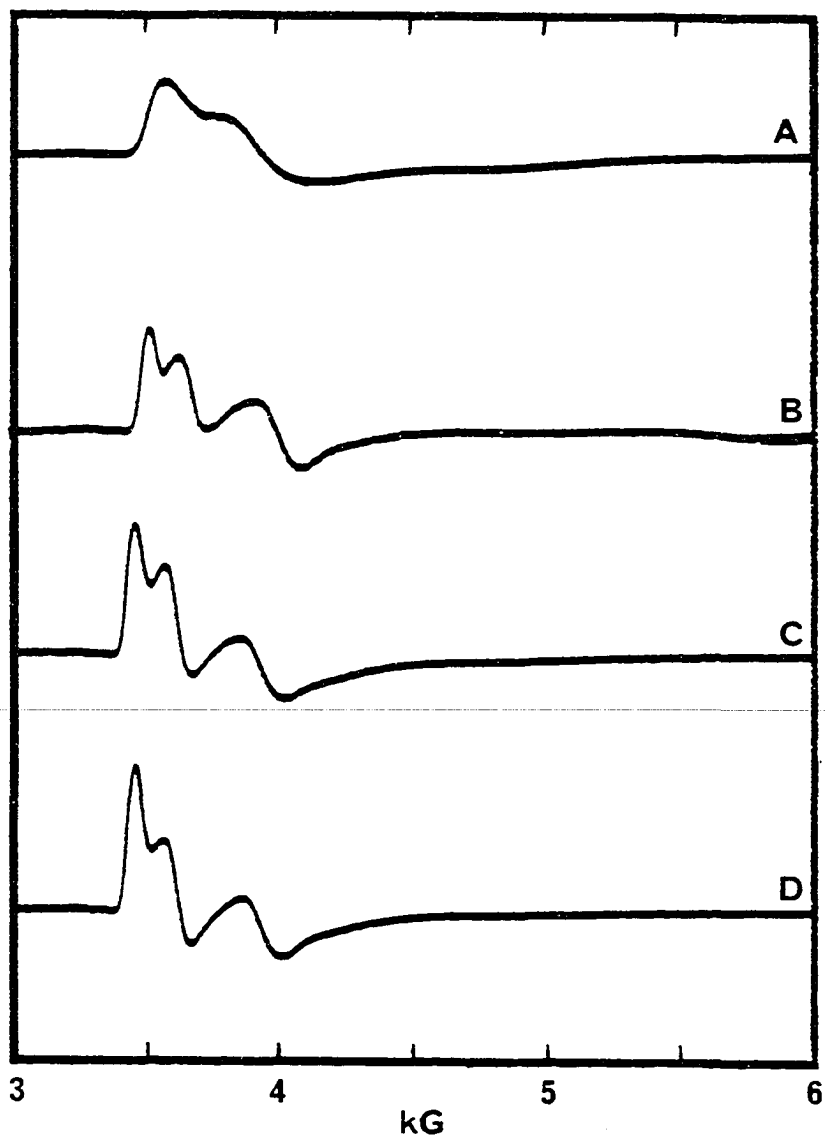


Figure III-21. EPR spectra following the extended anaerobic dialysis of $\mu\text{-S}^{2-}$ -semi-metHr: 2.1 mM protein in 50 mM Tris/acetate pH 8.0 at 4 °C

Dialysis times: A) 0 days, B) 3 days, C) 7 days, D) 20 days. Instrument parameters: temperature 4 K; frequency, 9.4216 GHz; power, 101 μW ; modulation amplitude, 16 G at 100 kHz; time constant, 0.2 s; receiver gain, 1.25×10^4

and $\mu\text{-S}^{2-}\text{semi-metHr}$ to $(\text{semi-met})_{\text{R}}$ indicate that the two predominant components in the observed spectra are due to $\mu\text{-S}^{2-}\text{semi-metHr}$ and $(\text{semi-met})_{\text{R}}$. After 20 days, there appears to be little or no reduction in overall EPR intensity, and the major contribution is from $(\text{semi-met})_{\text{R}}$.

3. $\mu\text{-S}^{2-}\text{semi-metHr}$ + ligand anions

Both EPR and UV-visible spectra confirm the observation by Freier et al. (65) that no reaction occurs when excess azide is added to $\mu\text{-S}^{2-}\text{semi-metHr}$ under anaerobic conditions at room temperature. Similar experiments with fluoride and nitrite also indicate a lack of reactivity of $\mu\text{-S}^{2-}\text{semi-metHr}$ with ligand anions.

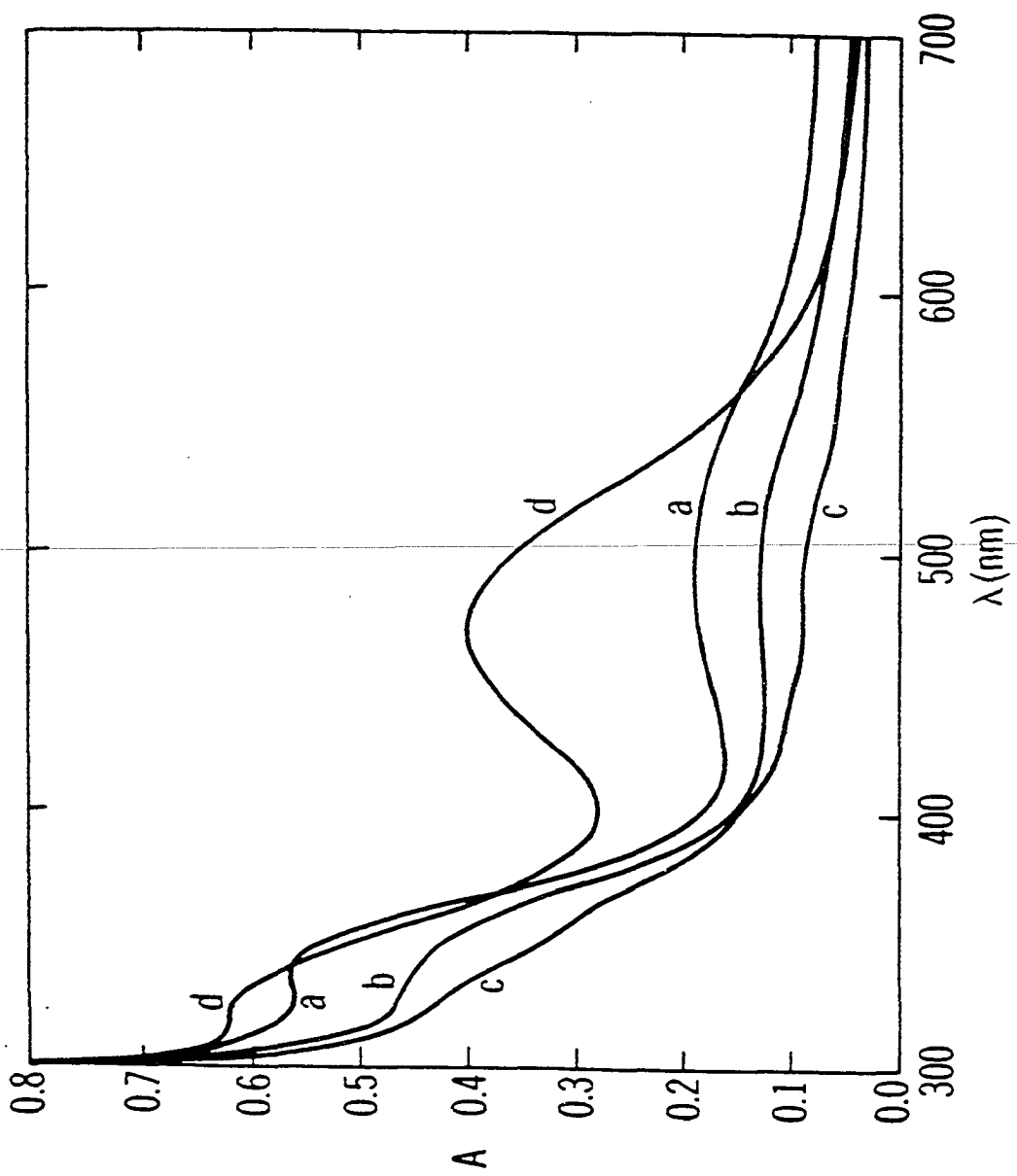
4. $\mu\text{-S}^{2-}\text{semi-metHr}$ + O_2

Freier et al. (65) reported that the resonance Raman spectrum of $\mu\text{-S}^{2-}\text{semi-metHr}$ was converted to that of oxyHr when the $\mu\text{-S}^{2-}\text{semi-metHr}$ was exposed to air. However, when following the same reaction by absorption and EPR spectroscopy in this laboratory, oxyHr is not the observed product. The absorption spectrum of the reaction product of $\mu\text{-S}^{2-}\text{semi-metHr}$ exposed to air is shown in Figure III-22 and consists of faint shoulders at approximately 320 nm, 360 nm and 500 nm. Addition of excess NaN_3 to this product results in the formation of semi-metN_3^- identified by its absorption

and EPR spectra (52, 54, 55). Monitoring of the reaction by EPR confirms the presence of semi-metHr, with subtle differences being observed depending on the presence or absence of perchlorate. The EPR spectra for each case are shown in Figure III-23 and III-24. $\mu\text{-S}^{2-}$ semi-metHr in Tris/perchlorate must be exposed to air for at least 15 minutes at room temperature before any changes are observed in the EPR signal. In the absence of perchlorate, i.e., in Tris/acetate, $\mu\text{-S}^{2-}$ semi-metHr samples frozen within 2 minutes after exposure to O_2 show changes in the EPR spectrum. At times much earlier than 40 minutes exposure of $\mu\text{-S}^{2-}$ semi-metHr to O_2 , the EPR spectra contain significant contributions from the $\mu\text{-S}^{2-}$ semi-metHr signal. The spectra after long reaction times have nearly the same g values (Figure III-23c: 2.02, 1.95, 1.86 and 1.72; Figure III-24b: 2.02, 1.95, 1.86 and 1.71). The difference is the persistence of the prominent 1.71 feature in perchlorate compared to its decrease in intensity in acetate. With the exception of the $g = 2.02$ feature, the products of reactions of $\mu\text{-S}^{2-}$ semi-metHr with O_2 have EPR spectra very similar to those observed during the conversion of $(\text{semi-met})_O$ towards $(\text{semi-met})_R$ reported by Wilkins and Harrington (1). For comparison purposes, EPR spectra were obtained during conversion of $(\text{semi-met})_O$ towards $(\text{semi-met})_R$ in the presence and absence of perchlorate and are given in Figures III-25 and III-26. In Tris/acetate pH 8.0

Figure III-22. Absorption spectra obtained during aerobic incubation of 0.16 mM μ -S²⁻ semi-metHr in 50 mM Tris/acetate pH 8.0 at room temperature

Cell pathlength = 1 cm. Reaction times: a) immediately after removal of excess sulfide by passage over a Sephadex G-25 column, b) 25 minutes, and c) 115 minutes in order of decreasing A_{500} , d) addition of NaN_3 at 150 minutes yields semi-metN₃⁻ spectrum (λ_{max} 470, 320sh)



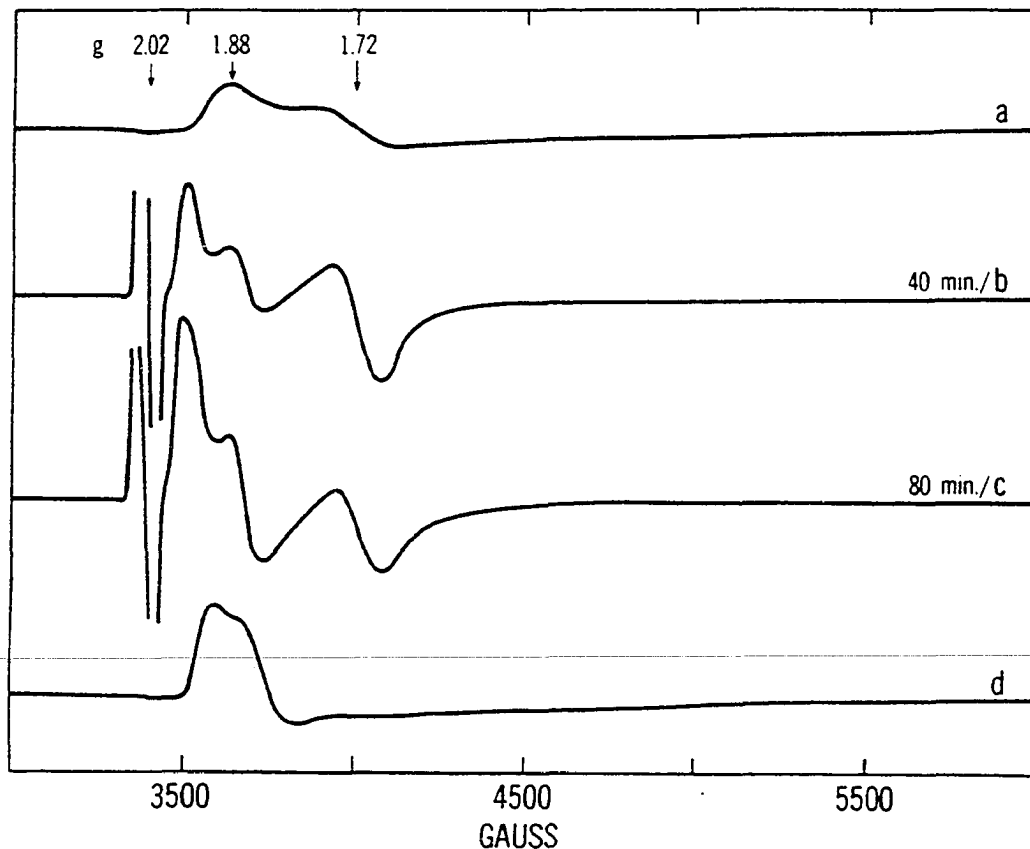


Figure III-23. EPR spectra observed during incubation of 1.94 mM μ -S²⁻semi-met in 50 mM Tris/acetate pH 8.0 at room temperature

a) before exposure to air, b) and c) after exposure to air for the indicated times, d) after addition of excess N_3^- to sample in c). Sample in c) had been passed over a Sephadex G-25 column before freezing. Instrument parameters: temperature 4 K; frequency, 9.750 GHz; power, 100 μ W; modulation amplitude, 16 G at 100 kHz; time constant, 0.2 s; receiver gain, 5.0×10^4

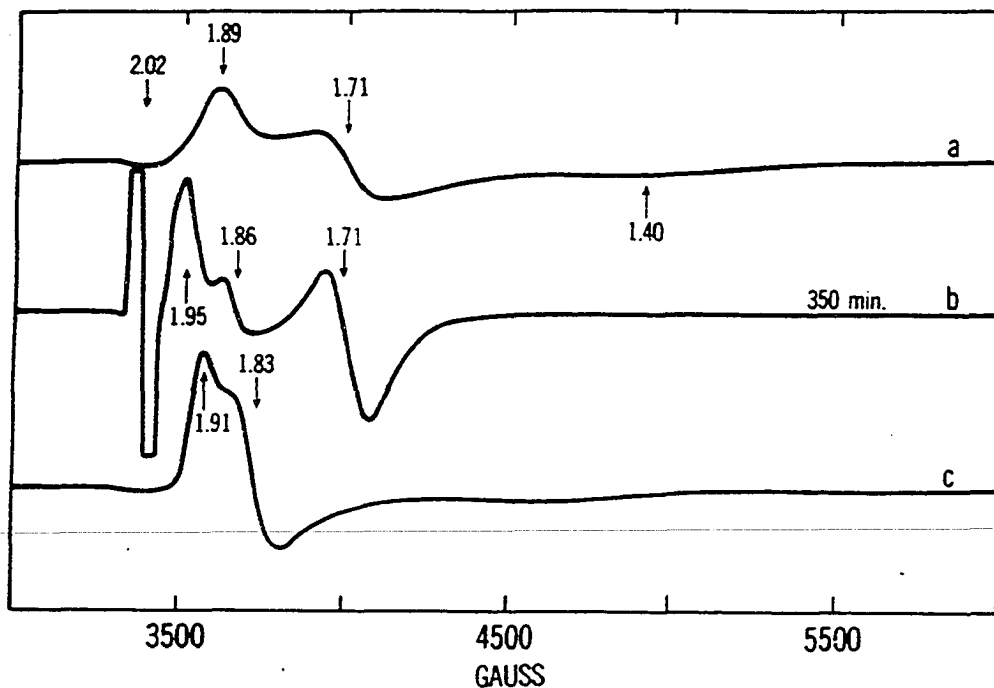


Figure III-24. EPR spectra observed during aerobic incubation of 1.94 mM μ -S²⁻ semi-met in 50 mM Tris/perchlorate pH 8.0 at room temperature

a) immediately after removal of excess S²⁻ by passage over a Sephadex G-25 column, b) after 350 minute exposure to air, c) after addition of NaN₃ (0.515 M) at 345 minute exposure to air. Instrument parameters: temperature 4 K; frequency, 9.750 GHz; power, 100 μ W; modulation amplitude, 16 G at 100 kHz; time constant, 0.2 s; receiver gain, 5.0×10^4

(Figure III-25) the final spectrum is not obtained until after ~ 50 minutes, almost twice the reaction time reported by Wilkins and Harrington (1, 55). In Tris/perchlorate (Figure III-26) the same conversion towards (semi-met)_R occurs, but the spectrum obtained after ~ 50 minutes in Tris/acetate is not observed until ~ 120 minutes in Tris/perchlorate. Comparison of spectra in Figures III-25 and III-23 (both in Tris/acetate) show that the product upon oxidative loss of sulfide from $\mu\text{-S}^{2-}$ -semi-metHr generates a spectrum that resembles the 8 minute spectrum during the conversion of (semi-met)_O towards (semi-met)_R. Upon oxidative loss of sulfide from $\mu\text{-S}^{2-}$ -semi-metHr similar EPR spectra are obtained at 40 minutes in Tris/acetate and 350 minutes in Tris/perchlorate (Figures III-23b and III-24b). These reaction times are consistent with the slowing effect of perchlorate on the (semi-met)_O towards (semi-met)_R conversion illustrated by comparison of Figures III-25 and III-26. A reasonable interpretation of these results is that (semi-met)_O is the initial product upon oxidative loss of sulfide from $\mu\text{-S}^{2-}$ -semi-metHr and implies that $\mu\text{-S}^{2-}$ -semi-metHr is in a conformation resembling that of (semi-met)_O when it loses sulfide oxidatively. The anaerobic loss of sulfide from $\mu\text{-S}^{2-}$ -semi-metHr discussed above (Figure III-21) occurs over several days and can be interpreted as due to a slow conformational change of $\mu\text{-S}^{2-}$ -semi-metHr to one more prone to loss of sulfide,

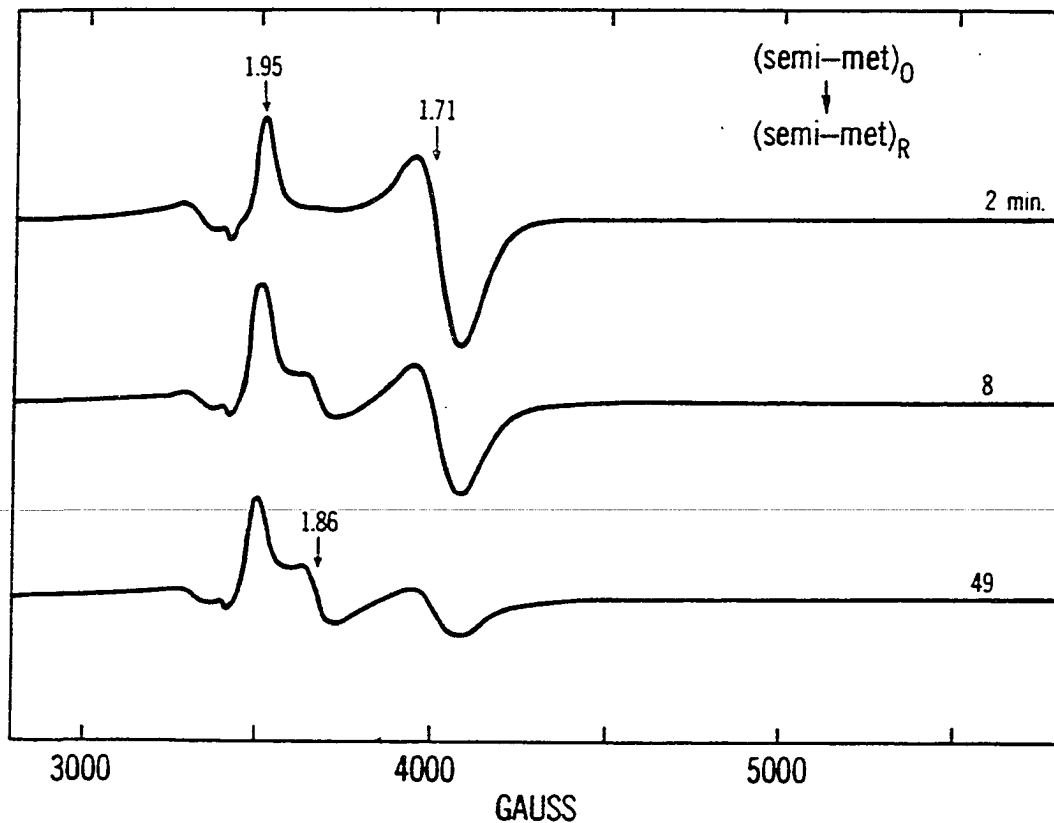


Figure III-25. EPR spectra obtained during anaerobic incubation of (semi-met)₀ for the indicated times in 50 mM Tris/acetate pH 8.0

Instrument parameters: temperature, 4 K;
 frequency, 9.569 GHz; power, 100 μ W;
 modulation amplitude, 16 G at 100 KHz; time
 constant, 0.2 s; receiver gain, 6.3×10^4 . The
 feature at ~ 3300 G is from the EPR cavity

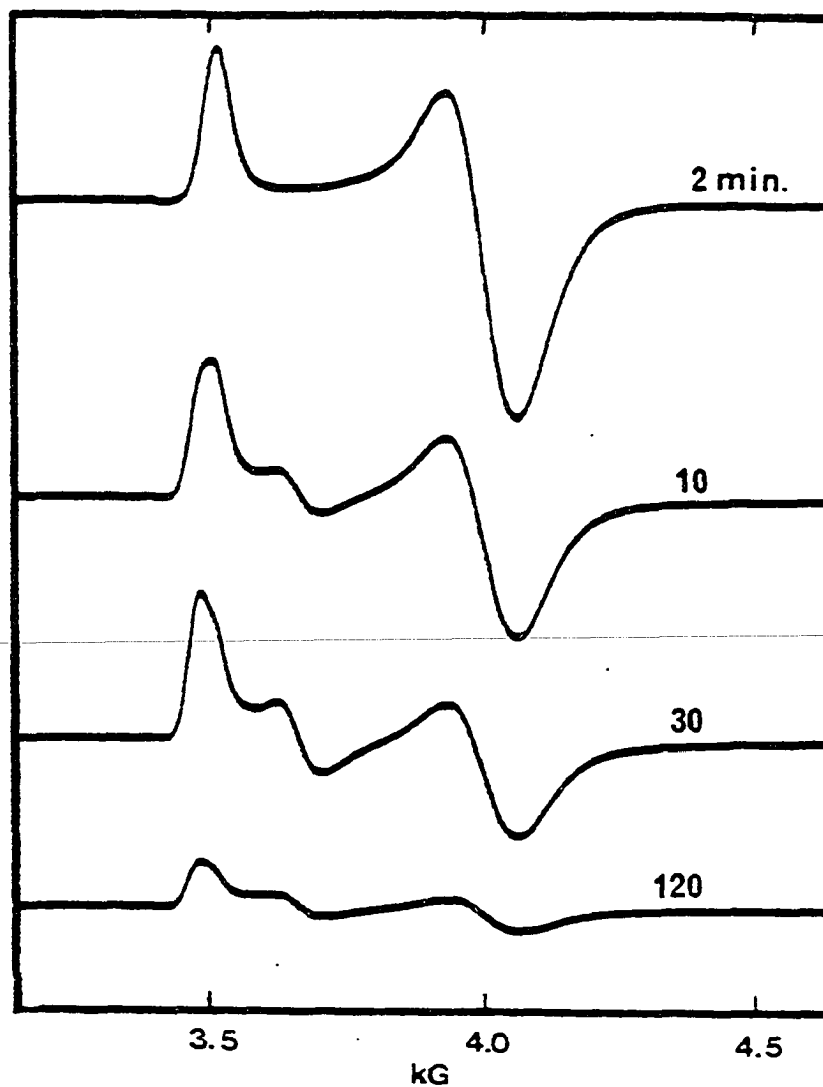
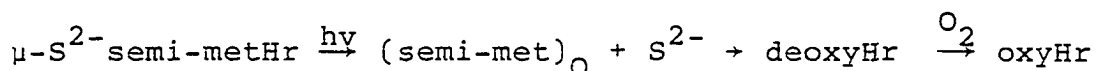


Figure III-26. Conversion of $(\text{semi-met})_O$ towards $(\text{semi-met})_R$ in 50 mM Tris/perchlorate pH 8.0 at room temperature as monitored by EPR

Instrument parameters: temperature 4.1 K; power, 100 μW ; modulation amplitude, 16 G at 100 kHz; time constant, 0.2 s; receiver gain, 1.25×10^4

perhaps resembling that of (semi-met)_R.

The results of Freier et al. (65) mentioned above are probably due to a photochemical reaction during laser irradiation of aerobic solutions of μ -S²⁻-semi-metHr. Our observations that prolonged laser irradiation of anaerobic solutions of μ -S²⁻-semi-metHr result in the formation of deoxyHr crystals and that (semi-met)_O is rapidly reduced to deoxyHr by sulfide make it possible to explain the results of Freier et al. by the following series of reactions:



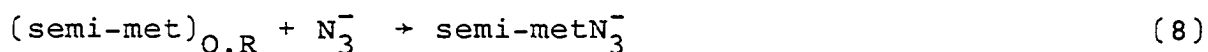
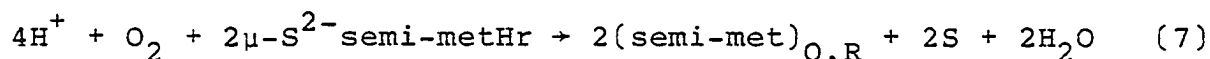
The rapid photochemically induced release of relatively large amounts of S²⁻ coupled with the limited amount of O₂ expected in a sealed Raman tube explains the formation of oxyHr rather than the thermal product (semi-met)_O. The proposed photochemically-induced release of the μ -sulfido bridge is supported by the fact that the exchange of the μ -oxo bridge of metmyoN₃⁻ is known to be light catalyzed (19).

The sharp g = 2.02 signal appearing in the EPR spectra for the reaction of μ -S²⁻-semi-metHr with O₂ has power saturation behavior very different from that of any of the semi-metHr derivatives (see Appendix A for power saturation curve). Since passage of the protein solution over a Sephadex G-25 column does not eliminate the g = 2.02 signal, the

radical must be associated with the protein. A similar EPR signal at $g = 2.01$ has been attributed to a cysteinyl disulfide radical (Cys-S-S \cdot) generated during oxidation of [4Fe-4S] centers in A.v Fd I (120). The $g = 2.02$ (but not the semi-met) signal disappears upon addition of dithiothreitol, ascorbate or sodium azide. The first two reagents likely cause reduction of the radical. A similar reduction is observed for the reaction of $g = 2.01$ of A.v Fd I with dithiothreitol. The loss of the $g = 2.02$ signal upon addition of N_3^- is illustrated in Figures III-23c and III-24d and can be rationalized by conformational changes occurring upon azide binding that could destabilize the Cys-S-S \cdot by increasing its exposure to water. Azide binding is known to greatly increase the reactivity of Cys-50 with sulfhydryl reagents (63).

As already mentioned, addition of azide to the product of the reaction of μ -S²⁻-semi-metHr with O_2 yields semi-metN₃⁻. By either double integration of the EPR spectra or using the absorbance at 470 nm (see Table I-2), 90 - 100 % of the initial protein concentration can be accounted for as semi-metN₃⁻. Figure III-27 shows the optical absorption spectra resulting from addition of excess N_3^- to μ -S²⁻-semi-metHr simultaneously with exposure to air. Two isosbestic points at ~ 544 nm and ~ 385 nm suggest that μ -S²⁻-semi-metHr and semi-metN₃⁻ are the only two species present. This result can be explained in terms of oxygen's reacting with the bridging

sulfide rather than directly at the iron atoms. The semi-metN₃⁻ would then be produced by a two-step sequence shown in reactions 7 and 8. The formation constant



for P. gouldii semi-metN₃⁻ (reaction 8) at pH 8.2 exceeds 10³ M⁻¹cm⁻¹, and the half-life for reaction 8 should be a few seconds under the conditions of Figure III-27 (52). Thus, the (semi-met)_{O,R} intermediates are never present in significant concentrations during the two-step reaction sequence. EPR spectra obtained over the time course of the same reaction are also consistent with a mixture of only μ-S²⁻-semi-metHr and semi-metN₃⁻ as shown in Figure III-28. Comparison of the simulations in Figure III-28B with the actual spectra in Figure III-28A indicates that ~ 60 % semi-metN₃⁻ is present after 15 minutes under the experimental conditions used for Figure III-28A. The similar time courses in Figures III-24 and III-28A, which were conducted with stirred samples open to air, suggest that N₃⁻ does not significantly change the time course of reaction 7.

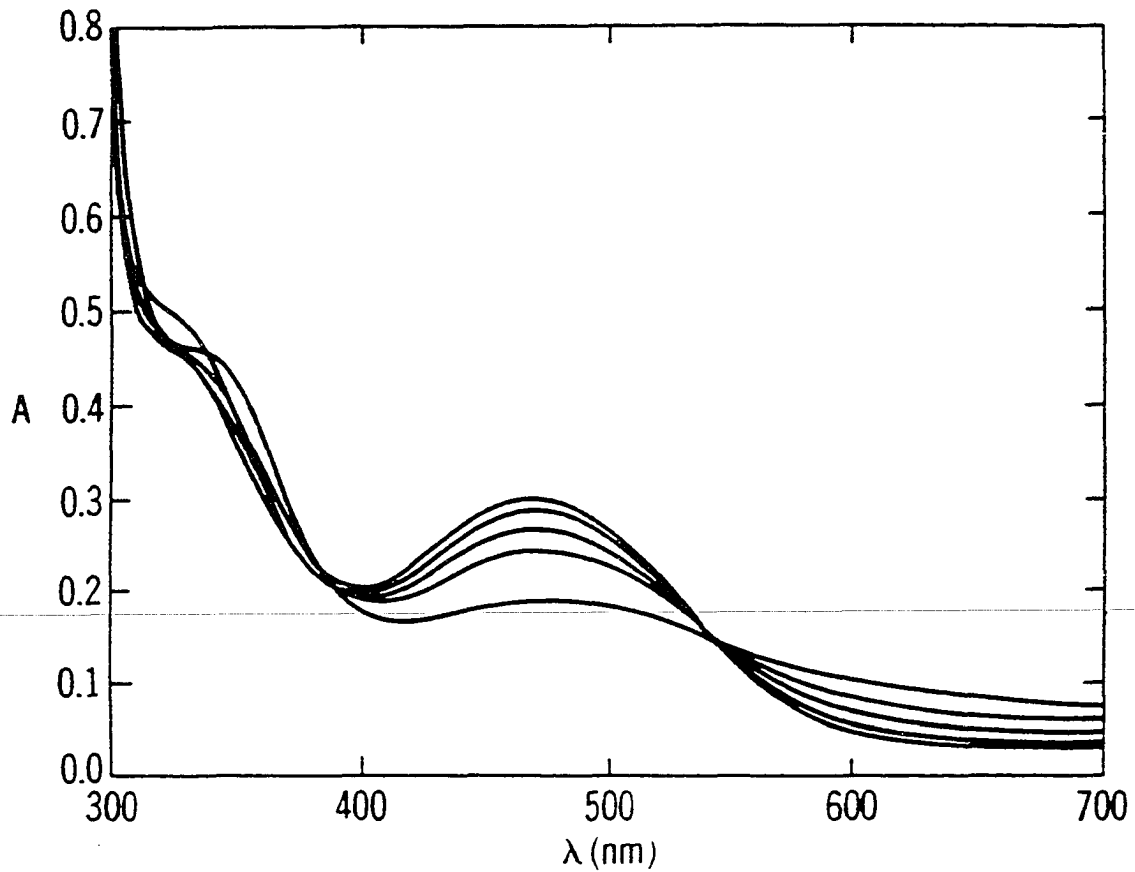


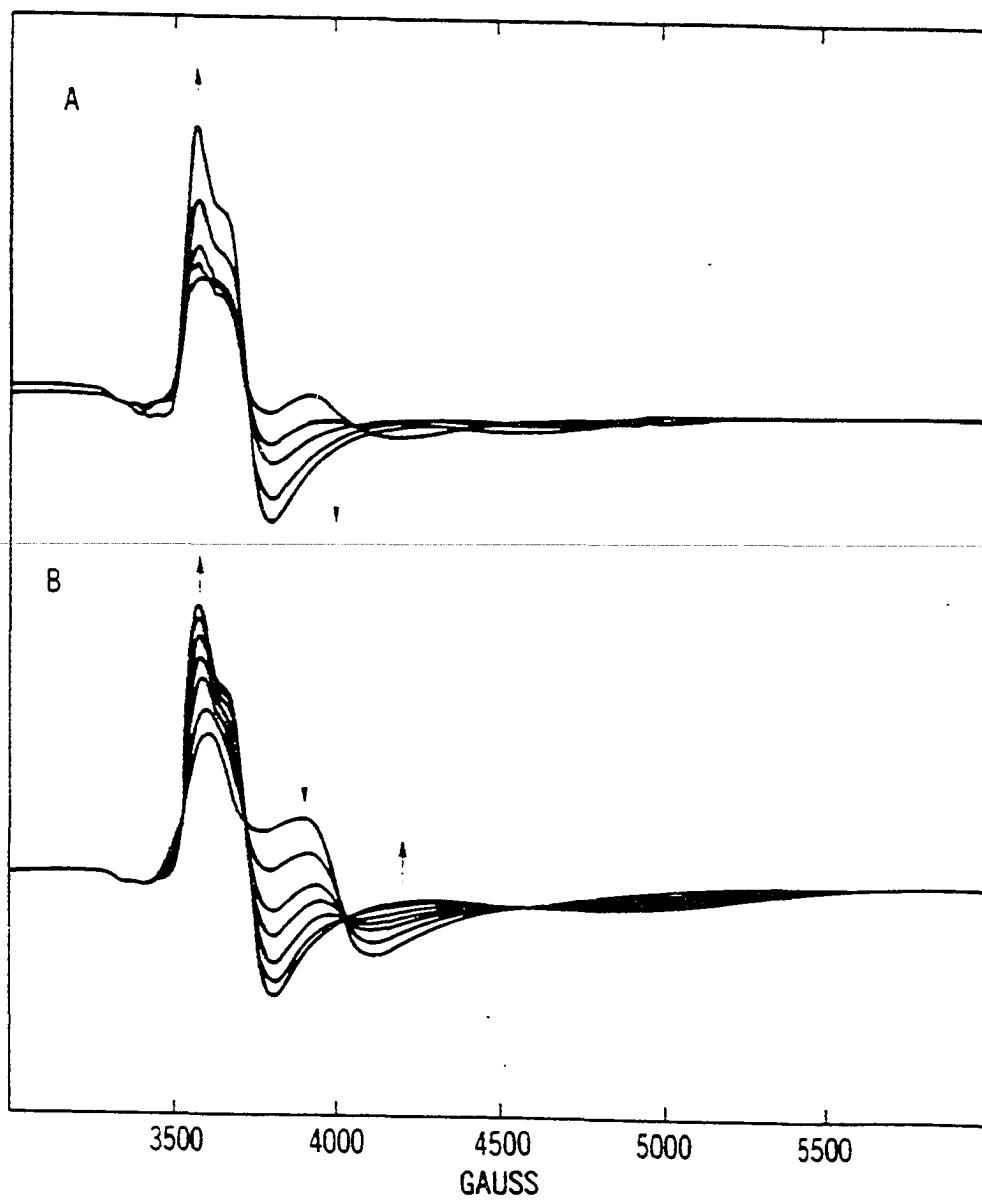
Figure III-27. Absorption spectra obtained during aerobic incubation of $0.125 \text{ mM } \mu\text{-S}^{2-}$ semi-metHr in 50 mM Tris/acetate pH 8.0 at room temperature in the presence of 6.5 mM NaN_3

Excess sulfide was removed by passage over a Sephadex G-25 column. Cell pathlength = 1 cm. Reaction times (min) in order of increasing A_{470} : 10, 25, 50, 115 and 295. The 295 minute spectrum has highest A_{320} and lowest A_{600}

Figure III-28. Aerobic reaction of $\mu\text{-S}^{2-}$ -semi-metHr with excess azide in 50 mM Tris/perchlorate at room temperature

A) EPR spectra obtained during aerobic incubation of 1.95 mM $\mu\text{-S}^{2-}$ -semi-metHr in the presence of 0.515 M NaN_3^- . Reaction times (min) in order of increasing intensity at the fields indicated by the vertical arrows: 15, 40, 63, 110, 345. Instrument parameters: temperature, 4 K; frequency, 9.750 GHz, power, 100 μW ; modulation amplitude, 16 G at 100 kHz; time constant, 0.2 s; receiver gain, 5.0×10^4

B) Computer simulation of EPR spectra resulting from mixture of $\mu\text{-S}^{2-}$ -semi-metHr and semi-met N_3^- . Percentages of $\mu\text{-S}^{2-}$ -semi-met: 100, 75, 50, 35, 20, 8 and 0. Arrows indicate directions of decreasing $\mu\text{-S}^{2-}$ -semi-metHr content



5. μ -S²⁻metHr + ligand anions

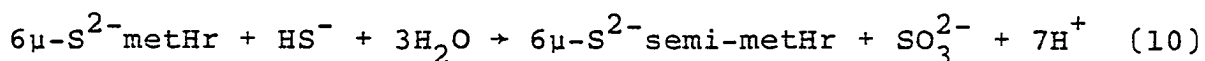
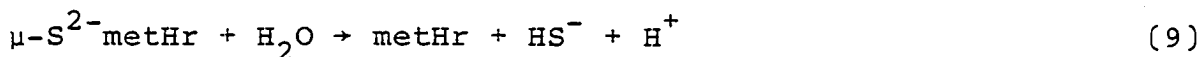
Addition of a 100-250 fold molar excess of N_3^- , SCN^- , CN^- or Cl^- to solutions of μ -S²⁻metHr in either Tris/acetate or Tris/perchlorate buffer pH 8.0 fails to significantly perturb the absorption spectrum of μ -S²⁻metHr for at least one hour at 4 °C. Similarly the resonance Raman spectrum of μ -S²⁻metHr in Tris/perchlorate pH 8.0 is unperturbed even after several hours incubation at 4 °C in the presence of excess N_3^- except for the appearance of a weak peak at 371 cm^{-1} , indicative of a small proportion of metN₃⁻ (60). Therefore, the UV-visible and resonance Raman spectra give no indication of a stable μ -S²⁻metHr/anion adduct under conditions where these adducts are known to form for metHr (121). If an anion adduct does exist, it is either very short-lived or extremely slow in forming under the given experimental conditions. Considering a bridging sulfide geometry for the sulfideHrs, the absence or fleeting nature of an anion addition to the iron site of μ -S²⁻metHr compared to that of metHr can be rationalized on steric and electronic grounds. Replacement of the bridging oxygen with the more electron donating sulfur could reduce the tendency of the five-coordinate iron to add a sixth ligand, especially an anion. Sulfur-containing ligands coordinated to iron most often stabilize coordination spheres of less than six (110). Evidence accumulated over several years has shown that the anion coordination site in metHr is

sterically restricted to ligands consisting of three or fewer non-hydrogen atoms (1, 29, 32). Upon substitution of the bridging sulfide for the oxide, the increase in bridge bond distances discussed in Section III-C coupled with the larger ionic radius of sulfide could result in increased steric restrictions at the anion binding site. According to Stenkamp (University of Washington, personal communication) if azide were to bind at the five-coordinate iron in $\mu\text{-S}^{2-}\text{metHr}$, the middle nitrogen atom of azide would be within the Van der Waal's radius of the bridging sulfide indicating that with a bridging sulfide there may no longer be room at the iron site for an additional ligand.

6. Stability of $\mu\text{-S}^{2-}\text{metHr}$

In anaerobic solutions $\mu\text{-S}^{2-}\text{metHr}$ slowly autoreduces to form $\mu\text{-S}^{2-}\text{semi-metHr}$. In light of the rather positive reduction potential measured for the $\mu\text{-S}^{2-}\text{metHr}/\mu\text{-S}^{2-}\text{semi-metHr}$ couple, this autoreduction is not surprising. At room temperature the first signs of the $\mu\text{-S}^{2-}\text{semi-metHr}$ EPR signal in a relatively concentrated sample of $\mu\text{-S}^{2-}\text{metHr}$ (1.68 mM) in Tris/acetate pH 8.0 are observed after 12 hours with the maximum $\mu\text{-S}^{2-}\text{semi-metHr}$ concentration (0.82 spins/2Fe) being detected after 48 hours. Changes in the absorbance spectrum are observed within an hour of diluting the protein in preparation of the UV-visible sample. The presence of

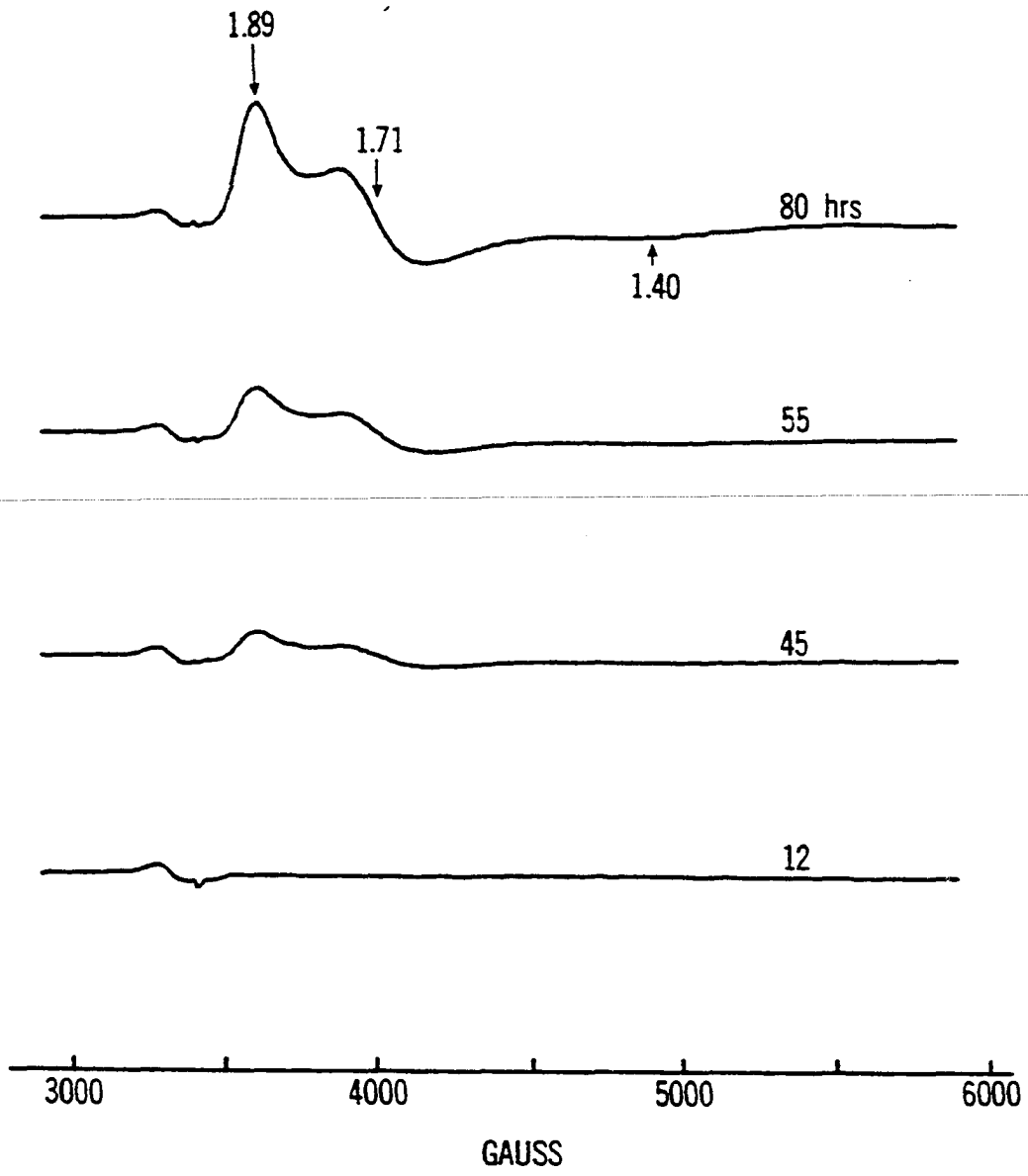
perchlorate stabilizes $\mu\text{-S}^{2-}\text{metHr}$ against autoreduction. In anaerobic Tris/perchlorate pH 8.0 $\mu\text{-S}^{2-}\text{metHr}$ is stable for several days at 4 °C and for much longer when frozen. At room temperature in anaerobic Tris/perchlorate pH 8.0, no significant changes in the absorption spectrum occurs for ~ 6 hours. However, over the course of three days at room temperature a shoulder at 340 nm, a decrease in visible absorbance and an EPR spectrum, which are all characteristic of $\mu\text{-S}^{2-}\text{semi-metHr}$, develop. As shown in Figure III-29, no EPR signal is seen before 44 hours incubation time, and the maximum signal (0.81 spins/2Fe) is observed at 80 hours. Based on these spin quantitations, the autoreduction can be explained in terms of reactions 9 and 10. Theoretically, 14.3 % of the sulfide needs to dissociate via reaction 9 to



reduce the remaining 85.7 % $\mu\text{-S}^{2-}\text{metHr}$ to $\mu\text{-S}^{2-}\text{semi-metHr}$ via reaction 10. Based on the measured potentials for the reduction of $\mu\text{-S}^{2-}\text{metHr}$ to $\mu\text{-S}^{2-}\text{semi-metHr}$ (283-312 mV) and the sulfite/sulfide reduction potential (-120 mV) (104), reaction 10 is thermodynamically feasible.

Figure III-29. EPR spectra observed at the indicated times during anaerobic incubation at room temperature of 1.78 mM μ -S²⁻metHr in 50 mM Tris/perchlorate pH 8.0

Instrument parameters: temperature 4 K; frequency, 9.57 GHz, power, 100 μ W; modulation amplitude, 16 G at 100 kHz; time constant, 0.2 s; receiver gain, 3.2×10^4 . Double integration gives the following spins/2 Fe: 12 hours, 0; 45 hours, 0.04; 55 hours, 0.14; 80 hours, 0.81. The weak feature at \sim 3300 G is from the EPR cavity



The autoreduction of $\mu\text{-S}^{2-}\text{metHr}$ is accelerated in the presence of ligand anions. As discussed above, there is no evidence for formation of stable ligand anion adducts of $\mu\text{-S}^{2-}\text{metHr}$. However, these ligand anions could conceivably cause dissociation of the bridging sulfide in $\mu\text{-S}^{2-}\text{metHr}$ by "attack" of the ligand anion at the five-coordinate iron. The increased rate of autoreduction can thus be viewed as an acceleration of reaction 9 by ligand anion. Due to the tight binding of azide to metHr, the autoreduction in this case should theoretically result in 14.3 % metN_3^- and 85.7 % $\mu\text{-S}^{2-}\text{semi-metHr}$. Starting with $\mu\text{-S}^{2-}\text{metHr}$ in Tris/acetate anaerobically at room temperature, addition of a 570-fold molar excess of azide results in the maximum $\mu\text{-S}^{2-}\text{semi-metHr}$ concentration (0.85 spins/2Fe) as monitored by EPR after 11 hours as shown in Figure III-30. During this time period, no EPR signal is observed in the absence of added ligand anions. Thus autoreduction is accelerated 4-5 fold at a molar ratio of $\text{N}_3^-/\mu\text{-S}^{2-}\text{metHr} = 570$. The anaerobic reaction of $\mu\text{-S}^{2-}\text{metHr}$ plus azide results in an absorption spectrum that has a broad peak at 470 nm and a shoulder at 340 nm. The shoulder at 340 nm is indicative of $\mu\text{-S}^{2-}\text{semi-metHr}$. Since the EPR spectra of this reaction show development of only the $\mu\text{-S}^{2-}\text{semi-metHr}$ signal, formation of semi-metN_3^- need not be considered. The broad peak at 470 nm is presumably

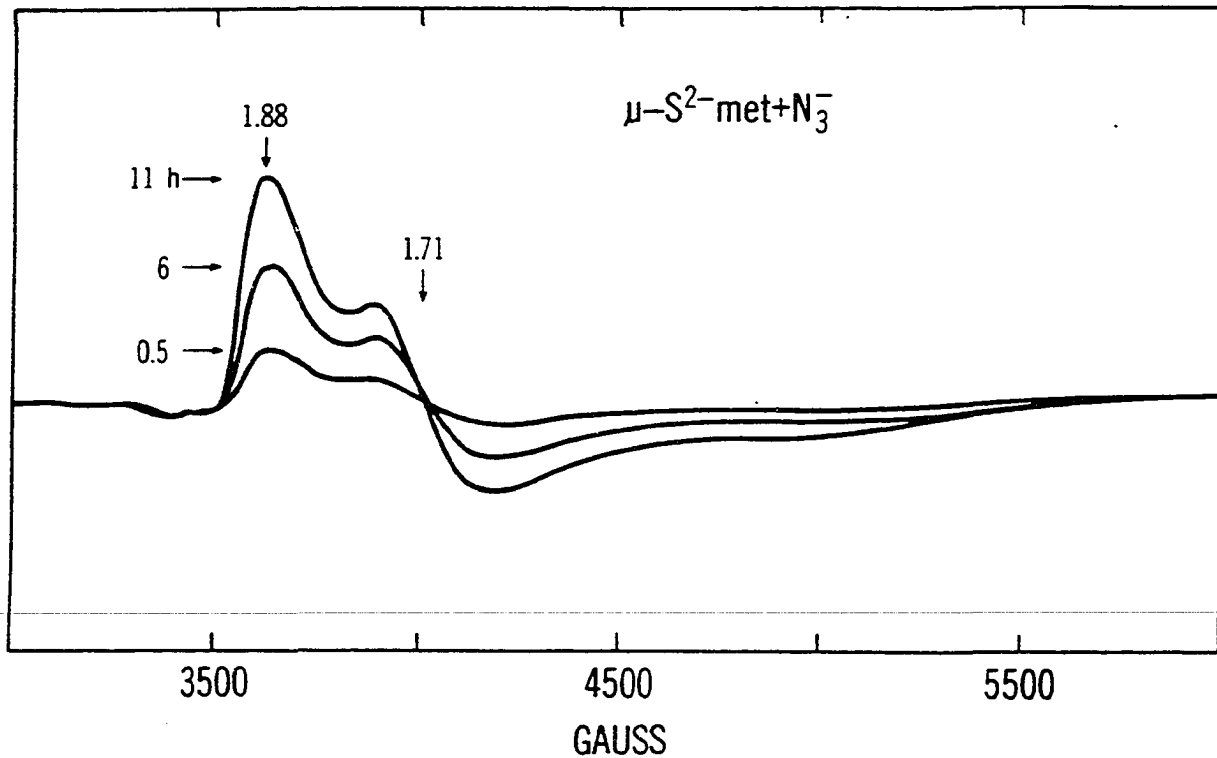


Figure III-30. EPR spectra observed during anaerobic incubation at room temperature of 1.48 mM $\mu\text{-S}^{2-}\text{-met}$ in 50 mM Tris/acetate pH 8.0 in the presence of 0.84 mM NaN_3 .

Instrument parameters: temperature 4 K; frequency, 9.569 GHz; power, 100 μW ; modulation amplitude, 16 G at 100 kHz; time constant, 0.2 s; receiver gain, 5.0×10^4 . Double integration gives the following spins/2Fe (time): 0.07 (0.5h); 0.5 (6h); 0.85 (11h). Times are listed in order of increasing intensity at $g = 1.88$

due to $\mu\text{-S}^{2-}$ -semi-metHr containing $\sim 15\%$ metN_3^- . Other ligands also accelerate the anaerobic autoreduction of $\mu\text{-S}^{2-}$ -metHr in the order $\text{N}_3^- > \text{CN}^- \sim \text{SCN}^- > \text{Cl}^-$.

Addition of one equivalent of $\text{Fe}(\text{CN})_6^{3-}$ to $\mu\text{-S}^{2-}$ -metHr in Tris/perchlorate under anaerobic conditions inhibits the autoreduction. When the $\mu\text{-S}^{2-}$ -metHr control (no $\text{Fe}(\text{CN})_6^{3-}$ added) contains its maximum $\mu\text{-S}^{2-}$ -semi-metHr concentration (88 hours), the $\mu\text{-S}^{2-}$ -metHr plus $\text{Fe}(\text{CN})_6^{3-}$ solution is EPR silent. This inhibition of autoreduction by $\text{Fe}(\text{CN})_6^{3-}$ is probably due to oxidations of both sulfide which dissociates from $\mu\text{-S}^{2-}$ -metHr via reaction 9 and $\mu\text{-S}^{2-}$ -semi-metHr which may be formed via reaction 10.

7. $\mu\text{-S}^{2-}$ -metHr + sulfide

Sulfide can also be used as a source of reducing equivalents for preparing $\mu\text{-S}^{2-}$ -semi-metHr from $\mu\text{-S}^{2-}$ -metHr. The UV-visible spectra of the reaction of $\mu\text{-S}^{2-}$ -metHr with sulfide using $\text{H}_2\text{S}_{(g)}$, NaSH or $\text{Na}_2\text{S}\cdot 9\text{H}_2\text{O}$ as the sulfide source indicate that the reduction reaction is complete within the time of mixing under conditions using molar ratios of 1.0 to 4.0 for sulfide/ $\mu\text{-S}^{2-}$ -metHr. EPR quantitations which confirm that $\sim 100\%$ of the protein is $\mu\text{-S}^{2-}$ -semi-metHr. Using a molar ratio of 0.2 sulfide/ $\mu\text{-S}^{2-}$ -metHr, the reduction is complete within 3 1/2 hours. This result is additional evidence for reaction 10 occurring during autoreduction of

$\mu\text{-S}^{2-}\text{metHr}$.

8. $\mu\text{-S}^{2-}\text{metHr}$ + reducing agents other than sulfide

Reaction of $\text{Na}_2\text{S}_2\text{O}_4$ with $\mu\text{-S}^{2-}\text{metHr}$ mimics the fast reduction of the $\mu\text{-S}^{2-}\text{metHr}$ by sulfide. Addition of one reducing equivalent of dithionite/mole $\mu\text{-S}^{2-}\text{metHr}$ gives quantitative formation of the $\mu\text{-S}^{2-}\text{semi-metHr}$ EPR signal within 0.5 minutes after mixing. Table III-9 indicates the $\mu\text{-S}^{2-}\text{semi-metHr}$ concentrations determined from double integration of EPR spectra, and the percentage of the total protein in the EPR active form. These relatively rapid reductions ($\mu\text{-S}^{2-}\text{metHr}$ + sulfide or dithionite) are more consistent with bridging than terminal sulfide based on analogies to the corresponding $\mu\text{-oxo}$ bridged derivatives. For terminal anion adducts of metHr such as metN_3^- , only the dissociated form reacts with reducing agents, and the reactions occur over much longer time periods (122).

UV-visible and EPR spectra indicate that $\text{Fe}(\text{CN})_6^{4-}$ reduces $\mu\text{-S}^{2-}\text{metHr}$ to $\mu\text{-S}^{2-}\text{semi-metHr}$ relatively slowly, and approximately 100-fold molar excess of ferrocyanide over protein is necessary for completion of the reaction in 15 minutes. Excess thiosulfate and sulfite do not undergo any detectable reaction with $\mu\text{-S}^{2-}\text{metHr}$. These latter two results are consistent with the postulated reaction 10.

Table III-9. Concentrations of $\mu\text{-S}^{2-}$ -semi-metHr present in reaction mixtures of $\mu\text{-S}^{2-}$ -metHr plus one equivalent of dithionite. Reactions carried out at 25 °C in 50 mM Tris/acetate pH 8.0

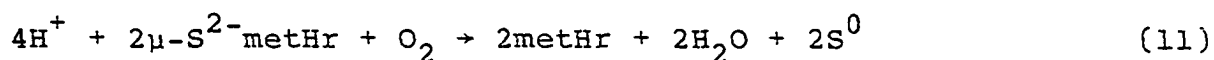
Reaction time (min.)	$[\mu\text{-S}^{2-}\text{-semi-metHr}]^a$ (mM)	Percent total Hr as $\mu\text{-S}^{2-}$ -semi-metHr
0.5	0.58	96 %
5.0	0.66	109 %
10.0	0.64	106 %

^a $\mu\text{-S}^{2-}$ -semi-metHr concentrations determined by double integration of EPR spectra.

9. $\mu\text{-S}^{2-}$ -metHr + O₂

In the presence of O₂, $\mu\text{-S}^{2-}$ -metHr is unstable relative to metHr. The binuclear iron center of $\mu\text{-S}^{2-}$ -metHr slowly reverts to the oxo-bridge configuration accompanied apparently by oxidation of sulfide. In aerobic Tris/perchlorate pH 8.0 at room temperature, the absorption spectrum of $\mu\text{-S}^{2-}$ -metHr (53.9 μM) changes smoothly over the course of 12 hours to that of metHr as shown in Figure III-31. Two isosbestic points at ~ 400 nm and ~ 320 nm are observed indicating the presence of only two species. A slight turbidity develops during the latter stages of the reaction attributable to precipitation of

S^0 . Examination of 0.1 mL aliquots of the reaction mixture at 4 K show that the $\mu-S^{2-}$ -metHr \rightarrow metHr transformation is not accompanied by the development of any significant EPR intensity. Lack of an EPR signal throughout the course of the reaction and formation of only $metN_3^-$ upon addition of azide suggest that O_2 is oxidizing the sulfide in a manner shown in reaction 11. $\mu-S^{2-}$ -metHr is never exposed to significant



concentrations of free sulfide in aerobic solutions because sulfide dissociation (reaction 9) in Tris/perchlorate is not appreciable on the time scale of reaction 11, i.e., autoreduction does not occur during this time period. If $\mu-S^{2-}$ -metHr in Tris/acetate is exposed to O_2 in the absence of perchlorate, there is a slightly different result. During the reaction, two EPR active species with g values 2.02 and 1.94, 1.88 and 1.71 are generated. These signals are very similar to ones observed during early times in the $\mu-S^{2-}$ -semi-metHr plus O_2 reaction discussed earlier in this section. However, in the present case the semi-metHr signals (g = 1.94, 1.88 and 1.71) account for no more than 6 % of the total protein concentration. Apparently due to the faster rate of autoreduction of $\mu-S^{2-}$ -metHr in Tris/acetate than in Tris/perchlorate, a minor pathway consisting of reactions 9,

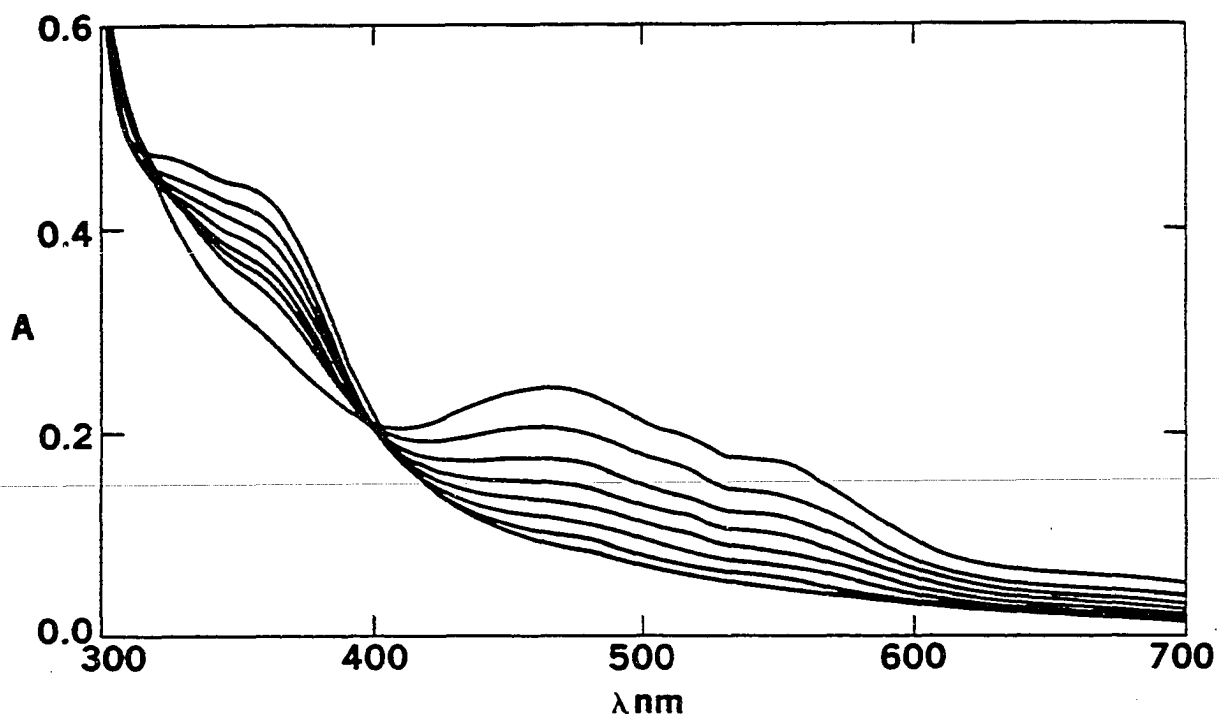


Figure III-31. Absorption spectra observed during aerobic incubation of 53.9 μM $\mu\text{-S}^{2-}\text{metHr}$ in 50mM Tris/perchlorate pH 8.0 at room temperature

Path length = 1 cm. With time the spectra show a decrease in absorbance at 464 nm and an increase at 360 nm. The second scan was recorded 4 hours after the initial scan. Succeeding spectra are at ~ 1 hour intervals

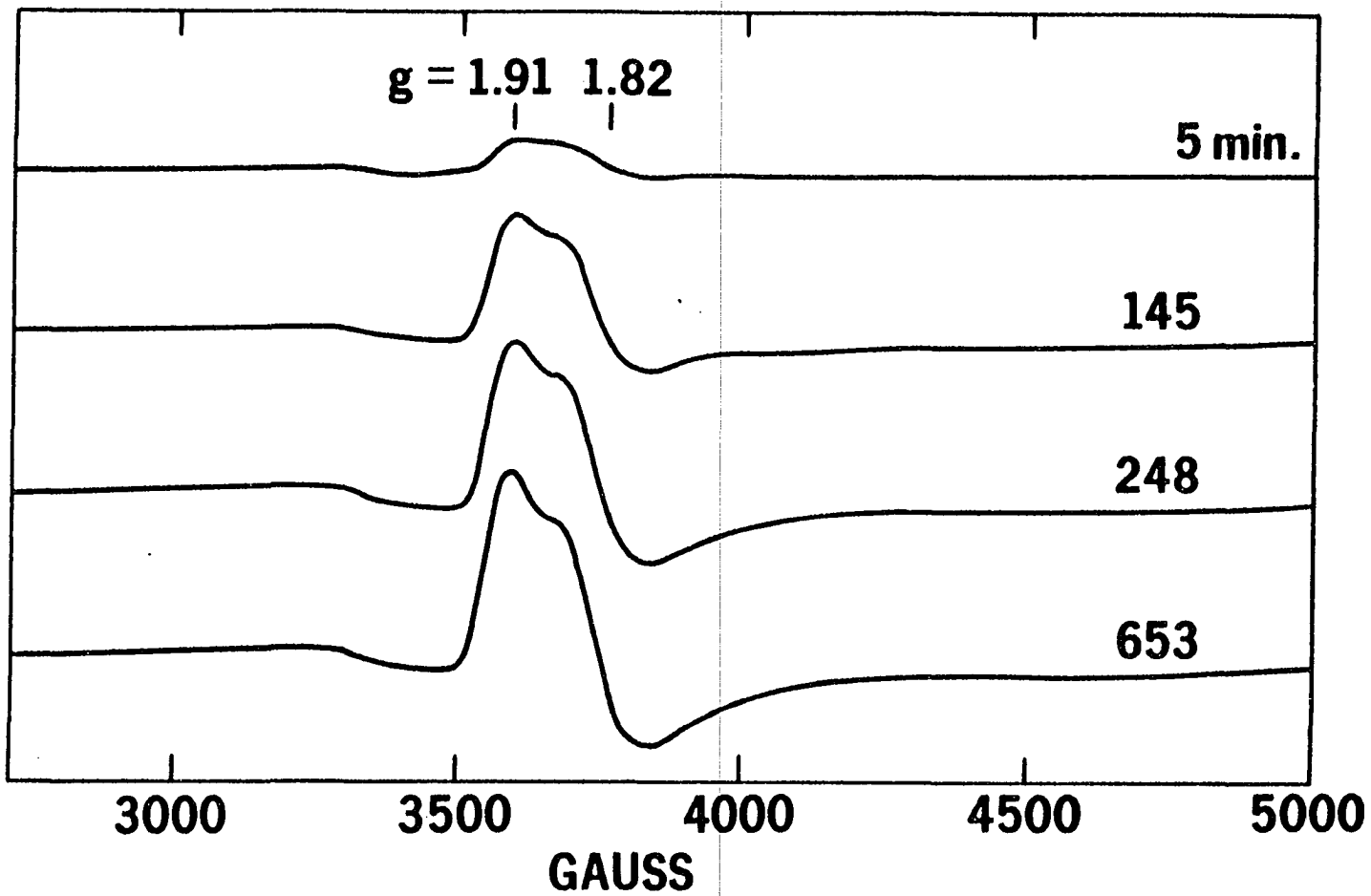
10 and 7 competes with the major pathway, reaction 11, which is the only one seen in perchlorate buffer. These various pathways are illustrated in Scheme III-4. The oxidation of $\mu\text{-S}^{2-}\text{metHr}$ with $\text{Fe}(\text{CN})_6^{3-}$ or H_2O_2 does not occur on a time scale faster than autoreduction. This makes oxidation difficult to detect, and product identification is hampered by reaction mixtures containing numerous species.

When an aerobic solution of $\mu\text{-S}^{2-}\text{metHr}$ in Tris/acetate is incubated in the presence of a 550-fold molar excess of N_3^- , the characteristic EPR (54) and UV-visible (55) spectra of semi-met N_3^- develop in the course of ~ 10 hours as illustrated in Figures III-32 and III-33. As indicated in the legend for Figure III-32, double integration of the semi-met N_3^- EPR signal shows that 81 % of the $\mu\text{-S}^{2-}\text{metHr}$ is converted to semi-met N_3^- . At longer reaction times than those shown in Figure III-33, conversion to met N_3^- is indicated in aerobic solutions by a decrease in the EPR intensity and by development of the characteristic UV-visible spectrum (32). Thus acceleration of the autoreduction pathway by azide (reactions 9 and 10) results in suppression of the reaction of $\mu\text{-S}^{2-}\text{metHr}$ with O_2 (reaction 11). The resulting $\mu\text{-S}^{2-}\text{semi-metHr}$ then undergoes its usual aerobic reaction 7 followed by binding of azide (reaction 8).

Aerobic incubation of $\mu\text{-S}^{2-}\text{metHr}$ in Tris/perchlorate in the presence of a 267-fold molar excess of NaN_3 when followed

Figure III-32. EPR spectra observed during aerobic incubation at room temperature of 1.41 mM μ -S²⁻methHr in 50mM Tris/acetate pH 8.0 in the presence of 0.76 M NaN_3

Instrument parameters: temperature, 4 K; frequency, 9.57 GHz; power, 100 μ W; modulation amplitude, 16 G at 100 kHz; time constant, 0.2 s; receiver gain, 4×10^4 . Double integration gives the following spins/2Fe: 5 minutes, 0.13; 145 minutes, 0.43; 248 minutes, 0.69; 653 minutes, 0.81



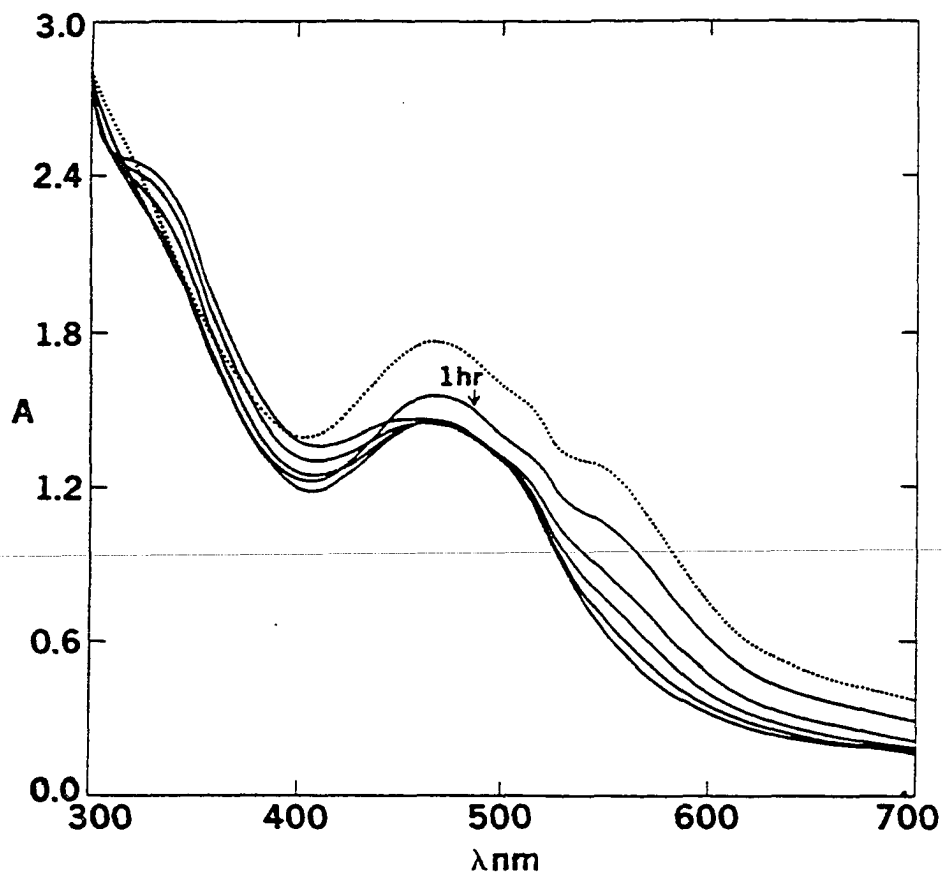


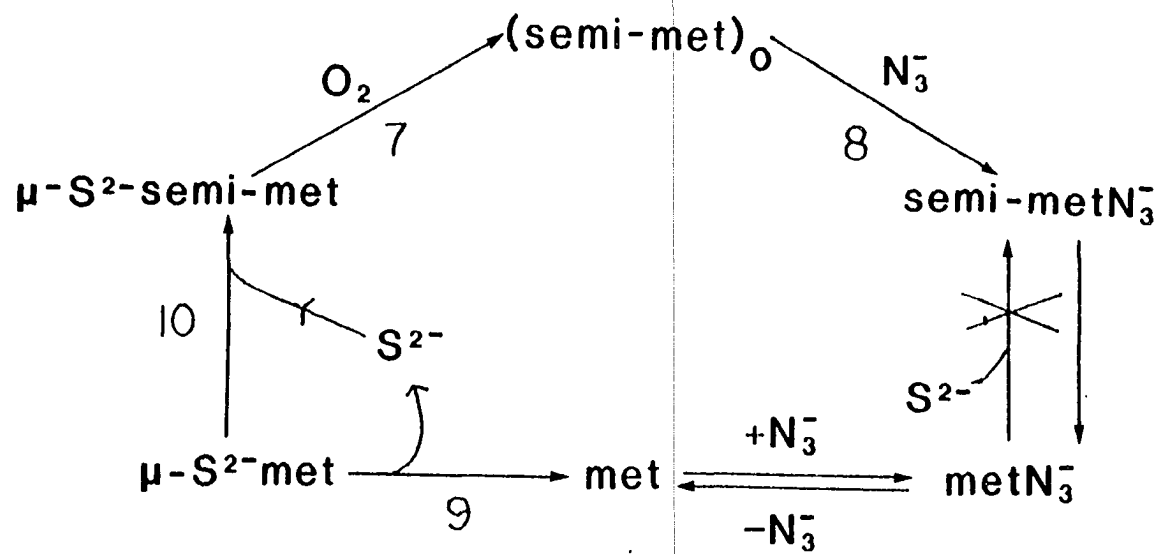
Figure III-33. Absorption spectra observed during aerobic incubation at room temperature of $0.35 \text{ mM } \mu\text{-S}^2\text{-metHr}$ in $50 \text{ mM Tris/perchlorate pH } 8.0$ containing 0.16 M NaN_3

Pathlength = 1 cm. Dotted spectrum was taken immediately after addition of NaN_3 . Solid curves were obtained at 2 hour intervals starting 1 hour after the initial scan

by EPR reveals a mixture containing ~ 40 % $\mu\text{-S}^{2-}$ -semi-metHr and ~ 60 % semi-metN₃⁻ when the maximum EPR signal is obtained. The EPR signal after 365 minutes is similar to the 35 % $\mu\text{-S}^{2-}$ -semi-metHr signal simulated in Figure III-28B and integrates to 0.9 spins/2Fe. The appearance of $\mu\text{-S}^{2-}$ -semi-metHr as an intermediate in Tris/perchlorate but not in Tris/acetate is consistent with the slowing of $\mu\text{-S}^{2-}$ -semi-metHr reaction with O₂ (reaction 7) in Tris/perchlorate relative to Tris/acetate. In the presence of excess azide, addition of one molar equivalent of sulfide does not result in reduction to semi-metN₃⁻ (see Sections II-A and III-A). Thus, a reaction pathway through $\mu\text{-S}^{2-}$ -semi-metHr is the only possibility for preventing formation of metN₃⁻ as a major product in the aerobic reaction of $\mu\text{-S}^{2-}$ -metHr with N₃⁻. Scheme III-5 summarizes the proposed reaction pathway. At reaction times greater than 10 hours, the aerobic solutions of $\mu\text{-S}^{2-}$ -metHr plus N₃⁻ show decreased EPR intensities, and the optical spectra indicate conversion to metN₃⁻.

When the aerobic reaction of $\mu\text{-S}^{2-}$ -metHr with azide is irradiated with a 150 watt projector bulb, conversion to metN₃⁻ occurs within an hour. This result is consistent with rapid photochemically induced release of significant amounts of sulfide; the resulting metHr then ligates the azide before reduction of metHr by sulfide can occur. An alternative possibility is that irradiation increases the rate of reaction 11.

Scheme III-5



IV. CONCLUSIONS

A. Formation and Structure of the Chalcogenide
Derivatives of Hemerythrin

The structure of the sulfide derivatives at the semi-met and met oxidation levels as determined by the previously discussed work is depicted in Figure IV-1. The most important conclusions from this work about the structure of the sulfide derivatives of Hr are: (i) the purple sulfide derivative first reported in 1965 (63) is at the semi-met oxidation level; (ii) a sulfide derivative at the met oxidation level can be prepared from it; (iii) the semi-met and met sulfide derivatives contain one bridging sulfide at each iron site; (iv) sulfide does interact with deoxyHr; however, the nature of the interaction is not well-characterized.

Exposure of metHr to sulfide under anaerobic conditions results in a one-electron reduction to the semi-met level followed by replacement of the μ -oxo bridge between the irons with a single sulfide. This reaction sequence is substantiated by the analogous reaction of metHr with selenide where the two steps are well-separated. Titration of metHr with sulfide indicates that a molar ratio of 1.2 sulfide/Hr is required for complete formation of μ -S²⁻-semi-metHr. This stoichiometry suggests that ~ 0.2 moles of sulfide/mole Hr are

oxidized to sulfite leaving one sulfide to be substituted into the bridge.

The sulfide bridge is maintained upon ferricyanide oxidation of $\mu\text{-S}^{2-}$ -semi-metHr to the met oxidation level and upon subsequent dithionite or sulfide reduction back to $\mu\text{-S}^{2-}$ -semi-metHr. The presence of a single sulfide in the $\mu\text{-S}^{2-}$ -metHr form is substantiated by chemical analyses which show 1 sulfide/2 irons. Analysis of the resonance Raman spectrum reveals Fe-S-Fe symmetric and asymmetric vibrations which are characteristic of a sulfur-bridged system with a bridge angle of approximately 80° .

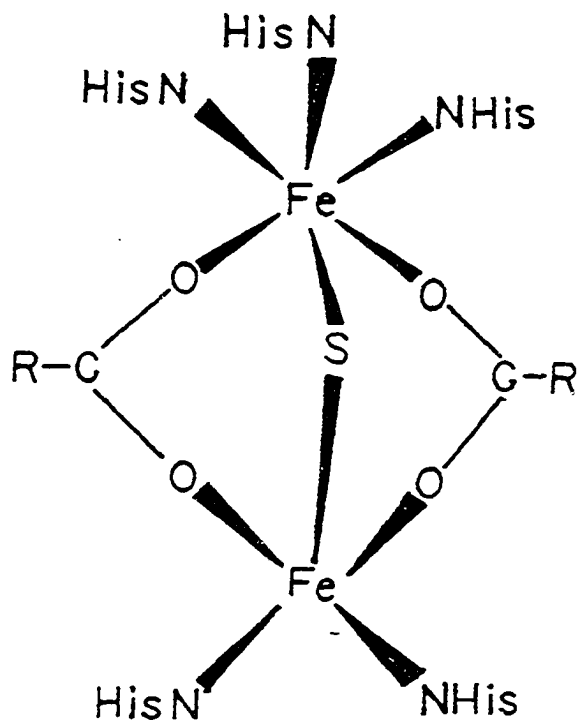


Figure IV-1. Iron site of the $\mu\text{-S}^{2-}$ -Hrs

Presently, there is no direct evidence for a μ -hydroxo or μ -oxo bridge in (semi-met)_O or _R or semi-metN₃⁻. However, the above conclusions about the μ -sulfido bridges in μ -S²⁻metHr and μ -S²⁻semi-metHr tend to support the idea that a μ -oxo or μ -hydroxo bridge persists at the semi-met oxidation level in the absence of sulfide and that it is more labile than at the met level.

μ -S²⁻metHr can only be prepared via oxidation of μ -S²⁻semi-metHr. The assumption that the purple sulfide derivative was at the met oxidation level and the lack of reversibility in the μ -S²⁻metHr \rightarrow metHr step explains why μ -S²⁻metHr was not discovered earlier. Recently, Maroney et al. (61) have provided evidence that the magnetic coupling between the irons in semi-metN₃⁻ is approximately 10-fold weaker than in metN₃⁻. This result is consistent with a μ -hydroxo bridge in semi-metHr rather than a μ -oxo bridge as in metHr. A μ -hydroxo bridge would be more labile and would explain the replacement of the bridging ligand by a sulfide at the semi-met but not the met oxidation level.

When the sulfide has been introduced into the iron site it is quite likely that the Fe-S-Fe angle is considerably smaller than that of the original Fe-O-Fe angle, and that severe steric restrictions are generated at the iron site. These restrictions are the most likely reason for the lack of stable anion adducts of the sulfide derivatives of Hr at

either the met or semi-met oxidation levels. Both metHr and semi-metHr form stable azide adducts (see Scheme III-4), whereas both $\mu\text{-S}^{2-}$ -metHr and $\mu\text{-S}^{2-}$ -semi-metHr do not. Although one could argue that the lack of azide binding to $\mu\text{-S}^{2-}$ -semi-metHr is due to reduction of the exposed iron, the fact that azide can bind to deoxyHr suggests that electronic factors alone do not prevent azide binding to $\mu\text{-S}^{2-}$ -semi-metHr.

Although $\mu\text{-S}^{2-}$ -semi-metHr cannot be reduced by dithionite, EPR data from experiments of deoxyN₃⁻ reacted with sulfide indicate that there is an interaction of sulfide with deoxyHr. The nature of the sulfide/deoxyHr interaction is not clear. Since all attempts at oxidizing the sulfide/deoxyHr complex back to the original $\mu\text{-S}^{2-}$ -metHr form have failed, it seems probable that the sulfide is not in a bridging position.

B. Comparison of Reactivity of the μ -Sulfidehemerythrins and μ -oxo Containing Hemerythrins

The reactivity and probably reaction pathways of the μ -sulfideHrs relative to the μ -oxo containing Hrs are summarized in Scheme III-4 (Section III-F). Introduction of a sulfide into the iron site has a considerable effect on the protein's reactivity. The main conclusions from the reactivity studies are: (i) replacement of the μ -oxo bridge by a μ -sulfido bridge results in a positive shift of the

met/semi-met reduction potential of approximately 200 mV; (ii) the μ -sulfideHrs exist as two conformers, which may resemble (semi-met)_O and (semi-met)_R; (iii) μ -S²⁻metHr undergoes a slow autoreduction to μ -S²⁻semi-metHr upon anaerobic incubation; (iv) ligand anions accelerate this autoreduction; (v) reactions of μ -S²⁻semi-metHr and μ -S²⁻metHr with O₂ result in semi-met and metHr, respectively; O₂ appears to react with bound sulfide, since the reactions with O₂ are much faster than the anaerobic dissociation of sulfide; (vi) perchlorate binding to the μ -S²⁻Hrs slows both oxidative loss of sulfide and autoreduction.

C. Comparison of the Iron Site in the μ -S²⁻hemerythrins with Those of Other Fe-S Centers

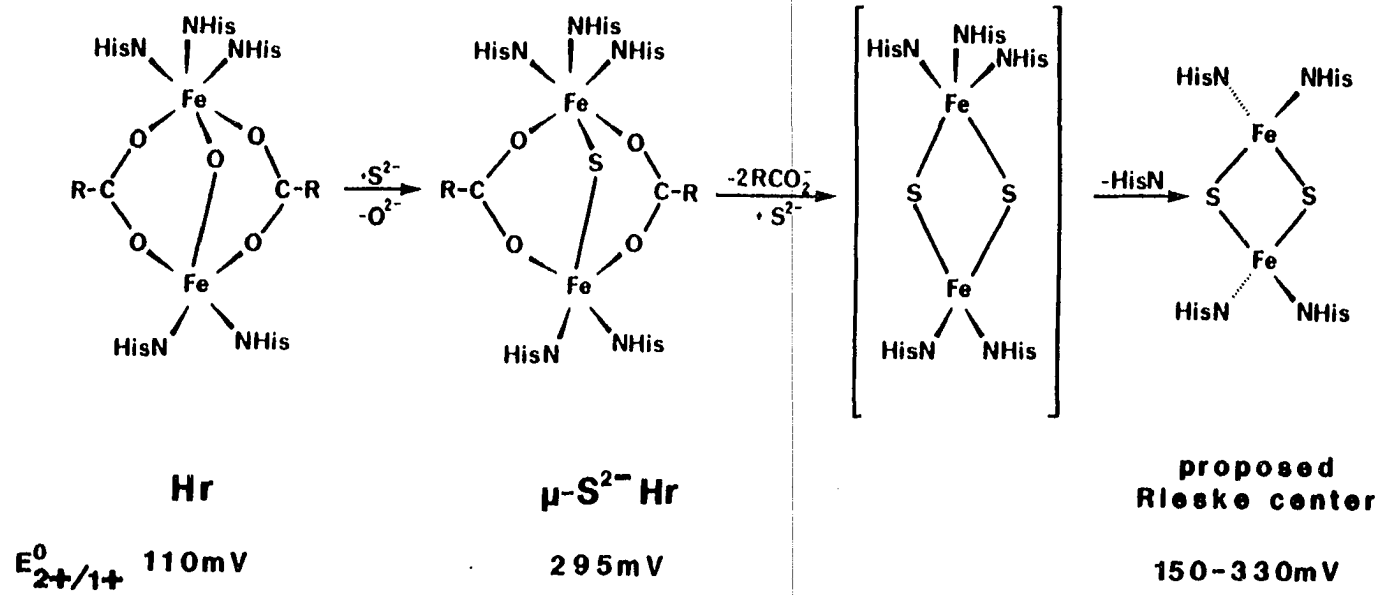
Some interesting parallels can be drawn between the iron sites in the μ -sulfideHrs and [2Fe-2S] centers in iron-sulfur proteins. The oxidation levels of μ -S²⁻metHr and μ -S²⁻semi-metHr correspond to oxidized and reduced [2Fe-2S] centers, respectively. Both the μ -S²⁻metHr and oxidized [2Fe-2S] centers consist of an antiferromagnetically coupled pair of high-spin Fe(III) ions and an S = 0 ground spin state. Both μ -S²⁻semi-metHr and reduced [2Fe-2S] centers have a trapped valence Fe(III)Fe(II) configuration and an S = 1/2 ground state. Reduction of μ -S²⁻semi-metHr with retention of the

sulfide is not observed, and correspondingly, a "superreduced" [2Fe-2S] center having two Fe(II) has yet to be identified (110). The reactions of the $\mu\text{-S}^{2-}$ Hrs and several ferredoxins with dioxygen result in the acid labile sulfide being removed from a bridging position and converted into sulfur in the zero oxidation state (123). One would not expect exact parallels in physical or chemical properties between the $\text{Fe}_2\text{S}(\text{O}_2\text{CR})_2$ core of the sulfideHrs and the Fe_2S_2 core of [2Fe-2S] ferredoxins, especially since most of the latter cores are known or suspected to be attached to the protein exclusively via two terminal thiolate ligands per iron (110). However, this work demonstrates that a stable iron-sulfur center can exist in a protein without thiolate ligation to iron and raises the possibility that such centers naturally occur in as yet undiscovered proteins.

Recently, a new Rieske-type (i.e., high potential) [2Fe-2S] iron-sulfur protein from Thermus thermophilus which contains equimolar cysteine and iron has been reported (71). The detailed structure of the iron site in any Rieske iron-sulfur protein is not yet known. However, in Thermus thermophilus protein at least one terminal ligand per iron must be something other than cysteine thiolate. The visible spectrum of this protein in the oxidized form bears a striking resemblance to that of $\mu\text{-S}^{2-}$ metHr. The $\text{Fe}_2\text{S}(\text{O}_2\text{CR})_2^{2+/1+}$ reduction potential for $\mu\text{-S}^{2-}$ Hr (283-312 mV) falls within the

range of the Rieske iron-sulfur centers (150-330 mV) (124, 125). The Fe_2S_2 core of the [2Fe-2S] centers which are presumably attached to the protein exclusively via terminal thiolate ligands as is the case for spinach ferredoxin have rather negative reduction potentials for the $\text{Fe}_2\text{S}_2^{2+/1+}$ couple (-400 to -450 mV versus NHE) (110). Based on electrostatic considerations, terminal ligation by neutral imidazoles rather than negatively charged thiolates should lead to a significant increase in this value. The reduction potential for $\mu\text{-S}^{2-}\text{Hrs}$ is in agreement with this expectation. These rather positive reduction potentials are apparently responsible for the autoreduction of $\mu\text{-S}^{2-}\text{metHr}$ as well as of at least one of the Rieske centers (126). The ^{57}Fe Mössbauer data for the Rieske protein from Thermus thermophilus are more consistent with 4 than 5 of 6-coordination (71, 127). Both the sulfide/iron ratio and Mössbauer data for this Rieske protein are significantly different from those of $\mu\text{-S}^{2-}\text{metHr}$ discussed in Section III-C. Therefore, despite the resemblance in optical and EPR spectra, the center in $\mu\text{-S}^{2-}\text{metHr}$ is apparently different from the Rieske center. Nonetheless, one can hypothetically construct a reasonable model for the Rieske center starting from that in $\mu\text{-S}^{2-}\text{metHr}$. The sequence of transformations is diagrammed in Scheme IV-1. Our data indicate that replacement of a bridging O^{2-} by S^{2-} induces an ~ 200 mV positive shift in reduction potential. Replacement

Scheme IV-1



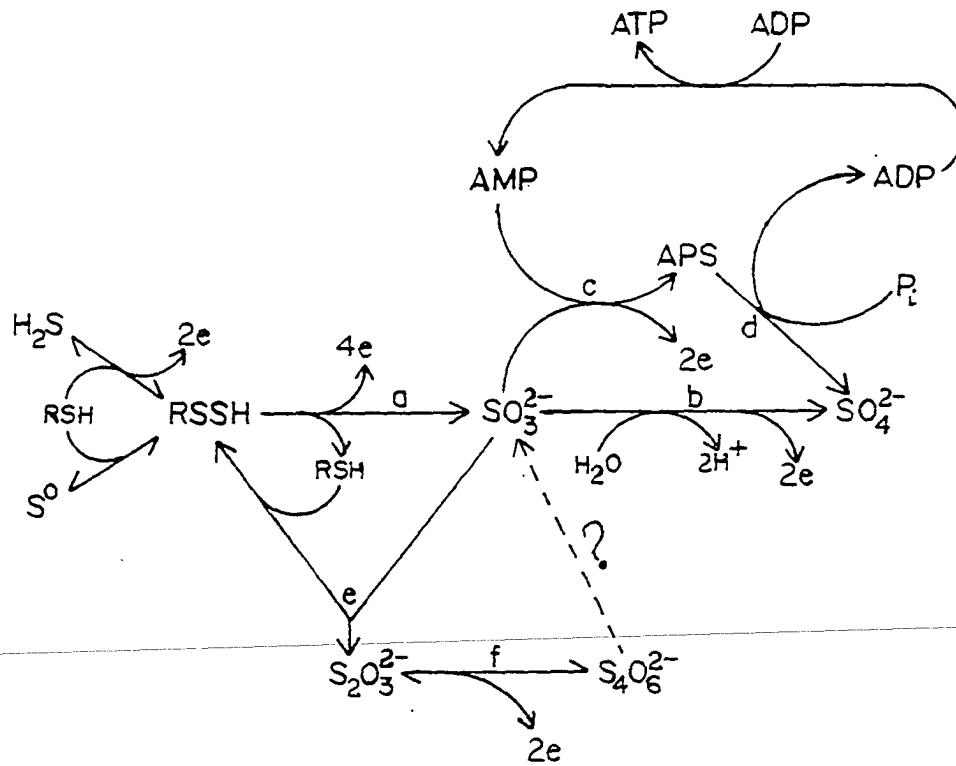
of the two bridging carboxylates by a second bridging S^{2-} might cause a further positive shift, perhaps to a value out of the above range for Rieske centers. However, removal of a histidine ligand from the originally 6-coordinate iron accompanied by transformation to tetrahedral geometry should have the opposite effect on reduction potential, thus conceivably negating any increase. Note that these transformations can occur with no change in overall charge on the center. Overall charge must play an important role in the positive shift in reduction potentials observed for the Rieske centers. Substitution of terminal S by N without changing the overall charge is insufficient. Terminal pyrrolate ($C_4H_4N^-$), when substituted for terminal thiolate on a synthetic Fe_2S_2 core, results in a negative shift in reduction potential (127). The amino acid composition of the Rieske protein from Thermus thermophilus requires that at least two terminal ligands per $[2Fe-2S]$ center be other than cysteine thiolate (71). The structure proposed in Scheme IV-1 is consistent with those data.

D. Comparison of the Reactivity of the $\mu-S^{2-}$ -hemerythrins with Sulfide Metabolism

Although there are similarities between the structure of the $\mu-S^{2-}$ -Hrs and several naturally occurring $[2Fe-2S]$ centers,

physiological parallels between the reactivity of metHr with sulfide and sulfide metabolism in living organisms are not readily apparent. Biological oxidation of H_2S to S^0 occurs in lithotrophic (sulfur-oxidizing) bacteria. These bacteria utilize electron flow from reduced sulfur compounds to O_2 (or NO_3^- for anaerobic strains) together with respiratory chain phosphorylation to generate ATP and reducing power for CO_2 assimilation. Bacteria of genus Thiobacillus oxidize sulfide, sulfur zero, thiosulfate and sulfite to sulfate. Scheme IV-2 summarizes the proposed routes for inorganic sulfur metabolism in these bacteria (128). It is interesting to note that the thiosulfate-oxidizing enzyme in this proposed pathway has a molecular weight of 115,000 and contains two moles of non-heme iron (129). The reaction of metHr with sulfide is the manner in which sulfide can be introduced into the bridging position in Hr. Once the $\mu\text{-S}^{2-}\text{Hrs}$ have been formed, the production of SO_3^{2-} seems to occur only during the autoreduction of $\mu\text{-S}^{2-}\text{metHr}$. Although intermediates in this reduction reaction have not been identified, it seems highly unlikely that the route from sulfide to sulfite in $\mu\text{-S}^{2-}\text{Hr}$ is analogous to the pathway in sulfide-oxidizing bacteria.

It is generally believed that the primeval atmosphere of earth was devoid of O_2 and that, as a result, primitive organisms depended upon compounds such as sulfate and nitrate as electron acceptors for terminal respiration. The



Scheme IV-2

- a) sulfur oxidizing enzyme
- b) sulfite oxidase
- c) APS reductase
- d) ADP sulfurylase
- e) thiosulfate splitting enzyme
- f) thiosulfate oxidizing enzyme

APS adenosine
5'-phosphosulfate

possibility exists that metHr could have had a role in the transport and or storage of sulfide used in sulfide metabolism of the putative ancestors of the present-day sipunculids. The idea of an oxygen-carrying protein being utilized for sulfide transport is not without precedent. The giant tube worms Riftia pachyptila found on the ocean floor near the hydrothermal vents at depths of 9000 feet or more contain a protein which appears to function in the transport of both sulfide and molecular oxygen. Somehow these worms incorporate living bacteria into their bodies, and it is believed that sulfide taken up from the vent water is transported via the sulfide binding protein to these symbiotic bacteria (130, 131).

On the other hand, binding of sulfide by metHr could be a mechanism for prevention of sulfide toxicity. A small percentage of metHr in the worms' blood could conceivably bind and oxidize sulfide, thereby preventing it from reducing and deoxygenating oxyHr or under conditions of low oxygen tension, metHr could react with and immobilize sulfide until there is enough O_2 present to oxidize it to S^0 .

V. LITERATURE CITED

1. Wilkins, R. G., Harrington, P. C. In "Advances in Inorganic Biochemistry", Vol. 5; Theil, E. C., Eichhorn, G. L. and Marzilli, L. G., Eds.; Elsevier Biomedical: New York, 1983; pp 51-85.
2. Manwell, C. Rev. Physiol. 1960, 22, 191-244.
3. DePhillips, H. A., Jr. Arch. Biochem. Biophys. 1971, 144, 122-125.
4. Mangum, C. P.; Kondon, M. Comp. Biochem. Physiol. 1975, 50, 777-785.
5. Rossi-Fanelli, A.; Antonini, E.; Caputo, A. Advan. Prot. Chem. 1964, 19, 73-78.
6. Okamura, M. Y.; Klotz, I. M. In "Inorganic Biochemistry", Eichhorn, G. L., Ed.; Elsevier: New York, 1973; pp 320-343.
7. de Waal, D. J. A.; Wilkins, R. G. J. Biol. Chem. 1976, 251, 2339-2343.
8. Wald, G.; Allen, D. W. J. Gen. Physiol. 1957, 40, 593-608.
9. Klippenstein, G. L.; Van Ripper, D. H.; Oosterum, E. A. J. Biol. Chem. 1972, 247, 5959-5963.
10. Klotz, I. M.; Keresztes-Nagy, S. Biochemistry 1963, 2, 445-452.
11. Klippenstein, G. L. Biochemistry 1972, 11, 372-380.
12. Manwell, C. Comp. Biochem. Physiol. 1960, 1, 277-285.
13. Subramanian, A. R.; Holleman, J. W.; Klotz, I. M. Biochemistry 1968, 7, 3859-3867.
14. Klippenstein, G. L.; Holleman, J. W.; Klotz, I. M. Biochemistry 1968, 7, 3868-3878.
15. Klotz, I. M.; Klippenstein, G. L.; Hendrickson, W. A. Science 1976, 192, 335-344.
16. Keresztes-Nagy, S.; Klotz, I. M. Biochemistry 1963, 2, 923-927.

17. Langerman, N. R.; Klotz, I. M. Biochemistry 1969, 8, 4746-4752.
18. Klapper, M. H.; Klotz, I. M. Biochemistry 1968, 7, 223-231.
19. Tan, K. H.; Keresztes-Nagy, S.; Frankfater, A. Biochemistry 1975, 14, 4280-4285.
20. Tan, K. H.; Keresztes-Nagy, S.; Frankfater, A. Biochemistry 1975, 14, 4286-4291.
21. Klippenstein, G. L.; Cote, J. L.; Ludham, S. E. Biochemistry 1976, 15, 1128-1136.
22. Liberatore, F. A.; Truby, M. F.; Klippenstein, G. L. Arch. Biochem. Biophys. 1974, 160, 223-229.
23. Darnall, D. W.; Garbett, K.; Klotz, I. M.; Aktipis, S.; Keresztes-Nagy, S. Arch. Biochem. Biophys. 1969, 133, 103-107.

24. Hendrickson, W. A. In "Invertebrate Oxygen-Binding Proteins"; Lamy, J. and Lamy, L., Eds.; Marcel Dekker: New York, 1981; pp 503-515.
25. Hendrickson, W. A.; Klippenstein, G. L.; Ward, K. B. Proc. Nat. Acad. Sci. USA 1975, 72, 2160-2164.
26. Stenkamp, R. E.; Sieker, L. C.; Jensen, L. H.; Loehr, J. S. J. Mol. Biol. 1976, 100, 23-34.
27. Sheridan, R. P.; Levy, K. M.; Salemme, F. R. Proc. Natl. Acad. Sci. USA 1982, 79, 4545-4549.
28. Ward, K. B.; Hendrickson, W. A.; Klippenstein, G. L. Nature, 1975, 257, 818-821.
29. Kurtz, D. M. Jr.; Shriver, D. F.; Klotz, I. M. Coord. Chem. Rev. 1977, 24, 145-178.
30. Sanders-Loehr, J.; Loehr, T. M. In "Advances in Inorganic Biochemistry", Vol. 1; Theil, E. C., Eichhorn, G. L. and Marzilli, L. G., Eds.; Elsevier Biomedical: New York, 1979; pp 235-252.

31. Harrington, P. C.; Wilkins, R. G.; Muhoberac, B. B.; Wharton, D. C. In "The Biological Chemistry of Iron"; Dunford, H. B., Dolphin, D., Raymond, K. N., and Sieker, L., Eds.; D. Reidel Publishing Company: New York, 1982; pp 145-160.
32. Garbett, K.; Darnall, D. W.; Klotz, I. M.; Williams, R. J. P. Arch. Biochem. Biophys. 1969, 103, 419-434.
33. Elam, W. T.; Stern, E. A.; McCallum, J. D.; Sanders-Loehr, J. J. Am. Chem. Soc. 1982, 104, 6369-6373.
34. Hendrickson, W. A.; Co, M. S.; Smith, J. L.; Hodgson, K. O.; Klippenstein, G. L. Proc. Natl. Acad. Sci. USA 1982, 79, 6255-6259.
35. Elam, W. T.; Stern, E. A.; McCallum, J. D.; Sanders-Loehr, J. J. Am. Chem. Soc. 1983, 105, 1919-1923.
36. Stenkamp, R. E.; Sieker, L. C.; Jensen, L. H. J. Am. Chem. Soc. 1984, 106, 618-622.
37. Stenkamp, R. E.; Sieker, L. C.; Jensen, L. H. J. Inorg. Biochem. 1983, 19, 247-253.
38. Dunn, J. B. R.; Shriver, D. F.; Klotz, I. M. Biochemistry 1975, 14, 2689-2695.
39. Kurtz, D. M., Jr.; Shriver, D. F.; Klotz, I. M. J. Am. Chem. Soc. 1976, 98, 5033-5035.
40. Stenkamp, R. E.; Sieker, L. C.; McCallum, J.; Sanders-Loehr, J. Proc. Natl. Acad. Sci. USA, submitted.
41. Stenkamp, R. E.; Sieker, L. C.; Jensen, L. H. J. Mol. Biol. 1978, 126, 457-466.
42. Armstrong, W. H.; Spool, A.; Papaefthymiou, G. C.; Frankel, R. G.; Lippard, S. J. J. Am. Chem. Soc. 1984, 106, 3653-3667.
43. Garbett, K.; Darnall, D. W.; Klotz, I. M. Arch. Biochem. Biophys. 1971, 142, 455-470.
44. Okamura, M. Y.; Klotz, I. M.; Johnson, G. E.; Winter, M. R. C.; Williams, R. J. P. Biochemistry 1969, 8, 1951-1958.

45. Garbett, K.; Johnson, C. E.; Klotz, I. M.; Okamura, M. Y.; Williams, R. J. P. Arch. Biochem. Biophys. 1971, 142, 574-583.
46. Dawson, J. W.; Gray, H. B.; Hoenig, H. E.; Rossman, G. R.; Schredder, J. M.; Wang, R. H. Biochemistry 1972, 11, 461-465.
47. Armstrong, W. H.; Lippard, S. J. J. Am. Chem. Soc. 1984, 106, 4632-4633.
48. Murray, K. S. Coord. Chem. Rev. 1974, 12, 1-35.
49. Shiemke, A. K.; Loehr, T. M.; Sanders-Loehr, J. J. Am. Chem. Soc. 1984, 106, 4951-4956.
50. Freier, S. M.; Duff, L. L.; Shriver, D. F.; Klotz, I. M. Arch. Biochem. Biophys. 1980, 205, 449-463.
51. Solbrig, R. M.; Duff, L. L.; Shriver, D. F.; Klotz, I. M. J. Inorg. Biochem. 1982, 17, 69-74.

52. Harrington, P. C.; de Waal, D. J. A.; Wilkins, R. G. Arch. Biochem. Biophys. 1978, 191, 444-451.
53. Babcock, L. M.; Bradic, Z.; Harrington, P. C.; Wilkins, R. G.; Yoneda, G. S. J. Am. Chem. Soc. 1980, 102, 2849-2850.
54. Muhoberac, B. B.; Wharton, D. C.; Babcock, L. M.; Harrington, P. C.; Wilkins, R. G. Biochim. Biophys. Acta 1980, 626, 337-345.
55. Harrington, P. C., Wilkins, R. G. J. Am. Chem. Soc. 1981, 103, 1550-1556.
56. Nocek, J. M.; Kurtz, D. M., Jr.; Pickering, R. A.; Doyle, M. P. J. Biol. Chem. 1984, 259, 12334-12338.
57. Armstrong, F. A.; Harrington, P. C.; Wilkins, R. G. J. Inorg. Biochem. 1983, 18, 83-91.
58. Harrington, P. C.; Muhoberac, B. B.; Wharton, D. C.; Wilkins, R. G. Biochemistry 1981, 20, 6134-6139.
59. Martinsen, J.; Irwin, M. J.; Ho, P. S.; Hoffman, B. M.; Klotz, I. M. Biochim. Biophys. Res. Commun. 1983, 53, 231-232.

60. Irwin, M. J.; Duff, L. L.; Shriver, D. F.; Klotz, I. M. Arch. Biochem. Biophys. 1983, 224, 473-478.
61. Maroney, M. J.; Lauffer, R. B.; Que, L. Jr.; Kurtz, D. M., Jr. J. Am. Chem. Soc. 1984, 106, 6445-6446.
62. Harrington, P. C.; Wilkins, R. G. J. Inorg. Biochem. 1983, 19, 339-344.
63. Keresztes-Nagy, S.; Klotz, I. M. Biochemistry 1965, 4, 919-931.
64. Bayer, E.; Krauss, P.; Schretzmann, P. Z. Naturforsch. 1970, B25, 327-328.
65. Freier, S. M.; Duff, L. L.; Van Duyne, R. P.; Klotz, I. M. Biochemistry 1979, 18, 5372-5377.
66. Spiro, T. G.; Hare, J.; Yachandra, V.; Gewirth, A.; Johnson, M. K.; Remsen, E. In "Iron-Sulfur Proteins Metal Ions in Biology", Vol. 4; Spiro, T. G. Ed.; John Wiley and Sons: New York, 1982; pp 406-423.
-
67. Loach, P. A. In "Handbook of Biochemistry and Molecular Biology", 3rd ed. Vol I; Fasman, G. D., Ed.; CRC Press, Inc.: Cleveland, 1976; pp 123-129.
68. O'Reilly, J. E. Biochim. Biophys. Acta 1973, 292, 509-515.
69. Heineman, W. R.; Norris, B. J.; Goelz, J. F. Anal. Chem. 1975, 47, 79-84.
70. Malkin, R.; Chain, R. K.; Lam, E. Chemica Scripta 1983, 21, 75-80.
71. Fee, J. A.; Findling, K. L.; Yoshida, T.; Hille, R.; Tarr, G. E.; Hearshen, D. O.; Dunham, W. R.; Day, E. P.; Kent, T. A.; Munck, E. J. Biol. Chem. 1984, 259, 124-133.
72. Drago, R. S. "Physical Methods in Chemistry"; W. B. Saunders Company: Philadelphia, 1977; pp 316-350.
73. Orme-Johnson, W. H., Sands, R. H. In "Iron Sulfur Proteins II"; Lovenberg, W., Ed.; Academic Press: New York, 1973; pp 195-235.

74. Gibson J. F.; Hall, D. O.; Thornley, J. H. M.; Whatley F. R. Proc. Natl. Acad. Sci. USA 1966, 56, 987-990.
75. Palmer, G. In "Methods for Determining Metal Ion Environments in Proteins", Darnall, D. W., Wilkins, R. G., Eds.; John Wiley and Sons: New York, 1980; pp 153-181.
76. Eaton, S. S.; Eaton, G. R. Bull. of Magn. Reson. 1979, 1, 130-137.
77. Johnson, C. E. In "Topics in Applied Physics: Mössbauer Spectroscopy", Vol. 5; Gonser, U., Ed.; Springer Verlag: New York, 1975; pp 139-166.
78. Moss, T. H. Meth. Enzymol. 1972, 27, 919-941.
79. Drago, R. S. "Physical Methods in Chemistry"; W. B. Saunders Company: Philadelphia, 1977; pp 530-549.
80. Grasselli, J. G., Snavely, M. K., Bulkin, B. J. "Chemical Applications of Raman Spectroscopy", John Wiley & Sons: New York, 1981; pp 75-98.
81. Tu, A. T. "Raman Spectroscopy in Biology Principles and Applications"; John Wiley and Sons: New York, 1982, pp 3-43.
82. Wing, R. M.; Callahan, K. P. Inorg. Chem. 1969, 8, 871-874.
83. Klotz, I. M.; Klotz, T. A.; Fiess, H. A. Arch. Biochem. Biophys. 1957, 68, 284-299.
84. Averill, B. A.; Bale, J. R.; Orme-Johnson, W. H. J. Am. Chem. Soc. 1978, 100, 3034-3043.
85. Wertz, J. E.; Bolton, J. R. "Electron Spin Resonance. Elementary Theory and Practical Applications"; McGraw-Hill: New York, 1972; pp 450-466.
86. Aasa, R.; Vanngard, T. J. Mag. Reson. 1975, 19, 308-315.
87. Sjöberg, B. M.; Loehr, T. M.; Sanders-Loehr, J. Biochemistry 1982, 21, 96-102.
88. Rill, R. L.; Klotz, I. M. Arch. Biochem. Biophys. 1970, 136, 507-514.

89. Rill, R. L.; Klotz, I. M. Arch. Biochem. Biophys. 1971, 147, 226-241.
90. Eibeck, R. E. Inorganic Synthesis 1963, 7, 128-131.
91. Irwin, M. J.; Duff, L. L.; Shriver, D. F.; Klotz, I. M. Arch. Biochem. Biophys. 1983, 224, 473-478.
92. Laurie, S. H.; Pratt, D. E.; Yong, J. H. L. Inorg. Chim. Acta 1984, 93, L57-L59.
93. McDonald, J. W.; Friesen, G. D.; Rosenhein, L. D.; Newton, W. E. Inorg. Chim. Acta 1983, 72, 205-210.
94. Segal, M. G.; Sykes, A. G. J. Am. Chem. Soc. 1978, 100, 4585-4588.
95. Fortune, W. B.; Mellon, M. G. Ind. Eng. Chem., Anal. Ed. 1938, 10, 60-64.
96. Fogo, J. K.; Popowsky, M. Anal. Chem 1949, 6, 732-734.

97. Golbeck, J. H.; Pietro, A. S. Anal. Chem. 1976, 73, 539-542.
98. Beinert, H. Anal. Chem. 1983, 131, 373-378.
99. Margoliash, E.; Frohwirt, N. Biochem. J. 1959, 71, 570-572.
100. Margoliash, E.; Walasek, O. F. Meth. Enzymol. 1967, 10, 339-348.
101. Margalit, R.; Schejter, A. Eur. J. Biochem. 1973, 32, 492-499.
102. Clark, P. E.; Webb, J. Biochemistry 1981, 20, 4628-4632.
103. York, J. L.; Bearden, A. J. Biochemistry 1970, 9, 4549-4554.
104. Krueger, R. J.; Siegel, L. M. Biochemistry 1982, 21, 2892-2904.
105. Harmer, M.; Sykes, A. G. In "Molybdenum Chemistry of Biological Significance", Newton, W. E.; Ofsuka, S., Eds.; Plenum Press: New York, 1980; pp 401-410.

106. Schwarzenbach, G.; Fischer, A. Helv. Chem. Acta 1960, 43, 1365-1390.
107. Yachandra, V. K.; Hare, J.; Gewirth, A.; Czernuszewicz, R.S.; Kimura, T.; Holm, R. H.; Spiro, T. G. J. Am. Chem. Soc. 1983, 105, 6462-6468.
108. Mitchell, P. C. H.; Parker, D. A. J. Inorg. Nucl. Chem. 1973, 35, 1385-1390.
109. Spiro, T. G.; Stein, P. Ann. Rev. Phys. Chem. 1977, 28, 501-521.
110. Berg, J. M.; Holm, R. H. In "Iron Sulfur Proteins"; Spiro, T. G., Ed; John Wiley: New York, 1982; pp 1-66.
111. Do, Y.; Simhan, E. D.; Holm, R. H. Inorg. Chem. 1983, 22, 3809-3812.
112. Reynolds, J. G.; Holm, K. Inorg. Chem. 1980, 19, 3257-3260.
-
113. Reem, R. C.; Solomon, E. I. J. Amer. Chem. Soc. 1984, 106, 8323-8325.
114. Bradić, Z.; Conrad, R.; Wilkins, R. G. J. Biol. Chem. 1977, 252, 6069-6075.
115. Dutton, P. L.; Wilson, D. F. Biochem. Biophys. Acta 1974, 346, 165-212.
116. Darnall, D. W.; Garbett, K.; Klotz, I. M. Biochem. Biophys. Res. Commun. 1968, 32, 264-271.
117. Bradić, Z.; Wilkins, R. G. Biochemistry 1983, 22, 5396-5401.
118. Burkey, K. D.; Gross, E. L. Biochemistry 1982, 21, 5886-5890.
119. Duff, L. L.; Klippenstein, G. L.; Shriver, D. F.; Klotz, I. M. Proc. Nat. Acad. Sci. USA 1981, 78, 4138-4140.
120. Morgan, T. V.; Stephens, P. J.; Derlin, F.; Stout, C. D.; Melis, K. A.; Burgess, B. K. Proc. Nat. Acad. Sci. USA 1984, 81, 1931-1935.
121. Melson, D. R.; Wilkins, R. G. Biochemistry 1976, 15, 1284-1290.

122. Olivas, E.; de Waal, D. J. A.; Wilkins, R. G. J. Inorg. Biochem. 1979, 11, 205-212.
123. Petering, D.; Fee, J. A.; Palmer, G. J. Biol. Chem. 1971, 246, 643-653.
124. Malkin, R.; Bearden, A. J. Biochim. Biophys. Acta 1978, 505, 147-181.
125. Bowyer, J. R.; Edwards, C. A.; Ohnishi, T., Trumpower, B. L. J. Biol. Chem. 1982, 257, 8321-8330.
126. Rieske, J. S.; Hansen, R. E.; Zaugg, W. S. J. Biol. Chem. 1964, 239, 3017-3022.
127. Coucouvanis, D.; Salifogulo, A.; Kanatzidis, M. G.; Simopoulous, A.; Papefthymiou, G. C. J. Am. Chem. Soc. 1984, 106, 6081-6082.
128. Siegel, L. M. In "Metabolic Pathways", Vol VII; Greenberg, D. M., Ed.; Academic Press: New York, 1975; pp 217-276.
-
129. Lyric, R. M.; Suzuki, I. Can. J. Biochem. 1970, 48, 355-363.
130. Arp, A. J.; Chidress, J. J. Science 1983, 219, 295-297.
131. Powell, M. A.; Somero, G. N. Science 1983, 219, 297-299.
132. Rupp, H.; Moore, A. L. Biochim. Biophys. Acta 1979, 548, 16-29.
133. Yim, M. B.; Kuo, L. C.; Makinen, M. W. J. Mag. Reson. 1982, 46, 247-256.
134. Poole, C. P., Jr. In "Electron Spin Resonance. A Comprehensive Treatise on Experimental Techniques", Wiley: New York, 1967; pp 695-733.
135. Skoog, D. A.; West, D. M. In "Fundamentals of Analytical Chemistry", Holt, Rinehard and Winston: New York, 1976; pp 357-362.

VI. ACKNOWLEDGEMENTS

I wish to thank Dr. Donald M. Kurtz, Jr. for the opportunity to carry out this work and the guidance he provided throughout its duration. The collaborative efforts with Dr. Peter Debrunner and Tim Sage at the University of Illinois for Mössbauer data and with Andrew Sheimke and Drs. Tom and Joane Loehr at the Oregon Graduate Center for the resonance Raman work were quite fruitful. I would like to thank them all for their invaluable input into this project.

Special thanks go to Dr. Dee-Hau Huang without whom the task of running low-temperature EPR spectra would have been considerably more frustrating and time-consuming. For always being willing to listen to ideas and offering helpful suggestions, I would like to thank my labmate, Judy Nocek.

A very special thank-you goes to my parents and my sister Ruth because without their support and encouragement I would have left the Chemistry Department at Iowa State University long before completion of this dissertation.

VII. APPENDIX A: EPR MICROWAVE POWER SATURATION CURVES
FOR HEMERYTHRIN DERIVATIVES AND THREE COPPER STANDARDS

In order to determine the concentration of an unknown paramagnetic species, the EPR spectra of both the unknown and the concentration standard must be obtained under non-saturating conditions. The signal amplitude (S) is dependent on the incident microwave power (P_0) according to the relationship $S/\sqrt{P_0} \propto (1 + P_0/P_{1/2})^{-b/2}$. The quantity $P_{1/2}$ is the power for half-saturation; the quantity b is a constant characteristic of the broadening mechanism. For representing power saturation data, the $\log (S/\sqrt{P_0})$ is plotted against $\log P_0$. The intersection of the asymptotic limits of the resulting saturation curve yields $P_{1/2}$. A line parallel to the abscissa indicates no saturation within that range of microwave power (132, 133, 134).

All plots given here were generated from EPR spectra in which the microwave power was varied while holding all other instrumental parameters constant. The signal amplitude was measured in centimeters and then normalized. Incident microwave power was always used in units of watts. The plots of $\log S/\sqrt{P_0}$ versus $\log P_0$ were used to confirm that EPR spectra to be integrated were recorded under non-saturating conditions.

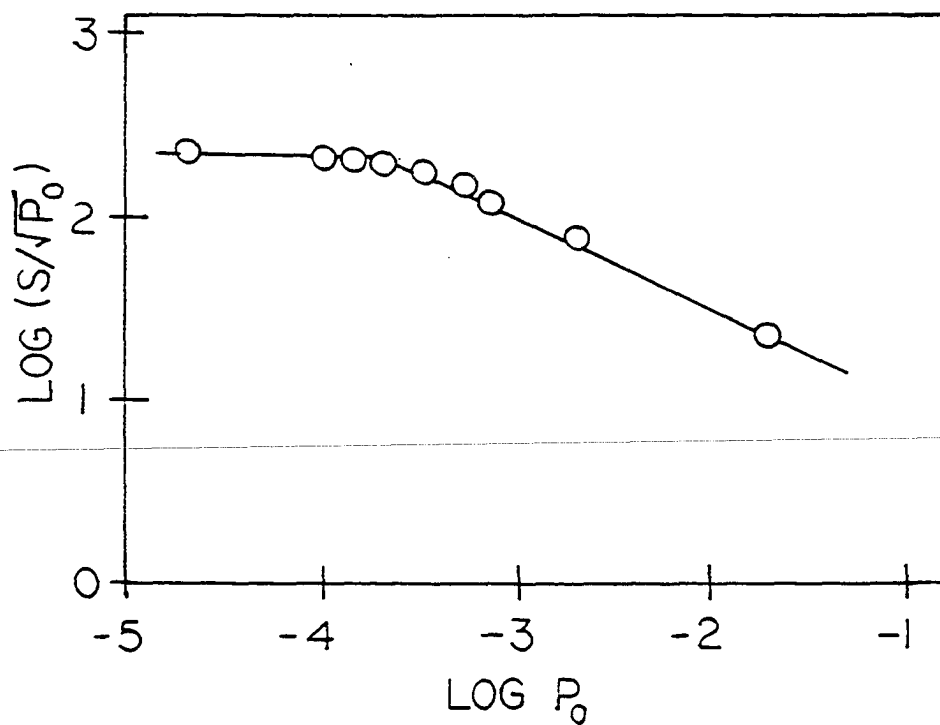


Figure A-1. Plot of $\log [S/\sqrt{P_0}]$ versus $\log P_0$ for 1.50 mM μ -S²-semi-methr in 50 mM Tris/acetate pH 8.0

Saturation curves for g -values 1.88, 1.70 and 1.40 are identical. Instrument parameters: temperature, 4.5 K; frequency, 9.569 GHz; modulation amplitude, 16 G at 100 kHz; time constant, 0.2 s; receiver gain, 1.25×10^4

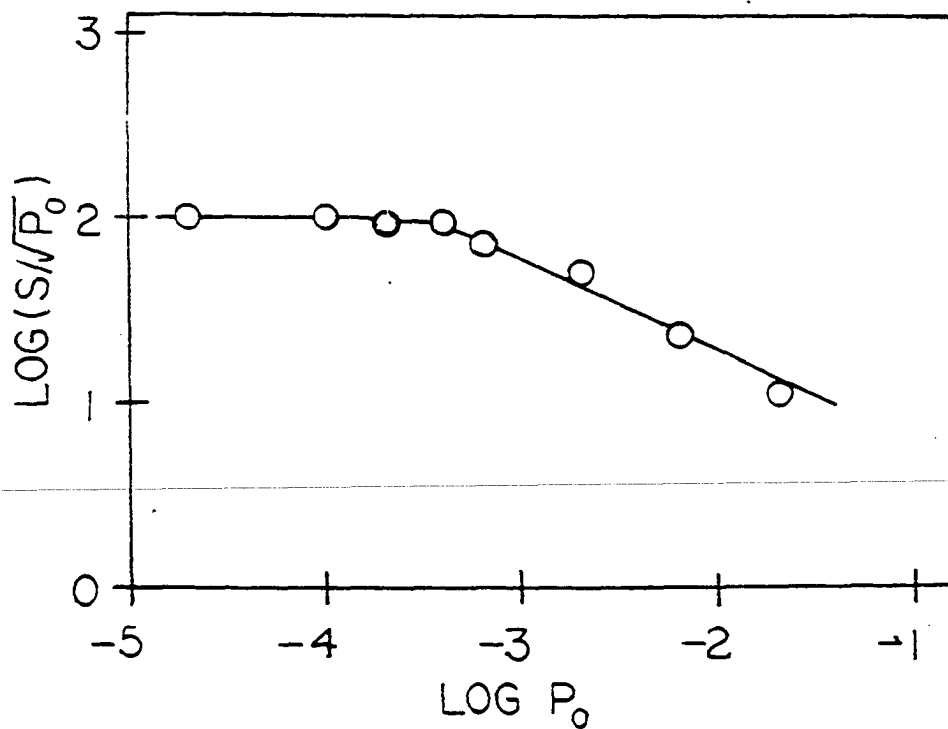


Figure A-2. Plot of $\log [S/\sqrt{P_0}]$ versus $\log P_0$ for 0.8 mM (semi-met)_R in 50 mM Tris/acetate pH 8.0

Saturation curves for features at g-values 1.95, 1.88 and 1.64 are identical. Instrument parameters: temperature, 4.5 K; frequency, 9.571 GHz; modulation amplitude, 16 G at 100 kHz; time constant, 0.2 s; receiver gain, 6.3×10^3

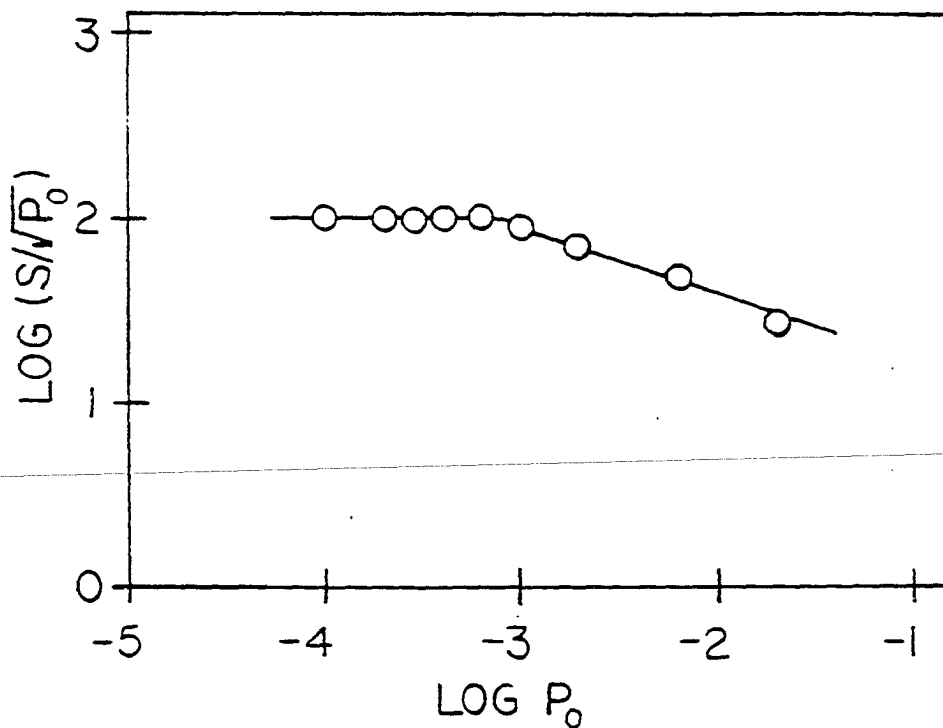


Figure A-3. Plot of $\log [S/\sqrt{P_0}]$ versus $\log P_0$ for 1.45 mM (semi-met)₀ in 50 mM Tris/acetate pH 8.0

Saturation curves for features with g-values 1.70 and 1.95 are identical. Instrument parameters: temperature, 4.3 K; frequency, 9.568 GHz; modulation amplitude, 16 G at 100 kHz; time constant, 0.2 s; receiver gain, 6.3×10^3

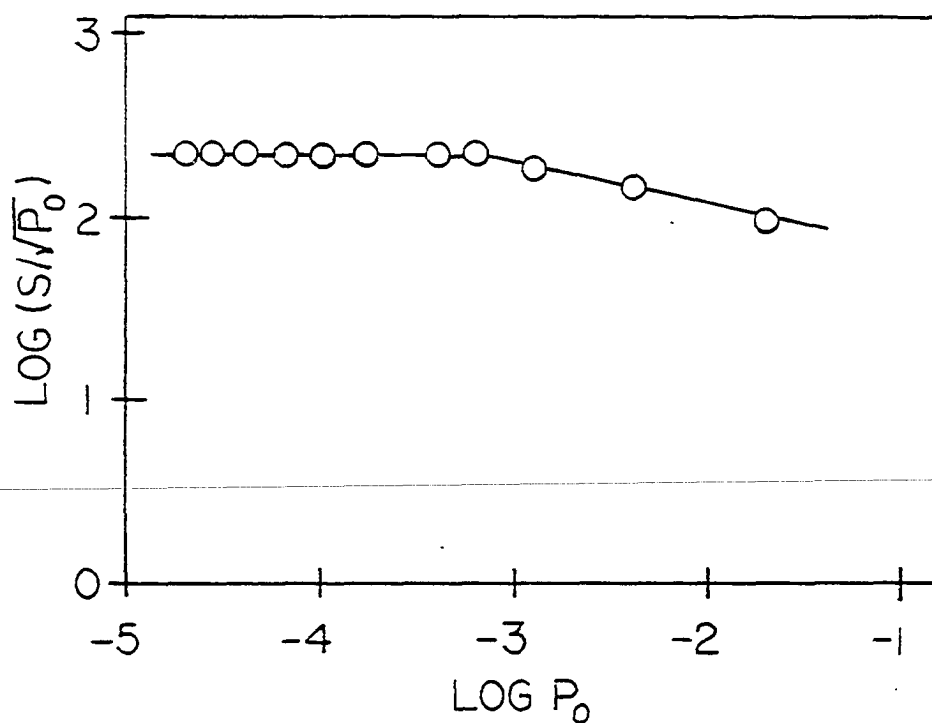


Figure A-4. Plot of $\log [S/\sqrt{P_0}]$ versus $\log P_0$ for 3.4 mM semi-metN₃ in 50 mM Bis/tris/sulfate pH 6.0

Saturation curves for features with g-values 1.90, 1.81 and 1.49 are identical. Instrument parameters: temperature, 4.4 K; frequency, 9.573 GHz; modulation amplitude, 16 G at 100 kHz; time constant, 0.2 s; receiver gain, 2.5×10^4

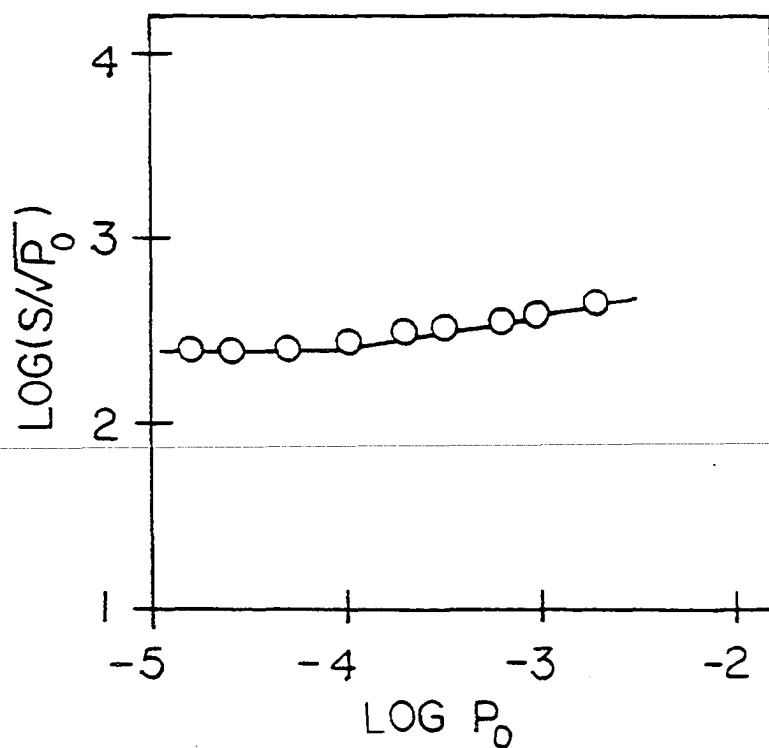


Figure A-5. Plot of $\log [S/\sqrt{P_0}]$ versus $\log P_0$ for 1.02 mM deoxyN₃⁻ in 50 mM Tris/acetate pH 8.0

Instrument parameters: temperature, 4.1 K;
frequency, 9.566 GHz; modulation amplitude, 16
G at 100 kHz; time constant, 0.2 s; receiver
gain, 6.3×10^4

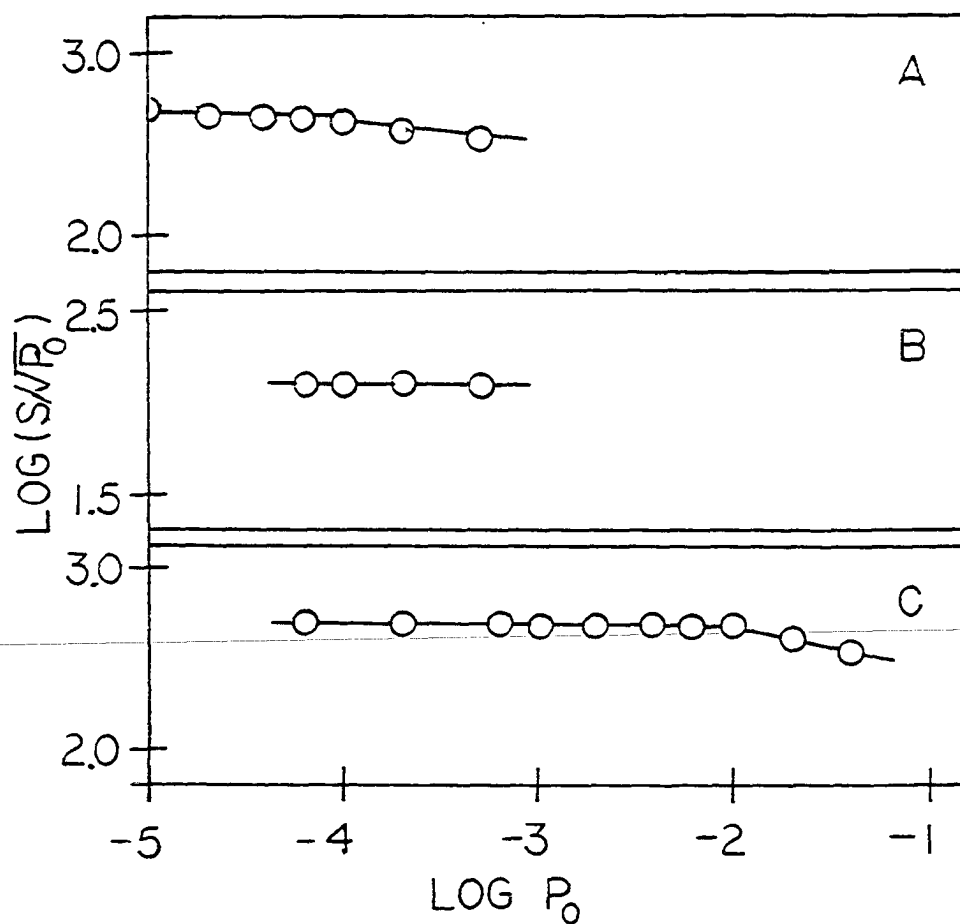


Figure A-6. Plots of $\log [S/\sqrt{P_0}]$ versus $\log P_0$ for 0.8 mM CuEDTA (A), 0.52 mM $\text{CuCl}_2 \cdot 5\text{H}_2\text{O}$ (B) and 1.00 mM $\text{CuSO}_4 \cdot 5\text{H}_2\text{O}$ (C)

Instrument parameters: temperature, 4.5 K; frequency, 9.561 GHz; modulation amplitude, 16 G at 100 kHz; time constant, 0.2 s; receiver gain, 5.0×10^4 (A), 4.0×10^4 (B) and 2.5×10^4 (C)

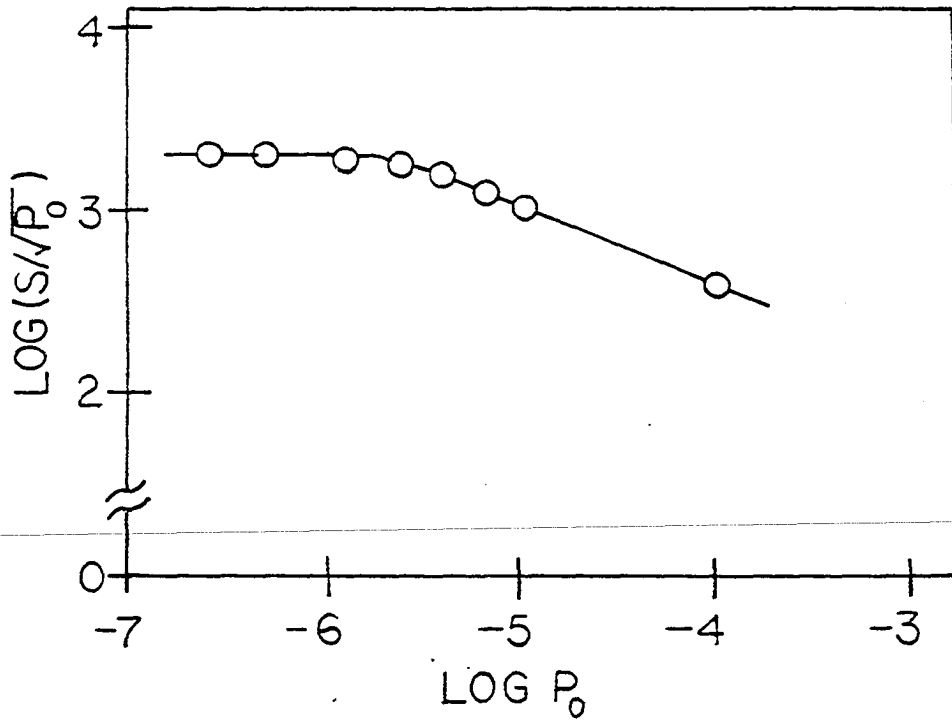


Figure A-7. Plot of $\log [S/\sqrt{P_0}]$ versus P_0 for $g = 2.02$ signal observed for the reaction of $\mu\text{-S}^2\text{-semi-methr}$ with O_2 in 50 mM Tris/acetate pH 8.0

Instrument parameters: temperature, 4.3 K; frequency, 9.570 GHz; modulation amplitude, 16 G at 100 kHz; time constant, 0.2 s; receiver gain, 1.6×10^4

VIII. APPENDIX B: IODOMETRIC TITRATION FOR THE
DETERMINATION OF SULFIDE CONCENTRATIONS (135)

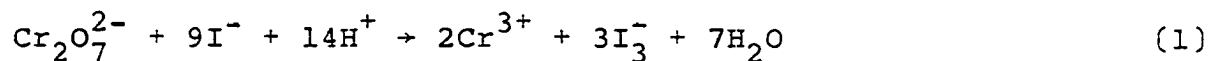
1) A solution approximately 0.1 N in I_2 was prepared in the following manner. Twenty-five grams of KI were dissolved in 20 mL H_2O . Twelve and seven-tenths grams of I_2 were added, and the solution was stirred until all the I_2 was dissolved. This solution was then filtered through a fine sintered glass frit and diluted to one liter. The solution was allowed to sit in the dark for several days.

2) A thiosulfate solution was prepared by dissolving 6.5 grams $Na_2S_2O_3 \cdot 5H_2O$ and 0.1 grams Na_2CO_3 in 500 mL of water which had been boiled and then cooled to room temperature. The final thiosulfate concentration was approximately 0.052 M.

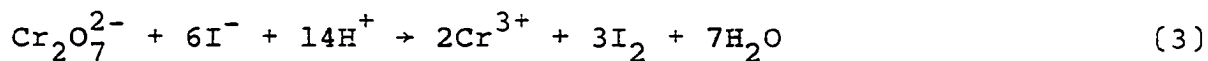
3) An 8.688 mM solution of dichromate was prepared by dissolving 0.6390 grams $K_2Cr_2O_7$ in 250 mL water.

4) One gram of KI was dissolved for every 25 mL of water used. Fifteen mL 1 M H_2SO_4 were added per 25 mL KI solution. The acid and KI solution were not mixed together until immediately before they were to be used since the solution turned yellow upon standing for a few minutes.

5) In order to standardize the thiosulfate solution, 25 mL (measured by buret) of the $K_2Cr_2O_7$ solution was mixed with 40 mL of the KI/H_2SO_4 solution. This dark red solution was allowed to stand covered for 5 minutes (reaction 1). Next, this solution was titrated with thiosulfate (reaction 2). When the reddish-brown color began to fade, several drops of starch were added making the solution appear dark blue. The titration was continued until the indicator turned a light blue-green.



or



6) The iodine solution was standardized against the thiosulfate solution (reaction 2 or 4). Again starch was used as the indicator.

7) To determine sulfide concentrations, a disposable syringe was used to transfer 1 mL of a stock sulfide solution into

30 mL of the standard I_2 solution. After all the sulfide had reacted (reaction 5 or 6), the remaining I_2 was titrated with thiosulfate using starch as the indicator (reaction 2 or 4).



or

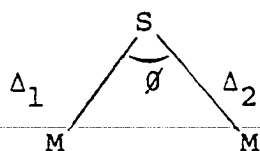


IX. APPENDIX C: CALCULATION OF Fe-S-Fe BRIDGING ANGLE
IN μ -SULFIDOMETHEMERYTHRIN FROM VIBRATIONAL FREQUENCIES

A. Calculation of Fe-S-Fe Angle from Resonance Raman Data

The secular equations from Wing and Callahan (82) were used for an M_2S instead of M_2O system.

1) Symmetry coordinates for M_2S



$$A_1: S_1 = 1/\sqrt{2}(\Delta_1 + \Delta_2)$$

$$B_2: S_2 = 1/\sqrt{2}(\Delta_1 - \Delta_2)$$

2) Secular Equations for M_2S

$$\nu_s: \lambda_s = [\mu_m + \mu_s (1 + \cos \phi)](k + k_{msm}); \text{ solving for } \cos \phi$$

$$\cos \phi = \frac{\lambda_s}{(k + k_{msm})\mu_s} - \frac{\mu_m}{\mu_s} - 1$$

$$\nu_{as}: \lambda_{as} = [\mu_m + \mu_s (1 - \cos \phi)](k - k_{msm}); \text{ solving for } \cos \phi$$

$$\cos \phi = - \frac{\lambda_{as}}{(k - k_{msm})\mu_s} - \frac{\mu_m}{\mu_s} + 1$$

$\lambda = (5.89 \times 10^{-7})\nu^2$, where ν is the frequency in cm^{-1} . k is the bridge M-S force constant; k_{msm} is the M-S-M bridge interaction constant. μ_{m} and μ_{s} are reciprocals of the masses of the metal atom and sulfur atom, respectively.

$$\lambda_{\text{s}} = 5.89 \times 10^{-7}(\nu_{\text{s}})^2 = 5.89 \times 10^{-7}(431)^2 = 0.109$$

$$\lambda_{\text{as}} = 5.89 \times 10^{-7}(\nu_{\text{as}})^2 = 5.89 \times 10^{-7}(327)^2 = 0.0630$$

$$\mu_{\text{m}} = 1/55.85 = 0.0179$$

$$\mu_{\text{s}} = 1/32.06 = 0.0312$$

If using the values of k and k_{msm} reported for an

$\text{Fe}_2\text{S}_2(\text{SCH}_2\text{CH}_3)_2$ model by Yachandra et al. (107) are used, one can solve for θ .

$$k = 1.44 \text{ mdyn/\AA}$$

$$k_{\text{msm}} = 0.27 \text{ mdyn/\AA}$$

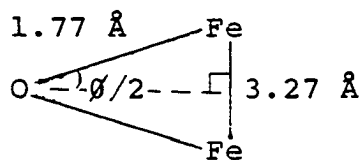
$$\text{Using } \nu_{\text{s}} = 431 \text{ cm}^{-1}, \theta = 62^\circ$$

$$\text{Using } \nu_{\text{as}} = 327 \text{ cm}^{-1}, \theta = 99^\circ$$

However, two different bridging angles are obtained with those values of k and k_{msm} . A good fit of the two frequencies can also be obtained using $k = 1.72 \text{ mdyn/\AA}$ and $k_{\text{msm}} = 0.27 \text{ mdyn/\AA}$. In this case the calculated $\theta = 79.6^\circ$ using either ν_{s} or ν_{as} .

B. Fe-S-Fe Angle Calculations Based on Retention of Fe-Fe Distance upon Replacement of S for O

1) metazideHr



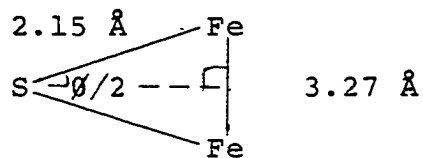
$$\sin (\phi/2) = \frac{(3.27/2)}{1.77} = 0.9237$$

$$\phi/2 = 67.5$$

$$\phi = 135^\circ$$

Reported value of ϕ is $135^\circ(41)$.

2) μ -S²⁻-metHr



Assuming a 0.35 \AA increase in bridge bond distances compared to those of metN_3^- .

$$\sin (\phi/2) = \frac{(3.27/2)}{2.15} = 0.7605$$

$$\phi/2 = 49/5^\circ$$

$$\phi = 99.0^\circ$$